MODELLING OF ADVECTION-DOMINATED TRANSPORT IN FLUID-SATURATED POROUS MEDIA

By

Wenjun Dong

May, 2006

Department of Civil Engineering and Applied Mechanics
McGill University, Montreal, QC, Canada, H3A 2K6

A thesis submitted to Faculty of Graduate Studies and Research
in partial fulfillment of the requirements for the degree of
Doctor of Philosophy

Library and
Archives Canada

Published Heritage
Branch

395 Wellington Street
Ottawa ON K1A 0N4
Canada

Bibliothèque et
Archives Canada

Direction du
Patrimoine de l'édition

395, rue Wellington
Ottawa ON K1A 0N4
Canada

Your file Votre référence
ISBN: 978-0-494-25131-7
Our file Notre référence
ISBN: 978-0-494-25131-7

NOTICE:
The author has granted a non-exclusive license allowing Library and Archives Canada to reproduce, publish, archive, preserve, conserve, communicate to the public by telecommunication or on the Internet, loan, distribute and sell theses worldwide, for commercial or non-commercial purposes, in microform, paper, electronic and/or any other formats.

The author retains copyright ownership and moral rights in this thesis. Neither the thesis nor substantial extracts from it may be printed or otherwise reproduced without the author's permission.

AVIS:
L'auteur a accordé une licence non exclusive permettant à la Bibliothèque et Archives Canada de reproduire, publier, archiver, sauvegarder, conserver, transmettre au public par télécommunication ou par l'Internet, prêter, distribuer et vendre des thèses partout dans le monde, à des fins commerciales ou autres, sur support microforme, papier, électronique et/ou autres formats.

L'auteur conserve la propriété du droit d'auteur et des droits moraux qui protège cette thèse. Ni la thèse ni des extraits substantiels de celle-ci ne doivent être imprimés ou autrement reproduits sans son autorisation.

In compliance with the Canadian Privacy Act some supporting forms may have been removed from this thesis.

While these forms may be included in the document page count, their removal does not represent any loss of content from the thesis.

Conformément à la loi canadienne sur la protection de la vie privée, quelques formulaires secondaires ont été enlevés de cette thèse.

Bien que ces formulaires aient inclus dans la pagination, il n'y aura aucun contenu manquant.

Canada

To my wife
Mrs. Congyue Zhang
for the time and support she gives to me

Also to my lovely twin girls
Xiao Wen Dong
Xiao Jun Dong

ABSTRACT

The modelling of contaminant transport in porous media is an important topic to geosciences and geo-environmental engineering. An accurate assessment of the spatial and temporal distribution of a contaminant is an important step in the environmental decision-making process. Contaminant transport in porous media usually involves complex non-linear processes that result from the interaction of the migrating chemical species with the geological medium. The study of practical problems in contaminant transport therefore usually requires the development of computational procedures that can accurately examine the non-linear coupling processes involved. However, the computational modelling of the advection-dominated transport process is particularly sensitive to situations where the concentration profiles can exhibit high gradients and/or discontinuities. This thesis focuses on the development of an accurate computational methodology that can examine the contaminant transport problem in porous media where the advective process dominates.

The development of the computational method for the advection-dominated transport problem is based on a Fourier analysis on stabilized semi-discrete Eulerian finite element methods for the advection equation. The Fourier analysis shows that under the Courant number condition of $Cr = 1$, certain stabilized finite element scheme can give an oscillation-free and non-diffusive solution for the advection equation. Based on this observation, a time-adaptive scheme is developed for the accurate solution of the one-dimensional advection-dominated transport problem with the transient flow velocity. The time-adaptive scheme is validated with an experimental modelling of the advection-dominated transport problem involving the migration of a chemical solution in a porous column. A colour visualization-based image processing method is developed in the experimental modelling to quantitatively determinate the chemical concentration on the porous column in a non-invasive way. A mesh-refining adaptive scheme is developed for the optimal solution of the multi-dimensional advective transport problem with a time- and space-dependent flow field. Such mesh-refining adaptive procedure is quantitative in the sense that the size of the refined mesh is determined by the Courant number criterion.

Finally, the thesis also presents a brief study of a numerical model that is capable to capture coupling Hydro-Mechanical-Chemical processes during the advection-dominated transport of a contaminant in a porous medium.

RÉSUMÉ

La modélisation du transport de contaminant dans des milieux poreux est une matière importante des géosciences et de la technologie géoenvironnementale. Une évaluation précise de la distribution spatiale et temporelle d'un contaminant est une étape importante dans le processus décisionnel environnemental. Le transport de contaminant dans des milieux poreux comporte habituellement des processus non linéaires complexes qui résultent de l'interaction des espèces chimiques migrante avec le milieu géologique. L'étude des problèmes pratiques dans le transport de contaminant exige donc habituellement le développement des procédures informatiques qui peuvent examiner avec exactitude les processus de couplage non linéaires impliqués. Cependant, la modélisation informatique du procédé de transport advection-dominé est particulièrement sensible aux situations où les profils de concentration peuvent montrer des gradients et/ou des discontinuités élevés. Cette thèse se concentre sur l'élaboration d'une méthodologie informatique précise qui peut examiner le problème de transport de contaminant dans des milieux poreux où le processus convectif domine.

L'élaboration de la méthode informatique pour le problème de transport advection-dominé est basée sur une analyse de Fourier des méthodes eulériennes, semi-discrète et stabilisées d'éléments finis pour l'équation d'advection. L'analyse de Fourier montre que sous la condition du nombre de Courant $Cr = 1$, certains schémas stabilisés d'éléments finis peuvent donner une solution d'oscillation libre et non-diffusive pour l'équation d'advection. Basé sur cette observation, un schéma de temps adaptatif est développé pour la solution précise du problème de transport advection-dominé unidimensionnel avec une vitesse d'écoulement transitoire. Le schéma de temps adaptatif est validé avec une modélisation expérimentale du problème de transport advection-dominé comportant la migration d'une solution chimique dans une colonne poreuse. Une méthode de traitement d'image basée sur la couleur est développée quantitativement dans la modélisation expérimentale, pour déterminer de manière non envahissante, la concentration chimique dans la colonne poreuse. Un schéma adaptatif de raffinement de maillage est développé pour la solution optimale du problème de transport convectif multidimensionnel avec un champ d'écoulement dépendant du temps et de l'espace. Un tel procédé adaptatif de raffinement de maillage est quantitatif dans le sens où la taille du maillage raffiné est déterminée par le critère du nombre de Courant. La thèse présente également une brève étude d'un modèle numérique qui est capable de capturer des processus de couplage Hydraulique-Mécanique-Chimique pendant le transport advection-dominé d'un contaminant dans un milieu poreux.

ACKNOWLEDGEMENTS

The author wishes to express his great gratitude to his supervisor, Professor A.P.S. Selvadurai, *William Scott Professor* and *James McGill Professor*, Department of Civil Engineering and Applied Mechanics at McGill University, for suggesting the topic of research, profound guidance, constant support, extensive reviewing of several drafts of the thesis and the research articles during author's doctoral program at McGill University.

The author would like to thank Professor Vincent H. Chu of the Department of Civil Engineering and Applied Mechanics at McGill University for his advice on an image processing method used in the experimental research of the thesis.

The author appreciates the academic discussions and friendly helps from his colleagues, Dr. Ali Shirazi, Dr. Qifeng Yu, Mr. Hani Ghiabi, Mr. Tuan Luu, Mr. Adrian Glowacki and Mr. Jason Kaden during author's doctoral study at McGill University.

The author wishes an appreciation to Mr. John Bartczak, the technician of Department of Civil Engineering and Applied Mechanics, McGill University, for his help in designing, manufacturing and assembling experimental apparatus of the thesis research. Appreciation also to Mr. Paul Selvadurai, research assistant of Department of Mechanical Engineering at McGill University, for his assistance with the experimental set up. Thanks also to Mr. Jack Goldsmith, the photographer of Instructional Communications Center at McGill University, for the professional instruction of the photography.

The author is also grateful for the help of Mrs. Sally Selvadurai for her expert and precise grammar corrections. Thanks also to Miss Vanessa Lysakoune for the revision of the French resume of the thesis.

The research conducted in this thesis was made possible through the financial assistance provided by the *Max Planck Research Prize in the Engineering Sciences* and the *NSERC-Discovery Grant* awarded to Professor A.P.S. Selvadurai.

Above all, the author wishes a great thank to his wife, Mrs. Congyue Zhang, for her patience, support, understanding and encouragement throughout author's research at McGill University. Special thanks are given to a truly friend and advisor, Mr. Danzi Jiamucuo, for his advising and encouragement throughout this research work.

TABLE OF CONTENTS

LIST OF TABLES

LIST OF FIGURES

CHAPTER 1
INTRODUCTION

1.1 Contaminant Transport in Porous Media

Groundwater is an important resource for human activities related to municipalities, agriculture and industry, and it makes up one-third of the drinking water supply on the earth. The rapid development of human economic activities in recent decades not only demands large quantities of water but also generates significant amounts and varieties of contaminants that ultimately find their way to the subsurface water resources. Sources of contaminants to the groundwater may come from agricultural, industrial and residential activity, as well as natural sources, and include the spillage of fertilizers and pesticides from agricultural practices, the leakage from both aboveground and underground fuel storage tanks and septic tanks, the leachate from waste disposal (i.e. municipal landfill, industrial radioactive deep waste repositories), chemical discharge from mine tailings impoundments and accidental spills, geothermal energy development, acid rain, de-icing salts, seawater intrusion in coastal aquifers, and groundwater-surface water interaction (Bedient et al., 1999; Vulliet et al., 2002). These chemicals may contaminate the groundwater, but can also migrate through geological media. Contamination of groundwater can make it unsuitable for use in the short term, and can render the contaminated aquifer unusable for decades. Furthermore, as the groundwater participates in the hydrologic cycle, contaminants can also move from disposal or spill sites to nearby lakes and rivers, polluting the surface water resources. The geo-environmental problems associated with the migration of contaminants with the groundwater (or contaminated groundwater) in the geosphere have received considerable attention over the past three decades. The study of the time- and space- dependent migration of a contaminant in porous media is a topic of current importance to environmental engineering (Bear and Verruijt, 1990; Bear and Bachmat, 1992; Banks, 1994).

Generally, groundwater constitutes the main agent for the transport of contaminants in geologic media (e.g. in saturated or aquifer zones). In this case, the transport process is composed of two basic processes: advection, due to the movement of the fluid in the pore space, and hydrodynamic dispersion that can consist of both molecular diffusion, due to concentration gradients based on Fick's law, and mechanical dispersion due to irregular movement of the pore fluids in the interstices of porous media. These irregularities can result from the pore scale tortuosity of the flow paths or the heterogeneity and anisotropy of the porous medium, due to the stratification characteristics and the presence of microcracks or fractures. Such inhomogeneous or anisotropic properties of porous media can also influence the time- and space-dependent distribution of the advective flow velocities. Besides these basic processes, the transport of a contaminant within groundwater can also occur by the natural convection due to the differences in density between the fresh and contaminated groundwater (Simmons et al., 2001).

Geologic media are generally composed of three phases: solid particles, pore fluids and gases (e.g. vapor and dry air) (Bishop, 1973; Bear and Verruijt, 1990; Thomas and He, 1995; 1997; Lewis and Schrefler, 1998), and therefore, apart from the movement of groundwater, the transport of contaminants is also influenced by the mechanical behaviour of solid particles and gas transfer inside the porous medium. The mechanical deformation of the solid skeleton of the porous medium can influence the contaminant transport through the soil by influencing the dissipation of the pore water pressure (Biot, 1941), which affects the seepage flow velocity based on Darcy's law. If the solid skeleton deforms, the force convection due to the mechanical movement of the solid particle should also be considered in any contaminant transport process in porous media. Contaminant transport in unsaturated or vadose zones is much more complex than in a saturated zone due to the effect of capillary forces and nonlinear soil characteristics with respect to the moisture content, and is usually influenced by the combined movement of multiphase gases (Bear, 1972; Philips, 1991; Charbeneau, 2000).

Two other important factors should be considered in the transport of contaminants in porous media: thermal effects and geochemical reactions, since both of them may have a significant impact on the chemical and physical behaviour of the fluids and the soil (saturated or unsaturated). The thermal expansion of the pore fluids and the porous skeleton due to temperature variations may become detectable, and thus can have a considerable influence on the contaminant transport, especially for the frost-related and heat generating reactive waste repository problems. On the other hand, organic and inorganic compounds in groundwater may react with their surrounding compounds and/or geological media during their transport, by means of sorption, aqueous complexation, ion exchange, mineral precipitation/dissolution, oxidation, biodegradation of the chemical species, etc. (Rubin, 1983). These geochemical reactions can not only modify the chemical composition of the transported contaminant dissolved in the groundwater, but also alter the chemical and physical properties of the soil skeleton, and consequently influence the contaminant transport process in the porous medium. One well-known example of such influences is the retardation of the contaminant transport process of due to the sorption process or the natural attenuation. Other examples of influences of chemical reactions on the contaminant transport may include the reduction of the elastic stiffness (Gerard et al., 1995; 1998; Le Bellégo et al., 2003; Li et al., 2003) and alteration of the permeability of the porous medium (Bear, 1972; Bourbie and Zinszner, 1985; Katz and Thompson, 1986; Doyen, 1988; Fredrich et al., 1993; 1995; Fredrich, 1999; Kieffer et al., 1999) due to the variation of the porosity caused by mineral precipitation and dissolution. In summary, the transport of contaminants in porous media is a complex coupling process and usually it should consider the mechanics, hydraulics, temperature, geochemistry and even air in the unsaturated zone (Figure 1.1).

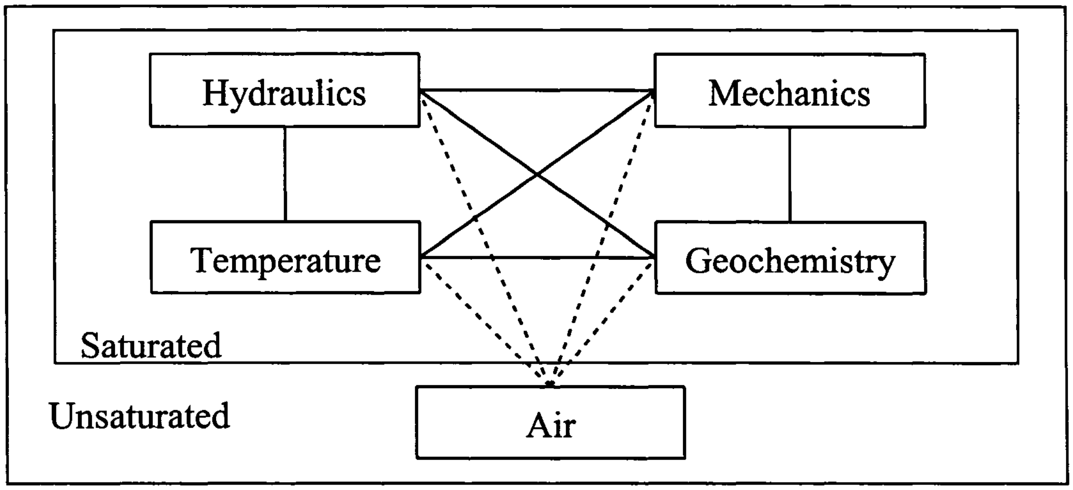

Figure 1.1 Coupling in contaminant transport in porous media (Following Vulliet et al., 2002)

1.2 Mathematical Modelling

A contaminant transported in porous media can render a large number of geologic sites and groundwater unsuitable for use. Therefore, the movement of contaminated groundwater is one of the most important environmental concerns, not only because it is a threat to human health but also because it may reduce the quality of the ground water resources, which are already in short supply because of the increased demand from human activities. The prediction of the time- and space-dependent movement of contaminants in porous media is important for contaminant management, groundwater remediation and soil cleanup. Generally, the contaminant transport in a porous medium can be described by the classical advection-dispersion equation, and two basic approaches can be used for its solution: an analytical approach and a computational approach. The study of the classical advection-dispersion-type equation through analytical means can be attempted only in a limited number of cases involving either a single spatial dimension or a high degree of spatial symmetry, usually requiring an assumption of linearity. Analytical solutions for one-, two- and three-dimensional advection-dispersion equation, containing a first order decay, a source term and certain forms of time- and space-dependent flow velocity, have been investigated and are available in the literature (Ogata and Banks, 1961; Sauty, 1980; Van Genuchten, 1981; Domenico, 1987; Leij and Dane, 1990; Wexler, 1992; Batu, 1993; Leij et al., 1993; Kocabas and Islam, 2000; Park and Zhan, 2001; Selvadurai, 2002a; 2003; 2004a,b). However, it should again be noted that, although the contaminant transport in porous media can basically be governed by the advection-dispersion equation, it is a complex nonlinear process that may include the deformation of the porous skeleton and pore fluids, gas and heat transfers, and geochemical reactions (Lewis and Schrefler, 1998; Smith, 2000; Peters and Smith, 2002). For such coupling transport problems, finding the analytical solutions is a challenge and these are not readily available in the literature; consequently computational modelling has become the preferred approach.

The mathematical modelling of the movement of fluids in a fluid saturated deformable porous medium can be described by the theory of poroelasticity (Biot,1941; 1955; 1956), which originates with the introduction of the concept of the effective stress by Terzaghi (1923). In a saturated porous medium, the effective stress is the inter-granular actual stress within the soil fabric and is defined as the difference between the total stress and pore water pressure. Applying this concept in the constitutive stress-strain relationship, Terzaghi (1923; 1943) proposed a consolidation theory to interpret the one-dimensional time-dependent deformation of the soil skeleton with pore pressure dissipation. Such consolidation theory can be considered as a one-dimensional counterpart of the theory of poroelasticity. For the partially saturated porous medium, the effective stress is determined not only by the total stress and pore fluid pressure but also by the air pressure (Alonso et al., 1990). With the constitutive stress-strain behaviour of the unsaturated soil (Bishop and Blight, 1963; Fredlund, 1979; Thomas and Cleall, 1999), the classical theory of poroelasticity can be extended to describe the moisture and gas transfers in deformable unsaturated porous medium (Thomas and He, 1995; 1997; Lewis and Schrefler, 1998).

Temperature gradient-induced thermal effects on the deformation of the porous medium and the moisture transfer have attracted a great deal attentions in the field of geomechanics in recent years, particularly for the performance assessment of the geological nuclear waste repositories. In such waste disposal systems, the mechanical deformation of the clay buffer (such as bentonite) is influenced by the thermal stress and the moisture movement (diffusion) caused by the temperature gradient. During the last decade, there have been many efforts to develop finite element models to simulate the strongly coupled Thermo-Hydro-Mechanical (THM) behaviours of the unsaturated buffer material. Such modelling should involve the solutions of the mass balance equations for water and air phases, the energy balance equation for heat transfer, and the momentum equilibrium equation for the porous medium (Nguyen et al., 2005). Recently, Hudson et al. (2001) reviewed the application of the THM model in the investigation of the long-term behaviour of bentonite-based buffers in a radioactive nuclear waste repository. Rutqvist et al. (2001) compared four element models for the thermohydromechanics of partially saturated geological media. The details of the formulation of the THM behaviour of an unsaturated soil have been well documented (e.g. Selvadurai and Nguyen, 1995; Thomas and He, 1995; 1997; Thomas et al., 1998; Lewis and Schrefler, 1998).

Geochemical reactions usually occur during the contaminant transport in porous media in the form of mass transfer, either between liquid phases or between liquid phases and solid phases of the contaminant. These geochemical reactions can generally be described by the chemical kinetics, which can be expressed by the Ordinary Differential Equation (ODE). If the reaction rate is sufficiently fast with respect to the local variation of the chemical concentration or the flow velocity, and the local equilibrium conditions are achieved, then the geochemical reaction can be described by the chemical reaction equilibrium, which can be expressed by a set of algebraic equations (Rubin, 1983). Nordstrom et al. (1976) reviewed more than 30 computational packages that are currently in use for the description of the chemical reaction equilibrium in porous media. Two approaches can be used to couple the chemical reaction equilibrium with the contaminant transport in porous media (Lewis et al., 1987). One approach is to incorporate the algebraic reaction equations directly into the transport equation and therefore both transport and chemical interaction can be described by a single reaction transport equation (Jennings et al., 1982; Kirkner et al., 1984). However, the computational models developed through this approach will vary with the different chemical reaction forms of the transported species. An alternative approach to simulating the reactive transport process is to separate the algebraic equation governing the chemical reaction equilibrium from the advection-diffusion equation. In this case, the iterative algorithm should be used for the solution of the chemical reactive transport process described by coupling the differential transport equation and algebraic reaction equation (Grove and Wood, 1979; Cederberg et al., 1985).

The advantage of the second approach is the possibility of using existing computer codes for the transport equation and the equilibrium calculation for large chemical systems (Lewis et al., 1987). Xu and Pruess (2001) used this approach to develop a Thermo-Hydro-Chemical (THC) model to investigate non-isothermal reactive geochemical transport in partially saturated fractured rocks. Both THM and THC models have been applied extensively for various engineering applications, including geothermal, nuclear waste repository, landfill, etc. However, the accurate analysis of the soil behaviour (saturated or unsaturated), in which the contaminant moves with the fluid flow, requires that both the thermal effect and the geochemical reaction be considered in the computational model (Cleall et al., 2004). In order to take this into consideration, a Thermo-Hydro-Mechanical-Chemical (THMC) model is necessary for the accurate simulation of the contaminant transport process in a deformable porous medium with thermal and chemical effects.

The above discussions indicate that the study of the contaminant transport in porous media usually needs to consider a set of completely coupled Partial Differential Equations (PDEs) governing the chemical migration, the mechanical behaviour of the porous skeleton, the moisture and gas movement, heat transfer and geochemical reactions. In order to obtain an accurate solution for such a coupled nonlinear transport problem by means of mathematical modelling, proper numerical schemes should be chosen for solving different PDEs. Due to the mathematical characteristic of the equations governing poroelastic behaviour of porous media and heat transfer, the conventional numerical method can be used to solve these equations without difficulty (Bathe, 1996; Lewis and Schrefler, 1998). Until now, many effective computational models have been developed for examining the poroelastic and THM behaviours of the unsaturated porous medium and some programming codes have been embedded into commercial software (ABAQUS, COSMOS, FEMLAB, FLAC, and PLAXIS, etc.). However, the conventional numerical methods encounter severe difficulty in modelling the linear transport equation with strong advection and the solution containing either high gradients or discontinuities; they introduce either numerical oscillations or artificial diffusion into the solution near its high gradients. Developing a high-order accurate stabilized numerical scheme for the advection or advection-dominated transport equation is an important topic in science and engineering, and it is an extremely important step in modelling the complex nonlinear coupled advection-dominated transport problem of a contaminant in a porous medium.

1.3 Numerical Difficulties for the Transport Equation

The classical advection-diffusion (or dispersion) equation is the basic form of many types of equations in solid and fluid mechanics, dynamics, heat transfer and water resources. Therefore its numerical modelling plays a very important role in science and engineering, for example, oil reservoir flow, transport of solutes in subsurface and surface water, the movement of aerosols and trace gases in the atmosphere. However, the presence of the first order spatial derivative (advective term) in the advection-diffusion equation usually causes great difficulty for the numerical modelling. The advection-diffusion equation can be classified as a mathematically hyperbolic-parabolic PDE. The dominance of either the hyperbolic or the parabolic character of the PDE depends on the magnitude of the *Péclet number* $\mathrm{Pe}\,(=\frac{vh}{2D}$, where v is the advective velocity or the characteristic speed of the equation, D is the diffusion coefficient, and h is the spatial discretization length). For the dominantly hyperbolic equation, conventional numerical schemes will encounter computational difficulties: higher-order methods, e.g. central method, second-order, Lax-Wendroff, Beam-Warming, etc., give rise to non-physical numerical oscillations near the leading edge of a sharp front in the solution, although they are less dissipative in the smooth regions of the solution. On the other hand, first-order methods, e.g. the upstream Lax-Friedrich schemes, can give oscillation-free solutions, but they usually posses a strong numerical diffusion that smears out the solution with a steep advective front, leading to inaccuracies. The above numerical phenomena can be demonstrated by the solutions for the one-dimensional linear steady and transient transport equations obtained from two basic finite difference methods, the *central method* and *backward upwind method*, expressed in terms of Péclet number and Fourier mode.

1.3.1 Péclet Number for the Steady Advection-Diffusion Equation

For the steady advection-diffusion equation, $vC_x - DC_{xx} = 0$, the numerical solutions given by the central and upwind finite difference schemes corresponding to the boundary conditions $C(0)=0$ and $C(1)=1$ applied on the domain $[0,l]$ can be written, respectively, in the following forms (Quarteroni and Valli, 1997)

$$\hat{C}_i^c = \frac{\left(\frac{1+\mathrm{Pe}}{1-\mathrm{Pe}}\right)^i - 1}{\left(\frac{1+\mathrm{Pe}}{1-\mathrm{Pe}}\right)^n - 1}, \quad i = 1, 2, \cdots, n-1 \tag{1.1a}$$

and

$$\hat{C}_i^u = \frac{(1+2\mathrm{Pe})^i - 1}{(1+2\mathrm{Pe})^n - 1}, \quad i = 1, 2, \cdots, n-1 \tag{1.1b}$$

where $\hat{C}_i^c$ and $\hat{C}_i^u$ are the numerical solutions at the node i given by the central and upwind schemes respectively. It is evident from equation (1.1) that $\hat{C}_i^c$ will exhibit an oscillatory behaviour since $\frac{1+\mathrm{Pe}}{1-\mathrm{Pe}} < 0$ when $\mathrm{Pe} > 1$ and such oscillations can be eliminated when $\mathrm{Pe} \leq 1$; in contrast, $\hat{C}_i^u$ does not possess oscillations for any value of the Péclet number. The one-sided upwind scheme has a strong physical meaning due to the fact that the flux by advection can only come from the upstream direction at any spatial point. However, using simple truncation error analysis, it can be shown that the upwind scheme introduces an artificial numerical diffusion to the central scheme for the advective term

$$v\frac{\hat{C}_{i+1} - \hat{C}_i}{h} = v\frac{\hat{C}_{i+1} - \hat{C}_{i-1}}{2h} - \frac{vh}{2}\frac{\hat{C}_{i+1} - 2\hat{C}_i + \hat{C}_{i-1}}{h^2} \tag{1.2}$$

The addition of artificial diffusion ensures that the corresponding artificial Péclet number is always smaller than unity, but it reduces the accuracy of the scheme. Therefore, the stability of the upwind scheme for the advection-dominated equation is obtained at the expense of accuracy, and this aspect can also be illustrated using a Fourier analysis.

1.3.2 Fourier Mode for the Transient Advection Equation

The exact solution of the transient purely advection equation, $C_t + vC_x = 0$, can be expressed as a sinusoidal function $C_\omega = \hat{C}_\omega(0)e^{i\omega(x-vt)}$. The sinusoidal solution of the transient advection equation with the central and upwind spatial discretizations on a regular grid can be written as (Vichnevetsky and Bowles, 1982)

$$C_{\omega,n} = \hat{C}_\omega(0)e^{i\omega\left(x_n - \frac{v\sin(\omega h)}{\omega h}t\right)} \tag{1.3a}$$

and

$$C_{\omega,n} = \hat{C}_\omega(0)e^{\frac{v}{h}[1-\cos(\omega h)]t} e^{i\omega\left(x_n - \frac{v\sin(\omega h)}{\omega h}t\right)} \tag{1.3b}$$

where ω is the spatial wave number, and $\hat{C}_\omega(0)$ is the Fourier transform of the initial condition of the dependent variable C. From sinusoidal solutions in (1.3), it is shown that the central finite difference scheme is conservative for the transient advection equation, i.e. the algorithmic amplitudes of the wave components in the solution remain constant. Therefore the central scheme is stable and consequently convergent based on the *Lax Equivalence theorem*, that the stability is necessary and sufficient to the convergence of a finite difference system of a well-posed linear Initial Boundary Value Problem (IBVP) or Initial Value Problem (IVP) if it is consistent with it. However, the phase velocities of high frequency wave components present in the sinusoidal solution of the central scheme are different from the characteristic speed v of the governing equation, and such a deviation in the traveling speeds will lead to an oscillatory wave train trailing or leading the "front" of the true solution. Although the upwind scheme has the same phase velocity distribution as the central difference scheme, the added artificial diffusion term resulting from the damping factor contained in the sinusoidal solution will smooth out the solution.

1.4 Development of Stabilized Numerical Methods

It is implied from (1.1) that the wiggles (or oscillations) in $\hat{C}^c$ can be avoided theoretically by adopting a mesh refinement such that $\mathrm{Pe} \le 1$. However, such a process can be costly in terms of the storage and the computation time associated with this type of mesh refinement, especially when the Péclet number is initially large. It is also impossible to implement a mesh refinement for the purely advection equation in which $D = 0$. From this point of view, an improvement in the numerical scheme being used should be considered instead. Development of an accurate computational model of the transport equation in the presence of a strong advective term, especially when the solution contains discontinuities or steep gradients, has been a challenge in computational fluid dynamics. Courant et al. (1952) introduced the upwind technique in the Finite

Difference Method (FDM) according to the characteristic direction determined by the coefficient of the advective term in the equation. Since then, many stabilized FDMs have been developed for the advection- (or convection) dominated problem, including the High-Order Upwind Scheme (Fromm, 1968), the Flux-Corrected Transport scheme (Boris and Book, 1973; Book et al., 1975, 1981), the Quadratic Upstream Interpolation method (QUICK) (Leonard,1979; Steffler, 1989) and the Total Variation Diminishing scheme (Harten, 1983). As the upwind scheme, the basic concept of these high-order stabilized FDMs is to add an artificial numerical diffusion to the high-order scheme for the advective term by means of either a flux limiter, a slope limiter or a total variation diminishing property, etc. (LeVeque, 1992; Morton, 1996), while maintaining the amount of such additional numerical diffusion “corrected”. Therefore, these stabilized computational schemes can be considered as combinations of high-order and first-order schemes; the weighting of the first-order scheme should be increased in the vicinity of the discontinuities or high gradients of the dependent variable while their weighting should be reduced elsewhere. This method is referred to as an “*optimal*” or “*smart*” upwind scheme (Figure 1.2). Purely finite difference approaches for the solution of the advection equation are relatively well established (Ganzha and Vorozhtsov, 1998). Although the smart upwind schemes provide much more stable solutions than conventional numerical scheme, particularly in treating the advective transport of discontinuous fronts, they are less well adapted to the treatment of three-dimensional problems with complex geometrical features. From this point of view, finite element methods have the

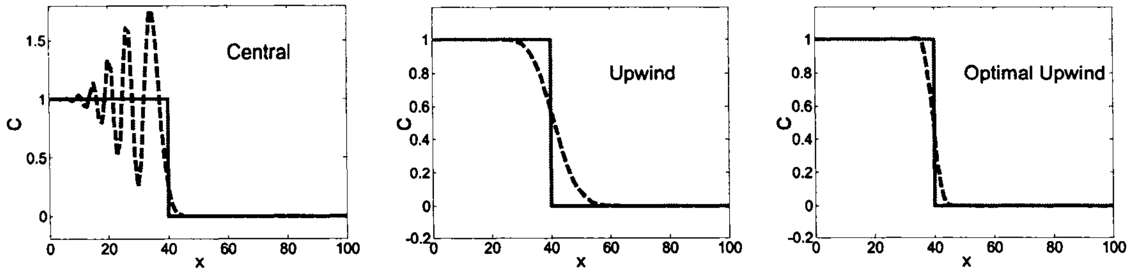

(a) (b) (c)

Figure 1.2 The demonstration of numerical simulations of the advection of a discontinuity obtained from (a) central scheme, (b) upwind scheme and (c) optimal upwind scheme convenience and flexibility in discretizing the physical domain of the problem with an unstructured mesh, and therefore they have been widely applied for the solution of engineering problems.

1.4.1 Classification

Finite element modelling of the advection equation has been the subject of extensive research over the past four decades and there is no universal agreement on the most judicious choice of a computational scheme that will yield reliable results for all situations. Among the Finite Element Methods (FEMs) for the advection-diffusion equation, there are two basic strategies to deal with the temporal and spatial terms of the governing equation. The first methodology is referred to as the *fully discrete* approximation, in which the governing PDE is discretized in the space-time domain $V \times [0,t^*]$ (where t^* is the time duration). The Space-Time Galerkin (ST-G) method is one such example (Varoglu and Liam Finn, 1982; Nguyen and Reynen, 1984; Oñate and Manzán, 1999). In the ST-G method, the integral form of the problem is discretized in the space-time slab $V^n = V^e \times I^n$ (where V^e is a elemental partition of V and $I^n = [t^n, t^{n+1}]$ is a time interval) by using the discontinuous Galerkin method, which weakly enforces the continuity of the unknown variable at the time interval I^n. The second methodology can be termed a *semi-discrete* approximation, in which the transient PDE is discretized spatially, first by a numerical method (e.g. the FDM, FEM, or Boundary Element Method (BEM)), and then transformed into a corresponding Ordinary Differential Equation (ODE), which is solved later using a time-integration scheme (e.g. Crank-Nicholson, Runge-Kutta methods etc.) (Zienkiewicz and Taylor, 2000). Fully discrete methods usually increase the dimension of the problem by one and hence introduce greater complexity to the computational procedure, especially for three-dimensional problems. From this point of view, the semi-discrete methods are more convenient and effective.

Numerical techniques used with the semi-discrete methods for solving the advection-diffusion equation can be classified into three types: *Eulerian*, *Lagrangian* and *Eulerian-Lagrangian* methods (Quarteroni and Valli, 1997). In Eulerian methods, the discretization in space is performed over a fixed spatial grid system, whereas in Lagrangian methods, such as the Method of Characteristics (MOC) (Garder et al., 1964; Douglas and Russell, 1982), the spatial discretization is performed either in a deforming grid or in the deforming coordinate in a fixed grid system. The MOC method can provide an efficient and accurate solution to the advective transport problem once the trajectory of the particle is determined, based on the theory of characteristics, which specifies that the material derivative of the unknown function along the characteristic curve is equal to zero. When the MOC techique is combined with the finite element method for the spatial discretization of the advective term, the consequent scheme is referred to as the Characteristic Galerkin method. However, the use of a moving grid in the Lagrangian method introduces further difficulties, such as mesh tangling, especially for inhomogeneous media with multiple sinks or sources and complex boundary conditions. From this viewpoint, the Eulerian method offers the advantage and convenience of a fixed grid or coordinate system.

Usually, most Eulerian methods work well with diffusion-dominated problems, but for advection-dominated transport problems, they either suffer from excessive numerical dispersion or give rise to non-physical oscillations as discussed in the previous section. The mixed Eulerian-Lagrangian methods (Neuman, 1981; 1984) attempt to combine the advantages of these two methodologies, in which the Operator Splitting techniques (Douglas and Rachfold, 1956; Yanenko, 1971; Marchuk, 1975; 1995; Khan and Liu, 1998a, b) are applied to the governing equation; the advective term is then solved using the Lagrangian approach, and the diffusive term, as well as the others, are solved using an Eulerian approach. Again, the accurate determination of the trajectory or the characteristic curve is a major challenge in the finite element modelling with elements of arbitrary shape. It should be noted that the contribution of the expansion of the unknown variable along the characteristic curve is equivalent to the addition of an artificial diffusion term to the governing equation, which leads to the same expression derived from the Taylor-Galerkin method (Zienkiewicz et al., 1985). A classification of the stabilized methods for the advection-diffusion equation is shown in Figure 1.3, and a brief summary table of selected stabilized methods is given in the Appendix. In the Eulerian finite element method, the conventional Galerkin discretization for the advective term in the governing advection-diffusion equation is equivalent to the central difference scheme; therefore, the conventional Galerkin method will introduce oscillations into the solution for the advective transport of a steep front. It can be noted from the discussions in the previous section that the Galerkin scheme for the advection equation can be stabilized by introducing the upwind scheme for the advective term in the governing equation. Based on this concept, there have been many so-called *Stabilized Eulerian Finite Element Methods* developed to date (Oñate, 1998; Codina, 1998).

In the late of 1970s, the upwind scheme was introduced into the finite element methods by using an asymmetric weighting function (Christie et al., 1976; Heinrich et al., 1977; Hughes, 1978; Griffiths and Mithchell, 1979; Heinrich and Zienkiewicz, 1979; Heinrich, 1980). In order to distinguish them from the conventional Galerkin method, such upwind finite element methods are referred to as a Petrov Galerkin scheme, in which the weighting function is different from the interpolating function. In this asymmetric weighting function, a perturbation in the form of the gradient of the weighting function is

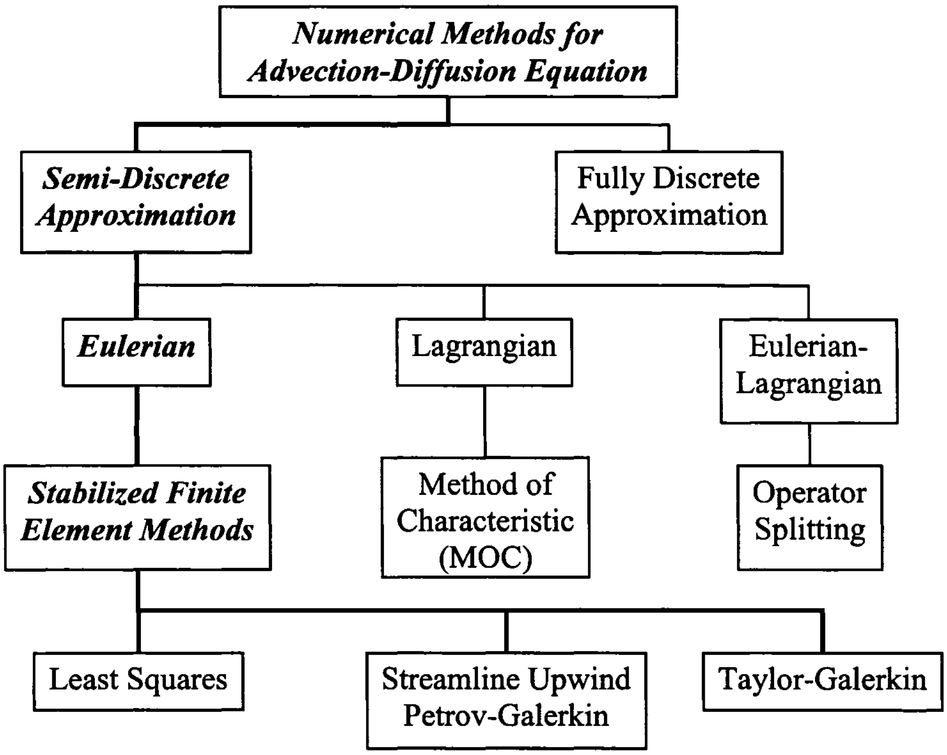

Figure 1.3 Stabilized methods for the advection-diffusion equation

introduced into the traditional Galerkin weighting function to take the upwind effect. The addition of such a perturbation is equivalent to the addition of an artificial diffusion to the advection-diffusion equation in the steady state condition. For multi-dimensional problems, the perturbation should also be added along the flow direction to avoid the crosswind diffusion (Hughes and Brooks, 1979; 1982). Using such a concept, Hughes and Brooks (1982) proposed a so-called Streamline Upwind Petrov Galerkin (SUPG) method, which is considered a milestone in the development of stabilized finite element methods for the advection equation. The importance of the SUPG scheme rests on the fact that the common form of the perturbation is given, which can be expressed as the scalar term $\tau \mathbf{v} \cdot \nabla w$, where $\mathbf{v}$ is the characteristic velocity vector, w is the weighting function, ∇ is the gradient and τ is the upwind parameter. The upwind parameter τ is also called the intrinsic time of the stabilized methods (Oñate et al., 1997) since it has a unit of time, and the different forms of τ can lead to different stabilized methods (Codina, 1998).

The perturbation added in the asymmetric weighting function will not only introduce an "artificial diffusion" term but also an "artificial convection" term in the discrete difference form of the advection equation, and both terms will influence the numerical behaviour of the corresponding stabilized finite element schemes. The perturbation parameter, τ, can be chosen such that the artificial convection term has the adjoint form of the convection (or advection) term of the equation and, consequently, the numerical scheme becomes symmetric (Wendland and Schmid, 2000), such as in the Least Squares method (Carey and Jiang, 1987a, b; 1988; Jiang, 1998). Here, the residual integral form of the equation is created by applying a variation on the integral square residual functional of the advection-diffusion equation, and τ is related to the time step Δt and flow velocity $\mathbf{v}$. On the other hand, τ can be chosen based on a Fourier analysis to ensure that numerical modelling can give an "optimal" solution of the transient advection-diffusion equation (Raymond and Garder, 1976; Kelly et al., 1980), such as in the SUPG method (Hughes and Brooks, 1982; Hughes and Mallet, 1986a) in which τ is related to the characteristic length of the element. The perturbation parameter can also take different values to generate different stabilized methods, such as the Talylor-Galerkin method corresponding to the Lax-Wendroff finite difference scheme (Lax and

Wendroff, 1960), in which the Taylor series expansion in time of the unknown variables is substituted into the original PDE to obtain the second-order or the third-order correction in time (Donea, 1984; Donea et al., 1984; 1987), where τ is defined with different formations for the temporal and spatial terms of the equation.

1.4.2 Theoretical Basis of Stabilized Methods

Using stabilized finite element methods for advection-dominated problems has existed for almost 30 years. The theoretical basis of stabilized methods was not investigated until the concepts of the *Bubble function* and the *variational multiscale model* were introduced in 1990s (Brezzi et al., 1992; Hughes, 1995). The mathematical basis relies on the physical explanation of the Péclet number. The Péclet number, which is interpreted as the Reynolds number for the fluid dynamics problem, can be considered as the ratio of the advective flux and the diffusive flux in a computational element. Originally, it reflects the relationship between the domain length and the mass diffusion length, $L_D = \sqrt{Dt_r}$, where $t_r = L/v$ is the residence time in the domain. Therefore, using the following derivations, it can be seen that the Péclet number reflects the ratio of the *system length* and the *mass diffusion length* (Figure 1.4(a))

$$\mathrm{Pe} = \frac{1}{2}\left(\frac{L}{L_D}\right)^2 = \frac{L^2}{2Dt_r} = \frac{L^2}{2DL/v} = \frac{vL}{2D} \tag{1.4}$$

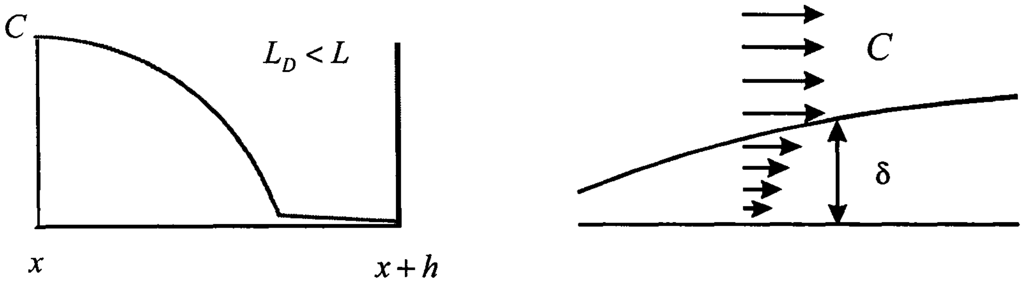

(a) (b)

Figure 1.4 The demonstration of (a) the mass diffusion length and (b) the boundary layer of the mass transport problem

Here, similarly to the boundary layer theory in fluid dynamics, there is also a boundary layer near the boundary plane encountered in a boundary value problem (Figure 1.4(b)).

Therefore, if $L_D >> L$ (i.e. $\mathrm{Pe} << 1$), the diffusion process is dominant over the element, and consequently the variation in the dependent variable C is smoothly varying from the upstream boundary to the downstream boundary of the element, without sudden change in amplitude (e.g. high gradient). If $L_D << L$ (i.e. $\mathrm{Pe} >> 1$), and condition on the upstream and downstream boundaries change rapidly, the dependent variable C will vary drastically in the element. It should be noted that even with $\mathrm{Pe} >> 1$, but if the boundary conditions change gradually, then the dependent variable C will vary smoothly over the element as in the first case. Since the diffusion length L_D is related to the residence time t_r, which is inversely proportional to the flow velocity v, then the greater the flow velocity, the thinner will be the diffusion boundary layer. For the advection-dominated transport problem with a high gradient in the dependent variable, the magnitude of the flow velocity is much higher with respect to the diffusivity coefficient and the diffusion length will be reduced within the domain. Therefore, in order to make the dependent variable vary "smoothly" within an element, the element length should be kept smaller than the diffusion length in the locations of high gradients or discontinuities of the dependent variable. For this case, more discretization elements would be necessary to ensure that there is at least one element within the boundary layer where the diffusive process will dominate (i.e. the mesh should be refined in the vicinity of the steep front of the solution).

The need for the mesh refinement at the steep front of the solution can be illustrated by the Fourier analysis in the frequency domain. It should be noted from the above discussions that if the dependent variable varies drastically over the element, where the elemental length is much longer than the diffusion length (i.e. $\mathrm{Pe} >> 1$), the overall behaviour of the unknown variable over the element can be considered discontinuous from the viewpoint of the discretization. This discontinuity is equivalent to the step wave (in the continuity sense). In the frequency domain, the step wave is composed of wave components of different frequencies and should include high frequency wave components (see Figure 1.5). In the conventional finite element space, a polynomial is used to construct the shape function and to interpolate the unknown variable over the computational domain. Such polynomial space can interpret low frequency wave components involved in the solution, which can be referred to as the *large scales* of the solution. The polynomial space is, however, inadequate for the high frequency wave components involved in a solution containing a discontinuity, which can be considered as the *fine scales* of the solution. Therefore, the polynomial finite element space with a coarse mesh cannot interpolate the fine scales (or high frequency wave components) included in the solution, and the mesh should be further refined to take into consideration the fine scale effects. As mentioned previously, such mesh refinement cannot guarantee that the polynomial finite element space will approach the solution space for the advection of a discontinuity (without diffusion), and recourse must be made for the advective transport of a discontinuity by the improvement of the finite element space.

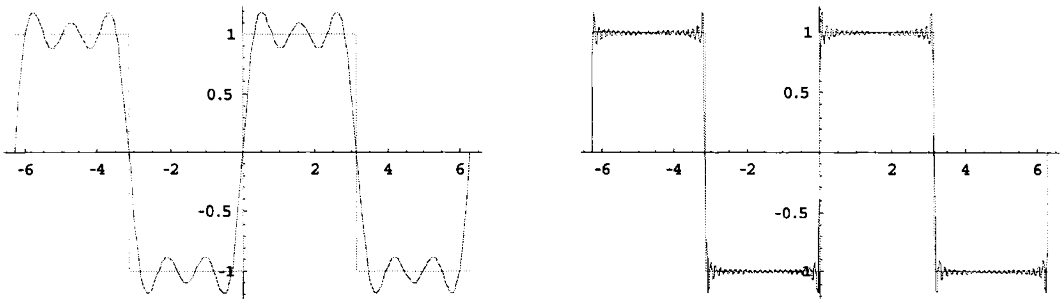

(a) (b)

Figure 1.5 A step wave and its Fourier series expansion with (a) 10 terms and (b) 50 terms

Since the normal low-order polynomial space cannot interpolate the discontinuities contained in the solution, the standard finite element space should be augmented by a high-order function space. The space of *bubble functions* is one choice that takes into consideration such fine scale effects included in the solution. The bubble functions are typically high-order polynomial functions which vanish on the elemental boundaries (Hughes, 1995), and they can be especially constructed via the solution of an element-level homogeneous Dirichlet boundary value problem (Franca and Macedo, 1998; Franca et al., 1998; Franca and Hwang, 2002), in which case they are referred to as the *residual-*

free bubbles (Brezzi et al., 1992; Brezzi and Russo, 1994; Franca and Farhat, 1995; Brezzi et al., 1997; 1998a, b). Another approach is to consider the effect of the unresolvable fine scales of the solution (or *subgrid scales*) on its resolvable coarse scales in the normal polynomial space by means of the elemental Green's function. This is the basic concept underlying the *variational multiscale model* (Hughes, 1995). Brezzi et al. (1997) showed the equivalence of the residual-free bubbles approach and the variational multiscale model for the advection-dominated transport problem. Both approaches add a stabilization term to the weighted residual integral form of the advection-diffusion equation (Codina, 1998). A detailed discussion about residual-free bubbles, the variational multiscale model and stabilized methods will be given in Chapter 2 and their inter-relationships are shown in Figure 1.6.

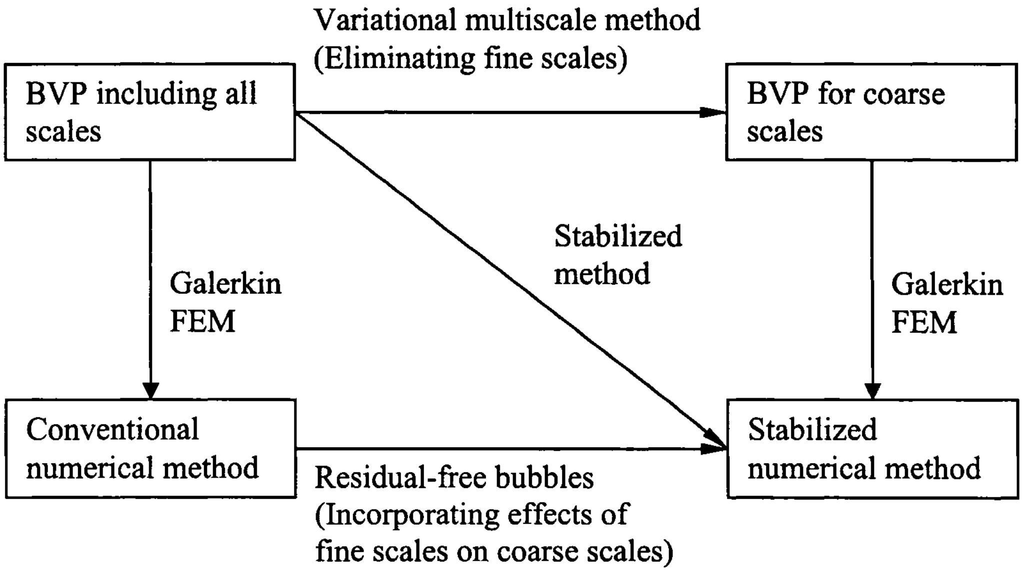

Figure 1.6 The relationship between residual-free bubbles, variational multiscale model and stabilized methods for the advection-diffusion equation (Following Brezzi et al., 1997)

1.5 Fourier Analysis of Stabilized Methods

Two mathematical analyses can be performed to evaluate and assess the numerical schemes developed for the solution of the advection-diffusion equation. Error analysis can provide insight into the error bounds of numerical schemes caused by the numerical truncation, and many stabilized methods can be derived from such error analysis (LeVeque, 1992; Morton, 1996; Wang and Hutter, 2001 and the references therein). Fourier analysis, on the other hand, can provide insight into the numerical properties of numerical schemes in the frequency domain, based on the fact that a step wave is composed of wave components of different frequencies and their amplitudes and phase velocities can be altered by the numerical scheme. If the numerical modelling is required to generate an accurate solution for the advective transport of a step wave, all the wave components involved in modelling such a step wave, should travel at the same speed without shape distortion. Because of this fact, Fourier analysis becomes one of the powerful methodologies for the investigation of the numerical behaviour of the computational methods for the advection-diffusion equation (Morton, 1980; Pereira and Pereira, 2001). Raymond and Garder (1976) conducted a Fourier analysis on the spatial discretization of the Petrov-Galerkin method for the advection equation to determine the optimum value of the upwind function of the scheme. Yu and Heinrich (1986) investigated the stability of the space-time Petrov-Galerkin method by means of the amplitude ratio (see also Richtmeyer and Morton, 1967). Sharkib and Hughes (1991) presented the Fourier stability and accuracy analysis of the space-time Galerkin/least-squares method applied to the time-dependent advection-diffusion transport problem. Tezduyar and Ganjoo (1986) used the algorithmic damping ratio (ADR) and algorithmic frequency ratio (AFR) procedures to develop and test the weighting functions, which were used in an improved Petrov-Galerkin method. Codina (1993a) used ADR and AFR to examine the stability of the forward Euler scheme in the SUPG method for the convection-diffusion equation. Cardle (1995) used a similar idea to determine the temporal weighting function that differs from the spatial weighting function in the Petrov-Galerkin method. All these investigations suggest that a Fourier analysis can be used to gain insight into the numerical behaviour of the stabilized numerical methods for the advection-dominated transport problem.

Most Fourier analyses in the literature have focused on the spatial discretization of the advection-diffusion equation. However, the temporal discretization of the governing equation also has an influence on the numerical behaviour of the schemes. For example, as shown in the section 1.3, the upwind method satisfies the von-Neumann stabilization condition for the steady advection equation (i.e. the amplitude of the sinusoidal solution is no greater than unity). For the transient advection equation, however, with the application of an explicit Euler time integration scheme, such stability is conditional and the Courant-Friedrichs-Lewy (CFL) condition should be satisfied (i.e. the Courant number $Cr = \frac{u\Delta t}{h} \leq 1$). The CFL condition represents a strong physical meaning in relation to the characteristics theory, wherein the *dependence domain of the numerical scheme* should include the *domain of the associated governing partial differential equation* (Figure 1.7). Otherwise, certain initial conditions determining the solution of the equation will not be included in the numerical model, leading to a diverging numerical solution of the equation.

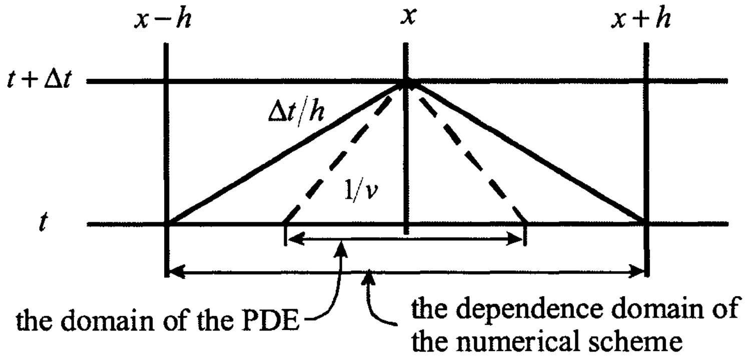

Figure 1.7 The dependence domain of the numerical scheme and the domain of the equation

Thus, the numerical performance of the computational method for the transport problem depends not only on spatial discretization but also on the time integration scheme of the governing equation. It should be noted that, besides the temporal and spatial discretizations, the overall behaviour of the stabilized numerical method for the advection-dominated transport problem is also influenced by the forms of the artificial diffusion and the artificial convection terms introduced by the stabilized scheme. Therefore, in order to assess the overall numerical performance of the stabilized numerical methods for the advection-dominated transport problem, all these factors should be included in the Fourier analysis. Based on the results of such a Fourier analysis, the conditions under which the stabilized numerical scheme can give an optimal solution for the advective transport problem, can be ascertained. Such Fourier analysis can also be used to develop a new numerical scheme that can give an *accurate* solution for the advection-dominated transport problem in porous media.

1.6 Rationale of Experimental Modelling

A mathematical model of a contaminant transport problem usually consists of three components: the model definition, the model parameters and the model approximation. The model definition describes basic processes involved in the transport problem, usually in terms of the mathematical equation as well as constraints such as initial and boundary conditions. The model parameters include the physical parameters governing the transport process, such as hydraulic conductivity, diffusivity and reaction rate or even the mechanical properties of the porous medium. The model approximation refers to the solution of the mathematical model for the prediction of the contaminant transport process with transport parameters and conditions. Two approaches, the analytical and the numerical, can be used for the model approximation, but generally only the numerical method can be used to solve complex coupling transport models. The quality of the mathematical model of the transport problem depends on the errors introduced by its three components. The error may already be embedded in the transport model when the model is created. This model definition error may result from the assumptions made by the modeller (e.g. small deformation of porous skeleton, local equilibrium of chemical reaction etc.), or from a lack of knowledge of the transport problem (e.g. constitutive stress-strain relationship of unsaturated soil, thermal and/or chemical induced alterations of the hydraulic and mechanical properties of the porous medium, and chemical reaction kinetics etc.). Such definition errors can be reduced by obtaining more knowledge about the contaminant and the porous medium.

The quality of the mathematical model cannot be improved if the model parameters are not well defined. Ill-defined model parameters result in errors in the mathematical model, and therefore the identification of the model parameters is an important aspect of any mathematical modelling process. The prediction process of unknown system states (e.g.

contaminant concentration) of the transport problem is referred to as the *forward problem*, while the determination of the transport parameters is referred to as the *inverse problem*, in which the parameters are taken as dependent variables and determined by fitting the observed system states (from laboratory experiments or field measurements). Besides the model definition and the model parameters, the model approximation may also introduce errors into the mathematical modelling of the contaminant transport problem in porous media, particularly for the advection-dominated transport problem due to the numerical difficulties discussed previously. The model approximation error may influence not only the accuracy of the model but also the identification of the transport parameters. Therefore, it is important to develop an accurate stabilized numerical scheme for the advection-dominated transport problem and validate it with experimental modelling, which should include the dominant transport characteristics associated with the numerical modelling. The results of the experimental modelling can also be used for the inverse problem of the mathematical modelling of the transport problem, to identify certain physical parameters that can be considered for the calibration procedures of the mathematical model. In this respect, this thesis will also study the experimental modelling of the advection-dominated transport processes in the porous medium.

1.7. Objectives and Scopes of the Research

The objective of this thesis is to develop accurate computational modelling of advection-dominated transport problems related to fluid saturated porous media. Such development is based on the assessment of the stabilized semi-discrete Eulerian FEMs proposed for the advection-dominated transport problem by means of a Fourier analysis. The result from the Fourier analysis can be used to derive the criterion for the optimal performance of the stabilized FEMs for the advection equation. Based on this criterion, not only a time-adaptive scheme can be developed for the accurate solution of one-dimensional advection-dominated transport problem, but also a mesh-refining adaptive scheme can be developed for optimal solution of multi-dimensional advective transport problems. As a complementary aspect of the mathematical modelling, an inverse analysis of transport problem is conducted in the study of an experimental modelling, which is set up for the validation of the proposed time-adaptive scheme. In this experimental modelling, a colour visualization-based image processing method will be developed to determine the transport process of a chemical solution on the cylindrical surface of a porous column in a non-invasive and quantitative way. Finally, the thesis will present a study on the time-adaptive mathematical modelling of the advection-dominated transport problem coupled with the Hydro-Mechanical-Chemical (HMC) processes involved in the porous medium. The thesis research work addresses the following aspects:

(i) Assessment of the stabilized semi-discrete Eulerian finite element methods, and derivation of the conditions for these methods to have optimum numerical performances for the advection equation, using a Fourier analysis conducted on both temporal and spatial discretizations of the governing transport equation.

(ii) Development of a time-adaptive scheme on the basis of Courant number criterion derived from the Fourier analysis, which can generate an oscillation-free and non-diffusive numerical solution for the advection-dominated transport problem with time- and space-dependent flow velocity.

(iii) Development of a colour visualization-based image processing method, which can used in the experimental modelling to determinate the advection-dominated transport processes of a chemical dye solution in an idealized porous column in a quantitative, economical and non-invasive way.

(iv) Identification of the hydrodynamic dispersion coefficient of the transport process in the porous column, which can be used in the validation procedure of the proposed time-adaptive scheme with the experimental results.

(v) Development of a mesh-adaptive scheme for modelling the linear and nonlinear three-dimensional axisymmetric advective transport in the porous medium, with time- and space-dependent flow fields due to the pore fluid pressure transients described by the piezo-conduction equation.

(vi) Development of a computational model for the advection-dominated contaminant transport problem coupled with Hydro-Mechanical-Chemical processes in the porous medium.

CHAPTER 2

COMPUTATIONAL MODELLING OF THE ADVECTIVE-DISPERSIVE TRANSPORT

In the first chapter, it was shown that although the contaminant transport in porous media can be described by the classical advection-diffusion equation, it is a complex nonlinear coupling process involving mechanics, hydraulics, heat transfer and geochemical reactions. For such coupled transport processes, it is necessary to use numerical modelling for the prediction of the migration of the contaminant in porous media. However, as mentioned in the previous chapter, the numerical model encounters major difficulties in simulating the first-order spatial derivative (or the advective term) in the classical linear advection-diffusion equation; the conventional numerical schemes introduce either non-physical oscillations or artificial diffusion into the solution, influencing the reliability and accuracy of the computational modelling. In order to overcome these numerical difficulties, many so-called stabilized computational schemes have been developed for the solution of the advection equation. The investigation of the numerical behaviour of stabilized schemes and the development of a higher-order accurate scheme for the advection-dominated transport problem is a necessary and important step in developing the complete coupling modelling of the nonlinear contaminant transport in porous media. In this chapter, the fundamental basis and structure of the stabilized finite element methods for the advection equation will be reviewed. Firstly, however, the basic Partial Differential Equation (PDE) governing the processes involved in a single component, the isothermal transport process of the contaminant in fully saturated homogenous porous media with small volume changes, which is the main objective throughout the thesis, will be described. A detailed derivation of the governing equations of the transport processes coupled with the elastic deformation of the porous medium will be given in Chapter 7.

2.1 Governing Equations

The basic equation governing the advective-dispersive transport of the contaminant through a non-deformable porous medium can be derived from the consideration of mass balance (Philips, 1991; Charbeneau, 2000; Selvadurai, 2000a,b). For the advective-dispersive transport of a contaminant through a control volume V, the conservation law requires the fluxes through the control volume to be equal to the accumulation of the contaminant in the void space of the control volume, i.e.

$$\sum Fluxes = \int_V n^* \frac{\partial C}{\partial t} \mathrm{d}V + \int_V \rho_b \frac{\partial C_s}{\partial t} \mathrm{d}V \tag{2.1}$$

where $C(\mathbf{x},t)$ is the concentration of dissolved contaminant per unit volume of the fluid contained in the pore space of the porous region V; $C_s(\mathbf{x},t)$ is the sorbed mass of contaminant per dry unit weight of solid skeleton (*mg/kg*) due to chemical reactions; $\mathbf{x}$ is a position vector; t is time; ρ_b is the bulk density of the solid phase (*kg/L*); n^* is the porosity of the porous medium, which is defined as the ratio of the volume of the voids V_v to that of the total volume of V. For a homogeneous non-deforming medium, the porosity can be assumed to be a constant. The first integral term in the Right Hand Side (RHS) of (2.1) represents the change rate of the contaminant in the void space of the control volume, the second integral term in the RHS of (2.1) represents the production or loss of the chemical species due to the sorption, chemical reaction, biological transformation and radioactive decay, which can act as a source-sink term. For the advective-dispersive transport process, the fluxes in (2.1) should include advective and dispersive fluxes through the surface S of the control volume V, i.e.

$$\sum Fluxes = -\oint_S (\mathbf{v} n^* C - n^* D \nabla C) \cdot \mathbf{n} \mathrm{d}S \tag{2.2}$$

where $\mathbf{v}$ is the flow velocity vector, D is the coefficient of hydrodynamic dispersion, which should include the molecular diffusion and the mechanical dispersion in the porous space, and $\mathbf{n}$ is the normal direction outward to the surface S. Using the Green's theorem and the Dubois-Reymond Lemma (see Selvadurai, 2002a), the advection-dispersion equation can be derived from (2.1) and (2.2) as

$$\frac{\partial C}{\partial t}+\frac{\rho_b}{n^*}\frac{\partial C_s}{\partial t}+\nabla\cdot(\mathbf{v}C)-\nabla\cdot(D\nabla C)=0 \tag{2.3}$$

The essential (Dirichlet), natural (Neumann) boundary conditions and the initial conditions for the transport problem through the control volume V are described as

$$C(\mathbf{x},t)=\widetilde{C}(\mathbf{x},t) \qquad \mathbf{x}\in S_{\mathrm{D}}, t\in[0,t^*] \tag{2.4a}$$

$$\mathbf{n}^{\mathrm{T}}\mathbf{v}C-\mathbf{n}^{\mathrm{T}}D\nabla C=\overline{q}_n \qquad \mathbf{x}\in S_{\mathrm{N}}, t\in[0,t^*] \tag{2.4b}$$

$$C(\mathbf{x},0)=C_0(\mathbf{x}) \qquad \mathbf{x}\in V \tag{2.4c}$$

$$C_s(\mathbf{x},0)=C_{s0}(\mathbf{x}) \qquad \mathbf{x}\in V \tag{2.4d}$$

where t^* is the total time duration and the control volume V is bounded by the surface $S=S_{\mathrm{D}}\cup S_{\mathrm{N}}$ with $S_{\mathrm{D}}\cap S_{\mathrm{N}}=0$. In general, for the groundwater movement in the porous medium, the flow velocities are determined by excess pore pressure $p(\mathbf{x},t)$ based on Darcy's law, i.e.

$$\mathbf{v}=\frac{\mathbf{v}'}{n^*}=-\frac{k}{n^*\gamma_w}\nabla p \tag{2.5}$$

where k is the hydraulic conductivity of the porous medium and γ_w is the unity weight of pore water. With compressible fluids and deformable porous media, the dissipation of excess pore pressure is influenced by the compressibilities of pore fluids and porous skeleton and therefore should be determined by either poroelasticity or poroplasticity (Biot, 1941; 1956; Selvadurai, 1996; Lewis and Schrefler, 1998). For the theory of poroelasticity (Biot, 1941; 1956), a set of partial differential equations describing the coupled elastic behaviour of saturated porous media and the dissipation of the excess pore pressure can be written as follows:

$$G\nabla^2\mathbf{u}+\frac{G}{1-2\nu}\nabla(\nabla\cdot\mathbf{u})-\alpha\nabla p=0 \tag{2.6}$$

$$\frac{k}{\gamma_w}\nabla^2 p=\frac{\partial}{\partial t}(\nabla\cdot\mathbf{u})+\frac{n^*}{K_f}\frac{\partial p}{\partial t} \tag{2.7}$$

where $\mathbf{u}=\{u_x,u_y,u_z\}^{\mathrm{T}}$ is the deformation vector of the soil skeleton; $G(=E/2(1+\nu))$ is the shear modulus; E and ν are, respectively, the elastic modulus and the Poisson ratio;

K_f is the bulk modulus of pore water; and α is the poroelastic parameter introduced by Biot and Willis (1957) to reflect the compressibility of pore fluid. For small volume changes of the porous medium, a suitable simplification for determining the dissipation of the excess pore pressure can be considered using the *piezo-conduction* or *elastic drive equation* (see e.g. Barenblatt et at., 1990; Selvadurai, 2000a, b; 2002a), which takes the following form for an isotropic porous medium with isotropic hydraulic conductivity characteristics

$$\frac{k}{\gamma_w}\nabla^2 p = (n^* \kappa_f + \kappa_s)\frac{\partial p}{\partial t} \tag{2.8}$$

where κ_f is the compressibility of the pore fluid and κ_s is the compressibility of the porous fabric. Furthermore, when the fluid is incompressible (i.e. $\nabla \cdot \mathrm{v} = 0$), the distribution of the excess pore pressure is governed by Laplace's equation, i.e.

$$\nabla \cdot (\frac{k}{\gamma_w}\nabla p) = 0 \tag{2.9}$$

The mechanism of the geochemical reactions between the species can be described by the kinetic rate laws via a set of ordinary differential equations for each species (Lichtner et al., 1996). For a single component geochemical system, this kinetic model for the reaction can be written as a general ordinary differential equation

$$\frac{\mathrm{d}C_s}{\mathrm{d}t} = \lambda_1(\lambda_2 C - \lambda_3 C_s) \tag{2.10}$$

where λ_i ($i = 1,2,3$) are reaction constants. If the local equilibrium condition is achieved very quickly in comparison with the variation of the concentration, then the mass transfer between the dissolved phase C and solid phase C_s of the contaminant during the chemical reaction can be described by the algebraic equations. For this case, $\lambda_1 \to \infty$, and the *isotherm*, which is the graphical relationship determined by laboratory experiments of the mass sorbed per unit mass of dry solids (C_s) and the concentration of the contaminant (C), can be used to determine λ_2 and λ_3. Two isotherms, namely the Langmuir and the Freundlich, are used widely (Bedient, 1999) and have the following forms

$$C_s = \frac{\alpha' \beta' C}{1+\alpha' C} \tag{2.11a}$$

$$C_s = K_d C^{1/N} \tag{2.11b}$$

where α' is an absorption constant related to the binding energy (*L/mg*), β' is the maximum amount of the solute that can be absorbed by the solid (*mg/kg*), N>0 is the Freundlich exponent, K_d is the Freundlich adsorption constant (Bedient, 1999). In this thesis, only the Langmuir isotherm sorption is used for representing the mass transfer between the liquid and solid phases of the contaminant in the nonlinear computations. The differential form (2.10) can be used for expressing the first-order irreversible reaction such as decay, attenuation and degradation, and in this type of reaction, $\lambda_1 = 1$, $\lambda_3 = 0$ and λ_2 is the reaction rate.

Generally, the study of the reactive transport problem in an elastically deformable and fully saturated porous medium should involve the advective-dispersive-reactive process governed by (2.3), pore pressure dissipation determined by poroelasticity, i.e. (2.6) and (2.7), and geochemical reaction described by kinetic model, i.e. by (2.9). For the small volume change of the porous medium, which is mainly considered in the thesis, the dissipation of the pore pressure can be plausibly determined using the piezo-conduction equation (2.8). For this case, the system of PDEs (2.3), (2.5), (2.8) and (2.10) are either linear and *weakly coupled* (i.e. the dissipation of the excess pore pressure can be solved independently of the transport problem), or nonlinear and *fully coupled* (i.e. the dissipation of the excess pore pressure is influenced by the chemical reaction). These PDEs can be classified as hyperbolic-parabolic for $C(\mathbf{x},t)$ (e.g. (2.3)), and either parabolic (e.g. (2.8)) or elliptic (e.g. (2.9)) for $p(\mathbf{x},t)$, depending upon the compressibility characteristics of the pore fluid and the porous skeleton.

2.2 Stabilized Computational Modelling

2.2.1 The Numerical Modelling

The basic concept underlying the numerical modelling of an Initial Boundary Value

Problem (IBVP), described by a set of Partial Differential Equations (PDE) and constraints (initial and boundary conditions etc.) applicable to a physical domain (finite or infinite), is that the domain is discretized by a set of the nodes, and the unknown field variables describing the physical phenomena are expressed by means of the interpolation function of their nodal values. Therefore, the infinite dimensional space of the solution of PDEs is approximated by a finite dimensional space containing computational nodal values. The objective of the numerical modelling is to seek the approximate nodal values of unknown variables by discretizing governing PDEs at the computational nodes. The nodal values of the unknown variable are determined by discrete difference equations which can be generally obtained from the weighted residual integral form of governing PDEs.

With the following definition of the advection-dispersion operator

$$L_t(C) = \frac{\partial C}{\partial t} + \nabla \cdot (\mathrm{v}C) - \nabla \cdot (D\nabla C) \tag{2.12}$$

and the denotation of $f = -\frac{\rho_b}{n^*}\frac{\partial C_s}{\partial t}$, the advection-dispersion equation (2.3) can be written in the following abbreviated form

$$L_t(C) = f \tag{2.13}$$

The general weighted residual integral form for the governing equation (2.13) with the initial and boundary conditions defined in (2.4) can be written as

$$\int_V w(L_t(C) - f)\mathrm{d}V = 0 \tag{2.14}$$

where w is a suitable weighting function. Usually the integral in (2.14) is calculated over a computational domain, which is decomposed into a union of subdomains. Different forms of the weighting function can lead to different numerical methods that result from the basic integral form (2.14).

In the Finite Element Method (FEM), the polynomial interpolation function is used as the weighting function, and therefore the finite element solution of (2.14) represents the orthogonal projection of the true solution of the problem into the finite element space

(Zienkiewicz and Taylor, 2000). When the weighting function is taken as unity, the integral (2.14) represents the mass balance over the element (or volume) and it leads to the Finite Volume Method (FVM) (Morton, 1996; LeVeque, 2002). By taking the weighting function as the Dirac delta function, the integral form (2.14) implies that the governing PDE (2.3) is satisfied at points, and thus leads to the Collocation method (Quarteroni and Valli, 1997). Replacing the differential derivatives with deference derivatives on the regular grid in the Collocation method leads to the Finite Difference Method (FDM). By defining the weighting function as the Fundamental solution of (2.13) and applying Green's theorem, the domain integral form (2.14) can be transformed into the Boundary Integral Equation, which is the basis of the Boundary Element Method (BEM) (Brebbia et al., 1984; Brebbia and Dominguez, 1992; Partridge et al., 1992). With the boundary integral equation, the BEM can be used for the modelling of the advective dispersive transport problem in a region of infinite extent (Zienkiewicz et al., 1977; Okamoto,1988; Okamoto and Kawahara, 1991; Bokota and Iskierka, 1995; Young et al., 2000; Driessen and Dohner, 2001). The primary difficulty associated with applying the BEM to the solution of the advection-dispersion equation is that it is usually difficult to obtain the fundamental solution for the transport problem.

The domain integration is usually required in numerical modelling to obtain algebraic equations for the nodal values of unknown variables of the system. This domain integration can be easily calculated over the predefined mesh, which provides the connectivity of nodes, via either an analytical formulation or quadrature rule. However, the mesh generation or mesh regeneration is generally a difficult task during the computation, especially for three-dimensional problems. Recently, a great deal of attention has been focused on meshfree (Liu, 2003; Atluri, 2004) or meshless particle approximations of the domain integration, in which the integral form in (2.14) is calculated over the local cell (or support domain) rather than the global mesh. Many methodologies have been developed based on such concepts, such as the Element Free Method (Belytschko et al., 1994), Moving Least Squares, Meshless Petrov-Galerkin (Atluri and Zhu, 1998; Lin and Atluri, 2000; Atluri et al., 2004), Smoothed Hydrodynamic Particle method (Liu et al., 1995), etc (see also Liu, 2003; Li and Liu, 2004; and references therein). The main advantage of meshfree methods is that they avoid the difficulties associated with the mesh generation and mesh regeneration especially for three-dimensional problems. However, there are difficulties in obtaining the exact (to machine accuracy) numerical integration of (2.11) in meshfree methods (Atluri et al., 1999; Liu and Yan, 1999).

2.2.2 The Galerkin Method

For the finite element solution of (2.13), the computational domain needs to be discretized with elements of arbitrary shape (such as two-dimensional triangles, quadrilaterals and three-dimensional bricks, trihedral elements, etc.) and the dependent field variable is represented with the shape function for each element. Denoting V^h and W^h as the spaces of the trial solution and the weighting function, respectively, i.e.

$$V_h = \{\hat{C} \mid \hat{C} \in H^1(V), \hat{C}(\mathbf{x},\cdot) = \tilde{C}(\mathbf{x},\cdot)\,\mathrm{on}\, S_\mathrm{D}\} \tag{2.15a}$$

$$W_h = \{w \mid w \in H^1(V), w(\mathbf{x}) = 0\,\mathrm{on}\, S_\mathrm{D}\} \tag{2.15b}$$

the variational form of the finite element approximation of the advection-dispersion equation (2.13) can be written as follows:

$$\text{Find } \hat{C} \in V_h \text{ such that } a(\hat{C},w) + (\mathbf{v}\hat{C},w)_{S_D} = (f,w) + (\tilde{q}_n,w)_{S_D} \text{ for } \forall w \in W_h \tag{2.16}$$

where $\hat{C}$ is the finite element solution of (2.13); $a(C,w) = (L_t(C),w)$ is a bilinear mapping from $V \times V$ to R corresponding to the differential operator $L_t(C)$, defined as the inner product on V, i.e.

$$a(C,w) = (L_t(C),w) = \int_V (\frac{\partial C}{\partial t} w + \nabla \cdot (\mathbf{v}C)w - \nabla w \cdot (D\nabla C))\mathrm{d}V \tag{2.17}$$

The equation in (2.16) is obtained by applying Green's theorem and is usually called the *weak form* of (2.13). If $V_h \equiv W_h$, then the variational form (2.16) is called *Galerkin* method. Usually $V_h \subset V$ is defined as the finite space of continuous polynomial functions with a prescribed degree, which are defined on each non-overlapping subdomain $K \in T_h$, and $T_h = \{K\}$ is a partition of the domain V. Therefore, for the advection-dispersion equation (2.13) with only the Dirichlet boundary condition, the weak form of the semi-discrete Galerkin method can be written as

$$\text{Find } \hat{C} \in V_h \text{ such that } a(\hat{C}, w) = (f, w) \text{ for } \forall w \in V_h \tag{2.18}$$

The approximate solution $\hat{C}$ can be expressed by the nodal values $C_i^h(t)$ and the interpolation function $N_i(\mathbf{x})$, i.e.

$$\hat{C}(\mathbf{x}, t) = \sum_{i=1}^{np} N_i(\mathbf{x}) C_i^h(t) \tag{2.19a}$$

and

$$N_i(\mathbf{x}) = \sum_{e=1}^{ne} \sum_{\alpha=1}^{ni} N_\alpha^e(\mathbf{x}) \Delta_{\alpha i}^e \tag{2.19b}$$

where *np* and *ne* are the total numbers of points and elements in the computational domain respectively, *ni* is the number of nodes in an element, $\Delta_{\alpha i}^e$ is the *Boolean* matrix, and $N_\alpha^e(\mathbf{x})$ is the local shape function. Because the shape function employed by FEM is expressed as an elemental polynomial, the continuity of the variable on each element is preserved. FEMs usually generate a large sparse algebraic matrix. But since they can use arbitrary-shaped elements, FEMs have the flexibility to examine domains with complex geometry.

2.2.3 The Stabilized Weighted Residual Integral

As discussed in Chapter 1, the standard Galerkin method that uses the simple polynomial space is inadequate to model the advection-dominated transport problem, especially with a solution that has a sharp gradient or discontinuity in the dependent variable. Therefore, the space V_h should be augmented and can be decomposed into two parts: $V_h = V_p \oplus V_b$, where V_p is the usual polynomial space and V_b is a closed subspace of the Hilbert space $H_0^1(V)$. Any weighting function w in W_h can be split in the following unique way

$$\hat{w} = w_p + w_b \in V_p \oplus V_b \tag{2.20}$$

and consequently, the variational problem (2.18) can be posed as follows: find

$\hat{C} = C_p + C_b \in V_p \oplus V_b$ such that

$$a(C_p + C_b, w_p) = (f, w_p) \quad \forall w_p \in V_p \tag{2.21a}$$

$$a(C_p + C_b, w_b) = (f, w_b) \quad \forall w_b \in V_b \tag{2.21b}$$

If the space V_b in the variational problem (2.21) is sufficiently large, such that $V_h = V_p \oplus V_b = H_0^1(V)$, then $C_p + C_b$ should represent the exact solution C. Here $C_p \in V_p$ can be regarded as *the resolvable large scale part of* C which is the projection of the exact solution on V_p, while $C_b \in V_b$ can be regarded as *the unresolvable subgrid-scale part of* C (Hughes, 1995), which can be represented with bubble functions (Brezzi et al., 1992).

In the stabilized finite element modelling, the computation is still performed in the conventional polynomial finite element space V_p, but the effect of the bubble C_b on the large scale C_p should be taken into the consideration. It should be noted from (2.21a) that if the definition of the bubble function C_b is known, then the stabilized finite element solution can be obtained in V_p. From the computational point of view, however, C_b is unresolvable in V_p, but it can be determined from the weak form shown in (2.21b), which leads to the following element-level homogeneous Dirichlet boundary value problem

$$(L_t(C_p), w_b) + (L_t(C_b), w_b) = (f, w_b) \tag{2.22}$$

The Euler-Lagrange equation of the problem (2.22) is

$$\begin{cases} L_t(C_b) = -(L_t(C_p) - f) & in\, V' \\ C_b = 0 & on\, S' \end{cases} \tag{2.23}$$

where $V' = \bigcup_{e=1}^{ne} V^e$ is the element interiors and $S' = \bigcup_{e=1}^{ne} S^e$ is the element boundaries. Since C_b varnishes on the elemental boundaries, it is also called the *residual-free bubble* (Franca and Russo, 1997). Brezzi et al. (1997) showed the equivalence of the variational multi-scale approach and the residual-free bubble approach. The solution of (2.23) for the subgrid-scale C_b can be expressed in terms of the elemental Green's function g, which satisfies

$$\begin{cases} L_t(g) = \delta & in\, V^e \\ g = 0 & on\, S^e \end{cases} \tag{2.24}$$

and δ is the Dirac delta function. Therefore

$$C_b(\mathbf{x},t) = -\int_{V^e} g(\mathbf{x},\mathbf{x}')(L_t(C_p) - f)(\mathbf{x}')\mathrm{d}\mathbf{x}' \tag{2.25}$$

If the Green's function $g(\mathbf{x},\mathbf{x}')$ is approximated by

$$g(\mathbf{x},\mathbf{x}') = \tau(\mathbf{x}')\delta(\mathbf{x}-\mathbf{x}') \tag{2.26}$$

then it is implied from (2.25) and (2.26) that

$$C_b(\mathbf{x},t) = -\tau(\mathbf{x})(L_t(C_p) - f)(\mathbf{x}) \tag{2.27}$$

Substituting (2.27) into (2.21a) gives the stabilized variational form for (2.13) on V_p as follows:

$$a(C_p, w_p) + (L_t(C_p) - f, \tau L_t^*(w_p))_{V'} = (f, w_p) \tag{2.28}$$

or in the weighted residual integral weak form as

$$a(C_p, w_p) + \sum_{e=1}^{ne} \int_{V^e} \tau L_t^*(w_p)[L_t(C_p) - f]\mathrm{d}V = (f, w_p) \tag{2.29}$$

where $L_t^*(C) = -\frac{\partial C}{\partial t} - \nabla\cdot(\mathbf{v}C) - \nabla\cdot(D\nabla C)$ is the adjoint operator of L_t defined by (2.12). It can be seen from (2.28) or (2.29) that the effect of C_b on C_p has been projected into the space V_p by adding a stabilized term to the conventional weak form of (2.13). Such stabilized term is also a weighted residual of (2.13) with a weighting function of $\tau L_t^*(w_p)$. For the semi-discrete Eulerian FEMs, the weighting function w_p is independent of time, and then the temporal derivative of the weighting function w_p

varnishes in $L_t^*(w_p)$. If linear elements are used in the formulation, then the second-order derivative of the weighting function is equal to zero, i.e. $\nabla^2 w_p = 0$, in $L_t^*(w_p)$. Consequently, only the first-order spatial derivative of w_p, i.e. $\mathbf{v} \cdot \nabla w_p$, is left in $L_t^*(w_p)$, leading to a general weighted residual integral form of stabilized semi-discrete Eulerian FEMs for the reactive transport equation (2.13)

$$\int_{V^e} w_p [L_t(C_p) - f] \mathrm{d}V + \sum_{e=1}^{ne} \int_{V^e} \tau \mathbf{v} \cdot \nabla w_p [L_t(C_p) - f] \mathrm{d}V = 0 \qquad (2.30)$$

With the bubble functions, Hughes (1995) proved that mapping $\tau(\mathbf{x})$ in (2.30) is equivalent to the intrinsic time τ in the SUPG method for the steady advection-diffusion equation. Different definitions of τ can also lead to different stabilized Eulerian FEMs, such as Taylor-Galerkin and Least Squares methods. The formulations of these stabilized semi-discrete Eulerian FEMs for the advection equation will be given in Section 2.4.

2.3 The Operator Splitting and the Method of Characteristics

Basically, the linear advective-dispersive transport process can be split into the advective contribution C_a and the dispersive contribution C_d; this means that the solution of the advection-dispersion equation can be considered as a combination or superposition of two parts, i.e. $C = C_a + C_d$. Therefore, the advection-dispersion equation can be separated into the advection part and the dispersion part based on Operator Splitting (OS) techniques (Marchuk, 1975; 1995) and they can be treated by different numerical schemes that favour their mathematical characters. The idea of an operator-splitting technique for the advective-dispersive transport can be described as follow: assuming that an approximation of the unknown variable of the problem at the time level $t = n\Delta t$, i.e. C^n, is computed, the approximation of C at $t = (n+1)\Delta t$, i.e. C^{n+1}, can be solved in the following two parts: the dispersion part governed by

$$\begin{cases} \dfrac{\partial C_d^{n+1}}{\partial t} - \nabla \cdot (D \nabla C_d) + \beta C_d = f \\ C_d^n = C^n \end{cases} \qquad (2.31)$$

and the advection part governed by

$$\begin{cases} \dfrac{\partial C}{\partial t} + \mathbf{v} \cdot \nabla C = 0 \\ C^n = C_d^{n+1} \end{cases} \tag{2.32}$$

where $\beta = \nabla \cdot \mathbf{v}$. Different numerical schemes can be used for these two kinds of problems. Mathematically, the diffusion (or dispersion) equation has a parabolic character and can be conveniently solved by the conventional Galerkin method. The advection equation has a hyperbolic character and usually gives rise to numerical difficulties (i.e. numerical oscillations) when the standard Galerkin method is applied. Theoretically, the Method of Characteristics (MOC) (Garder et al.,1964; Douglas and Russell, 1982) can be used to give an exact solution for the advection equation using the concept of the *characteristic curve* (line), which can be determined by

$$\mathbf{v} = \frac{\mathrm{D}\mathbf{x}}{\mathrm{D}t} \tag{2.33}$$

where $\mathrm{D}/\mathrm{D}t$ is the material or convected derivative defined by

$$\frac{\mathrm{D}}{\mathrm{D}t} = \frac{\partial}{\partial t} + \mathbf{v} \cdot \nabla \tag{2.34}$$

With the material derivative (2.34), the advection-dispersion equation (2.3) is reduced to

$$\frac{\mathrm{D}C}{\mathrm{D}t} - \nabla \cdot (D \nabla C) + \beta C = f \tag{2.35}$$

It can be deduced from the mass conservation law that the mass transport by the advective process along the characteristic curve should be constant, i.e.

$$\frac{\mathrm{DC}}{\mathrm{D}t} = \frac{\partial C}{\partial t} + \mathbf{v} \cdot \nabla C = 0 \tag{2.36}$$

Substituting (2.36) into (2.35) implies that only the diffusion equation needs to be solved along the characteristic curve. The suppression of the advective term in the equation is an interesting feature from a computational point of view, since this is often the source of numerical difficulties.

In multi-dimensional problems, however, the most difficult part of the MOC is to determine the characteristic curve in the Eulerian coordinate system. If the trajectory of a particle, located at the spatial point $\mathbf{x}_{ref} = \mathbf{x}$ at time $t = t_{ref} = t^{n+1}$, is denoted by $\tilde{\mathbf{x}}(\mathbf{x}_{ref}, t_{ref}; t)$, then the trajectory (or the characteristic curve) will be the solution of (2.33) with the initial condition of $\tilde{\mathbf{x}}(t^{n+1}) = \mathbf{x}$, which can be approximated by the second-order Taylor series expansion (Zienkiewicz and Codina, 1995)

$$\tilde{\mathbf{x}}(t^n) = \tilde{\mathbf{x}}(t^{n+1}) - \Delta t \mathbf{v}\left(\tilde{\mathbf{x}}(t^{n+1}), t^n\right) + O(\Delta t^2) = \mathbf{x} - \Delta t \mathbf{v}^n + O(\Delta t^2) \tag{2.37}$$

Using a similar procedure, an approximation of the advective part of C on the characteristic curve can be expressed as

$$C(\tilde{\mathbf{x}}(t^n), t^n) = C^n - \Delta t \mathbf{v} \cdot \nabla C^n + O(\Delta t^2) \tag{2.38}$$

As will be seen in the following section, (2.38) is equivalent to the formulation derived from the second-order Taylor-Galerkin method, one of the stabilized semi-discrete Eulerian methods for the advection equation.

2.4 Stabilized Semi-Discrete Eulerian Finite Element Methods

Since the advective term is the main source of difficulty associated with numerical modelling and only linear elements will be used throughout the thesis in modelling exercises, for the sake of completeness, this description will focus on the homogeneous advection equation with the application of the Euler time-integration scheme and the trapezoidal rule, i.e.

$$\frac{C^{n+1} - C^n}{\Delta t} + \mathbf{v} \cdot \nabla C^{n+\theta} = 0 \tag{2.39}$$

where $C^{n+\theta} = (1-\theta)C^n + \theta C^{n+1}$ and $\theta \in [0,1]$ is time weighting.

2.4.1 The Streamline Upwind Petrov-Galerkin Method

As mentioned in Chapter 1, the smart upwind FEM can be introduced into the finite element method by using an asymmetric weighting function. Such asymmetric weighting functions can be constructed by adding a perturbation to the standard Galerkin weighting function (Christie et al., 1976; Heinrich et al., 1977). Since such a perturbation should only be added in the vicinity of the discontinuity or the high spatial gradient of the dependent variable, it should be related to the gradient of the weighting function w. Furthermore, in order to avoid the "crosswind-diffusion" in multi-dimensional problems, this perturbation should also be added in the flow direction (Hughes and Brooks, 1979). Therefore, the additional perturbation should include the form of $\mathbf{v} \cdot \nabla w$. Based on these considerations, Hughes and Brooks (1982) developed the *Streamline Upwind Petrov-Galerkin* (SUPG) method for the advection equation, the weighted residual integral form of which can be written as

$$\int_V \left[w + \frac{\alpha_P h}{2\|\mathbf{v}\|} \mathbf{v} \cdot \nabla w \right] \left[\frac{\partial C}{\partial t} + \mathbf{v} \cdot \nabla C^{n+\theta} \right] \mathrm{d}V = 0 \tag{2.40}$$

where $\{(\alpha_P h/2\|\mathbf{v}\|)\mathbf{v} \cdot \nabla w\}$ is the perturbation added to the classical weighting function w, h is a characteristic length of an element and α_P is a non-dimensional upwind parameter. It should be noted that the formulation (2.40) follows the general stabilized weighted residual integral form (2.30) with a definition of $\tau = \alpha_P h/2\|\mathbf{v}\|$. For the steady state one-dimensional advection-diffusion equation, the SUPG scheme will be nodally exact on the piecewise element with the definition of $\alpha_P = \coth(\mathrm{Pe}) - (\mathrm{Pe})^{-1}$ (Christie et al., 1976). For the transient situation, the scheme can give an "optimal" solution for the advection equation when $\alpha_P = 2/\sqrt{15}$, based on a Fourier analysis conducted on the spatial discretization of the governing equation (Raymond and Garder, 1976). A discontinuity-capturing term can also be added to the weighting function to improve the performance of the SUPG scheme (Hughes and Mallet, 1986b). This discontinuity-capturing term involves a form of $\alpha' \mathbf{v}_{\|} \cdot \nabla w$ (where α' is a parameter and $\mathbf{v}_{\|} = (\mathbf{v} \cdot \nabla C)\nabla C/\|\nabla C\|^2$); therefore, it is a function of the gradient of the unknown variable which makes the scheme nonlinear even though the original governing PDE is linear. For simplicity, only the integral form (2.40) is considered in the ensuing discussions.

2.4.2 The Taylor-Galerkin Method

A further approach to developing a stabilized form for the advection equation is to substitute a Taylor series expansion in time of the unknown variable into the original advection equation to obtain a higher-order correction in time (Lax and Wendroff, 1960), and then use the Galerkin procedure to discretize the corresponding stabilized equation to generate a Taylor-Galerkin weighted integral form (Donea, 1984). For example, the Taylor expansion of the unknown variable C at the time step $n+1$ can be expressed as

$$C^{n+1} = C^n + \frac{\partial C}{\partial t}\Delta t + \frac{1}{2}\frac{\partial^2 C}{\partial t^2}\Delta t^2 + \frac{1}{6}\frac{\partial^3 C}{\partial t^3}\Delta t^3 + O(\Delta t^4) \tag{2.41}$$

If only the terms up to the second-order are considered in the above Taylor expansion and the pure advection equation is substituted into the expansion, a stabilized equation can be obtained as follows

$$\frac{C^{n+1} - C^n}{\Delta t} + \mathbf{v}\cdot\nabla C = \frac{\Delta t}{2}\|\mathbf{v}\|^2 \nabla^2 C \tag{2.42}$$

Applying the standard Galerkin procedure to the above stabilized equation gives a weak form of the second-order Taylor-Galerkin method for the advection equation expressed as

$$\int_V \frac{C^{n+1} - C^n}{\Delta t}\mathrm{d}V + \int_V \left[w + \frac{\Delta t}{2}\mathbf{v}\cdot\nabla w\right]\left(\mathbf{v}\cdot\nabla C^{n+\theta}\right)\mathrm{d}V = 0 \tag{2.43}$$

Similarly, if the terms up to the third order in the Taylor expansion (2.41) are considered and substituted into the advection equation, the corresponding stabilized equation can be expressed as

$$\left(1 - \frac{\Delta t^2}{6}\|\mathbf{v}\|^2 \nabla^2\right)\frac{C^{n+1} - C^n}{\Delta t} + \mathbf{v}\cdot\nabla C = \frac{\Delta t}{2}\|\mathbf{v}\|^2 \nabla^2 C \tag{2.44}$$

and the corresponding weak form of the third-order Taylor-Galerkin method for the advection equation can be written as

$$\int_V \left[w + \frac{\Delta t^2}{6}\|\mathbf{v}\|^2 \nabla w\cdot\nabla\right]\frac{C^{n+1} - C^n}{\Delta t}\mathrm{d}V + \int_V \left[w + \frac{\Delta t}{2}\mathbf{v}\cdot\nabla w\right]\left(\mathbf{v}\cdot\nabla C^{n+\theta}\right)\mathrm{d}V = 0 \tag{2.45}$$

It is noted, from the RHS of (2.42), that an artificial diffusion term is added to the original advection equation due to the Taylor series expansion. Furthermore, it can be seen from (2.44) that an artificial convection term also arises in the residual integral equation due to the consideration of more terms in the Taylor series expansion in (2.41). It can be also noted from the integral equations (2.43) and (2.45) that both second- and third-order Taylor Galerkin formulations for the advection equation follow the general stabilized weighted residual integral form (2.30), but with different definitions of τ for the temporal and spatial derivative terms of the governing equation.

2.4.3 The Least Squares Method

A different approach for deriving a weighted residual integral similar to (2.40) is to consider the variation on the least squares residual integral of the advection equation (Carey and Jiang, 1987a, b; 1988; Jiang, 1998)

$$J(C^{n+1}) = \frac{1}{2}\int_V \left[\frac{C^{n+1} - C^n}{\Delta t} + \mathbf{v}\cdot\nabla C^{n+\theta}\right]^2 \mathrm{d}V \tag{2.46}$$

By assigning a stationary condition $\delta J = 0$ with respect to C^{n+1}, and replacing the variation of the dependent variable δC^{n+1} by the weighting function w, a weighted residual integral form of the advection equation can be written as

$$\int_V [w + \theta\Delta t\mathbf{v}\cdot\nabla w]\left[\frac{C^{n+1} - C^n}{\Delta t} + \mathbf{v}\cdot\nabla C^{n+\theta}\right]\mathrm{d}V = 0 \tag{2.47}$$

Compared to the classical Galerkin method, a perturbation with the form of $\{\theta\Delta t\mathbf{v}\cdot\nabla w\}$ is added to the classical weighting function and the corresponding scheme can give rise to a symmetric matrix form for the advection equation. Like SUPG method, the formulation of least squares method also follows the general stabilized weighted residual integral form (2.30) with a definition of $\tau = \theta\Delta t$

2.4.4 The Modified Least Squares Method

Since the Least Squares method can generate a matrix in symmetric form for the non-adjoint advection equation, it presents a great advantage in examing the nonlinear problem, which usually contains iterative algorithm. Wendland and Schmid (2000) proposed a so-called 3S scheme (Symmetrical Streamline Stabilization) for the advection-dominated transport process, in which a parameter was introduced into the *upwind* term of the Least Squares (LS) scheme for improved performance for the advection-dominated transport problem. This is equivalent to using different perturbation parameters in the LS method for the temporal and the spatial terms of the advection equation, i.e.

$$\int_V [w+\theta\Delta t\mathbf{v}\cdot\nabla w]\frac{C^{n+1}-C^n}{\Delta t}\mathrm{d}V+\int_V [w+\alpha\theta\Delta t\mathbf{v}\cdot\nabla w]\mathbf{v}\cdot\nabla C^{n+\theta}\mathrm{d}V=0 \tag{2.48}$$

Therefore this scheme can be cataloged as the *Modified Least Squares* (MLS) method. In (2.48), α is the upwind parameter, which can be determined by Fourier analysis to achieve the optimum numerical performance of the MLS scheme for the advection equation.

2.5 The Stabilized Equation and the Artificial Péclet Numbers

2.5.1 The Stabilized Equation

It should be noted that in the derivation of the classical advection-dispersion equation (2.3) from (2.1) and (2.2), only the first-order Taylor expansions in space for the advective flux and the dispersive flux are used. However, if the advective transport process has a significant variation over the control volume, the first-order Taylor expansion in space is not sufficient and the second-order expansion should be considered, i.e.

$$[\mathbf{v}C](\mathbf{x}+\Delta\mathbf{x})=[\mathbf{v}C](\mathbf{x})+\nabla[\mathbf{v}C]\Delta\mathbf{x}+\frac{\Delta\mathbf{x}^{\mathrm{T}}}{2}\nabla^2[\mathbf{v}C]_{\mathbf{x}+\eta\Delta\mathbf{x}}\Delta\mathbf{x} \tag{2.49}$$

where $\eta\in[0,1]$. The last term in (2.49) represents the residual of Taylor expansion and can be expressed by

$$\frac{\Delta\mathbf{x}}{2}\nabla^2[\mathbf{v}C]_{\mathbf{x}+\eta\Delta\mathbf{x}}\Delta\mathbf{x}=\frac{\mathbf{h}_c^{\mathrm{T}}}{2}\nabla^2[\mathbf{v}C]\Delta\mathbf{x} \tag{2.50}$$

where $\mathbf{h}_c = (h_x, h_y, h_z\}^{\mathrm{T}}$ is referred to as the characteristic length vector of the control volume, which can be written as $\mathbf{h}_c = 2\tau\mathbf{v}$, and τ is the so-called intrinsic time scale. Considering (2.49) and (2.50) in (2.1) and (2.2), a stabilized form of the advection-dispersion equation (2.3) is obtained as follows (Oñate et al., 1997; Oñate, 1998):

$$\frac{\partial C}{\partial t} + \nabla \cdot (\mathbf{v}C) - \nabla \cdot (D\nabla C) - \tau \mathbf{v}^{\mathrm{T}} \nabla^2 [\mathbf{v}C] = f \tag{2.51}$$

If both advective and dispersive fluxes vary dramatically over the control volume, following the same procedure as in (2.49) gives

$$\begin{aligned} [\mathbf{v}C - D\nabla C](\mathbf{x} + \Delta\mathbf{x}) &= [\mathbf{v}C - D\nabla C](\mathbf{x}) + \Delta\mathbf{x}^{\mathrm{T}} \nabla [\mathbf{v}C - D\nabla C] \\ &\quad + \tau\mathbf{v}^{\mathrm{T}} \nabla^2 [\mathbf{v}C - D\nabla C] \Delta\mathbf{x} \end{aligned} \tag{2.52}$$

In addition, in the derivation of equation (2.3), the accumulation and reaction over the control volume are assumed to be constant. For the rapid transport flux, a more accurate consideration of the determination of the accumulation and reaction is to use a Taylor expansion in space, including a linear residual, i.e.

$$\begin{aligned} [\frac{\partial C}{\partial t} + rC] &= [\frac{\partial C}{\partial t} + rC](\mathbf{x}) + \Delta\mathbf{x}^{\mathrm{T}} \nabla [\frac{\partial C}{\partial t} + rC]_{x+\eta'\Delta\mathbf{x}} \\ &= [\frac{\partial C}{\partial t} + rC](\mathbf{x}) + \mathbf{h}_c'^{\mathrm{T}} \nabla [\frac{\partial C}{\partial t} + rC]_{x+\eta'\Delta\mathbf{x}} \\ &= [\frac{\partial C}{\partial t} + rC](\mathbf{x}) + \tau' \mathbf{v}^{\mathrm{T}} \nabla [\frac{\partial C}{\partial t} + rC](\mathbf{x}) \end{aligned} \tag{2.53}$$

where $\eta' \in [0,1]$, $\mathbf{h}_c'$ and τ' are quantities same as η, $\mathbf{h}_c$ and τ. Considering (2.52) and (2.53) in (2.1) and (2.2) and keeping $\tau = \tau'$, a generalized form of the stabilized advection-dispersion equation can be expressed as

$$r - \tau \mathbf{v}^{\mathrm{T}} \nabla r = 0, \quad \mathbf{x} \in V, t \in [0, t^*], t^* > 0 \tag{2.54}$$

where

$$r = f - L_t(C) \tag{2.55}$$

The corresponding stabilized Dirichlet and Neumann boundary conditions can be obtained using the similar procedure and can be written as follows:

$$C(\mathbf{x},t) - \widetilde{C}(\mathbf{x},t) = 0 \qquad \mathbf{x} \in S_{\mathrm{D}}, t \in [0, t^{*}] \tag{2.56a}$$

$$-\mathbf{n}^{\mathrm{T}}\mathbf{v}C + \mathbf{n}^{\mathrm{T}} D \nabla C + \bar{q}_n - \tau \mathbf{v}^{\mathrm{T}}\mathbf{n} r = 0 \qquad \mathbf{x} \in S_{\mathrm{N}}, t \in [0, t^{*}] \tag{2.56b}$$

The weighted residual form of (2.54) can be obtained by applying the Galerkin procedure

$$\begin{aligned} &\int_V w(r - \tau \mathbf{v}^{\mathrm{T}} \nabla r) \mathrm{d}V + \int_{S_D} \overline{w}(\hat{C} - \widetilde{C}) \mathrm{d}S \\ &\quad + \int_{S_N} \overline{\overline{w}}(-\mathbf{n}^{\mathrm{T}}\mathbf{v}C + \mathbf{n}^{\mathrm{T}} D \nabla C + \bar{q}_n - \tau \mathbf{v}^{\mathrm{T}}\mathbf{n} r) \mathrm{d}S = 0 \end{aligned} \tag{2.57}$$

where w, $\overline{w}$ and $\overline{\overline{w}}$ are weighting functions. Assuming $w = \overline{w} = 0$ on S_D and choosing $\overline{\overline{w}} = -w$ in (2.57) as well as applying the integration by parts leads to the following results:

$$\int_V (w + \tau \mathbf{v}^{\mathrm{T}} \nabla w) r \mathrm{d}V - \int_{S_N} w(-\mathbf{n}^{\mathrm{T}}\mathbf{v}C + \mathbf{n}^{\mathrm{T}} D \nabla C + \bar{q}_n) \mathrm{d}S = 0 \tag{2.58}$$

Equation (2.58) is identical to the weak form of the SUPG method for the advection-dispersion equation (2.3). Therefore, the standard Galerkin form for the stabilized equation (2.54) is equivalent to the SUPG formulation for the classical advection-dispersion equation (2.3).

2.5.2 The Artificial Péclet Numbers

Mathematically, the advection-dispersion equation (2.3) has either a *parabolic* or a *hyperbolic* dominance, depending on the Péclet number

$$\mathrm{Pe} = \frac{\|\mathbf{v}\| h}{2D} \tag{2.59}$$

When the Péclet number is small (in comparison to unity), the advection-dispersion equation (2.3) is dominantly parabolic with the result that most currently available numerical techniques can be used to solve the resulting PDE without difficulty. As the Péclet number increases (i.e. much greater than unity), the advection-dispersion equation (2.3) becomes dominantly hyperbolic with the result that the conventional numerical schemes break down in the vicinity of either a discontinuity or a location with a high gradient of the dependent variable. It can be seen from equations (2.40), (2.42), (2.45) and (2.47) that the Streamline Upwind Petrov-Galerkin (SUPG), the Taylor-Galerkin (TG), the Least Squares (LS) and Modified Least Squares (MLS) methods use asymmetric weighting functions to generate the stabilized form of the advection equation. As observed previously, for steady situations, the use of such asymmetric weighting functions is equivalent to the addition of an artificial diffusion term in the advection-dispersion equation as shown in (2.51) and (2.54). Since the Péclet number, by definition, reflects the ratio of the advective flux to the dispersive flux in the computational element, it can be used to indicate the amount of artificial diffusion introduced by the stabilized methods to the steady state equation. Table 2.1 presents the perturbations, the corresponding artificial diffusion coefficients and the Péclet numbers of SUPG, TG, LS and MLS schemes for the steady state situation. It can be seen from this Table that $\mathrm{Pe}_{\mathrm{TG}}$, $\mathrm{Pe}_{\mathrm{LS}}$ and $\mathrm{Pe}_{\mathrm{MLS}}$ are influenced by the magnitude of the flow velocity; they become greater as $\|\mathbf{v}\|$ approaches zero, with the assumption of a constant time step and characteristic length. Consequently, the stability of the TG, LS and MLS schemes can be

Table 2.1 Artificial diffusion coefficients and Péclet numbers

Schemes	Diffusion coefficient	Péclet number
SUPG	$\tilde{k}_{\mathrm{SUPG}} = \frac{1}{2}\alpha_P h\|\mathbf{v}\|$	$\mathrm{Pe}_{\mathrm{SUPG}} = \frac{\|\mathbf{v}\|h}{2\tilde{k}_{\mathrm{SUPG}}} = \frac{1}{\alpha_P}$
TG	$\tilde{k}_{\mathrm{TG}} = \frac{1}{2}\Delta t\|\mathbf{v}\|^2$	$\mathrm{Pe}_{\mathrm{TG}} = \frac{\|\mathbf{v}\|h}{2\tilde{k}_{\mathrm{LS}}} = \frac{h}{\|\mathbf{v}\|\Delta t} = \frac{1}{Cr}$
LS	$\tilde{k}_{\mathrm{LS}} = \theta\Delta t\|\mathbf{v}\|^2$	$\mathrm{Pe}_{\mathrm{LS}} = \frac{\|\mathbf{v}\|h}{2\tilde{k}_{\mathrm{LS}}} = \frac{h}{2\theta\|\mathbf{v}\|\Delta t} = \frac{1}{2\theta Cr}$
MLS	$\tilde{k}_{\mathrm{LS}} = \alpha\theta\Delta t\|\mathbf{v}\|^2$	$\mathrm{Pe}_{\mathrm{LS}} = \frac{\|\mathbf{v}\|h}{2\tilde{k}_{\mathrm{LS}}} = \frac{h}{2\theta\|\mathbf{v}\|\Delta t} = \frac{1}{2\alpha\theta Cr}$

influenced by a variation in the flow velocity within the domain, which can often be encountered in transport problems in geoenviromental engineering applications. On the other hand, Pe_{SUPG} is not influenced by the magnitude of the flow velocity, therefore better computational performance is associated with the SUPG scheme for advective transport problems with space-dependent flow velocity.

2.6 Discussion

In this chapter, the basic concept and general weighted residual integral form of the stabilized finite element method for the advection equation are reviewed and presented with the residual-free bubble functions and variational multi-scale approach. Four representations of the stabilized semi-discrete Eulerian finite element method for the advection equation, SUPG, TG, LS and MLS schemes, are also briefly described. Using the concept of the stabilized equation, the stabilities of these four semi-discrete stabilized finite element methods for the advection-dominated equation are assessed through the artificial Péclet numbers. However, such assessments are based on the assumption that the temporal derivative in the governing equation is computed accurately, or that the transport process is steady state. In the numerical formulation of the transient advection-dispersion equation by the semi-discrete method, the temporal derivative is usually discretized by the time integration scheme and therefore the temporal truncation has an influence on the corresponding numerical schemes for the advection-dispersion equation. The influence of the discretization of both temporal and spatial terms of the transient advection-dispersion equation on the numerical behaviour of stabilized semi-discrete Eulerian methods can be investigated through Fourier analysis, which will be the main focus of the next chapter.

CHAPTER 3

FOURIER ANALYSIS OF STABILIZED SEMI-DISCRETE EULERIAN METHODS

Fourier analysis is one mathematical tool that can be used to assess numerical methods for the solution of the transport equation. This is done by illustrating the alterations, introduced by the numerical schemes, of the algorithmic amplitude and phase velocity of wave components involved in the solution. Therefore, Fourier analysis can be used to reveal the mathematical nature, in a frequency domain, of the numerical difficulties involved in a specific numerical scheme for the advection equation. In this chapter, Fourier analysis is carried out to investigate the numerical performance of the stabilized semi-discrete Eulerian methods described in the previous chapter for the advection equation with the application of the Euler time integration scheme and the trapezoidal time rule. Such Fourier analysis is performed on the Modified Least Squares method (MLS) for the one-dimensional purely advection equation, but the corresponding analytical results for Petrov-Galerkin, Taylor-Galerkin and Least Squares methods are also presented. The variations of the algorithmic amplitudes and phase velocities of these stabilized schemes for the advection equation, with the dimensionless wave number vs. Courant number, are illustrated in this chapter. These illustrations show that the Courant number has a significant influence on the numerical behaviour of these stabilized schemes for the advection equation. Based on this observation, a Courant number criterion can be derived, under which the MLS scheme can generate an *oscillation-free* and *non-diffusive* numerical solution for the advection equation, particularly for the case involving a discontinuity.

3.1 Finite Difference Stencils

In this chapter, the following one-dimensional advection equation is considered for the purpose of assessing the stabilized semi-discrete Eulerian methods

$$\frac{\partial C}{\partial t} + v\frac{\partial C}{\partial x} = 0 \qquad (3.1)$$

where $C(x,t)$ is the scalar property of the species that is being transported (e.g. concentration of chemical or contaminant); x is the spatial coordinate; t is time; v is the field velocity or the characteristic speed of the equation. The general weak forms of the advection equation derived by several semi-discrete Eulerian stabilized FEMs have been given in Chapter 2. For completeness of the discussion in this chapter, the generalized residual integral form of the semi-discrete Eulerian FEM for the one-dimensional advection equation (3.1) with the application of the trapezoidal time rule is given as follows

$$\int_0^l \left[w + \tau_1 \mathrm{sign}(v)\frac{dw}{dx} \right] \frac{\partial C}{\partial t}\mathrm{d}x + \int_0^l \left[w + \tau_2\, \mathrm{sign}(v)\frac{dw}{dx} \right] (v\frac{\partial C^{n+\theta}}{\partial x})\mathrm{d}x = 0 \qquad (3.2)$$

where $C^{n+\theta} = (1-\theta)C^n + \theta C^{n+1}$; $\theta \in (0,1]$ is the time weighting; w is the standard Galerkin weighting function and $[0,l]$ is the interval of the computational domain. Also τ_i (i=1,2) in (3.2) are the perturbation parameters referred to as the upwind functions or the intrinsic times of the stabilized methods (Oñate et al., 1997). They should be chosen based on either the Least Squares method (LS) (Carey and Jiang, 1987a) such that the artificial convection term has the adjoint form of the convection term of the equation giving rise to symmetric computational schemes (Wendland and Schmid, 2000), or be based on a Fourier analysis to ensure that the numerical modelling can give an "optimal" solution of the advection-diffusion equation (Raymond and Garder, 1976), such as the Petrov-Galerkin (PG) Method (Hughes and Brooks, 1982). They can also take on different values to generate different stabilized methods, such as the second-and the third-order Taylor-Galerkin methods (TG2 and TG3) (Donea et al., 1984) or the MLS method. The expressions of upwind functions, τ_i (i=1,2), for several stabilized finite element methods, PG, TG2, TG3, LS and MLS methods, are listed in the Table 3.1, where h is the elemental length, Δt is the time step and α_P and α are the upwind parameters introduced respectively in the SUPG and MLS schemes. The integral form (3.2) with the piecewise linear elements can lead to the nodal difference equation of the advection

Table 3.1 Definitions of upwind functions for different methods

Schemes	τ_1	τ_2
PG	$\frac{1}{2}\alpha_p h$	$\frac{1}{2}\alpha_p h$
TG2	0	$\frac{1}{2}\lvert v\rvert\Delta t$
TG3	$\frac{1}{6}\lvert v\rvert^2\Delta t^2\frac{\mathrm{d}}{\mathrm{d}x}$	$\frac{1}{2}\lvert v\rvert\Delta t$
LS	$\theta\lvert v\rvert\Delta t$	$\theta\lvert v\rvert\Delta t$
MLS	$\theta\lvert v\rvert\Delta t$	$\alpha\theta\lvert v\rvert\Delta t$

Table 3.2 Finite difference stencils of stabilized semi-discrete methods

Schemes	Equivalent Finite Difference Stencils
PG	$\frac{1}{6}(\dot{C}_{j-1}+4\dot{C}_j+\dot{C}_{j+1})+\frac{\alpha_P}{4}(\dot{C}_{j-1}-\dot{C}_{j+1})+$ $\frac{v}{2h}(C_{j+1}^{n+\theta}-C_{j-1}^{n+\theta})-\frac{\alpha_P v}{2h}(C_{j-1}^{n+\theta}-2C_{j1}^{n+\theta}+C_{j+1}^{n+\theta})=0$
TG2	$\frac{1}{6}(\dot{C}_{j-1}+4\dot{C}_j+\dot{C}_{j+1})+$ $\frac{v}{2h}(C_{j+1}^{n+\theta}-C_{j-1}^{n+\theta})-\frac{\Delta t\, v^2}{2h^2}(C_{j-1}^{n+\theta}-2C_j^{n+\theta}+C_{j+1}^{n+\theta})=0$
TG3	$\frac{1}{6}(\dot{C}_{j-1}+4\dot{C}_j+\dot{C}_{j+1})-\frac{\Delta t^2 v^2}{6h^2}(\dot{C}_{j-1}-2\dot{C}_j+\dot{C}_{j+1})+$ $\frac{v}{2h}(C_{j+1}^{n+\theta}-C_{j-1}^{n+\theta})-\frac{\Delta t\, v^2}{2h^2}(C_{j-1}^{n+\theta}-2C_j^{n+\theta}+C_{j+1}^{n+\theta})=0$
LS	$\frac{1}{6}(\dot{C}_{j-1}+4\dot{C}_j+\dot{C}_{j+1})+\frac{\theta v\Delta t}{2h}(\dot{C}_{j-1}-\dot{C}_{j+1})+$ $\frac{v}{2h}(C_{j+1}^{n+\theta}-C_{j-1}^{n+\theta})-\frac{\theta\Delta t\, v^2}{h^2}(C_{j-1}^{n+\theta}-2C_j^{n+\theta}+C_{j+1}^{n+\theta})=0$
MLS	$\frac{1}{6}(\dot{C}_{j-1}+4\dot{C}_j+\dot{C}_{j+1})+\frac{\theta v\Delta t}{2h}(\dot{C}_{j-1}-\dot{C}_{j+1})+$ $\frac{v}{2h}(C_{j+1}^{n+\theta}-C_{j-1}^{n+\theta})-\frac{\alpha\theta\Delta t\, v^2}{h^2}(C_{j-1}^{n+\theta}-2C_j^{n+\theta}+C_{j+1}^{n+\theta})=0$

equation. The finite difference stencils of these stabilized semi-discrete methods for the advection equation (3.1) are given in Table 3.2.

The finite difference stencils listed in Table 3.2 can be expressed in the operator form (Vichnevetsky and Bowles, 1982) as follows:

$$\mathbf{A}_1 \cdot \dot{C}_j = \mathbf{A}_2 \cdot C_j \tag{3.3}$$

where the discrete operator $\mathbf{A}_i$ is of the form

$$\mathbf{A}_i \cdot = \sum_k a_i^{(k)} \mathbf{E}^{(k)} \cdot \tag{3.4}$$

and $\mathbf{E}^{(k)}$ is the space shift operator, $\mathbf{E}^{(k)} \cdot C_j \equiv C_{j+k}$. For the implicit semi-discretization, (3.3) can be expressed as

$$\dot{C}_j = \mathbf{A} \cdot C_j \tag{3.5}$$

where $\mathbf{A} = \mathbf{A}_1^{-1} \cdot \mathbf{A}_2$. The discrete operators $\mathbf{A}_1$ and $\mathbf{A}_2$ corresponding to the MLS scheme are defined by

$$\mathbf{A}_1(C_j) = \frac{1}{6}(C_{j-1} + 4C_j + C_{j+1}) + \frac{\theta v \Delta t}{2h}(C_{j-1} - C_{j+1}) \tag{3.6a}$$

$$\mathbf{A}_2(C_j) = \frac{v}{2h}(C_{j+1} - C_{j-1}) - \frac{\alpha\theta \Delta t\, v^2}{h^2}(C_{j-1} - 2C_j + C_{j+1}) \tag{3.6b}$$

3.2 Spectral Functions

Returning to the advection-diffusion equation, an exact solution can be written as

$$C(x,t) = \exp(i\omega x - \nu t) \tag{3.7}$$

In (3.7), ω is the *spatial wave number*, ν determines the temporal evolution of the solution and can be written as

$$\nu = \xi + i\Omega \tag{3.8}$$

where ξ is the *damping coefficient* and Ω is the *wave frequency*. Substituting (3.7) into (3.1) gives the following relationship

$$\xi = D\omega^2 \tag{3.9a}$$

$$\Omega = v\omega \tag{3.9b}$$

where D is the coefficient of diffusion included in the transport equation. For the purely advection equation, i.e. $D = 0$, the damping coefficient $\xi = 0$, and therefore the solution of the advection equation (3.1) should not decay in amplitude.

Similarly, the solution of the finite difference stencils (3.5) corresponding to the MLS scheme for the advection equation (3.1) can be written as

$$C_j(t) = C(x_j, t) = \exp[i\omega(x_j - vt)] \tag{3.10}$$

Substituting (3.10) into (3.5) gives

$$-(\xi^h + i\Omega^h)C_j(t) = \hat{A}(\omega)C_j(t) \tag{3.11}$$

where $\hat{A}(\omega)$ is the *spectral function* of the operator $\mathbf{A}$ in (3.5), which is defined as the function of ω, i.e.

$$\hat{A}(\omega) = \frac{\mathbf{A}_2 \cdot e^{i\omega x_n}}{\mathbf{A}_1 \cdot e^{i\omega x_n}} = \frac{\hat{A}_2(\omega)}{\hat{A}_1(\omega)} \tag{3.12}$$

Substituting the discrete operator $\mathbf{A}$ defined by (3.6) into (3.12) gives the spectral function of the MLS scheme for the advection equation (3.1) as follows

$$\hat{A}(\omega) = \frac{-v[6\alpha Cr\theta(1 - \cos(\omega h)) + i3\sin(\omega h)]}{h[(2 + \cos(\omega h)) - i3Cr\theta\sin(\omega h)]} \tag{3.13}$$

where $h = x_{j+1} - x_j$ is a spatial increment and $Cr = v\Delta t/h$ is the Courant number. Following the same procedure, the spectral functions of other stabilized semi-discrete Eulerian FEMs for the advection equation can also be obtained and they are listed in Table 3.3.

From equation (3.11), the following relationships can be obtained,

$$\xi^h = -\mathrm{Re}(\hat{A}(\omega)) \tag{3.14a}$$

$$\Omega^h = -\mathrm{Im}(\hat{A}(\omega)) \tag{3.14b}$$

Table 3.3 Expressions of spectral function $\hat{A}(\omega)$

Schemes	$\hat{A}(\omega)$
PG	$\dfrac{\frac{v}{h}[\alpha_P(\cos(\omega h)-1)-i\sin(\omega h)]}{\frac{1}{3}(\cos(\omega h)+2)-i\frac{\alpha_P}{2}\sin(\omega h)}$
TG2	$\dfrac{\frac{v}{h}\left[\frac{v\Delta t}{h}(\cos(\omega h)-1)-i\sin(\omega h)\right]}{\frac{1}{3}(\cos(\omega h)+2)}$
TG3	$\dfrac{\frac{v}{h}\left[\frac{v\Delta t}{h}(\cos(\omega h)-1)-i\sin(\omega h)\right]}{\frac{1}{3}\left[(\cos(\omega h)+2)-\frac{v^2\Delta t^2}{h^2}(\cos(\omega h)-1)\right]}$
LS	$\dfrac{\frac{v}{h}\left[\frac{2\theta v\Delta t}{h}(\cos(\omega h)-1)-i\sin(\omega h)\right]}{\frac{1}{3}(\cos(\omega h)+2)-i\frac{\theta v\Delta t}{h}\sin(\omega h)}$

Substituting (3.14) into (3.10) gives

$$\begin{aligned} C(x_j,t) &= \exp[-\xi^h t]\exp[i\omega(x_j-\frac{\Omega^h}{\omega}t)] \\ &= \exp[\mathrm{Re}(\hat{A}(\omega))t]\exp[i\omega(x_j-\frac{-\mathrm{Im}(\hat{A}(\omega))}{\omega}t)] \end{aligned} \tag{3.15}$$

If the variation of the unknown variable is considered only in the time interval $[t, t+\Delta t]$, then, from the equation (3.15), the *algorithmic amplitude* of the numerical operator $\mathbf{A}$ can be written as

$$\zeta^h = \left|\frac{C_j^{n+1}}{C_j^n}\right| = \exp[-\xi^h\Delta t] = \exp[\mathrm{Re}(\hat{A}(\omega))\Delta t] \tag{3.16}$$

and the *relative phase velocity* v^* of the numerical operator $\mathbf{A}$ has the form

$$\frac{v^*}{v} = \frac{\Omega^h}{v\omega} = \frac{-\operatorname{Im}(\hat{A}(\omega))}{v\omega} \tag{3.17}$$

Substituting the definition of $\hat{A}(\omega)$ in (3.13) into (3.16) and (3.17) leads to the algorithmic amplitude and the relative phase velocity of the MLS scheme for the advection equation (without applying the time integration), which are expressed as follows:

$$\zeta^h = \exp\left(-\frac{Cr[6\alpha Cr\theta(1-\cos(\omega h))(2+\cos(\omega h)) + -9Cr\theta\sin^2(\omega h)]}{[(2+\cos(\omega h))]^2 + [3Cr\theta\sin(\omega h)]^2} \right) \tag{3.18}$$

$$\frac{v^*}{v} = \frac{3\sin(\omega h)[6\alpha Cr^2\theta^2(1-\cos(\omega h)) + (2+\cos(\omega h))]}{\omega h[(2+\cos(\omega h))]^2 + [3Cr\theta\sin(\omega h)]^2} \tag{3.19}$$

where ωh is the *dimensionless wave number*. Expanding ζ^h and v^*/v in terms of ωh gives

$$\begin{aligned} \zeta^h &= 1 + Cr^2(1-\alpha)(\omega h)^2 \\ &+ \frac{Cr^2\theta}{12}(-\alpha + 6Cr^2\theta(1-\alpha)^2 - 12Cr^2\theta^2(1-\alpha))(\omega h)^4 + O\left((\omega h)^6\right) \end{aligned} \tag{3.20}$$

$$\begin{aligned} \frac{v^*}{v} &= 1 - Cr^2\theta^2(1-\alpha)(\omega h)^2 \\ &+ (-\frac{1}{180} + \frac{1}{12}\alpha Cr^2\theta^2 + Cr^4\theta^4(1-\alpha))(\omega h)^4 + O\left((\omega h)^6\right) \end{aligned} \tag{3.21}$$

Tables 3.4 and 3.5 show the expansions, in terms of ωh, of ζ^h and v^*/v of four other stabilized semi-discrete Eulerian FEMs for the advection equation without implementation of time integration.

It is shown from (3.20) and (3.21) that ζ^h and v^*/v for the MLS scheme should have higher accuracy in terms of ωh when $\alpha = 1$, which corresponds to the LS scheme. If $\theta = 0$, the algorithmic amplitude and the relative phase velocity defined by (3.20) and (3.21) correspond to the conventional Galerkin method. It is indicated from the expansion shown in Table 3.5 that the relative phase velocity of the PG scheme for the advection equation, obtained without applying the time integration, can reach the sixth order

Table 3.4 Expansions of ζ^h in terms of ωh (without time integration)

Schemes	$\zeta^h = \exp[\mathrm{Re}(\hat{A}(\omega))\Delta t]$
PG	$1-\frac{\alpha_P}{24}Cr(\omega h)^4+O((\omega h)^6)$
TG2	$1-\frac{1}{2}Cr^2(\omega h)^2+\frac{1}{24}Cr^2(3Cr^2-1)(\omega h)^4+O((\omega h)^6)$
TG3	$1-\frac{1}{2}Cr^2(\omega h)^2+\frac{1}{24}Cr^2(5Cr^2-1)(\omega h)^4+O((\omega h)^6)$
LS	$1-\frac{\theta}{12}Cr^2(\omega h)^4+O((\omega h)^6)$

Table 3.5 Expansions of v^*/v in terms of ωh (without time integration)

Schemes	$\frac{v^*}{v}=\frac{-\mathrm{Im}(\hat{A}(\omega))}{\omega v}$
PG	$1-(\frac{\alpha_P^2}{48}-\frac{1}{180})(\omega h)^4+O((\omega h)^6)$
TG2	$1-\frac{1}{180}(\omega h)^4+O((\omega h)^6)$
TG3	$1-\frac{1}{6}Cr^2(\omega h)^2+\frac{1}{360}Cr^2(10Cr^4-5Cr^2-2)(\omega h)^4+O((\omega h)^6)$
LS	$1-(\frac{Cr^2\theta^2}{12}-\frac{1}{180})(\omega h)^4+O((\omega h)^6)$

accuracy in ωh when the upwind function $\alpha_P = 2/\sqrt{15}$. This result was also obtained by Raymond and Garder (1976). Figures 3.1 to 3.5 show the variation of the algorithmic amplitude and the relative phase velocity of the Galerkin, PG, LS, TG2 and TG3 methods, with ωh within the time interval $[t, t+\Delta t]$.

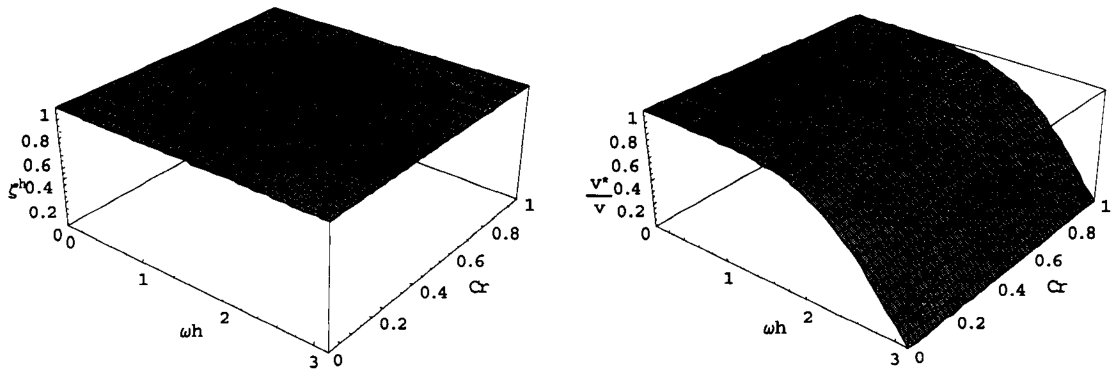

(a) (b)

Figure 3.1 Distributions of (a) the algorithmic amplitude and (b) the relative phase velocity of the Galerkin method

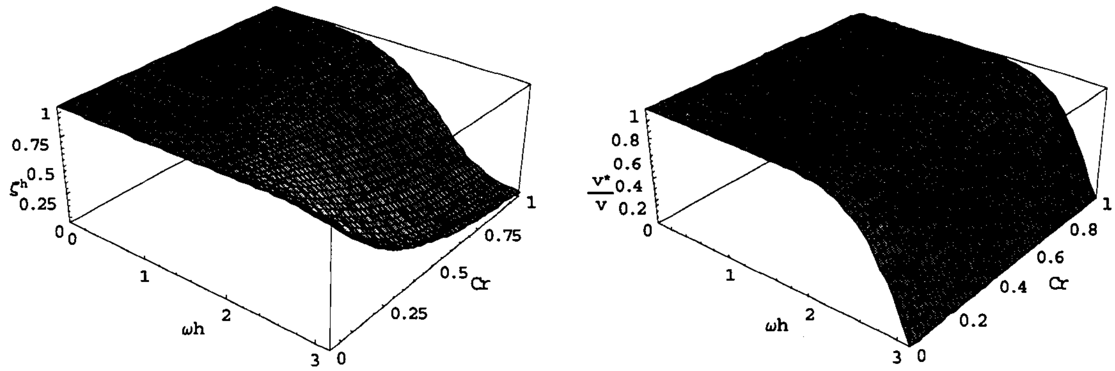

(a) (b)

Figure 3.2 Distributions of (a) the algorithmic amplitude and (b) the relative phase velocity of the Petrov-Galerkin method

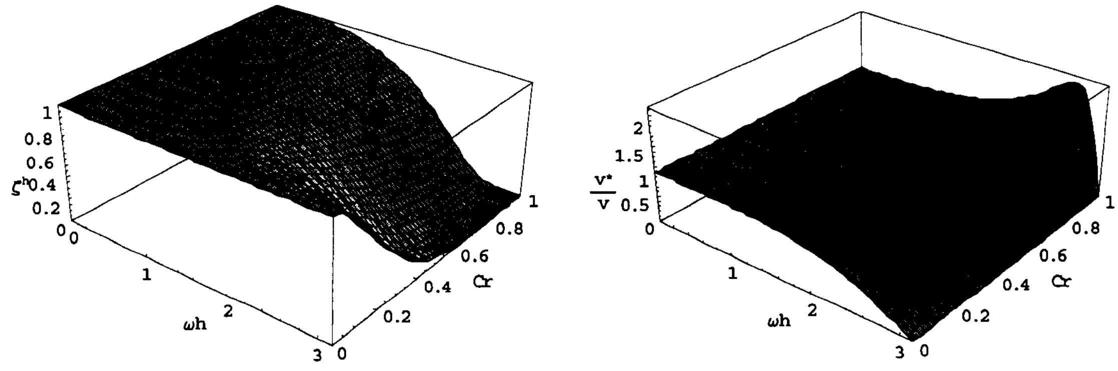

(a) (b)

Figure 3.3 Distributions of (a) the algorithmic amplitude and (b) the relative phase velocity of the Least Squares method

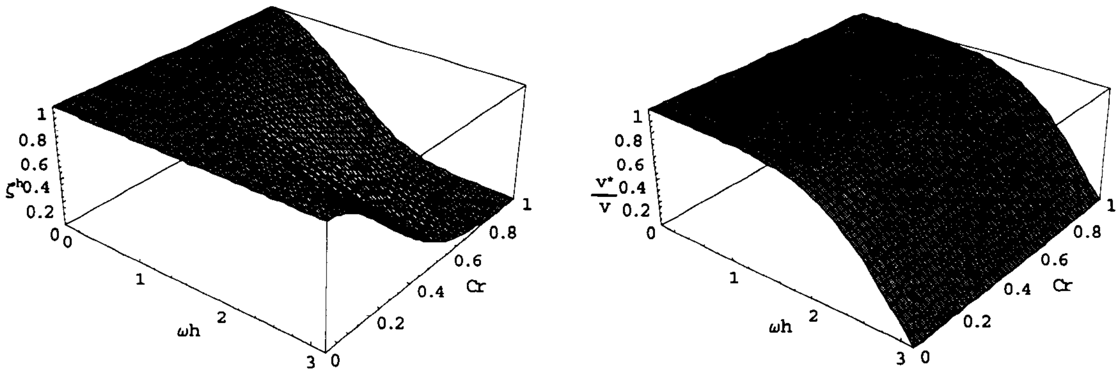

(a) (b)

Figure 3.4 Distributions of (a) the algorithmic amplitude and (b) the relative phase velocity of the second-order Taylor-Galerkin method

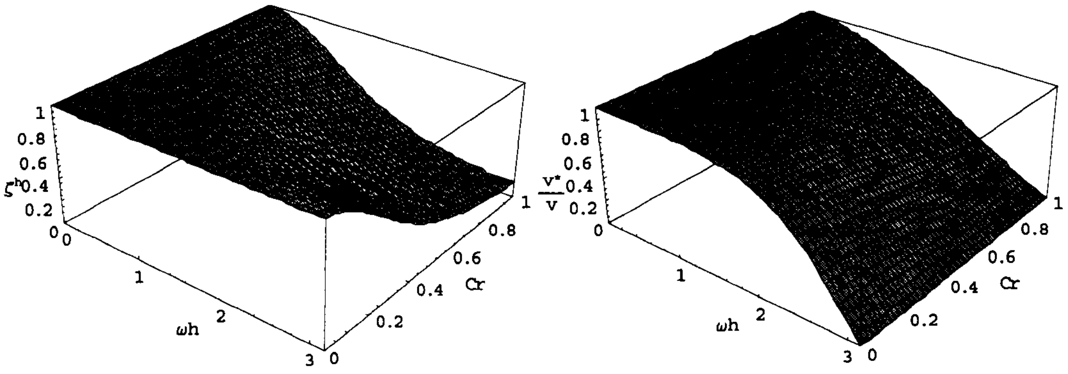

(a) (b)

Figure 3.5 Distributions of (a) the algorithmic amplitude and (b) the relative phase velocity of the third-order Taylor-Galerkin method

It should be noted that ζ^h and v^*/v discussed until now correspond to the spatial discretization of the advection equation using the stabilized FEMs concerned. This is based on the assumption that the temporal derivative in the advection equation is accurately computed in the time interval $[t, t+\Delta t]$. In the semi-discrete methods, however, the temporal derivative of the advection equation is also discretized by certain time integration schemes, such as forward Euler, backward Euler, Crank-Nicolson or Runge-Kutta methods, etc. Therefore the numerical behaviour of the stabilized semi-discrete methods for the advection equation is also influenced by the temporal discretization. In the following section, the influence of the temporal discretization together with the spatial discretization on the numerical performance of the stabilized semi-discrete Eulerian FEMs for the advection equation will be discussed using the Fourier analysis.

3.3 Fourier Analysis on Temporal and Spatial Discretizations

With the application of the trapezoidal time rule, the finite difference stencil of the MLS scheme for the advection equation (3.1) with the Euler time integration scheme can be written as follows:

$$C_j^{n+1} = C_j^n + \Delta t[\theta \mathrm{A} C_j^{n+1} + (1-\theta)\mathrm{A} C_j^n]. \tag{3.22}$$

Following (3.10), it can be assumed that the solution of (3.22) is of the following form

$$C_j^n = C(x_j, t_n) = \exp[i\omega x_j - \nu^h t_n] \tag{3.23}$$

where $\nu^h = \xi^h + i\Omega^h$, and $x_{j+1} - x_j = h$, $t_{n+1} - t_n = \Delta t$. With these notations, the above equation can be written as

$$C_j^n = \exp[-\xi^h t_n]\exp[i\omega(x_j - \frac{\Omega^h}{\omega} t_n)] \tag{3.24}$$

Substituting the discrete solution C_j^n in (3.24) into (3.22) gives

$$[\zeta^h e^{-i\Omega^h \Delta t}]C_j^n = z(\omega)C_j^n \tag{3.25}$$

where ζ^h is the *algorithmic amplitude* of the numerical operator described by (3.22), which is defined as

$$\zeta^h = \left|\frac{C_j^{n+1}}{C_j^n}\right| = \exp[-\xi^h \Delta t]. \tag{3.26}$$

and $z(\omega)$ is the *spectral function* of the numerical operator described by (3.22), which is defined as

$$z(\omega) = \frac{1 + \Delta t(1-\theta)\hat{A}(\omega)}{1 - \Delta t\theta \hat{A}(\omega)} \tag{3.27}$$

It is evident from (3.25) that the algorithmic amplitude ζ^h is equal to $|z(\omega)|$ of the scheme, and therefore the *von Neumann stabilization condition* (von Neumann, 1944) is

$$\zeta^h = |z(\omega)| \le 1 \tag{3.28}$$

Substituting the spectral function defined by (3.13) into (3.27) leads to the spectral function $z(\omega)$ of the MLS scheme for the advection equation (3.1) as follows

$$z(\omega) = \frac{[2+\cos(\omega h)] - 6\alpha Cr^2\theta(1-\theta)\,[1-\cos(\omega h)] - i3Cr\sin(\omega h)}{[2+\cos(\omega h)] + 6\alpha Cr^2\theta^2\,[1-\cos(\omega h)]} \tag{3.29}$$

Similarly, the spectral function $z(\omega)$ of other stabilized semi-discrete Eulerian FEMs for the advection equation (3.1) can also be obtained and they are listed in Table 3.6.

Table 3.6 Expressions for the spectral function $z(\omega)$

Schemes	$z(\omega)$
PG	$\frac{2[2+\cos(\omega h)] - 6\alpha_P Cr(1-\theta)[1-\cos(\omega h)] - i3[2Cr(1-\theta)+\alpha_P]\sin(\omega h)}{2[2+\cos(\omega h)] + 6\alpha_P Cr\theta[1-\cos(\omega h)] + i3(2Cr\theta-\alpha_P)\sin(\omega h)}$
TG2	$\frac{[2+\cos(\omega h)] - 3Cr^2(1-\theta)\,[1-\cos(\omega h)] - i3Cr(1-\theta)\sin(\omega h)}{[2+\cos(\omega h)] + 3Cr^2\theta\,[1-\cos(\omega h)] + i3Cr\theta\sin(\omega h)}$
TG3	$\frac{-[2+\cos(\omega h)] + Cr^2(2-3\theta)\,[1-\cos(\omega h)] + i3Cr(1-\theta)\sin(\omega h)}{-[2+\cos(\omega h)] - Cr^2(1+3\theta)\,[1-\cos(\omega h)] - i3Cr\theta\sin(\omega h)}$
LS	$\frac{[2+\cos(\omega h)] - 6Cr^2\theta(1-\theta)\,[1-\cos(\omega h)] - i3Cr\sin(\omega h)}{[2+\cos(\omega h)] + 6Cr^2\theta^2\,[1-\cos(\omega h)]}$

3.4 Algorithmic Amplitudes and Relative Phase Velocities

From (3.25), the following relationship can be derived

$$\zeta^h e^{-i\Omega^h \Delta t} = z(\omega) \tag{3.30}$$

which implies that the algorithmic amplitude and the wave frequency can be defined as follows:

$$\zeta^h = |z(\omega)| \tag{3.31}$$

$$\Omega^h = -\frac{\arg(z(\omega))}{\Delta t} \tag{3.32}$$

The phase velocity of the numerical scheme in (3.22) can be obtained from (3.32) as

$$v^* = \frac{\Omega^h}{\omega} = -\frac{\arg(z(\omega))}{\omega \Delta t} \tag{3.33}$$

With the consideration of $z(\omega)$ defined by (3.29), the algorithmic amplitude and the relative phase velocity of the MLS scheme can be expressed as

$$\zeta^h = |z(\omega)| = \frac{\sqrt{[2+\cos(\omega h) - 6\alpha Cr^2\theta(1-\theta)(1-\cos(\omega h))]^2 + 9Cr^2\sin^2(\omega h)}}{2+\cos(\omega h) + 6\alpha Cr^2\theta^2(1-\cos(\omega h))} \tag{3.34a}$$

$$\frac{v^*}{v} = -\frac{\arg(z(\omega))}{\omega v \Delta t} = \frac{1}{Cr\,\omega h}\arctan\left(\frac{3Cr\sin(\omega h)}{2+\cos(\omega h) - 6\alpha Cr^2\theta(1-\theta)(1-\cos(\omega h))}\right) \tag{3.34b}$$

Expanding (3.34) in terms of ωh gives

$$\begin{aligned}\zeta^h &= 1 + \frac{1}{2}Cr^2(1-2\alpha\theta)(\omega h)^2 \\ &\quad - \frac{1}{24}Cr^2[2\alpha\theta + 3Cr^2(1-4\alpha\theta(1-2\theta) - 8\alpha^2\theta^3)](\omega h)^4 + O\left((\omega h)^6\right)\end{aligned} \tag{3.35a}$$

$$\begin{aligned}\frac{v^*}{v} &= 1 - \frac{1}{3}\mathrm{Cr}^2[1-3\alpha\theta(1-\theta)](\omega h)^2 + \frac{1}{180}[-1+15\alpha Cr^2\theta(1-\theta) \\ &\quad + 36Cr^4(1-5\alpha\theta(1-\theta) + 5\alpha^2\theta^2(1-\theta)^2)](\omega h)^4 + O\left((\omega h)^6\right)\end{aligned} \tag{3.35b}$$

Following the same procedure, the expressions for the algorithmic amplitudes and the relative phase velocities of the PG, TG2, TG3 and LS schemes for the advection equation (3.1) with the application of the trapezoidal rule can be obtained, and their expansions in terms of the dimensionless wave number ωh are given in Table 3.7 and Table 3.8, respectively. From these expansions and equation (3.35), it is noted that the accuracy (compared to unity) of the algorithmic amplitudes and the phase velocities of the PG, TG2, TG3, LS and MLS schemes depends on the Courant number Cr and the time weighting θ. The upwind parameters α_p and α can also influence the numerical performance of PG and MLS schemes, and theoretically they can be determined such that the numerical schemes have a higher accuracy in the algorithmic amplitude and the phase velocity.

Table 3.7 Expansions of ζ^h in terms of ωh (with trapezoidal rule)

Schemes	$\zeta^h = \lvert z(\omega) \rvert$
PG	$1+\frac{1}{2}Cr^2(1-2\theta)(\omega h)^2+[Cr^4(\theta^3-\theta^2+\frac{\theta}{2}-\frac{1}{8})-\frac{\alpha_P Cr}{24}](\omega h)^4+O((\omega h)^6)$
TG2	$1-Cr^2\theta(\omega h)^2+\frac{1}{24}Cr^2[-1+3Cr^2(1-2\theta+4\theta^2+8\theta^3)](\omega h)^4+O((\omega h)^6)$
TG3	$1-Cr^2\theta(\omega h)^2+\frac{1}{24}Cr^2[-1+Cr^2(1+2\theta+12\theta^2+24\theta^3)](\omega h)^4+O((\omega h)^6)$
LS	$1+\frac{1}{2}Cr^2(1-2\theta)(\omega h)^2+[Cr^4(\theta^3-\theta^2+\frac{\theta}{2}-\frac{1}{8})-\frac{1}{12}Cr^2\,\theta](\omega h)^4+O((\omega h)^6)$

Table 3.8 Expansions of v^*/v in terms of ωh (with trapezoidal rule)

Schemes	$\frac{v^*}{v}=-\frac{\arg(z(\omega))}{\omega v\Delta t}$
PG	$1-\frac{1}{3}Cr^2(1-3\theta+3\theta^2)(\omega h)^2+[\frac{1}{720}(15\alpha_P^2-4)+\frac{\alpha_P Cr}{24}(1-2\theta)$ $+Cr^4(\frac{1}{5}-\theta+2\theta^2-2\theta^2+\theta^4))(\omega h)^4+O((\omega h)^6)$
TG2	$1-\frac{1}{6}Cr^2(-1+6\theta^2)(\omega h)^2+[-\frac{1}{180}+\frac{1}{24}Cr^2(1-2\theta)$ $+\frac{1}{20}Cr^4(-1+5\theta-5\theta^2+20\theta^4))(\omega h)^4+O((\omega h)^6)$
TG3	$1-Cr^2\theta^2(\omega h)^2+\frac{1}{180}[-1+5Cr^2(1-3\theta)$ $+Cr^4(-4+15\theta+45\theta^2+180\theta^4))(\omega h)^4+O((\omega h)^6)$
LS	$1-\frac{1}{3}Cr^2(1-3\theta+3\theta^2)(\omega h)^2+[-\frac{1}{180}+\frac{1}{12}Cr^2\theta(1-\theta)$ $+Cr^4(\frac{1}{5}-\theta+2\theta^2-2\theta^2+\theta^4))(\omega h)^4+O((\omega h)^6)$

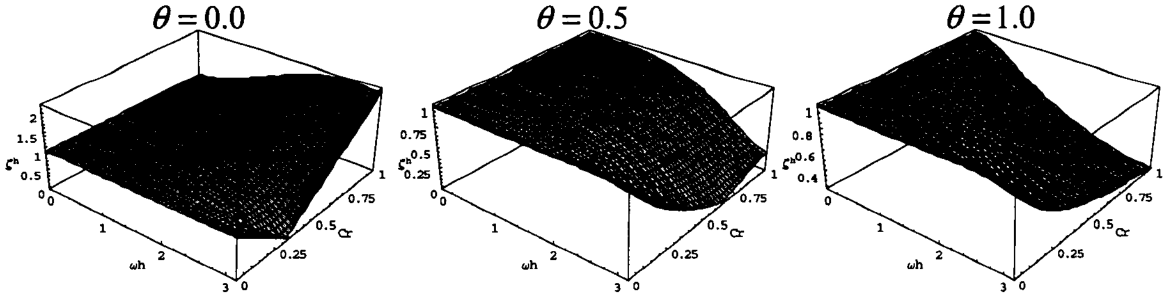

(a) PG

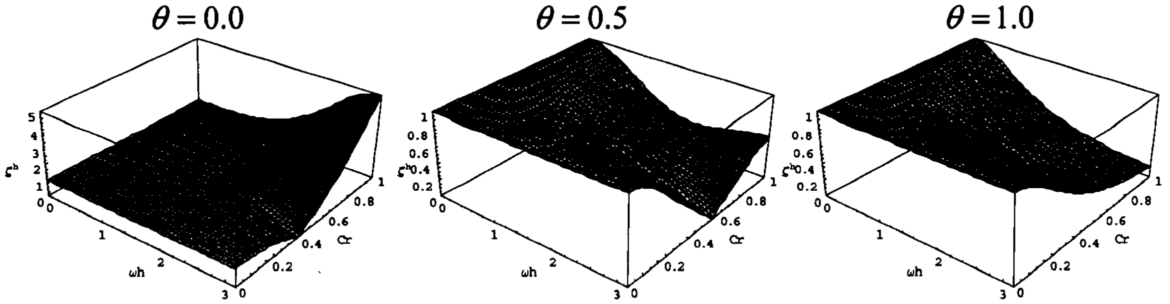

(b) TG2

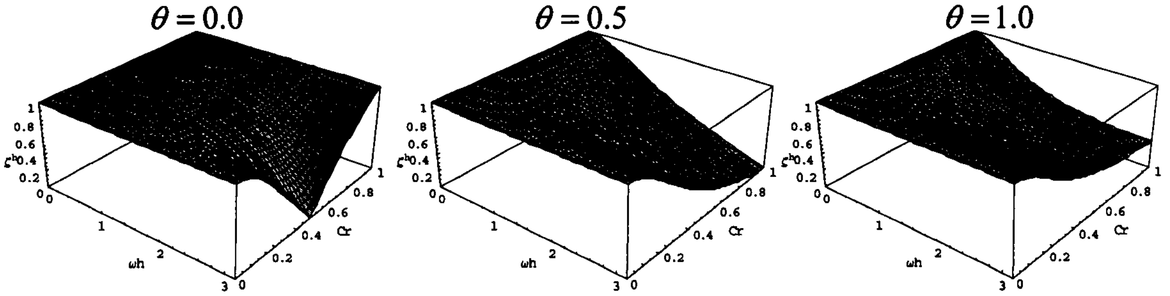

(c) TG3

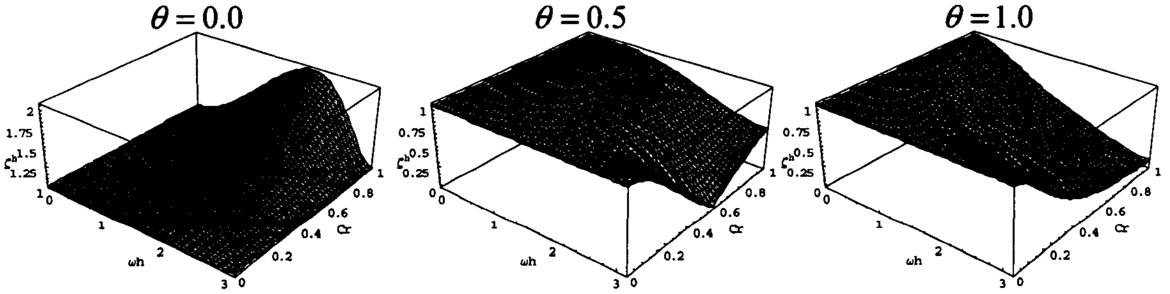

(d) LS

Figure 3.6 Distributions of the algorithmic amplitudes of the stabilized semi-discrete Eulerian FEMs with different time weightings

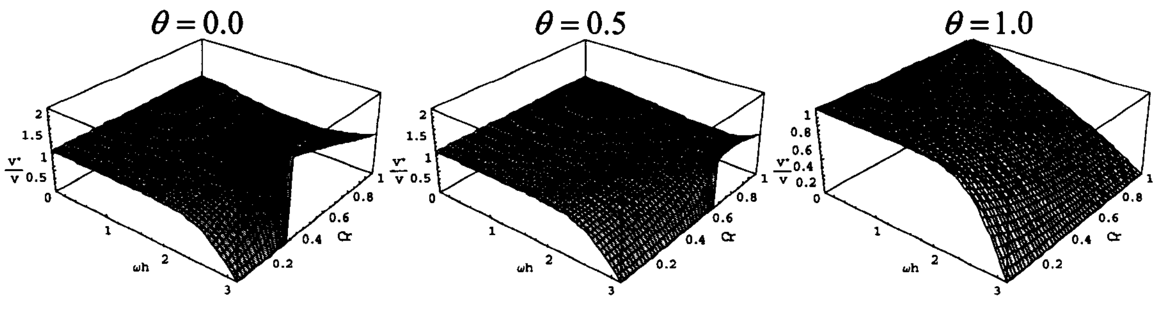

(a) PG

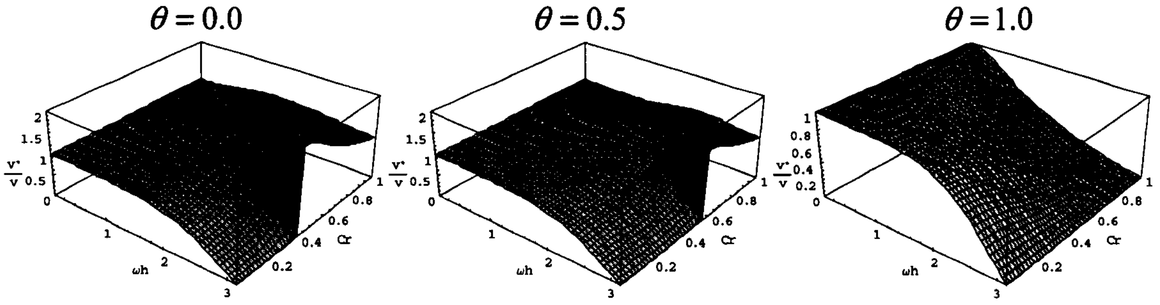

(b) TG2

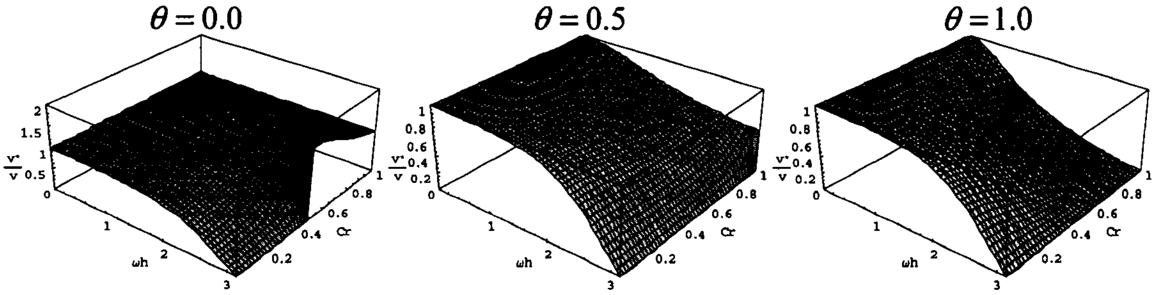

(c) TG3

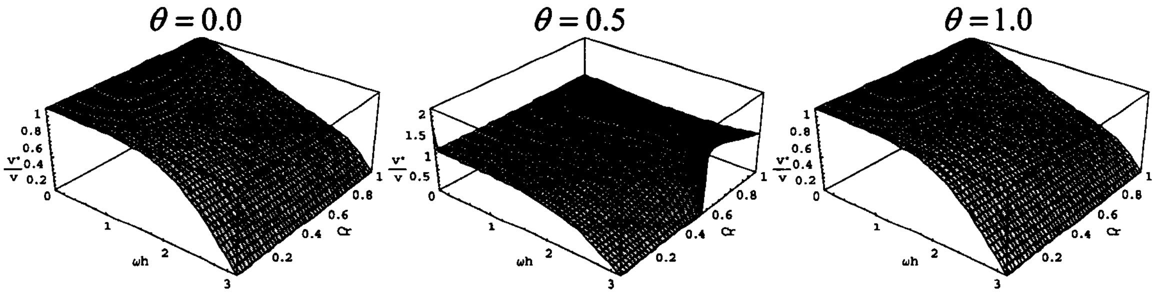

(d) LS

Figure 3.7 Distributions of the relative phase velocities of the stabilized semi-discrete Eulerian FEMs with different time weightings

Figures 3.6 and 3.7 shows, respectively, the distributions of the algorithmic amplitudes and relative phase velocities of PG (with $\alpha_P = 1/\sqrt{15}$), TG2, TG3 and LS (or MLS with $\alpha = 1$) schemes for the advection equation (3.1) with different time weighting over the plane of Courant numbers vs. dimensionless wave number. It is implied from the Figures 3.6 and 3.7 that these four stabilized semi-discrete schemes will have different numerical performances for the advection equation using different time integrations. All the schemes satisfy the von Neumann stabilization condition (i.e. $|z(\omega)| < 1$) when $\theta \geq 0.5$; but when $\theta = 0$, the corresponding explicit PG, TG2 and LS schemes become unstable since $|z(\omega)| \geq 1$ for certain values of the dimensionless wave numbers ωh.

3.5 α and θ in the MLS Scheme

The introduction of the upwind parameter α in the MLS scheme provides an opportunity to improve the numerical behaviour of the scheme for the advection equation (3.1). It is shown from (3.35) that the accuracy of the algorithmic amplitude ζ^h and the relative phase velocity v^*/v can reach at least the 4th order in terms of ωh if α and θ satisfy the following criteria

$$\begin{cases} 1 - 2\alpha\theta = 0 \\ 1 - 3\alpha\theta(1-\theta) = 0 \end{cases} \tag{3.36}$$

which implies that

$$\begin{cases} \alpha = 3/2 \\ \theta = 1/3 \end{cases} \tag{3.37}$$

Figure 3.8 shows the distribution, over the plane of ωh vs. Cr, of ζ^h and v^*/v of the MLS scheme with the values of α and θ defined by (3.37).

It is noted from Figure 3.8 that when $Cr = 1$, both the algorithmic amplitude and the relative phase velocity of the MLS scheme are equal to unity for all the dimensionless wave numbers. In fact, keeping $Cr = 1$ and substituting (3.37) into (3.34) results in

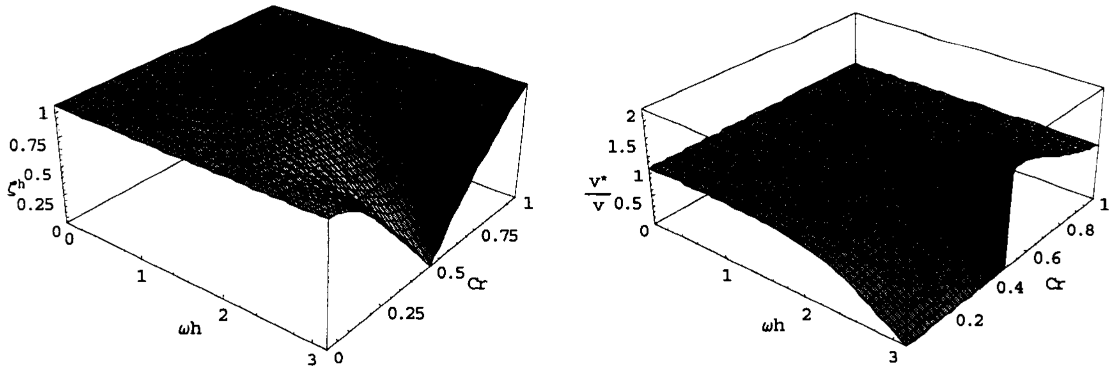

(a) (b)

Figure 3.8 Distributions of (a) the algorithmic amplitude and (b) the relative phase velocity of the MLS scheme with $\alpha = 3/2$ and $\theta = 1/3$ for the advection equation over the plane of ωh vs. Cr

$$\zeta^h\Big|_{\alpha=\frac{3}{2},\theta=\frac{1}{3},Cr=1} = 1 \tag{3.38a}$$

$$\frac{v^*}{v}\Bigg|_{\alpha=\frac{3}{2},\theta=\frac{1}{3},Cr=1} = 1 \tag{3.38b}$$

It should also be noted from (3.34b) that, even under the condition of $Cr = 1/2$ and with the values of α and θ defined by (3.37), $v^* = v$, i.e.

$$\frac{v^*}{v}\Bigg|_{\alpha=\frac{3}{2},\theta=\frac{1}{3},Cr=\frac{1}{2}} = 1 \tag{3.39}$$

It follows from (3.38) that for $Cr = 1$ and α and θ determined by (3.37), there are no errors in the algorithmic amplitude and the phase velocity of the MLS scheme for all ωh, and therefore all wave components included in the solution obtained from the MLS scheme will travel at the same speed without shape distortion. Consequently, the MLS scheme with α and θ determined by (3.37) can generate an accurate solution for the advection equation when Cr is kept equal to unity. This conclusion is confirmed by the numerical computation presented in the ensuing section.

3.6 Numerical Analyses

In this section, an advective transport problem with a constant flow velocity $v = 0.5 m/s$ in a one-dimensional region of $V = [0, 30m]$ is considered. The computational domain is discretized into 60 elements with identical element size of $h = 0.5m$. The initial condition for the concentration is set equal to zero everywhere in the domain, and the transport problem is subject to boundary conditions $C(0,t) = 1$ and $C_x(30,t) = 0$ at the left and right sides of the domain respectively. The PG scheme with $\alpha_P = 1/\sqrt{15}$ and $\theta = 1/2$, and the MLS scheme with $\alpha = 3/2$ and $\theta = 1/3$ are used to simulate the above one-dimensional transport problem. Two time steps are chosen such that the Courant number is equal to ½ and 1, corresponding to the mesh size and the magnitude of the flow velocity. Figures 3.9 and 3.10 illustrate the computational results over the plane of the space vs. time obtained from the PG and MLS schemes respectively, corresponding to two different Courant number conditions, i.e. $Cr = 1/2$ and $Cr = 1$. It is evident that the PG method introduces oscillations in the vicinity of the discontinuity involved in the solution for both Courant number conditions. Although the MLS scheme introduces oscillations in the vicinity of the discontinuity of the solution for $Cr = 1/2$, it can generate an accurate solution for the advective transport or a step wave under the condition of $Cr = 1$ because of (3.38). Based on this observation, it can be concluded that either a time-adaptive or mesh-adaptive procedure should be coupled with the MLS scheme for the accurate solution of the advective transport problem with the transient flow velocity, in which the time step or the mesh size is automatically selected in terms of the Courant number criterion of $Cr = 1$. This will be discussed in the chapter that follows.

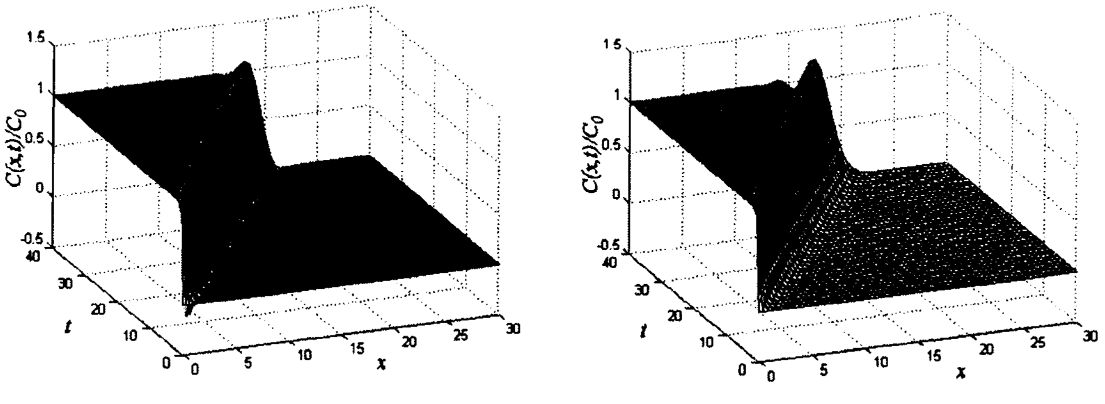

(a) (b)

Figure 3.9 Computational results for the one-dimensional advective transport problem obtained from the PG method with $\alpha_p = 2/\sqrt{15}$ and $\theta = 1/2$ under different Courant number conditions, (a) $\Delta t = 0.5s$, $Cr = 0.5$ and (b) $\Delta t = 1.0s$, $Cr = 1.0$

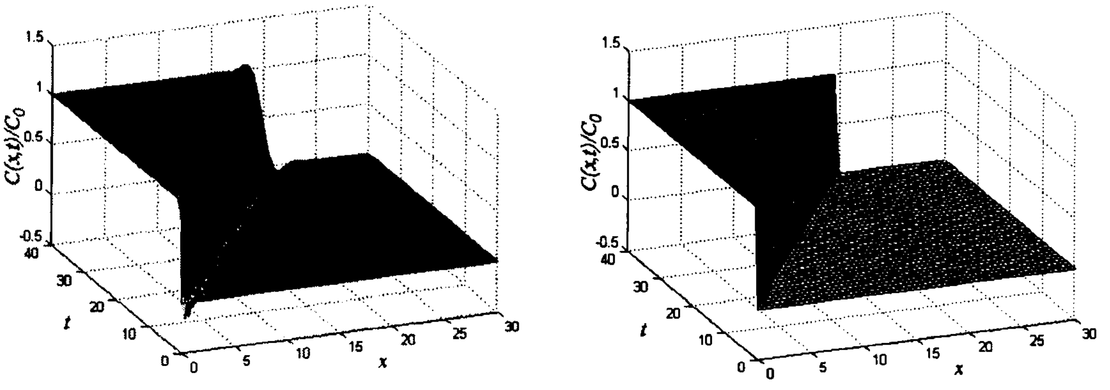

(a) (b)

Figure 3.10 Computational results for the one-dimensional advective transport problem obtained from the MLS method with $\alpha = 3/2$ and $\theta = 1/3$ under different Courant number conditions, (a) $\Delta t = 0.5s$, $Cr = 0.5$ and (b) $\Delta t = 1.0s$, $Cr = 1.0$

3.7 Discussion

In this chapter, a Fourier analysis was used to assess several stabilized semi-discrete Eulerian FEMs for the advection equation. From these assessments it is shown that the Modified Least Squares scheme with time weighting and upwind parameters defined by (3.37) can generate an accurate numerical solution for the advection equation, with the solution containing a discontinuity, under the Courant number condition of $Cr = 1$. This conclusion is substantiated through a numerical computation conducted at the end of this chapter. The numerical advantage of the MLS scheme can be extended with the application of a time-adaptive procedure for the accurate solution of the transport process with a transient flow velocity, which will be discussed in the ensuing chapter. Several issues related to the Fourier analysis carried out in this chapter, however, need to be discussed:

(i) Although the error of the phase velocity of the MLS scheme with α and θ defined by (3.37) is zero for all dimensionless wave numbers when $Cr = 1/2$, the deviation of the algorithmic amplitude from unity will also lead to oscillations in the numerical solution for the advection equation, especially in the vicinity of a discontinuity in the solution. This phenomenon was observed through the numerical computation.

(ii) It should be noted that the expression of the spectral function $z(\omega)$ in the MLS scheme given in (3.29) with α and θ defined by (3.37) is identical to the expression of $z(\omega)$ for the TG3 method shown in Table 3.6 with $\theta = 0$, and both have the following expression

$$z(\omega) = \frac{[2+\cos(\omega h)] - 2Cr^2\,[1-\cos(\omega h)] - i3Cr\sin(\omega h)}{[2+\cos(\omega h)] + Cr^2\,[1-\cos(\omega h)]} \tag{3.40}$$

It implies that the MLS scheme with α and θ defined by (3.37) and the explicit TG3 scheme have the same distributions of the algorithmic amplitude and the phase velocity over the plane of Courant number and dimensionless wave number. Therefore, both schemes can generate an accurate solution for the advection equation.

(iii) Although an upwind parameter is also introduced in the PG scheme, it is shown, from the expansion expression shown in Table 3.8, that the phase velocity of the PG method can only reach 2nd order accuracy in terms of the dimensionless wave number for all possible values of α and θ, and the same result can be obtained with the LS scheme.

(iv) Comparing the integral form (3.2) and the upwind functions given in Table 3.1, it should be noted that the different numerical performances between the PG and LS schemes and the TG3 and MLS schemes might result from their different formations for the advection equation. The former two schemes use the same weighting function for the temporal and spatial derivatives of the advection equation, while the latter two schemes use different weighting functions for temporal and spatial derivatives of the advection equation. More effort should be done in the future to discover a general conclusion or structure for the stabilized methods that can generate accurate solutions for the advection equation.

CHAPTER 4

TIME-ADAPTIVE SCHEME FOR THE TRANSPORT WITH PRESSURE TRANSIENTS

It has been shown from the Fourier analysis conducted in Chapter 3 that the Courant number has a significant influence on the numerical performance of stabilized semi-discrete Eulerian schemes for the advection equation. With a Courant number criterion of $Cr = 1$, the Modified Least Squares (MLS) scheme with a specific upwind function and time weighting, i.e. $\alpha = 3/2$ and $\theta = 1/3$, can generate an oscillation-free and non-diffusive numerical solution for the advection equation. This indicates that a time-adaptive procedure can be used in conjunction with the MLS scheme for the accurate solution of the advection-dominated transport process involving transient flow velocities. In this chapter, such a time-adaptive MLS scheme is proposed and will be used for accurately modelling the advective transport in a one-dimensional porous domain; here, the time-dependent flow velocity is induced by the pore pressure transient described by the piezo-conduction equation that accounts for the compressibility characteristics of the system. However, a Fourier analysis conducted in this chapter will show that this numerical advantage of the MLS scheme for the advection equation does not hold true for the advection-dispersion equation. In this case, it is necessary to use the operator-splitting technique with the MLS scheme for advection-dominated transport problems. Therefore, we develop a time-adaptive operator-splitting computational scheme in this chapter to simulate an advection-dominated transport process of the contaminant from a cavity in a spherically symmetric, fully saturated porous medium. In this numerical modelling, an infinite element is used for solving the piezo-conduction equation to obtain the accurate distribution of pressure potential, which is governed by the potential condition on the cavity boundary and the regularity condition at infinity of the porous region.

4.1 The Courant Number and the Time-Adaptive Scheme

The numerical demonstration at the end of the previous chapter showed that the MLS scheme, with $\alpha = 3/2$ and $\theta = 1/3$, can give an accurate numerical solution (in the sense that there is no artificial diffusion or oscillation in the solution) of the one-dimensional advective transport process with a constant flow velocity under the Courant number condition $Cr = 1$. Combining this with a time-adaptive and/or a mesh adaptive procedure, the numerical advantage can be extended to model advective transport with a transient flow velocity. In such adaptive procedures, the time step or the elemental size, in a location with a high gradient or the discontinuity of the solution, should be determined using the following Courant number criterion, based on the magnitude of the flow velocity and characteristic length of the element:

$$(Cr)_{ie} = \frac{|v|_{ie} \Delta t}{h_{ie}} = 1 \tag{4.1}$$

where Δt is the time step; *ie* indicates the elements where the high gradient or the discontinuity of the solution is located; h_{ie} and $|v|_{ie}$ are, respectively, the characteristic length and the magnitude of the flow velocity of the element.

For the purpose of validation, the time-adaptive MLS scheme is first used to model the advective transport process with the following time decaying flow velocity

$$v = v_0 \exp(-\frac{k}{l} t) \tag{4.2}$$

where k is the Dupuit-Forchheimer hydraulic conductivity related to the conventional area averaged hydraulic conductivity $\tilde{k}$ by the relation $k = \tilde{k}/n^*$ and n^* is the porosity, l is the length parameter corresponding to the size of the domain. The decaying flow velocity (4.2) can be induced by the exponential decay in the flow potential boundary condition. Figure 4.1 shows the computational results for such an advective transport problem with $k = 0.03m/day$, $l = 30m$ and $v_0 = 0.5m/s$ obtained using the MLS scheme both with and without the time-adaptive procedure. The initial time step is chosen as $\Delta t = 1.0s$ such that $Cr = 1$ at the start of the transport process. By introducing a time-adaptive procedure, which satisfies the Courant number criterion (4.1) in the element near the location of the steep front of the solution during the computations, the MLS scheme generates an accurate solution to advective transport process with the decaying flow velocity given in (4.2). Without a time-adaptive feature, the MLS scheme gradually introduces oscillations in the vicinity of the discontinuity of the solution, due to the deviation of the Courant number from unity, resulting from the decay of the flow velocity.

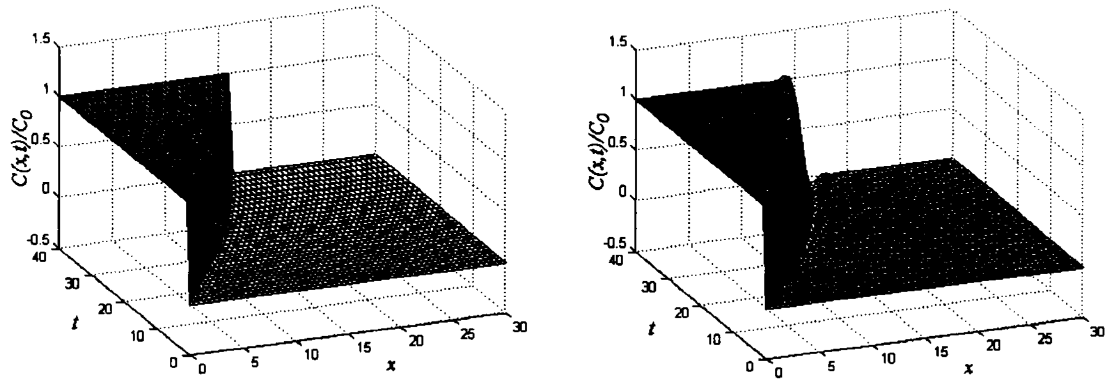

(a) (b)

Figure 4.1 Computational results for the one-dimensional advective transport problem with the exponential decaying flow velocity obtained using the MLS scheme, (a) with the time-adaptive procedure and (b) without the time-adaptive procedure

4.2 The One-Dimensional Advective Transport

4.2.1 Governing Equations

In this section, the time-adaptive MLS scheme is used to model the one-dimensional advective transport problem of a chemical species in a fluid-saturated porous medium. The advective flow velocity in the porous medium is governed by Darcy's law, which for an isotropic porous medium is expressed by

$$v = -k\frac{\partial \phi}{\partial x} \tag{4.3}$$

where k is the Dupuit-Forchheimer hydraulic conductivity, ϕ is the hydraulic potential inducing flow, which consists of the datum potential ϕ_D and the pressure potential ϕ_p, i.e. $\phi = \phi_D + \phi_p$. For a constant datum potential, the temporal and spatial distribution of the hydraulic pressure potential in the linear elastic deformable porous medium can be determined by the theory of poroelasticity developed by Biot (1941) (see also Lewis and Schrefler, 1998). However, with the small volumetric deformation of the porous skeleton, the coupled behaviour between the deformation of the porous medium and the pore fluid can be simplified by the piezo-conduction equation (Barenblatt et al., 1990; Selvadurai, 2000a, b; 2002b). Considering the compressibilities of the pore fluid and the porous skeleton, as well as the mass conservation during the flow, the PDE governing the one-dimensional advective flow potential can be reduced to the following classical piezo-conduction equation for ϕ_p

$$D_p \frac{\partial^2 \phi_p}{\partial x^2} = \frac{\partial \phi_p}{\partial t} \tag{4.4}$$

subject, respectively, to the boundary condition and the regularity condition

$$\phi_p(0,t) = \phi_0 \mathrm{H}(t)\,;\; \phi_p(\infty,t) \to 0 \tag{4.5}$$

as well as the initial condition

$$\phi_p(x,0) = 0\,;\; x \in [0,\infty) \tag{4.6}$$

In (4.5), $\mathrm{H}(t)$ is the Heaviside step function, ϕ_0 is a constant. This reduction is equivalent to assuming that the pressure head is much higher than the datum head. It also should be noted that for the purpose of examining the pressure transient, the domain is assumed to be semi-infinite. The pressure diffusion coefficient D_p in (4.4) is given by

$$D_p = \frac{k}{S_s} = \frac{k}{\gamma_w[n^* \kappa_f + \kappa_s]} \tag{4.7}$$

where S_s is referred to as the specific storage of the porous system, κ_f is the compressibility of the pore fluid and κ_s is the compressibility of the porous skeleton.

Also, consideration of mass conservation of the chemical within a control volume gives the following continuity equation for the advective transport process:

$$\frac{\partial C}{\partial t}+v\frac{\partial C}{\partial x}+C\frac{\partial v}{\partial x}=0 \tag{4.8}$$

The third term on the LHS of (4.8) is non-zero if the fluid is considered to be compressible. It is evident that the governing PDEs (4.4) and (4.8) are weakly coupled, in the sense that the velocity field is assumed to be uninfluenced by the chemical transport process. The appropriate solution applicable to the diffusion problem (4.4) can be obtained in exact closed form through the consideration of Laplace transform techniques (Selvadurai, 2000a). The resulting solution takes the form

$$\phi_p(x,t)=\phi_0 \operatorname{erfc}\left(\frac{x}{2\sqrt{D_p t}}\right) \tag{4.9}$$

where $\operatorname{erfc}(x)$ is the complimentary error function defined by

$$\operatorname{erfc}(x)=1-\frac{2}{\sqrt{\pi}}\int_0^x e^{-\zeta^2}d\zeta \tag{4.10}$$

From (4.3) and (4.9), the fluid velocity in the porous medium of semi-infinite extent can be expressed in the form

$$v(x,t)=-k\frac{\partial \phi_p}{\partial x}=k\phi_0\left(\frac{1}{\sqrt{\pi D_p t}}\exp\left(-\frac{x^2}{4D_p t}\right)\right) \tag{4.11}$$

Substituting (4.11) into (4.8) gives the PDE governing the advective transport process with the transient flow velocity as follows

$$\frac{\partial C}{\partial t}+k\phi_0\left(\frac{\exp\left(-\frac{x^2}{4D_p t}\right)}{\sqrt{\pi D_p t}}\right)\frac{\partial C}{\partial x}-k\phi_0\left(\frac{x\exp\left(-\frac{x^2}{4D_p t}\right)}{2\sqrt{\pi}(D_p t)^{3/2}}\right)C=0 \tag{4.12}$$

which is subject to the initial condition

$$C(x,0)=0 \quad ; \qquad x\in[0,\infty) \tag{4.13}$$

and the boundary condition

$$C(0,t)=C_0\mathrm{H}(t) \tag{4.14}$$

as well as the regularity condition

$$C(x,t)\to 0 \quad ; \qquad \text{as } x\to\infty \tag{4.15}$$

For the flow process to be transient, the compressibility of the pore fluid and/or the compressibility of the porous skeleton should be non-zero. In the absence of these compressibilities, the flow process is steady state and is governed by the Laplace's equation with the consequence that, for a solution to exist, the domain should be finite.

4.2.2 Numerical Computations

For the purpose of computation, an advective transport process in a semi-infinite region $(0,\infty)$ is considered in this section, which is subject to the flow potential boundary conditions of $\phi(0)=\phi_0$ and $\phi(\infty)=0$. The Dupuit-Forchheimer hydraulic conductivity of the porous medium is taken as $k=0.03m/day$. The porous aquifer material and the fluid are assumed to be compressible with the typical compressibility values of $\kappa_s=1.0\times10^{-8}$ m^2/N and $\kappa_f=4.4\times10^{-10}$ m^2/N (Freeze and Cherry, 1979)

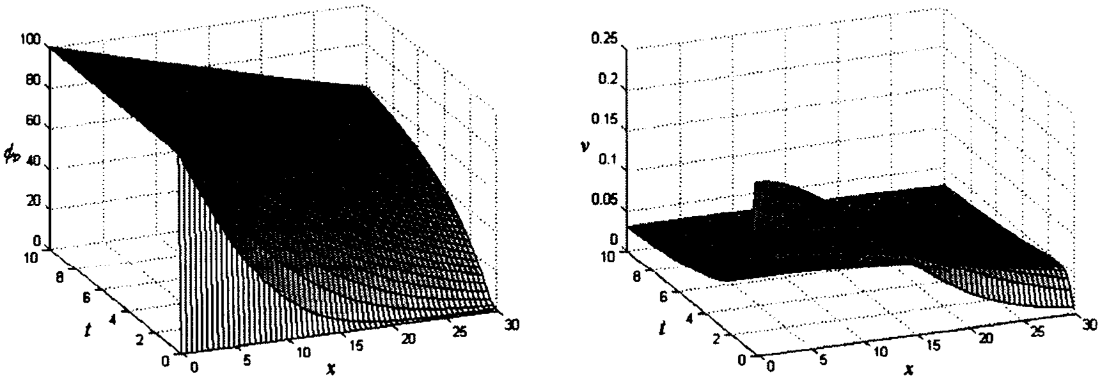

(a) (b)

Figure 4.2 Distributions of (a) the flow potential and (b) the flow velocity in the time-space region during a period of 10 days respectively, and the porosity is taken as $n^* = 0.3$. Using these values, the specific storage of the porous system is approximately equal to $S_s = 1.0 \times 10^{-8}\ m^2 / N$. We first assume that the advective transport is initiated by a constant flow potential $\phi_0 = 100\,m$ applied at the boundary $x = 0$. Figure 4.2 shows the distributions of the flow potential and the flow velocity over a finite region $V = [0,30m]$ obtained from analytical solutions (4.9) and (4.11) respectively, during a period of 10 days. It is noted from Figure 4.2 that the flow velocity varies to a large extent over the domain at the beginning of the transport process due to the large variations of the potential.

A finite domain of $V = [0,30m]$ is used for the finite element modelling of the advective transport process with the flow velocity shown in Figure 4.1, and the regularity condition at an infinite location is replaced with a Neumann boundary condition applied downstream of the domain. The finite domain is discretized into 300 elements and the MLS scheme, both with and without the time-adaptive procedure, is used to obtain computational estimates for the advective transport process. The corresponding numerical solutions are shown in Figure 4.3, and they indicate that without the time-adaptive procedure, the MLS scheme introduces oscillations into the solution due to the variations in the magnitude of the flow velocity. The time-adaptive MLS scheme, however, gives an

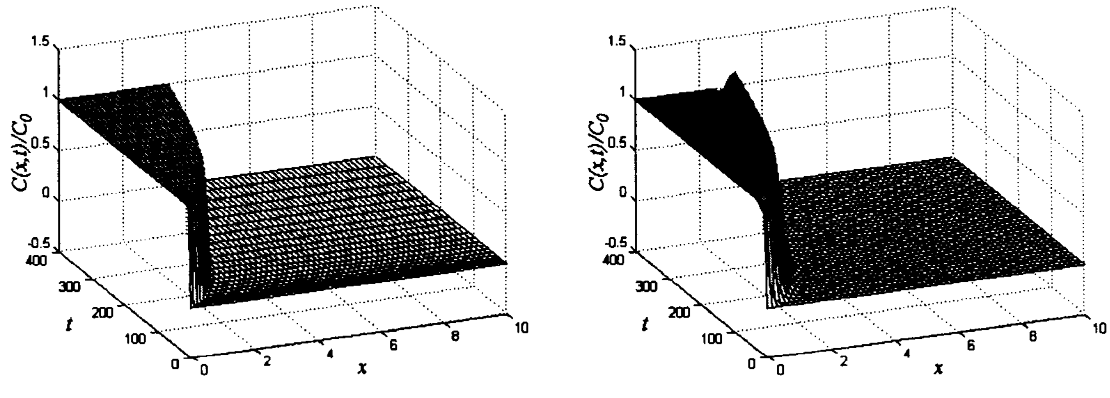

(a) (b)

Figure 4.3 Computational results during a period of 400 days for the advective transport with the transient advective flow velocity obtained from the MLS scheme (a) with the time-adaptive procedure and (b) without the time-adaptive procedure oscillation-free and non-diffusive computational solution for the advective transport with time-dependent flow velocity. Using the time-adaptive scheme, the initial time step of $\Delta t = 0.2\,days$ increases to $\Delta t = 33\,days$ at the end of the computation, in order to satisfy the constraint (4.1) imposed by the Courant number criterion.

In the remainder of this section, further transient characteristics of the flow potential, caused by the time-dependent boundary condition, are considered for above advective transport problem. Firstly, the flow potential boundary condition with an exponential

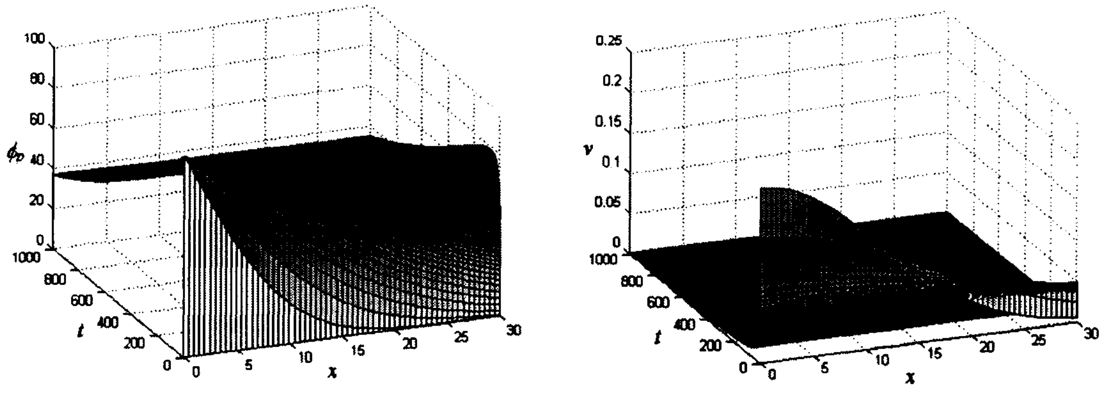

(a) (b)

Figure 4.4 Distributions of (a) the flow potential and (b) the flow velocity in the time-space region during a period of 1000 days corresponding to the decaying boundary potential

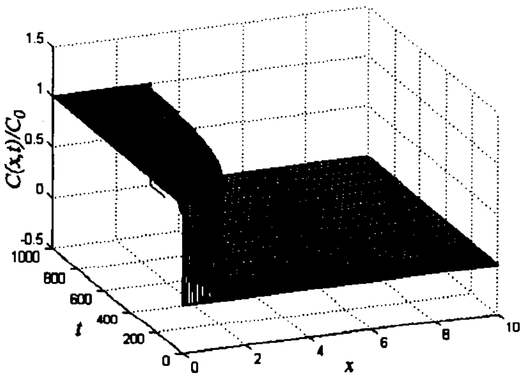

Figure 4.5 Computational results during a period of 1000 days for the advective transport with the transient flow velocity, obtained using the time-adaptive MLS scheme

decay in time is considered in the numerical computation using the time-adaptive scheme

$$\phi_0 = \phi^* \exp(-\frac{k}{l}t) \tag{4.16}$$

where $\phi^* = 100\,m$. This variation can approximate the chemical entry under a gravity flow. Figure 4.4 illustrates the distribution of the flow potential and the flow velocity over the domain during a 1000-day period. It should be noted that the flow velocity decays to almost zero after 500 days. Figure 4.5 illustrates the numerical results within a finite region of $[0,10m]$ obtained from the time-adaptive MLS method using 100 elements. The initial time step of $\Delta t = 5\,days$ increases to $\Delta t = 647\,days$ due to the variation of the flow velocity at the location of the steep front of the solution, which implies that the chemical will migrate only $0.1m$ (element length) within 647 days. It should also be noted that the advective transport process of the contaminant almost stops due to low flow velocity.

Next, a decaying boundary flow potential with a pulse is considered in the numerical computation, which is defined by the following time-dependent potential history:

$$\phi_0 = \begin{cases} \phi^* \exp(-\frac{k}{l}t), & t \le 500days \\ \phi^* \exp[-\frac{k}{l}(t-500)], & t > 500days \end{cases} \tag{4.17}$$

Figure 4.6 illustrates the distribution of the flow potential and the flow velocity over the finite domain V for a duration of 1000 days. Figure 4.7 shows the corresponding numerical results within the finite region of $[0,10m]$, obtained using the time-adaptive MLS scheme with 100 elements. Again, with the time-adaptive procedure that satisfies the Courant number criterion (4.1), the initial time step of $\Delta t = 5\,days$ increases to $\Delta t = 142\,days$ at the end of the computation due to the decay of the flow velocity. It should be noted from the numerical results shown in Figure 4.7 that the advective transport process of a contaminant in the porous medium is accelerated at t=500*days* resulting from the application of a pulse in the flow boundary potential.

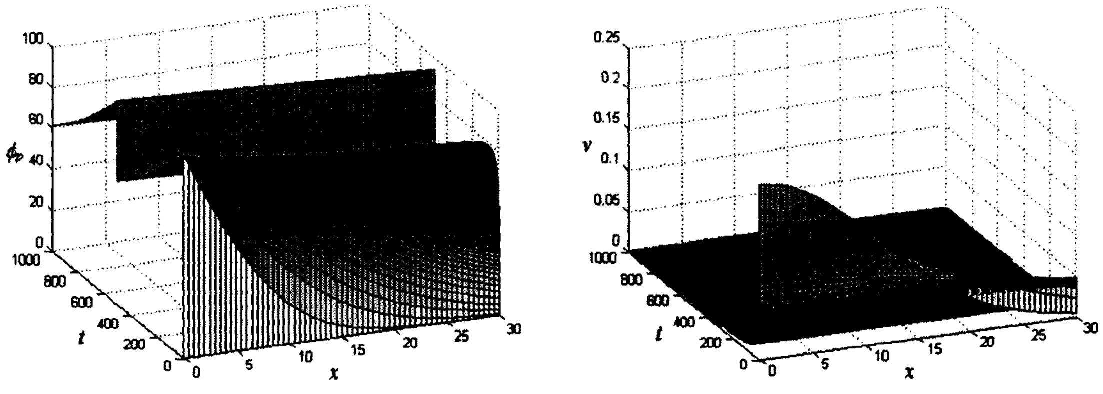

(a) (b)

Figure 4.6 Distributions of (a) the flow potential and (b) the flow velocity in the time-space region during a period of 1000 days corresponding to the decaying boundary potential with a pulse

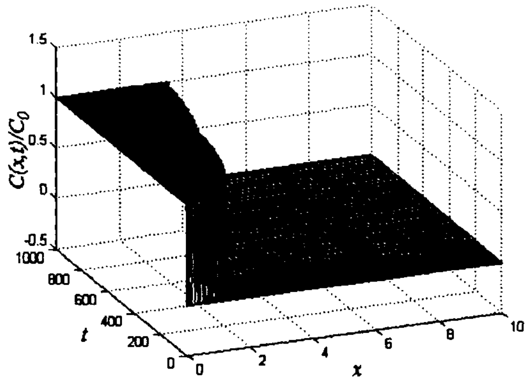

Figure 4.7 Computational results during a period of 1000 days for the advective transport with the transient flow velocity determined by the decaying boundary potential with a pulse, obtained using the time-adaptive MLS scheme

4.3 Rationale for the Operator Splitting Technique

It is shown from the numerical computations in the previous section that the time-adaptive MLS scheme with $\alpha = 3/2$ and $\theta = 1/3$ can give an accurate solution for the advective transport with transient flow velocities. As indicated in Chapter 1, however, the transport of contaminants in porous media involves complex processes, which usually include advection, hydrodynamic dispersion and chemical reaction etc. For such situations, the classical one-dimensional advection-dispersion equation (4.8) takes on the form including advection, dispersion and reaction terms, i.e.

$$\frac{\partial C}{\partial t}+\frac{\partial (vC)}{\partial x}-D\frac{\partial^2 C}{\partial x^2}+rC=0 \tag{4.18}$$

where D is the hydrodynamic dispersion coefficient and r is a first-order decay coefficient. Applying the MLS scheme to the advection-dispersion-reaction equation (4.18) leads to the following weighted residual integral form over a one-dimensional region $[0,l]$

$$\begin{aligned}&\int_0^l [w+\theta\Delta t r w]\left[\frac{C^{n+1}-C^n}{\Delta t}+v\frac{\partial C^{n+\theta}}{\partial x}-D\frac{\partial^2 C^{n+\theta}}{\partial x^2}+rC^{n+\theta}\right]\mathrm{d}x\\&+\int_0^l \theta\Delta t v\frac{\mathrm{d}w}{\mathrm{d}x}\left[\frac{C^{n+1}-C^n}{\Delta t}-D\frac{\partial^2 C^{n+\theta}}{\partial x^2}+rC^{n+\theta}\right]\mathrm{d}x+\int_0^l \alpha\theta\Delta t v\frac{\mathrm{d}w}{\mathrm{d}x}v\frac{\partial C^{n+\theta}}{\partial x}\mathrm{d}x=0\end{aligned} \tag{4.19}$$

The introduction of the upwind parameter α in (4.19) ensures consistency with the MLS formulation for the purely advection equation. When $\alpha=1$, the integral form (4.19) will correspond to the LS scheme. The finite difference stencil corresponding to the integral form (4.19), with a piecewise linear element, can be written as

$$\begin{aligned}&(1+\theta\Delta t\, r)\frac{1}{6}(\dot{C}_{j-1}+4\dot{C}_j+\dot{C}_{j+1})+\frac{\theta v\Delta t}{2h}(\dot{C}_{j-1}-\dot{C}_{j+1})=\\&-\frac{v}{2h}(C_{j+1}^{n+\theta}-C_{j-1}^{n+\theta})+\left[(1+\theta\Delta t\, r)D+\alpha\theta\Delta t\, v^2\right]\frac{1}{h^2}(C_{j-1}^{n+\theta}-2C_j^{n+\theta}+C_{j+1}^{n+\theta})\\&-(1+\theta\Delta t\, r)r\frac{1}{6}(C_{j-1}^{n+\theta}+4C_j^{n+\theta}+C_{j+1}^{n+\theta})\end{aligned} \tag{4.20}$$

Following the procedure presented in Chapter 3, the spectral function $z(\omega)$ of the MLS scheme for the advection-dispersion-reaction equation (4.18), with the application of the forward Euler time integration scheme and the trapezoidal time rule, can be expressed in the following form

$$z(\omega)=\frac{1+(1-\theta)\Delta t\,A(\omega)}{1-\theta\Delta t\,A(\omega)}=\frac{-(1-\theta)(Cr)a_1+[1-(1-\theta)(Cr)(Da)]a_2-i(Cr)b_1}{\theta(Cr)a_1+(1+\theta(Cr)(Da))a_2} \tag{4.21}$$

where $A(\omega)$ is a spectral function of the finite spatial difference stencil described by (4.20) which can be expressed as

$$A(\omega) = -\frac{v}{h}\left[\frac{a_1 + (Da)a_2 + ib_1}{a_2 - i\theta(Cr)b_1}\right] \tag{4.22}$$

and

$$\begin{cases} a_1 = 6\left[(1 + \theta\, Cr\, Da)Pe^{-1} + \alpha\theta\, Cr\right]\left[1 - \cos(\omega h)\right] \\ a_2 = (1 + \theta\, Cr\, Da)\left[2 + \cos(\omega h)\right] \\ b_1 = 3\sin(\omega h) \end{cases} \tag{4.23}$$

In (4.21) and (4.22), $Cr = v\Delta t/h$ is the Courant number, $Pe = vh/D$ is the Péclet number and $Da = rh/v$ is the Damköhler number. The algorithmic amplitude and the relative phase velocity of the MLS scheme for the advection-dispersion-reaction equation (4.18) can be written in the expansion form in terms of the dimensionless wave number ωh as

$$\zeta^h = |z(\omega)| = \frac{c_1}{c_2} + \frac{Cr(Cr - 2Cr\theta c_1 \alpha - 2c_1 c_2 Pe^{-1})}{2c_1 c_2{}^3}(\omega h)^2 + O((\omega h)^4) \tag{4.24a}$$

$$\begin{aligned} \frac{v^*}{v} = \frac{1}{c_1 c_2} - \frac{Cr(Cr - 3\alpha c_1 c_2 Cr\theta(1-\theta) - 3Pe^{-1}c_1 c_2{}^2(1-\theta))}{3c_1{}^3 c_2{}^3}(\omega h)^2 \\ + O((\omega h)^4) \end{aligned} \tag{4.24b}$$

where

$$\begin{cases} c_1 = 1 - (1-\theta)Cr\, Da \\ c_2 = 1 + \theta\, Cr\, Da \end{cases} \tag{4.25}$$

It is evident from (4.24) and (4.25) that the algorithmic amplitude and phase velocity (and hence the numerical performance) of the MLS scheme for (4.18) are influenced by the Courant Number Cr, the Péclet number Pe and the Damköhler Number Da. In this case, it is impossible to choose the upwind function α and the time weighting θ such that $\zeta^h \equiv 1$ and $v^* \equiv v$ for all values of the dimensionless wave number ωh. Even for the advection-dispersion equation (i.e. $r = 0$ in (4.18)), the non-zero Péclet number will have an influence on the distribution of the algorithmic amplitude and the phase velocity of the MLS scheme. Such an influence will make it difficult to determine the optimal values of the upwind function and the time weighting involved in the semi-discrete MLS scheme. For example, with $Da = 0$ in (4.21), the spectral function $z(\omega)$ of the MLS scheme for the advection-dispersion equation becomes

$$z(\omega)=\frac{-6(1-\theta)Cr(Pe^{-1}+\alpha\theta\, Cr)(1-\cos(\omega h))+(2+\cos(\omega h))-i3Cr3\sin(\omega h)}{6\theta\, Cr(Pe^{-1}+\alpha\theta\, Cr)(1-\cos(\omega h))+(2+\cos(\omega h))} \qquad (4.26)$$

The corresponding algorithmic amplitude and relative phase velocity determined by (4.26) can be expressed as follows:

$$\zeta^h=\frac{\sqrt{[2+\cos(\omega h)-6Cr(1-\theta)(Pe^{-1}+\alpha Cr\theta)(1-\cos(\omega h))]^2+9Cr^2\sin^2(\omega h)}}{2+\cos(\omega h)+6\alpha Cr^2\theta^2(1-\cos(\omega h))} \qquad (4.27a)$$

$$\frac{v^*}{v}=\frac{1}{Cr\,\omega h}\arctan\left(\frac{3Cr\sin(\omega h)}{2+\cos(\omega h)-6Cr(1-\theta)(Pe^{-1}+\alpha Cr\theta)(1-\cos(\omega h))}\right) \qquad (4.27b)$$

Figure 4.8 shows the distributions of the algorithmic amplitude and the relative phase velocity of the MLS scheme with $\alpha=3/2$ and $\theta=1/3$ for the advection-dispersion equation with $Pe=50$ corresponding to Cr=1 in the region of $\omega h\in[0,\pi]$. It is shown from Figure 4.8 that $\zeta^h\equiv 1$ and $v^*/v\equiv 1$ are no longer satisfied for all $\omega h\in[0,\pi]$ under the condition of $Cr=1$. The fact that ζ^h is greater than unity for some ωh makes the numerical scheme unstable in the vicinity of the discontinuity or high gradient of the solution.

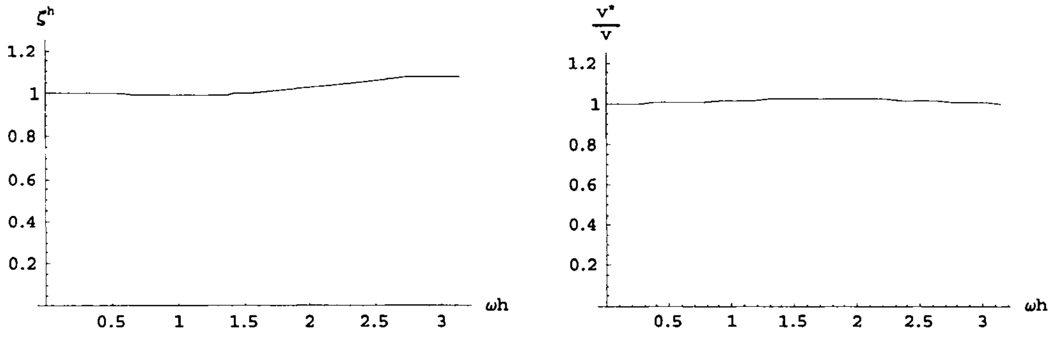

(a) (b)

Figure 4.8 Distributions of (a) the algorithmic amplitude and (b) the relative phase velocity of the MLS scheme for the advection equation corresponding to Cr=1

This phenomenon can be observed during the numerical computation of the advective-dispersive transport problem with a sharp front moving at a constant flow velocity v=0.5m/s and with a dispersion coefficient $D=0.005m^2/s$. The time step is set at

$\Delta t = 1.0s$, and consequently the Courant number is equal to unity everywhere in the domain. The computational domain is discretized with piecewise linear elements with length of $h = 0.5m$, resulting in $Pe = 50$. Figure 4.9 shows the numerical results of above advective-dispersive transport problem obtained from the MLS method. As expected, severe oscillations were introduced into the numerical solution near the sharp gradient of the dependent variable, and such oscillations increase as D increases. Figure 4.10 shows the distributions of the algorithmic amplitude of the MLS scheme for the advection-dispersion equation over the plane of ωh vs. Cr corresponding to the cases where $Pe = 50$ and $Pe = 5$. It can be seen from these distributions that the Courant number should be kept less than unity in order that the algorithmic amplitude is no greater than the value of unity required to ensure the stability of the numerical scheme. However, the fact that the algorithmic amplitude is smaller than unity implies that the artificial diffusion will be introduced by the numerical scheme.

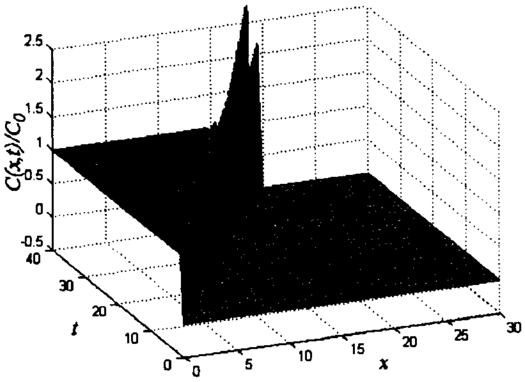

Figure 4.9 Numerical results for the advection-dispersion equation with a constant flow velocity v=0.5m/s and the dispersion coefficient $D = 0.005m^2 / s$, obtained from the MLS scheme corresponding to Courant number Cr=1

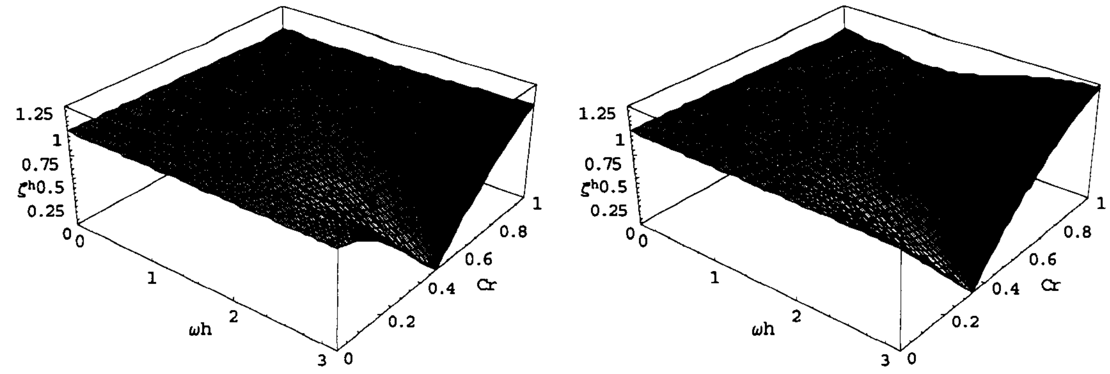

(a) (b)

Figure 4.10 Distributions of the algorithmic amplitude of the MLS scheme for the advection-dispersion equation over the plane of ωh vs. Cr corresponding to (a) Pe=50 and (b) Pe=5

In order to obtain an accurate solution for the advection-dominated transport problem, the *operator splitting* technique should be applied to separate the advection-dispersion equation into advection and dispersion parts based on the separate physical processes. In such operator splitting procedure, the approximation C^{n+1} of dependent variable C at $t=(n+1)\Delta t$ is solved in two sequent steps. First, an intermediate diffusive contribution C_d to the known approximation C^n of C at the time level $t=n\Delta t$ is determined by the following diffusion part

$$\begin{cases} \dfrac{\partial C_d}{\partial t} - D\dfrac{\partial^2 C_d}{\partial x^2} + \beta C_d = 0 \\ C_d^n = C^n \end{cases} \tag{4.28}$$

where $\beta = \dfrac{\partial v}{\partial x} + r$. Then such intermediate state C_d^{n+1} is used as the initial condition to determine the solution C^{n+1} containing the advective contribution, using the following advection part

$$\begin{cases} \dfrac{\partial C}{\partial t} + v\dfrac{\partial C}{\partial x} = 0 \\ C^n = C_d \end{cases} \tag{4.29}$$

The diffusion and advection parts are discretized with different numerical schemes based on their different mathematical natures (i.e. either parabolic or hyperbolic). The conventional Galerkin method is used to solve the diffusion part directly, and the time-adaptive semi-discrete MLS scheme is used to solve the advection part. In the section that follows, this operator splitting scheme will be used to compute the spherically symmetric advective dispersive transport in an infinite region.

4.4 Spherically Symmetric Transport in a Semi-Infinite Region

4.4.1 Governing Equations

In this section, we restrict attention to a practical advective-dispersive-reactive transport problem of a chemical species in an isotropic fluid-saturated porous region from a spherical cavity of radius of $a(a > 0)$ due to pressurization. Such transport problems can be encountered during deep geological disposal of chemical wastes in pressurized cavities terminating in small diameter boreholes (Figure 4.11). The PDE governing the spherically symmetric advection-dispersion-reaction in the fluid saturated porous medium is governed by

$$\frac{\partial C}{\partial t} + v_R \frac{\partial C}{\partial R} + C\left(\frac{\partial v_R}{\partial R} + \frac{2}{R} v_R\right) = D\nabla_R^2 C - rC \tag{4.30}$$

Figure 4.11 A schematic drawing of the contaminant transport from a spherical cavity for deep geological disposal of hazardous chemicals

with the initial condition

$$C(R,0)=0 \quad ; \qquad R\in[a,\infty) \tag{4.31}$$

and subject to the boundary condition

$$C(a,t)=C_0\mathrm{H}(t) \tag{4.32}$$

as well as the regularity condition

$$C(R,t)\to 0 \quad ; \qquad \text{as } R\to\infty \tag{4.33}$$

In (4.30), $\nabla_R^2=\dfrac{\partial^2}{\partial R^2}+\dfrac{2}{R}\dfrac{\partial}{\partial R}$, R is the radial coordinate and v_R is the radial flow velocity. The radial fluid flow is determined by the temporal and spatial distribution of the pressure potential ϕ_p governed by the spherically symmetric form of the piezo-conduction equation

$$D_p\left\{\frac{\partial^2\phi_p}{\partial R^2}+\frac{2}{R}\frac{\partial\phi_p}{\partial R}\right\}=\frac{\partial\phi_p}{\partial t} \tag{4.34}$$

subject, respectively, to the boundary condition and the regularity condition

$$\phi_p(a,t)=\phi_0\mathrm{H}(t);\ \phi_p(\infty,t)\to 0 \tag{4.35}$$

and the initial condition

$$\phi_p(R,0)=0;\ R\in[a,\infty) \tag{4.36}$$

4.4.2 The Coordinate Transformation

The integrals included in the stabilized weighted residual form of the advection-dispersion-reaction equation (4.30) are constructed in the spherical coordinate system (R,ϕ,θ). Due to the spherical symmetry of (4.30), these integrals are actually performed over the volume V; this in turn can be reduced to a line integral as follows:

$$\int_V F(R)dV=\int_0^{2\pi}\int_0^{\pi}\int_a^{\infty}F(R)R^2\sin\phi\, dR\,d\phi\, d\theta=4\pi\int_a^{\infty}F(R)d(\frac{R^3}{3}) \tag{4.37}$$

where $F(R)$ represents the integral functions involved in the stabilized weak form of (4.30). These integrals over the three-dimensional space can be converted to integrals involving a linear space x using the following coordinate transformation

$$y = R^3/3 \tag{4.38}$$

With the coordinate transform (4.38), the spherically radial advection-dispersion-reaction equation (4.30) in the radial space R can be converted into its one-dimensional counterpart in the linear space x. Equation (4.39) presents a transformed form of the spherically symmetric purely advection equation in the new coordinate system

$$\frac{\partial C}{\partial t} + v_y \frac{\partial C}{\partial y} = 0 \tag{4.39}$$

where v_y is the transformed advective flow velocity defined as

$$v_y = R^2 v_R \tag{4.40}$$

4.4.3 The Advective Transport with the Steady Flow

As a numerical example, an advective transport problem from the spherical cavity in a fully saturated porous medium with a Dupuit-Forchheimer hydraulic conductivity $k = 0.03m/day$ is first examined analytically and numerically. The cavity has a radius of $a = 3m$ and is subject to the boundary conditions of the flow potential $\phi_p(a,t) = 100\,m$ and the concentration $C(a,t) = 1$ (see Figure 4.11). The porous system is assumed to be incompressible, and consequently D_p becomes infinity. For this case, the diffusion-type piezo-condution equation (4.34) reduces to a Laplace's equation, i.e.

$$\frac{\mathrm{d}^2\phi_p}{\mathrm{d}R^2} + \frac{2}{R}\frac{\mathrm{d}\phi_p}{\mathrm{d}R} = 0 \tag{4.41}$$

The analytical solution of (4.41) subject to the boundary condition $\phi_p(a) = \phi_0$ can be expressed as

$$\phi_p = \frac{a\phi_0}{R} \tag{4.42}$$

and the flow velocity can be evaluated in the form

$$v_R = -k\frac{\mathrm{d}\phi_p}{\mathrm{d}R} = k\frac{a\phi_0}{R^2} \tag{4.43}$$

Selvadurai (2002a) presented an analytical solution for the spherically symmetric advective transport with the established steady-state flow velocity field obtained by (4.43) in a porous medium of infinite extent. The solution takes the form

$$\frac{C(R,t)}{C_0} = H[1-\lambda(\rho)] \tag{4.44}$$

where

$$\lambda(\rho) = \frac{a^2}{3\phi_0 k}\left[\rho^3 - 1\right];\ \rho = \frac{R}{a} \tag{4.45}$$

Figure 4.12(a) shows the analytical solution to the advective transport processes given by (4.44) for a period of 100 days.

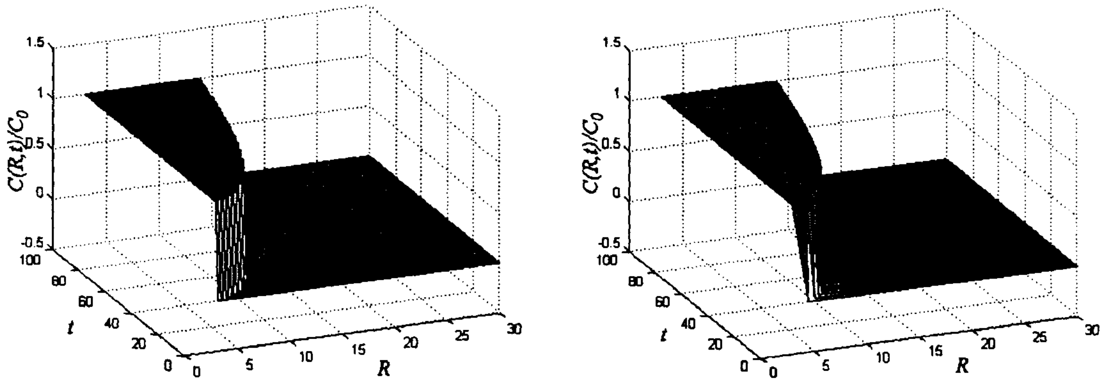

(a) (b)

Figure 4.12 Profiles of (a) an analytical solution (Selvadurai, 2002a) and (b) the numerical results for spherically symmetric advective transport in a porous medium during a period of 100 days

For the purpose of the numerical computation, a finite region $a \le R \le b$ and $b = 30m$ is taken as a computational domain. A homogeneous Neumann boundary condition is applied on the outer boundary, i.e. $C_R(b,t) = 0$, to replace the regularity condition. With the coordinate transform (4.38), the MLS scheme with $\alpha = 3/2$ and $\theta = 1/3$ is used to model this spherically symmetric advective transport problem in the spherically symmetric one-dimensional space. It should be noted that the radial flow velocity (4.43) has a strong spatial dependency, but such space dependency can be eliminated in the linear space through the use of the coordinate transformation (4.38), which makes the transformed flow velocity constant, i.e. $v_y = ka\phi_0$. Therefore, the time step for the computation of the advective transport in linear space can be chosen to satisfy the Courant number criterion $Cr = 1$. Figure 4.12(b) shows the corresponding computational results obtained from the MLS scheme with the aid of the coordinate transformation. The results are almost identical to the analytical solution shown in Figure 4.12(a). The numerical advantage of the MLS scheme provides the possibility for the numerical modelling to capture little physical diffusion (or dispersion) involved in the advection-dominated transport process without the introduction of oscillations or artificial diffusion. Figure 4.13 shows the computational results of the advective-dispersive transport problem with

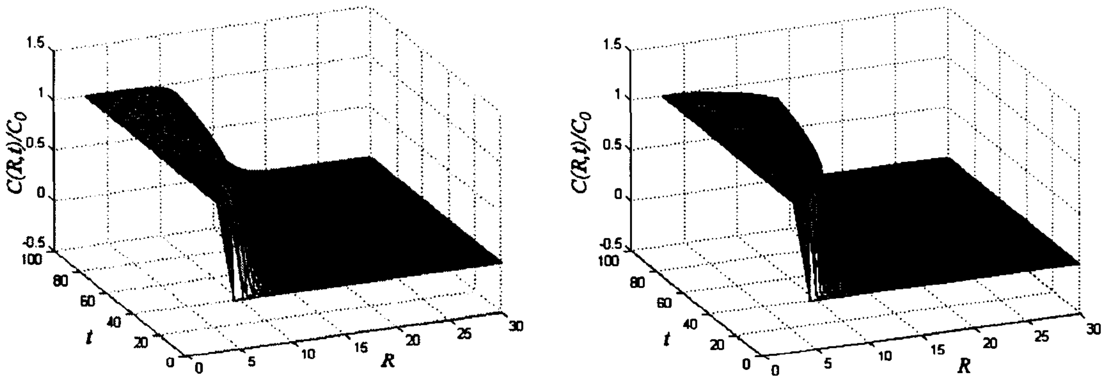

(a) (b)

Figure 4.13 Numerical results during a period of 100 days for (a) the spherically symmetric advective-dispersive transport with $D = 0.05m^2 / day$ and (b) the advective-reactive transport with $r = 0.002 / day$

$D = 0.05 m^2 / day$, and advective-reactive transport problem with $r = 0.002 / day$, for a discontinuous spherically symmetric front migrating from the cavity, obtained using the time-adaptive OS-MLS scheme.

4.5 An Infinite Element Approach for the Piezo-Conduction Equation

In the above numerical modelling of the transport problem from the cavity, the porous system is assumed to be incompressible, and consequently the distribution of the stationary advective flow velocity in the semi-infinite region can be determined analytically. As mentioned previously, if the pore fluid and solid skeleton are compressible, the pore pressure potential has a transient nature, which can be described by a piezo-conduction equation (4.34). The analytical solution of the piezo-conduction equation (4.34) subject to the boundary, regularity and initial conditions defined by (4.35) and (4.36) can be obtained using a Laplace transform technique, and it has the following form

$$\phi_p(R,t) = \frac{a\phi_0}{R}\operatorname{erfc}\left(\frac{R-a}{2\sqrt{D_p t}}\right) \tag{4.46}$$

With this analytical distribution of the pressure potential, the Darcy flow velocity can be determined based on Darcy's law as follows

$$v_R(R,t) = -k\frac{\partial \phi_p}{\partial R} = ak\phi_0\left(\frac{\exp\left(-\frac{(R-a)^2}{4D_p t}\right)}{\sqrt{\pi D_p t}\,R} + \frac{1}{R^2}\operatorname{erfc}\left(\frac{R-a}{2\sqrt{D_p t}}\right)\right) \tag{4.47}$$

In practical situations, the potential boundary conditions may vary with time, and the diffusion coefficient may vary spatially due to the inhomogeneity of the porous medium or the geochemical reactions. For these cases, a numerical approach has to be used for the solution of the piezo-conduction equation. In addition, the boundary and regularity conditions of the pressure potential in (4.35) imply that the pressure potential, and consequently the Darcy flow field, should be determined in such a way that the infinite extent of the porous region should be taken into consideration. In view of these considerations, an infinite element is developed for the analysis of the piezo-conduction equation (4.34). Figure 4.14 illustrates the finite computational domain and the infinite element for the pressure distribution and the contaminant transport.

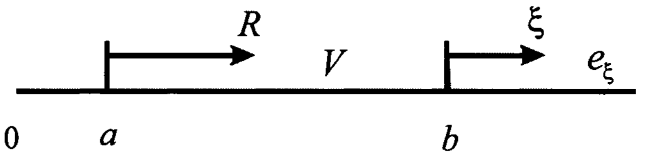

Figure 4.14 One dimensional finite computational domain Ω and infinite element e_ξ

The key issue in the construction of an infinite element for the mass transfer problem in an infinite medium relates to the choice of a so-called mass transfer function (Zhao and Valliappan, 1994). A general form of the mass transfer function for the transient infinite element can be derived from the analytical solution of a representative problem. With the analytical solution of the piezo-conduction equation (4.46), the flow potential at the intersection ($R = b$) of the finite domain and infinite element can be expressed as follows:

$$\phi(b,t) = \frac{a\phi_0}{R}\operatorname{erfc}\left(\frac{b-a}{2\sqrt{D_p t}}\right) \tag{4.48}$$

Therefore, the flow potential at any point, say $b+\xi$, within the infinite element can be expressed as

$$\phi(b+\xi,t) = \phi(b,t)F(\xi,t) \tag{4.49}$$

where $\xi \geq 0$, and $F(\xi,t)$ is the mass transfer function for the infinite element, which takes the following form:

$$F(\xi,t) = \frac{1}{\operatorname{erfc}(\lambda)}\operatorname{erfc}\left(\frac{b+\xi-a}{2\sqrt{D_p t}}\right) \tag{4.50}$$

where $\lambda = \dfrac{b-a}{2\sqrt{D_p t}}$. The mass transfer function can be considered as the shape function in the infinite element (i.e. $N_b = F(\xi, t)$). With such a shape function and its derivative

$$\frac{\partial F(\xi,t)}{\partial \xi} = \frac{-1}{\sqrt{\pi D_p t}\ \mathrm{erfc}(\lambda)} \exp\left(-(\frac{b+\xi-a}{2\sqrt{D_p t}})^2 \right) \tag{4.51}$$

the piezo-conduction equation (4.34) can be reduced to the matrix equation

$$[\mathbf{K}]_\xi \{\phi\} + [\mathbf{M}]_\xi \{\frac{\partial \phi}{\partial t}\} = 0 \tag{4.52}$$

where

$$[\mathbf{K}]_\xi = 4\pi \int_0^\infty D_p \frac{\partial N_b}{\partial \xi} \frac{\partial N_b}{\partial \xi} (b+\xi)^2 \mathrm{d}\xi = \frac{4\pi}{\mathrm{erfc}(\lambda)^2} \mathbf{K}_b \tag{4.53a}$$

$$[\mathbf{M}]_\xi = 4\pi \int_0^\infty N_b N_b (b+\xi)^2 \mathrm{d}\xi = \frac{4\pi}{\mathrm{erfc}(\lambda)^2} \mathbf{M}_b \tag{4.53b}$$

and $\mathbf{K}_b$ and $\mathbf{M}_b$ in (4.53) are defined by

$$\mathbf{K}_b = \frac{1}{\pi t} \int_0^\infty \exp\left(-(\frac{b+\xi-a}{\sqrt{D_p t}})^2 \right) (b+\xi)^2 \mathrm{d}\xi \tag{4.54a}$$

$$\mathbf{M}_b = \int_0^\infty \mathrm{erfc}(\frac{b+\xi-a}{2\sqrt{D_p t}})^2 (b+\xi)^2 \mathrm{d}\xi \tag{4.54b}$$

The infinite integrals in (4.54) can be evaluated using the *adaptive Simpson quadrature* (Gander and Gautschi, 2000). The matrix equation of the infinite element formulation, (4.52), is combined with the finite element formulation of (4.34) to obtain the accurate pressure distribution over the finite element domain. Figure 4.15 shows the pressure distributions over the spherically symmetric finite region within a 100-day period, obtained from the analytical solution (4.46) and the infinite element model. During the computations, the values for the compressibilities for the porous aquifer material and the fluid are assumed to be $\kappa_s = 1.0\times10^{-8}\ m^2/N$ and $\kappa_f = 4.4\times10^{-10}\ m^2/N$ respectively

(Freeze and Cherry, 1979), the porosity is taken as $n^* = 0.3$ and the Dupuit-Forchheimer hydraulic conductivity for the porous medium is taken as $k = 0.03 m/day$. It can be observed from the Figure 4.15 that the infinite element model generates an accurate flow potential distribution in the finite region that is very close to the analytical solution. Figure 4.16 illustrates the distribution of radial flow velocity over the finite domain for a 100-day period as determined from the analytical solution (4.47) and the numerical pressure potential shown in Figure 4.15(b).

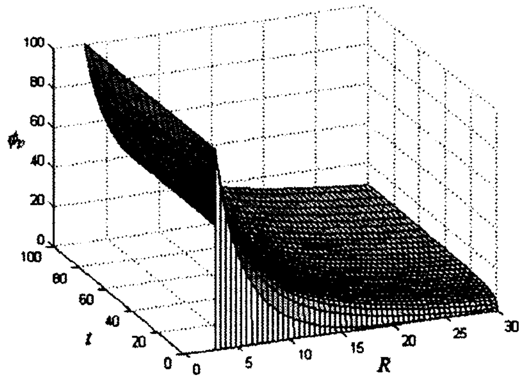

(a) (b)

Figure 4.15 Distributions of the pressure potential during a 100-day period obtained by (a) the analytical solution and (b) the infinite element model

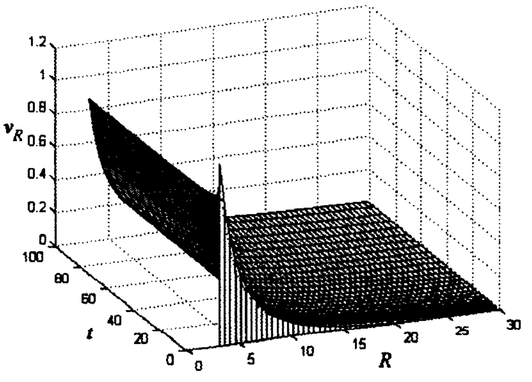

(a) (b)

Figure 4.16 Distributions of the radial flow velocity during a 100-day period obtained by (a) the analytical solution and (b) the infinite element model

With the flow velocity field determined using an infinite element model, the spherically symmetric contaminant transport problem from the spherical cavity in a porous medium of infinite extent is examined computationally with the time-adaptive OS-MLS scheme. Figure 4.17 shows the corresponding computational results for both the purely advective and the advective-dispersive-reactive transport problem with $D = 0.05m^2/day$ and $r = 0.002/day$, in an infinite porous region obtained from the time-adaptive scheme with an initial time step of $\Delta t = 2.34days$.

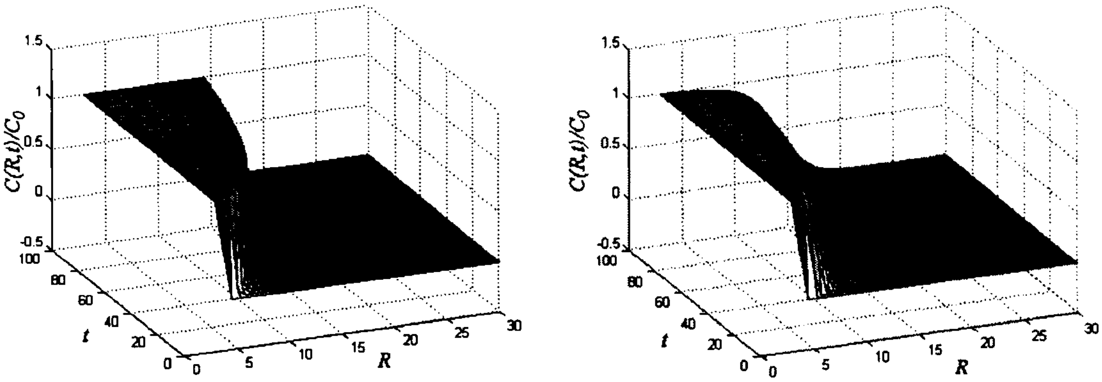

(a) (b)

Figure 4.17 Computational results during a 100-day period for (a) an advective transport and (b) an advective-dispersive-reactive transport in the spherically symmetric region

In section 4.2, the influence of the variation of the flow potential boundary condition on the transport processes was considered in the numerical computation via an analytical solution of the pressure potential, by changing the corresponding boundary parameter in the solution. However, any change in the analytical solution will lead to a simultaneous alteration in the distribution of the pressure potential over the domain. As shown previously, the transient distribution of the pressure potential in the compressible porous medium can be governed by the piezo-conduction equation and the regularity condition at a remote (infinite) location. Therefore, the realistic redistribution of the pressure potential considered in the practical transport problem, due to the variation of the boundary condition, should be determined by the diffusion problem, and the infinite element model can be used for the consideration of the effect of the regularity condition.

In the following section, the infinite element model is used to compute the influence of a decaying potential boundary, with a pulse, on the spherically symmetric advective-dispersive transport process. The variation in the boundary potential is given by

$$\phi_0 = \begin{cases} \phi^* \exp(-\frac{k}{l}t), & t \le 200days \\ \phi^* \exp[-\frac{k}{l}(t-200)], & t > 200days \end{cases} \tag{4.55}$$

Figure 4.18 shows the distributions of the pressure potential and the flow velocity over the domain corresponding to the potential boundary condition (4.55) as obtained from the infinite element model. The influence of the pulse on the distribution of the flow potential and flow velocity at the downstream boundary of the computational domain can be clearly seen in Figure 4.18.The time-adaptive OS-MLS scheme with the initial time step of $\Delta t = 0.1days$ is used to model such a transport problem from the cavity, driven by the transient flow velocity shown in Figure 4.18(b). The corresponding numerical results for a duration of 400 days are shown in Figure 4.19.

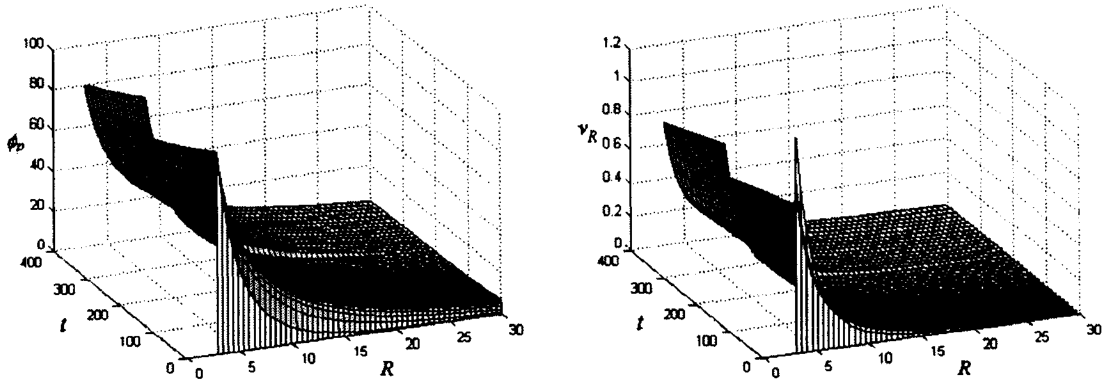

(a) (b)

Figure 4.18 Distributions of (a) the flow potential and (b) the radial velocity in the spherically symmetric region corresponding to the decaying boundary flow potential with a pulse

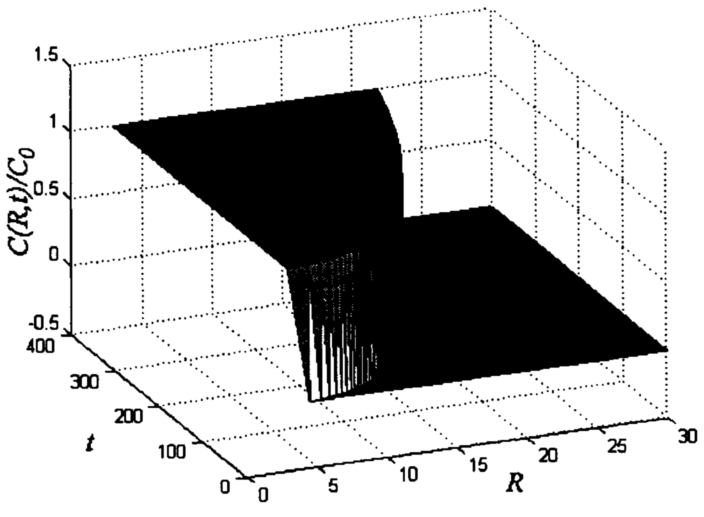

Figure 4.19 Numerical results of the transport process from the cavity with decaying boundary flow potential during a period of 400 days

4.6 Discussion

In conventional modelling of the advective transport problem, it is often assumed that the migration of the contaminant or chemical species within a fluid-saturated medium is initiated by steady Darcy flow applicable to an incompressible fluid. For most soils, this is a useful approximation, particularly when considering the incompressible nature of the pore fluid in comparison to that of the porous soil fabric. When the compressibilities of the porous skeleton the pore fluid are comparable, the pore pressure dissipation in porous media will have a transient nature, which can introduce the time-dependent Darcy flow velocity to the transport problem. A further class of time-dependent velocity fields can be introduced to the transport problem as a result of the time-dependent variation in the boundary potential. In this chapter, a simplified approach was utilized for the treatment of the coupled behaviour between the deformations of the pore fluid and the porous medium that is restricted to predominantly volumetric deformations of the materials. In such cases, the fluid pressure responsible for the Darcy flow in the porous medium is governed by the *piezo-conduction equation*, which leads to not only a space-dependent but also a time-dependent flow field.

A time-adaptive scheme was proposed in this chapter to examine the contaminant transport in a fluid-saturated porous medium with the time-dependent flow velocities determined by a transient pore pressure, due to the compressibility characteristics of the pore fluid and that of the porous medium. Such a time-adaptive scheme is developed based on the Fourier analysis conducted in Chapter 3, and it is sufficient for the accurate solution of the spatially one-dimensional transport problem. Chapter 6 will develop a mesh-adaptive scheme for the optimum solution of the multi-dimensional transport problem, in which a time- and space-dependent flow field is usually not uniformly distributed along the steep front of the solution. In this chapter, it was implicitly assumed in the computations that the chemical being transported induces no changes to either the compressibility characteristics of the pore fluid or the hydraulic characteristics of the porous medium. For those cases with chemically-induced alterations of the hydraulic conductivity and compressibility of the porous medium, the flow velocities will be governed by the solution of fully coupled PDEs of deformations of the porous skeleton and the pore pressure dissipation in the porous medium.

CHAPTER 5

EXPERIMENTAL MODELLING OF THE TRANSPORT IN A POROUS COLUMN

In the previous chapters, several stabilized numerical methods for the advection equation were investigated via a Fourier analysis, and based on this investigation, a time-adaptive operator-splitting numerical scheme was developed for modelling the advection-dominated transport with transient flow velocity. Such a numerical scheme was successfully used in the previous chapter to give the accurate solution of the advective-dispersive-reactive transport problem in the mathematically one-dimensional region where the time-dependent flow field is governed by the transient pore pressure. In this chapter, the time-adaptive scheme will be validated with an experimental modelling of the advection-dominated transport process in a porous medium. The experimental modelling is stimulated by considering the migration of a non-reactive red chemical dye solution through an idealized porous column consisting of glass beads, in which the advective flow is induced by the potential gradient that may have a variation in time. The transient transport phenomenon of the chemical dye solution on the cylindrical surface of the glass bead column is recorded by digital camera. A colour visualization-based image processing model is developed, using the "Image Processing Toolbox" in the MATLAB software package, to determine the distribution of the concentration of the dye solution along the surface of the porous column in a non-invasive way. The experimental results together with an inverse analysis are used to identify the coefficient of hydrodynamic dispersion involved in the transport process in the experimental modelling. The corresponding identified parameters are then used in the validation process of the time-adaptive operator-splitting scheme for the advection-dominated transport problem developed in Chapter 4. Finally, a comparison of experimental, analytical and numerical results of the transport process of a dye plug driven by a transient flow in the porous column is presented at the end of the chapter.

5.1 Image Visualization-Based Techniques

Experimental work is an important aspect in modelling the transport processes of contaminants in porous media, both for the validation of theoretical and numerical models as well as for the identification of parameters governing physical phenomena. All these aspects require that the experimental model give an accurate simulation of the physical transport process of the chemical in the pore space within the porous medium. A key aspect of any experimentation associated with the advective-dispersive transport of a chemical through a porous medium involves the measurement of the concentration of the chemical within the pore space. An important constraint on such measurements is that the procedure should be non-invasive. The presence of any measuring device or probe within the porous medium (Bear, 1961; Robbins, 1989) would represent an anomaly that could influence the flow pattern and in turn affect the advective transport processes within the porous medium. With the advent of efficient technologies for the visualization and the processing of digital information, digital imaging techniques have been successfully applied in a number of areas in the pure and applied sciences and they have become powerful tools in the field of geomechanics and geo-environmental engineering (Garbocai et al, 1999; Asundi, 2002; Gonzalesz and Woods, 2002).

Recent technological advancements in image analysis offer great potential for the accurate and effective quantification of the solute transport process in porous media. Several image-based techniques have been developed to visualize the transport pattern of contaminants in porous media to overcome the difficulties encountered due to the random structure of the soil skeleton, and they can be classified into two categories. The first category is referred to as *computed tomography techniques*, such as X-ray tomography (Warner et al, 1989; Coles, 1999), Nuclear Magnetic Resonance Imaging (NMRI) (Majors et al, 1991; Shattuck et al, 1997; Grenier et al, 1997), Positron Emisson Tomography (Park and McNeil, 1996; Khalili et al, 1998). In such methods, a three-dimensional tomographic imaging technology, which was originally applied in the medical field, is used for the measurement of a radioactive tracer in the fluid to obtain information about multi-phase porous medium systems in a non-invasive way. The disadvantages of computed tomography methods include the low resolution of the image, the small length scale of the sample and the large time interval of the measurement.

The second category of imaging methods is referred as *optical visualization techniques*, such as Photoluminescent Volumetric Imaging (PVI) (Montemagno and Gray, 1995). In such methods, the illuminable fluoropores, excited by electromagnetic energy such as laser or ultra-violet light, are used as the tracer to simulate the solute transport processes; a Charged Coupled Device (CCD) digital camera is used to record the movement of the tracer in the porous medium. More recently a dye visualization-based technique has been employed to determine the solute transport pattern in a porous medium (Corapcioglu and Fedirchuk, 1999; Huang et al, 2002). In the study by Corapcioglu and Fedirchuk (1999), the dye solution was used as the tracer to simulate the solute transport processes in an idealized porous medium consisting of glass beads. In a similar study by Huang et al (2002), an ultra-violet light source located behind the sample was used to excite the fluorescent dye tracer and to minimize the image noise introduced by the reflected and diffusive ambient light. This particular methodology, however, introduces light dispersion effects that can influence the accuracy of the quantitative evaluations of experimental results and should be avoided in experimental modelling.

Due to its efficiency and simple implementation, dye visualization-based imaging technologies have been applied to many problems encountered in civil engineering, such as the evolution of heterogeneities in porous media (Dawe et al 1992; Caruana and Dawe, 1996), the measurement of deformations of geomaterials (Allersma, 1990; Macari et al, 1997), microbubble behaviour in porous media (Burns and Zhang, 1999), determination of diffusivity in porous media (Meyerhoff and Hesse, 1997), non-aqueous phase liquid solubilization in pore networks (Jia et al, 1999), the movement of bed-load (Papanicolaou et al, 1999), particle shape analysis (Shin and Hryciw, 2004; Chandan et al, 2004). All these applications indicate that dye visualization-based imaging methods can be used to determine the transport processes of chemicals in porous media in an economical and quantitative way during laboratory experimental studies.

5.2 The Advective-Dispersive Transport in a Porous Column

Photographic and schematic views of the experimental configuration used for modelling the movement of the chemical dye solution in the idealized porous column are shown in

Figures 5.1 and 5.2 respectively. The apparatus consists of a series of precision manufactured glass cylinders of internal diameter 15*cm*, length 61*cm* and wall thickness 0.50*cm* that are connected to form a one-dimensional column 102*cm* length. The use of the smooth walled glass cylinders both minimizes damage due to the abrasion of the interior surface by the porous material and provides a relatively distortion free transparent surface for the observation of the chemical dye migration pattern. The porous medium consists of a packed bed of glass spheres (of specific gravity approximately 2.5) with sizes ranging from 150μm -212μm. The glass beads are placed in the column with water to a height of 61 *cm* and to a porosity roughly corresponding to 38.5%. The Dupuit-Forchheimer hydraulic conductivity of the porous column is determined by conducting conventional falling head tests and it was measured as $k = 2.05\times10^{-4} m/s$. A water soluble *sodium chloride acid red dye* is mixed with water to make a dye solution at a concentration of 1*g/L*. This dye solution is placed above the porous column under the condition of no flow (valve closed) and used as the tracer to illustrate the transport

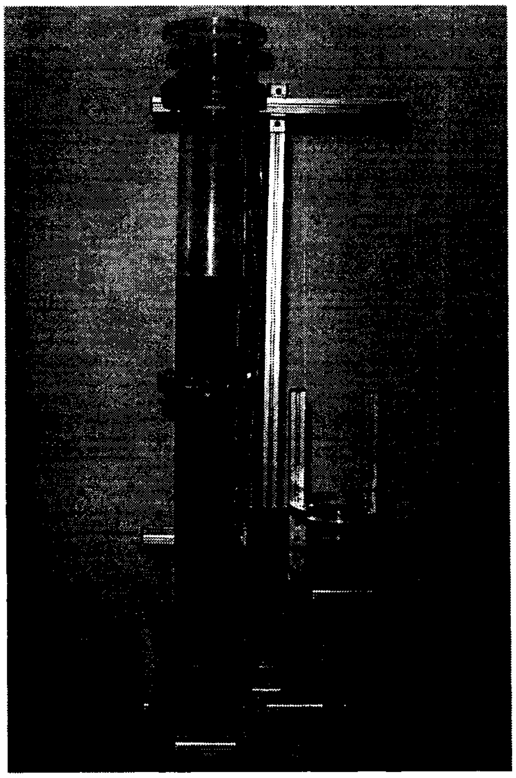

Figure 5.1 A photographic view of the column apparatus

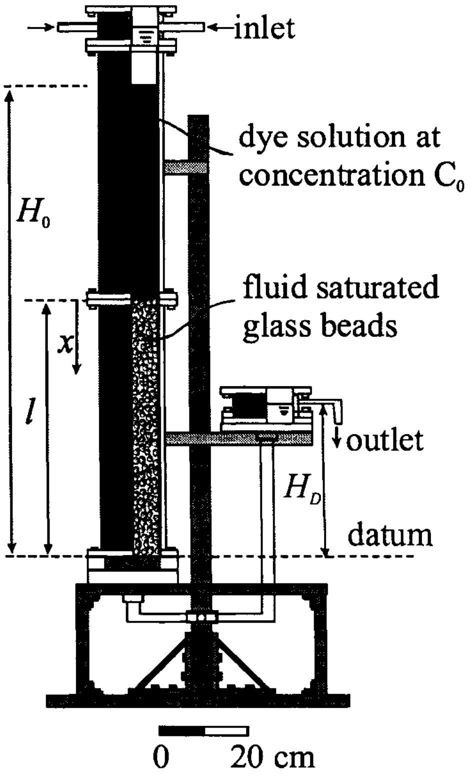

Figure 5.2 A schematic view of the experimental column

process in the porous column. Careful placement of the chemical dye solution is necessary for eliminating the premature migration of the chemical dye solution into the porous region with the result that the porous medium section of the column can be regarded as free of any chemical dye. Furthermore, since the preparation time for the experiment is sufficiently short, the initial diffusion from the column of the dye solution to the water-saturated porous medium can be neglected. The transport of the dye solution through the porous column is caused by a gradient of the hydraulic potentials applied at the inlet and outlet boundaries of the porous column. The hydraulic potential at the outlet boundary of the porous column is kept fixed but the hydraulic potential at the inlet boundary is kept either constant or decaying with time, resulting in an advective flow velocity that is uniform in space but either constant or exponentially varying in time.

5.3 The Governing Equation and an Analytical Solution

The non-reactive advective-dispersive transport of the chemical dye solution in the fluid-saturated and non-deformable porous column can be described by in the following Initial Boundary Value Problem (IBVP) (Philips, 1991; Charbeneau, 2000; Selvadurai, 2000a),

$$\begin{cases} \dfrac{\partial C}{\partial t} + v_0 \exp(-\lambda t)\dfrac{\partial C}{\partial x} - \dfrac{\partial}{\partial x}\left(D\dfrac{\partial C}{\partial x}\right) = 0, \quad x \in [0,l], t \in [0,t^*] \\ C(x,0) = 0, \; x \in [0,l] \\ C(x,t)\big|_{x=0} = C_0 \mathrm{H}(t), \; \dfrac{\partial C}{\partial x}\bigg|_{x=l} = 0 \end{cases} \tag{5.1}$$

where $C(x,t)$ is the concentration of the chemical dye solution measured per unit volume of the fluid; x is the spatial coordinate; t is time; t^* is total time duration; D is the coefficient of the hydrodynamic dispersion including the molecular diffusion (D^*) and the mechanical dispersion (D_L) (Bear, 1972); v_0 is the advective flow velocity which is defined as $v_0 = k(H_0 - H_D)/l$ based on Darcy's law; k is the Dupuit-Forchheimer measure of the hydraulic conductivity of the porous medium and l is the length of the porous column. The parameter λ occurring in (5.1) is defined as $\lambda = k/l$ which can be interpreted by appeal to Darcy flow in the porous column. In the boundary conditions of

(5.1), C_0 is a constant concentration and $\mathsf{H}(t)$ is the Heaviside step function. For constant flow velocity and dispersion coefficient, an analytical solution of the initial boundary value problem defined by (5.1) was given by Ogata and Banks (1961) and takes the form

$$\frac{C(x,t)}{C_0} = \frac{1}{2}\left[\operatorname{erfc}\left(\frac{x-vt}{2\sqrt{Dt}}\right) + \exp\left(\frac{xv}{D}\right)\operatorname{erfc}\left(\frac{x+vt}{2\sqrt{Dt}}\right)\right] \tag{5.2}$$

where $\operatorname{erfc}(\alpha)$ is the complimentary error function which is defined by (4.10).

5.4 Image Processing Model

The transport of the dye solution in the porous column is physically a three-dimensional process, and a key aspect of experimental modelling of such a transport process involves the measurement of the concentration of the chemical dye solution within the glass bead column. An essential constraint on the measurement of the chemical dye concentration in the porous column is that the procedure should be non-invasive, and the presence of a measuring device within the porous medium would influence the flow pattern and consequently the transport processes. One effective non-invasive way to measure the dye concentration is to use computed tomographic imaging technology to measure a radioactive tracer introduced into the pore fluid to illustrate the flow transport pattern inside the porous medium. But this methodology usually encounters difficulties in obtaining a high resolution for the image, the need for a large scale sample and the fast acquisition of image samples. Since the experimental modelling of the transport process in a porous column performed in this chapter is carried out to validate the numerical scheme developed in the previous chapter for the advection-dominated transport problem, only the transport process of the dye solution at the interface between the glass tube and cylindrical surface needs to be measured for validation purposes. Due to this consideration and the physical arrangement of the test column, an easily implemented colour visualization-based *image processing* technique can be used to determine the chemical dye concentration along the surface of the porous column. In this image processing method, the dye solution is used as the tracer and a digital camera is used to record the colour images of the migration of the chemical dye solution along the cylindrical surface of the glass bead column. Based on the fact that different concentrations of the dye solution in the glass bead column can be illustrated by different colors or grey intensities, the quantitative distribution of the concentration of the dye solution along the surface of the porous column can be determined by colour image means. In this section, the basic steps involved in the image processing procedure will be described, including

- image acquisition
- image enhancement
- image calibration
- image quantification.

5.4.1 Image Acquisition

Since the colour representation will be used as an indication of the concentration of the chemical dye solution along the column, the acquisition of the colour image is an important stage in the image processing procedure. The transport of the dye solution along the cylindrical interface between the glass container and the porous column is recorded at specific time intervals using a CCD (Charge Coupled Device) digital camera with a digital sensor capacity of 5 Mega pixels. A strong diffusive light placed in front of the column was used to eliminate any influence of ambient lighting. The camera was positioned in front of the porous column and at the mid-point level of the spatial range of interest, and its settings, such as the shutter speed, aperture and white balance, determined under the conditions of the diffusive lighting, were maintained the same for all experiments, including the calibration exercises. An image strip of 915×20 pixels, which is approximately $60cm$ long and $1.5cm$ wide, is extracted from the photographic image along the cylindrical surface of the porous column for the purpose of determining the concentration of the dye solution along the visible cylindrical surface of the test column. Since the diameter of the glass tube is much greater than the width of the image strip, any light distortion due to the curvature of the glass tube can be neglected in the analysis of the extracted image strip. A typical record of the migration of the chemical dye solution through the porous column is shown in Figure 5.3.

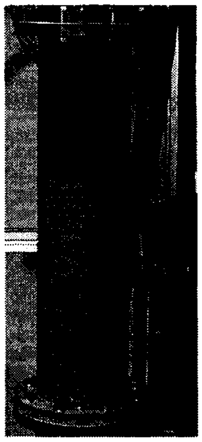

Figure 5.3 A typical photographic record

5.4.2 Image Enhancement

It should be noted from Figure 5.3 that the visual image of the migration of the dye solution through the porous column, recorded by the digital camera, contains not only the colour of the fluids in the pore space (i.e. either the chemical dye solution in the dye-dosed zone or water in the water-saturated zone) but also the colour of the glass beads adjacent to the cylindrical surface of the column. Only the colour distribution of fluids in the pore space should be considered for the purpose of the image analysis. In order to obtain the colour distribution of the dye solution of different concentrations in the pore space, the image can be enhanced by interpreting the colour of the glass beads as *noise* imposed on the colour representation of the dye solution and by removing it from the image. The photographic records captured by the digital camera are *truecolour* images in the form of two dimensional digital arrays of pixels. The realistic area porosity on the surface between the glass tube and the glass bead column is larger than the volumetric porosity of the column that is 38.5% (Garbocai et al., 1999). For glass spheres, the theoretical estimates for the area porosity on the surface of glass beads range from 47.5% for a cubic packing to 26% for a hexagonal packing (Corapcioglu and Fedirchuk, 1999). Therefore, it can be assumed that area porosity over a section at the interface between the glass tube and the porous column is close to 40%. Consequently, it can be concluded that approximately 40 percent of the pixels in an image of the sample contains the colour representing the pore fluids in pore space and 60 percent of pixels contains the colour contribution from glass beads. Furthermore, since an image strip of a physically 60-centimeter long porous column contains 915 pixels in length, a 5×5 pixel neighborhood in the image strip should correspond to a $1 \times 1\ cm^2$ area on the cylindrical surface of the glass bead column, the size of which is about 50 to 70 times of the diameter of the glass bead. Such $1 \times 1\ cm^2$ area can be considered as a REV (Representative Elementary Volume) on the surface of the glass bead column. Therefore it can be concluded that for a 5×5 pixel neighborhood in the image strip, on average, 10 out of 25 pixels (i.e. 40%) contain the colour representing the dye solution in the pore space and the remaining 15 pixels contain the colour representative of the glass beads.

The truecolour image at each pixel is composed of the three primary colours, *r*ed, *g*reen and *b*lue, i.e. (r, g, b) (Russ, 1994), and it can be transformed from the RGB colour space into an *HSI* colour space expressed in terms of the *H*ue, *S*aturation and *I*ntensity. The intensity I is defined as $I = (r + g + b)/3$ and it can reflect the colour variation in the grey scale. For example, for a typical image shown in Figure 5.4(a), the variation in the *r*, *g*, *b* colour components along a vertical line at the centre of the column are shown in Figure 5.4(b) and the corresponding intensity profile along this vertical line is shown in Figure 5.4(c). It should be noted from Figure 5.4(b) that the *red* colour component of the image in both dye-dosed and water-saturated zones in the image is almost uniformly distributed. The green and blue colour components, however, vary significantly in these

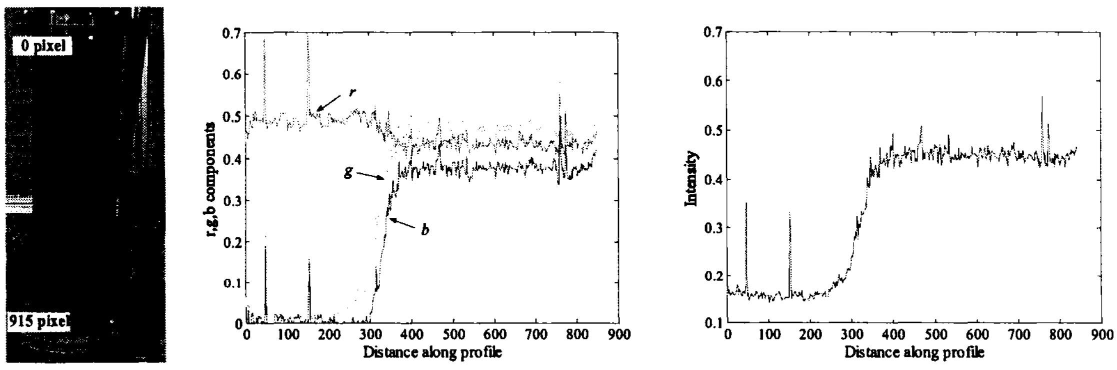

(a) (b) (c)

Figure 5.4 The distribution of the *r*, *g*, *b* colour components and the intensity along the vertical profile line, (a) an original image, (b) *r*, *g*, *b* colour components, (c) intensity zones, resulting in a low intensity in the dye-dosed zone and a high intensity in the water-saturated zone, which can be observed in Figure 5.4(c). The oscillations in the intensity profile correspond to the colour noise due to the light reflection resulting from the glass spheres adjacent to the surface of the column. In general, because of the light reflection, the intensity of the glass spheres is lower than that of the ambient solutions in both the dye-dosed zone and the water-saturated zone. Since large glass bead particles introduce the worst noise into the image, the larger glass beads, with the size ranging from and $650\mu m$ -$850\mu m$, were used as the porous medium in the illustration shown in Figure 5.4 for a more clear demonstration of the colour and intensity variation phenomenon.

In conclusion, if 25 pixels in the above 5×5 neighbourhood taken from the dye-dosed zone are sorted in terms of the intensity increment, then the top 10 elements in the ordered set will contain the colour representing the dye solution in the pore space and the remaining 15 elements will contain the colour related to the glass spheres. A similar result can be obtained for the 5×5pixel neighbourhood taken from the water-saturated zone in the image since the intensity of the water in the pore space is also higher than that of the glass spheres in the contact region. A median of the top 10 elements of the ordered colour set is chosen to replace the colour at the central pixel of the 5×5 neighbourhood. Therefore, if the colour at this central pixel corresponds to a glass sphere, then it will be replaced by the colour of its ambient fluids using the *order-statistics filtering procedure* just described (Gonzalesz and Woods, 2002). The colour representation of the glass beads can be removed from the image by applying the order-statistics filtering to each pixel in the image. After the order-statistics filtering process, a *linear spatial filtering procedure* is then applied to smooth the image by means of a weighted averaging of a pixel with its neighboring 24 pixels. In this procedure, the value at the central pixel in the 5×5 neighborhood is replaced by the weighted average of the 25 elements of the 5×5 array.

Figure 5.5 shows an example of the image enhancement procedure. The image strip shown in Figure 5.5(a) is extracted from the photographic record contained in Figure 5.4(a). Some white spots can be observed in both the dye-dosed and water-saturated zones in the image due to the light reflection from certain glass spheres adjacent to the surface of the porous column. These reflection spots correspond to large oscillations in the intensity profile shown in Figure 5.4(b), and they can be removed by using the image filtering procedure described above. A schematic diagram of the 5×5 pixel image neighbourhood isolated from the original image is shown in Figure 5.5(b). This 5×5 image array is sorted in terms of the intensity increment (Figure 5.5(c)). The colour median of the top 10 elements in the ordered set is then selected for the replacement of the colour of the central pixel in the 5×5 pixel neighbourhood. Then, a linear smoothing filter is applied to the image with a weighted kernel shown in Figure 5.5(d). The final enhanced image, shown in Figure 5.5(e), contains a noise-free colour distribution.

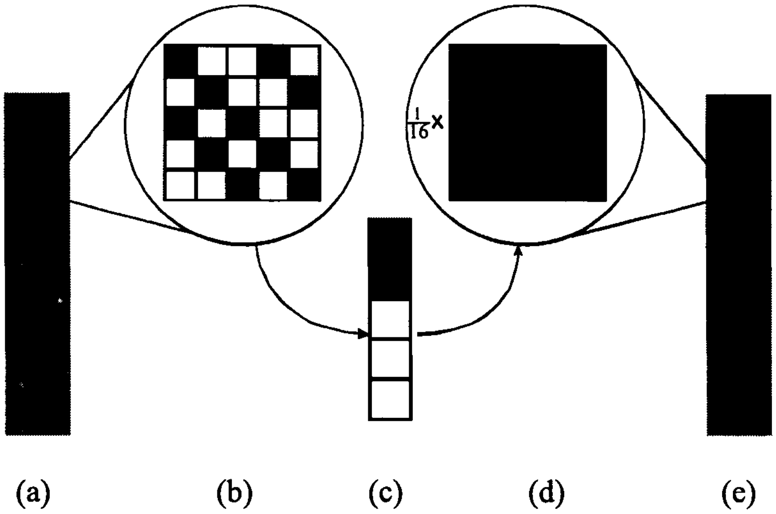

Figure 5.5 The image enhancement procedure, (a) an original image, (b) a schematic view of the 5×5 pixel neighborhood taken from the original image, (c) the ordered colour set of the neighbourhood in the intensity increment, (d) the colour redistribution of the 5×5 pixel array and the weighting kernel and (e) the consequent enhanced image

5.4.3 Image Calibration

The colour distribution in the enhanced images, which are also the truecolour images, can be expressed in terms of the pixel position (i, j) in the following form

$$\begin{cases} r_{ij} = r(i,j) \\ g_{ij} = g(i,j) \\ b_{ij} = b(i,j) \end{cases} \tag{5.3}$$

If the relationship between the primary colour coordinates (r, g, b) and the concentration of the chemical solution, C, is known, i.e.

$$C = C(r, g, b) \tag{5.4}$$

then the quantitative concentration of the dye solution at each pixel in the image can be determined from the colour representation. This process is called the *image quantification*. In order to determine this mapping from the colour to the concentration level, preliminary tests should be performed to calibrate the concentration level of the chemical dye solution in its *in situ* condition within the porous column. In the preliminary calibration tests, the glass beads were placed to the reference porosity in seven dye solutions of known concentrations, 0, 0.05, 0.1, 0.25, 0.5, 0.75 and 1.0 *g/L*, to develop a relationship between the concentrations of the dye solution and their colour counterparts within the porous column. Figure 5.6 presents the photographic records of the seven columns saturated with the dye solution at different concentrations.

The narrow image strips are extracted from these photographic records along the porous column to make seven colour image samples. These image samples were enhanced to extract the colour representation of the dye solution in the pore space by using the image filtering procedure described previously. The corresponding enhanced images shown in Figure 5.7(a) indicate that the colour image varies with the concentration of the chemical dye solution in the porous medium. These colour images can therefore be used as the database for interpreting the concentration of the dye solution on the cylindrical surface of the porous column, and they represent seven points in the planes of the concentration of the dye solution *vs.* the primary ***r***ed, ***g***reen and ***b***lue colour components shown in Figure 5.7(b). A *cubic spline interpolation* is applied to these sample points to generate smooth piecewise polynomial curves for each colour component (Figure 5.7(b)). These interpolating curves represent a mapping (i.e. (5.4)) between the concentration of the dye solution and its colour counterpart in the pore space, and they can be used as the reference in the image quantification procedure to convert the colour representation to the quantitative estimate of the dye concentration in the pore space on the cylindrical surface of the porous column.

(a) (b) (c) (d) (e) (f) (g)

Figure 5.6 The photographic records of seven calibration samples in fine glass bead columns with the dye solution concentration of (a) 0.0, (b) 0.05, (c) 0.1, (d) 0.25, (e) 0.5, (f) 0.75, (g) 1.0 *g/L*

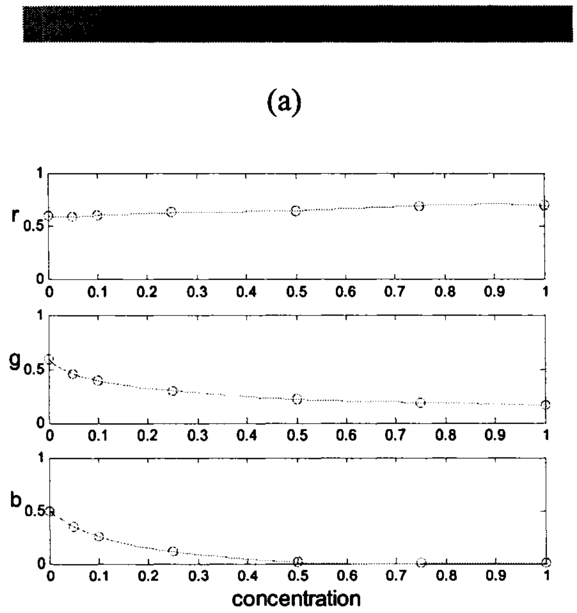

(a)

(b)

Figure 5.7 (a) Enhanced images of seven calibration samples and (b) their corresponding cubic spline fittings for 3 colour components

5.4.4 Image Quantification

The colour-concentration mapping (5.4) used to quantify the images is defined on a colour set B created by the interpolating curves of seven calibration samples shown in Figure 5.7(b). However, the observed colour $(r_{ij}^{ob}, g_{ij}^{ob}, b_{ij}^{ob})$ at a pixel (i, j) in the image of the transport process of the dye solution in the porous column, captured by a digital camera and enhanced through the image filtering procedure, may not necessarily belong to the colour set *B*, i.e. $(r_{ij}^{ob}, g_{ij}^{ob}, b_{ij}^{ob}) \notin B$, due to either experimental errors or the filtering process. Therefore, the projection $(r'_{ij}, g'_{ij}, b'_{ij})$ of the observed colour $(r_{ij}^{ob}, g_{ij}^{ob}, b_{ij}^{ob})$ in *B* should be used for the purpose of colour quantification at the pixel (i, j) of the image. The projected colour $(r'_{ij}, g'_{ij}, b'_{ij})$ in *B* can be determined by means of a *shortest distance* concept: i.e.

$$P(r'_{ij}, g'_{ij}, b'_{ij}) = \min_{(r,g,b)\in B} P(r, g, b) \qquad (5.5)$$

where P represents a Euclidean norm of $(r_{ij}^{ob}, g_{ij}^{ob}, b_{ij}^{ob})$ to the colour set *B*, i.e.

$$P(r, g, b) = \sqrt{(r_{ij}^{ob} - r)^2 + (g_{ij}^{ob} - g)^2 + (b_{ij}^{ob} - b)^2} \qquad (5.6)$$

By substituting $(r'_{ij}, g'_{ij}, b'_{ij})$ into the mapping (5.4) determined from the interpolating curves shown in Figure 5.7(b), the quantitative concentration of the chemical dye solution at the pixel (i, j) can be determined as

$$C_{ij} = C(r'_{ij}, g'_{ij}, b'_{ij}). \qquad (5.7)$$

Figure 5.8 shows the image quantification procedure used to digitize the colour distribution of the concentration of the dye solution in the visible pore space during its transport in the porous column. A photographic record of the transport of the dye solution along the porous column captured by the digital camera at a specified time is shown in Figure 5.8(a). The corresponding enhanced image strip extracted from the central part of the column in the photograph is shown in Figure 5.8(b). The colour equivalent of the concentration profile determined using the image quantification procedure is shown in Figure 5.7(c) and a colourbar shown in Figure 5.7(d) reflects the colour-concentration mapping. Finally, the numerical values for the normalized concentration are shown in Figure 5.7(e).

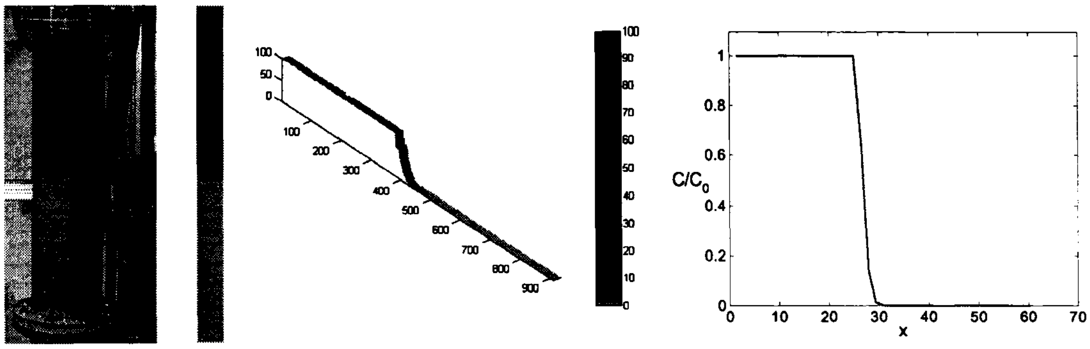

(a) (b) (c) (d) (e)

Figure 5.8 The quantification of the concentration distribution of the dye solution at the cylindrical surface of the porous column, (a) a photographic record, (b) an image strip, (c) the colour quantification, (d) the colourbar and (e) the quantitative distribution of the dye concentration

5.5 Experimental Results

By applying the image enhancement and image quantification procedures shown in Figure 5.8 to a sequence of images obtained at specified time intervals, the transport process of the dye solution at the visible cylindrical surface of the glass bead column can be quantified. Figure 5.9 shows the quantitative estimates of the transport processes, over the plane of dimensionless variables $X(=x/l)$ vs. $T(=kt/l)$, of the dye solution with the concentration of 1.0 *g/L* on the cylindrical surface of the glass bead column. The migration of the dye solution takes place with a constant Darcy flow velocity v (= $k(H_0 - H_D)/n^*l$)= 2.18×10^{-4} *m/s*, initiated by the initial boundary hydraulic potentials $H_0 = 0.70m$ and $H_D = 0.45m$ applied, respectively, at the inlet and outlet boundaries of the porous column. The constant movement of the breakthrough front of the dye solution can be clearly seen in Figure 5.9. The fact that the Reynolds number $\mathrm{Re}(=\rho vd/\mu = 0.033 \sim 0.046)$ associated with the flow in the column is much lower than unity points to the applicability of Darcy's law.

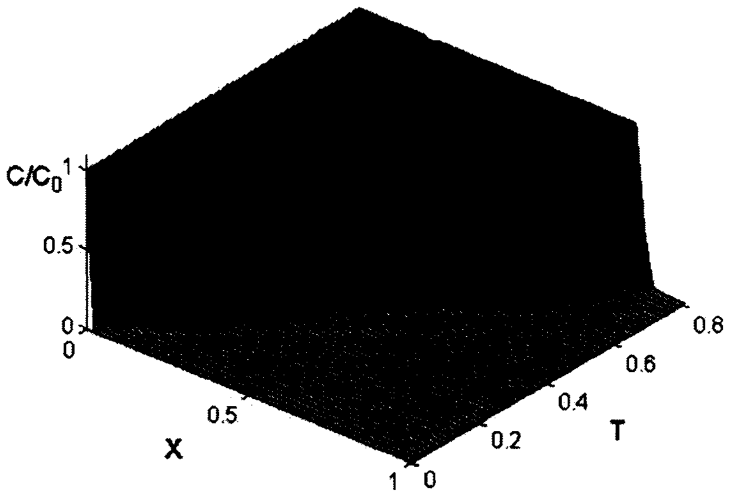

Figure 5.9 Experimental results of the transport process of the chemical dye solution in the porous column

5.6 Inverse analysis

5.6.1 Parameter Identification

The transport process of the dye solution in the hydraulically homogeneous column of glass beads is governed by the hydraulic conductivity of the porous medium and the hydrodynamic dispersion coefficient of the chemical dye solution in the column of glass beads. The hydraulic conductivity of the porous column can be measured by conducting conventional constant or falling head tests, but the measurement of the hydrodynamic dispersion coefficient is less straightforward and usually requires a formal *parameter identification* application. Compared with the initial boundary value problem stated by (5.1), which is usually called the *forward problem*, the parameter identification process can be referred to as the *inverse problem* (Sun, 1994). In the forward problem, the temporal and spatial distribution of the chemical concentration over the domain is determined by the governing equation and system parameters via analytical or mathematical approaches; while in the inverse problem, the system parameters (such as the hydrodynamic dispersion coefficient) are determined by the observation of the temporal and spatial distribution of the chemical concentration. A widely used approach for the determination of the physical parameters in the field of geological sciences is the *time lag method* (Grathwohl, 1998). Here, however, an *indirect method* will be used for the identification of the coefficient of the hydrodynamic dispersion of the dye solution in the column of glass beads, since this method provides a general approach which can be used to identify physical parameters in other fields such as hydrology, geology, ecology etc. (Gottlieb and DuChateau, 1996). The basic concept underlying the indirect method for parameter identification is to transfer the inverse problem into an *optimization problem* by means of the Output Least Squares (OLS) criteria of the difference between the observation and the calculation of system states (e.g. the concentration of the contaminant) (Sun, 1994). Such methods usually require the *adjoint state* equation of the system, and the different derivations of the adjoint state equation will lead to different indirect methods. Isakov (1998) has addressed the issues of the convergence, uniqueness and stability of the inverse problem.

The optimization problem used in this section for identifying the hydrodynamic dispersion coefficient D was created by using the OLS criterion relating the *observed* and *estimated* distributions of the chemical dye concentration, which is expressed as

$$J(D) = \left\| C(\cdot,\cdot,D) - C_i^{ob}(\cdot,\cdot) \right\|_{\Omega}^{2} = \int_0^{t^*}\int_0^{l} \left(C(x,t,D) - C_i^{ob}(x,t) \right)^2 \mathrm{d}x\mathrm{d}t \rightarrow \min_p \qquad (5.8)$$

where $J(D)$ is the objective function of the optimization problem; $C_i^{ob}(x,t)$ is the experimentally observed chemical dye concentration along the column obtained from the image processing technique; $C(x,t,D)$ is the estimated chemical dye concentration obtained from either an analytical solution or a computational modelling; and the dot in the expression refers to the independent variable. The optimal problem (5.8) can be solved by means of Newton-type methods (Modified-Newton, Quasi-Newton, etc), in which the descent orientation of $J(D)$ is required. In general, it is difficult to directly calculate the orientation of the descent direction of $J(D)$, since the objective function of the optimization problem (5.8) has a complex form, and cannot be expressed as a straightforward mathematical function. It is, however, shown from the *Fréchet derivative* that the descent direction of $J(D)$ can be determined by the adjoint state of the dye concentration.

5.6.2 The Fréchet Derivative and the Steepest Descent Direction

It can be assumed that the concentration of the chemical dye solution C is a function of the spatial coordinate x, the time t and the hydrodynamic dispersion coefficient D, i.e. $C = C(x,t;D)$. The hydrodynamic dispersion coefficient D can also be a function of the distance x and the time t, and it can admit a small increment of the form $\delta D = \varepsilon\eta(x,t)$, where ε is a scalar parameter, $\eta(x,t)$ is a given function in the space $L^2(\Omega)$ and $\Omega = [0,l]\times[0,t^*]$. The *Fréchet derivative* of C with respect to D along the direction η can be defined as

$$\dot{C} = \lim_{\varepsilon\to 0^+} \frac{C(x,t;D+\varepsilon\eta) - C(x,t;D)}{\varepsilon} = C'_D(x,t;D)\eta(x,t) \tag{5.9}$$

Assuming that $D^* \in L^2(\Omega)$ is the optimal parameter of the equation (5.7), $\forall D \in U_{ad}$ (where U_{ad} is an admissible set of D) and $\forall \varepsilon \in [0,1]$ such that $(1-\varepsilon)D^* + \varepsilon D = D^* + \varepsilon(D - D^*) \in U_{ad}$, the following relationship can be made

$$J(D^*) \le J((1-\varepsilon)D^* + \varepsilon D) = J(D^* + \varepsilon(D - D^*)) \tag{5.10}$$

with the result

$$\frac{1}{\varepsilon}\left[J(D^* + \varepsilon(D - D^*)) - J(D^*)\right] \ge 0. \tag{5.11}$$

From the definition of the *Fréchet derivative*, the following inequality can be obtained as ε approaches zero

$$J'(D^*)(D - D^*) \ge 0. \tag{5.12}$$

It is implied from (5.12) that the descent direction of $J(D)$ should be equal to $-J'(D^*)$.

For the purpose of determining the derivation of $J(C)$, the adjoint state ψ of the concentration is introduced, which satisfies the following *adjoint* problem of the original IBVP defined by (5.1)

$$\begin{cases} \dfrac{\partial \psi}{\partial t} + v\dfrac{\partial \psi}{\partial x} + \dfrac{\partial}{\partial x}(D\dfrac{\partial \psi}{\partial x}) = 2(C - C^{ob}) \\ \psi(x,t^{*})\Big|_{x=0} = 0,\ \dfrac{\partial \psi}{\partial x}\Big|_{x=l} = 0,\ \ x \in [0,l], t \in [0,t^{*}] \end{cases} \tag{5.13}$$

where C^{ob} is the observed value of C. Applying the *Fréchet derivative* to the IBVP defined by (5.1) gives

$$\begin{cases} \dfrac{\partial \dot{C}}{\partial t} + v\dfrac{\partial \dot{C}}{\partial x} - \dfrac{\partial}{\partial x}(D\dfrac{\partial \dot{C}}{\partial x}) - \dfrac{\partial}{\partial x}(\eta\dfrac{\partial C}{\partial x}) = 0,\ \ x \in [0,l], t \in [0,t^{*}] \\ \dot{C}(x,0) = 0,\ \ x \in [0,l] \\ \dot{C}\Big|_{x=0} = 0,\ \left(D\dfrac{\partial \dot{C}}{\partial x} + \eta\dfrac{\partial C}{\partial x}\right)\Bigg|_{x=l} = 0,\ \ t \in [0,t^{*}] \end{cases} \tag{5.14}$$

Multiplying the first equation in (5.13) by $\dot{C}$, then integrating the result over the domain Ω and taking into consideration the first equation in (5.14) leads to the following relationship

$$\begin{aligned} \int_0^{t^{*}}\int_0^{l} \eta \frac{\partial C}{\partial x}\frac{\partial \psi}{\partial x}\,\mathrm{d}x\mathrm{d}t &= \int_0^{t^{*}}\int_0^{l} 2\left(C(x,t;D^{*}) - C_i^{ob}\right)\dot{C}\,\mathrm{d}x\mathrm{d}t \\ &= 2\left(C(\cdot,\cdot;D) - C_i^{ob}, \dot{C}(\cdot,\cdot;D)\right)_{\Omega} \end{aligned} \tag{5.15}$$

Alternatively, with the definition of $J(D)$ and taking the inner product of $J'(D)$ and η, the following relationship can be obtained

$$\begin{aligned} J'(D)\eta &= \lim_{\varepsilon \to 0^{+}} \frac{J(D+\varepsilon\eta) - J(D)}{\varepsilon} \\ &= \lim_{\varepsilon \to 0^{+}} \frac{1}{\varepsilon}\left\{ \left\| C(\cdot,\cdot,D+\varepsilon\eta) - C_i^{ob}(\cdot,\cdot)\right\|_{\Omega}^{2} - \left\| C(\cdot,\cdot,D) - C_i^{ob}(\cdot,\cdot)\right\|_{\Omega}^{2} \right\} \\ &= 2\left(C(\cdot,\cdot;D) - C_i^{ob}, \dot{C}(\cdot,\cdot;D)\right)_{\Omega} \end{aligned} \tag{5.16}$$

Comparing (5.15) and (5.16) gives

$$J'(D)\eta = \int_0^{t^{*}}\int_0^{l} \eta \frac{\partial C}{\partial x}\frac{\partial \psi}{\partial x}\,\mathrm{d}x\mathrm{d}t \tag{5.17}$$

Since η is an arbitrary function, the direction of the steepest descent of $J(D)$ can be expressed as follows

$$-\nabla J(D) = -J'(D) = -\int_0^{t^*}\int_0^{l}\frac{\partial C}{\partial x}\frac{\partial \psi}{\partial x}\mathrm{d}x\mathrm{d}t \tag{5.18}$$

5.6.3 The Hydrodynamic Dispersion

With the descent direction of the objective function $J(D)$ defined by (5.18), a Quasi-Newton iterative algorithm (Murray, 1972; Engelman et al, 1981; Soria and Pegon, 1990; Gottlieb and DuChateau, 1996) can be used to solve the optimization problem stated by (5.8) to identify the hydrodynamic dispersion coefficient D based on the experimental observations. In order to ensure that the estimated parameter is physically admissible, a constraint, i.e. $D_l \le D \le D_u$ (where D_l and D_u represent the lower and upper limits of the hydrodynamic dispersion coefficient D, respectively), needs to be applied to the optimization problem. For the purpose of the inverse analysis exercise, the experimental results for the transport of the chemical dye solution in the porous column shown in Figure 5.9 are used for the identification of D. Figure 5.10 shows the flowchart for a quasi-Newton iterative procedure for the optimization problem (5.8). Table 5.1 gives the iterative results of the quasi-Newton algorithm for the hydrodynamic dispersion coefficient of the transport of the dye solution in the porous column with the initial estimate $D_0 = 5\times10^{-9} m^2/s$. Finally, the hydrodynamic dispersion coefficient is identified as

$$D = 1.361\times10^{-8}\, m^2/s\,. \tag{5.20}$$

Figure 5.11 shows the comparison of experimental results taken at time t=360s for the transport of the dye solution in the porous column with the results given by the analytical solution (5.2) and the operator splitting MLS scheme using the hydrodynamic dispersion coefficient D defined by (5.20). In the numerical computation, the spatial domain is discretized into 200 elements with the element length of $h = 0.003m$. With such elemental size, the Péclet number has a value as $Pe = v\,h/D = 48$ over the computational domain, and therefore the transport process of the dye solution is advection dominant.

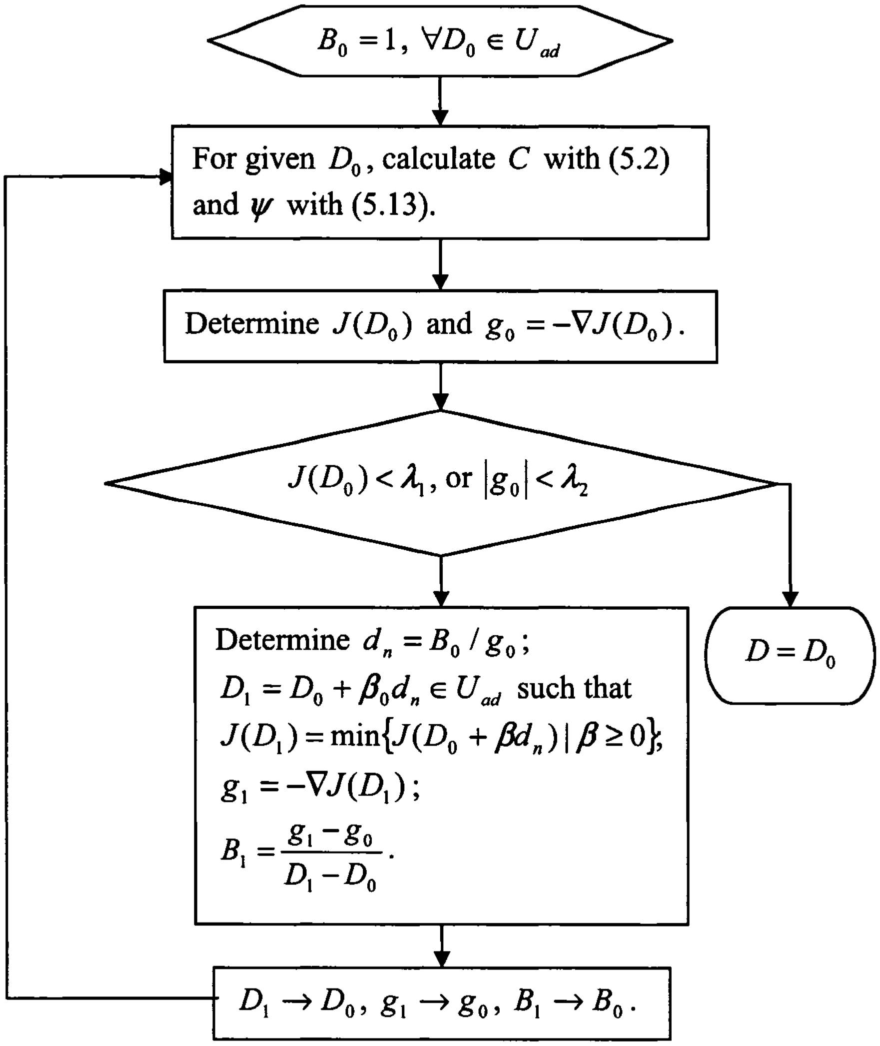

Figure 5.10 The flowchart of the quasi-Newton iterative procedure for the optimization problem of the inverse analysis, where λ_1 and λ_2 are two tolerance criteria

Table 5.1 Iterative results for identification of D

D_0 (m^2/s)	Iteration	J	$-\nabla J$	D (m^2/s)	$\psi(n)$
5×10^{-9}	1	8.694×10^{-2}	4.686×10^{2}	1.147×10^{-8}	1.464×10^{1}
	2	2.317×10^{-2}	1.155×10^{2}	1.314×10^{-8}	4.626×10^{1}
	3	2.025×10^{-2}	7.230×10^{1}	1.361×10^{-8}	3.414×10^{0}

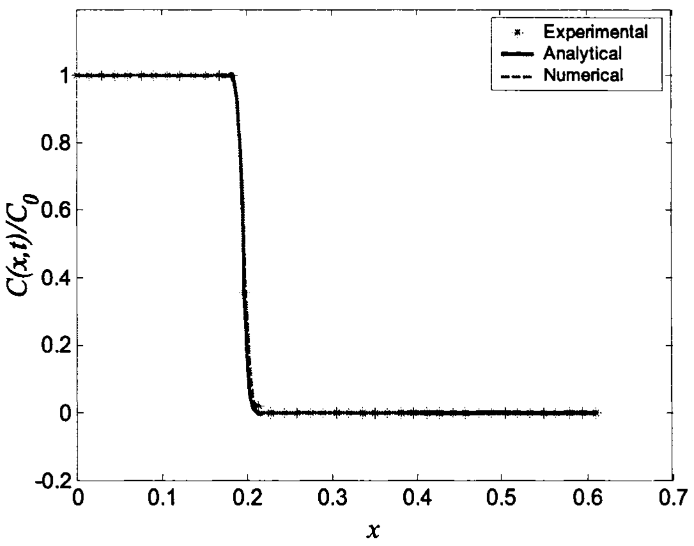

Figure 5.11 Experimental, analytical and numerical results at t=360s for the transport process of the chemical dye solution in the porous column

As mentioned previously, the process of hydrodynamic dispersion in the porous medium generally includes both a molecular diffusion component characterized by D^* and a mechanical dispersion component characterized by D_L, i.e. $D = D_L + D^*$. The diffusion of the contaminant in natural porous media is influenced by the tortuosity, constrictivity and effective transport-through porosity of the porous medium, and therefore its value should be lower than that applicable to the diffusion of the chemical species in water. The molecular diffusion of a chemical in liquid depends on the interactive forces between the molecules which account for a frictional drag and therefore they are mainly affected by the dynamic viscosity of the fluid. Several empirical correlations have been developed to determine the effective diffusion coefficient D^* of a chemical in porous media (Grathwohl, 1998). The largest estimated value of D^* should be lower than $2.0\times10^{-9} m^2/s$ (Freeze and Cherry, 1979). Based on the physical properties of the porous column and the basic chemical components of the dye used in this experiment, the value for the molecular diffusion in the transport processes of the dye solution in the porous column can be estimated at $D^* = 1.0\times10^{-10} m^2/s$. According to the identified hydrodynamic dispersion coefficient (5.20), the dominant dispersive process during the transport of the dye solution in the porous column is through mechanical dispersion. The mechanical dispersion coefficient, D_L, is generally assumed to be directly proportional to the magnitude of the flow velocity (Taylor, 1953; Bear and Bachmat, 1992), and for one-dimensional problems it has a form $D_L = \alpha_{\mathrm{L}}|v|$, where α_{L} is referred to as the *longitudinal dispersivity* and $|v|$ is a velocity norm. Using the values of D and D^* thus obtained, the longitudinal dispersivity, α_{L}, of the dye solution in the glass bead column can be evaluated as

$$\alpha_L = \frac{D - D^*}{|v|} = 6.186 \times 10^{-5}\, m \tag{5.21}$$

The determined dispersivity can be used in an analytical solution or numerical modelling to simulate an advective-dispersive transport process in the porous column with a transient flow field.

5.7 The Comparison of Analytical, Numerical and Experimental Results

In this section, the *transport of a plug of the chemical dye* in the glass bead column with a time-dependent flow velocity is considered. The chemical plug is located in the region [0.155*m*, 0.305*m*] within the porous column, and is allowed to migrate through the column driven by a falling upper boundary hydraulic potential. The reducing hydraulic potential gives rise to a spatially uniform advective flow velocity in the porous column but with a time-dependent variation of a negative exponential form. The initial inlet and outlet boundary potentials applied to the porous column are set as $H_0 = 0.96m$ and $H_D = 0.26m$ respectively. Figure 5.12(a) shows a photographic record of the movement of the plug of chemical dye solution during its transport in the porous column at a specific time $\tilde{t} = 210s$. Figure 5.12(b) shows the experimental results for the normalized concentration over the plane of the dimensionless variables X and T, obtained by using the image processing technique.

Selvadurai (2004b) gave an analytical solution for the transport problem of a chemical plug in an infinite region with an exponential decaying flow velocity and constant dispersion coefficient, which can be written as follows

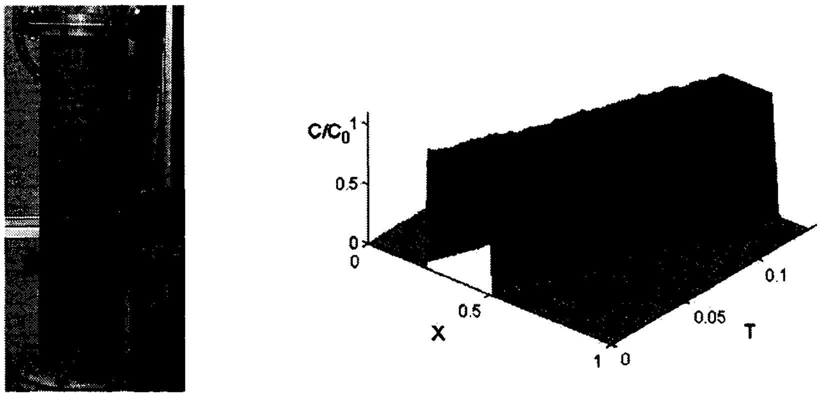

(a) (b)

Figure 5.12 A typical photographic record (a) and experimental results (b) of the transport processes of the chemical dye plug with the time dependent flow velocity in the glass bead column

$$\frac{C(x,t)}{C_0}=\frac{1}{2}\operatorname{erf}\left(\frac{-x-a+v_0\dfrac{\{1-\exp(-\lambda t)\}}{\lambda}}{2\sqrt{Dt}}\right)-\frac{1}{2}\operatorname{erf}\left(\frac{-x-b+v_0\dfrac{\{1-\exp(-\lambda t)\}}{\lambda}}{2\sqrt{Dt}}\right),\ x<v_0t \qquad (5.22a)$$

$$\frac{C(x,t)}{C_0}=\frac{1}{2}\operatorname{erfc}\left(\frac{x-b-v_0\dfrac{\{1-\exp(-\lambda t)\}}{\lambda}}{2\sqrt{Dt}}\right)-\frac{1}{2}\operatorname{erfc}\left(\frac{x-a-v_0\dfrac{\{1-\exp(-\lambda t)\}}{\lambda}}{2\sqrt{Dt}}\right),\ x\geq v_0t \qquad (5.22b)$$

where $a \leq b$, and $[a,b]$ represents a finite or infinite interval region which is initially occupied by the chemical. The analytical solution (5.22) can give an approximation to the transport of the dye plug in the porous column considered in this section. Figure 5.13(a) shows this analytical approximation with $[a,b]=[0.155,0.305]$ and the approximated dispersion coefficient is determined by

$$\widetilde{D}=D^{*}+\alpha_L v_0\exp(-\frac{k\widetilde{t}}{l})=3.16\times10^{-8}m^2/s \qquad (5.23)$$

The other transport parameters, such as k and λ, take the same values as defined before. Figure 5.13(b) shows the corresponding numerical results obtained from the time-adaptive operator-splitting MLS scheme developed in Chapter 4. In the numerical computation, the hydrodynamic dispersion coefficient depends on the transient flow velocity and is defined as $D = D^{*} + \alpha_{L}|v|$, where the longitudinal dispersion α_{L} is determined from (5.21).

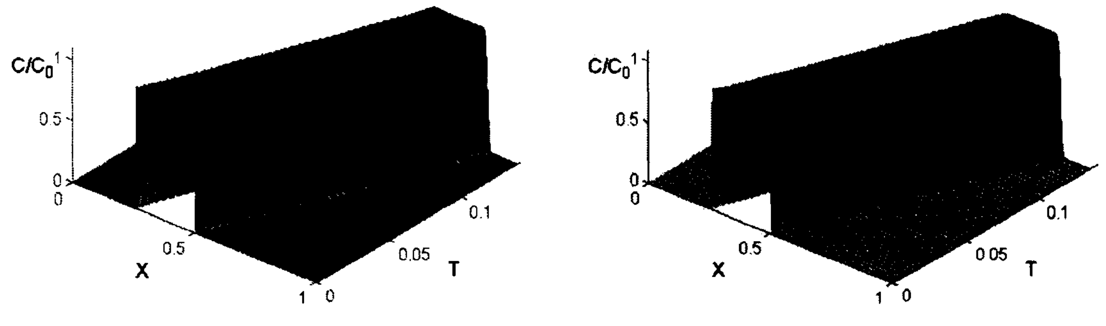

(a) (b)

Figure 5.13 The results of (a) the analytical solution and (b) the numerical simulation obtained using the time-adaptive operator splitting MLS scheme for the transport process of the chemical dye plug with the time-dependent flow velocity in the glass bead column

Figure 5.14 shows the comparison of the experimental results evaluated at the specific time $\tilde{t}$ obtained from the image processing method, the analytical solution given by (5.22) with D determined by (5.23) and the computational estimates derived from the five stabilized schemes discussed in Chapter 2. In the numerical computations, the time-adaptive procedure and operator splitting technique discussed in Chapter 4 are used. The Crank-Nicolson time integration scheme is used with the PG, TG2 and LS schemes, and the Euler forward time integral scheme is used with TG3 scheme. In the MLS scheme, the upwind parameter and time weighting are determined by (3.37). It is shown from Figure 5.14 that the MLS and TG3 schemes give oscillation-free and non-diffusive numerical solutions for the advection-dominated transport of the dye plug, which are very close to the analytical solution. The difference between them is due to the values of the hydrodynamic dispersion coefficients used in the analytical solution and the numerical modellings. The PG and LS schemes give similar numerical results due to their similar distributions of the algorithmic amplitude and the phase velocity (see Chapter 3), and both of these introduce oscillations into the numerical solution near its steep gradient. Finally, the TG2 scheme generates an overdiffusive solution to the transport problem of the dye plug. The close resemblance between the experimental results, analytical solutions and numerical simulations obtained from the time-adaptive operator-splitting MLS and TG3 schemes shown in Figure 5.11 indicates the effectiveness of the image processing technique in determining the quantitative distribution of the dye concentration in the visible pore space of the porous glass bead medium, as well as the accuracy of the time-adaptive operator-splitting scheme for the advection-dominated transport problems developed in the previous chapter.

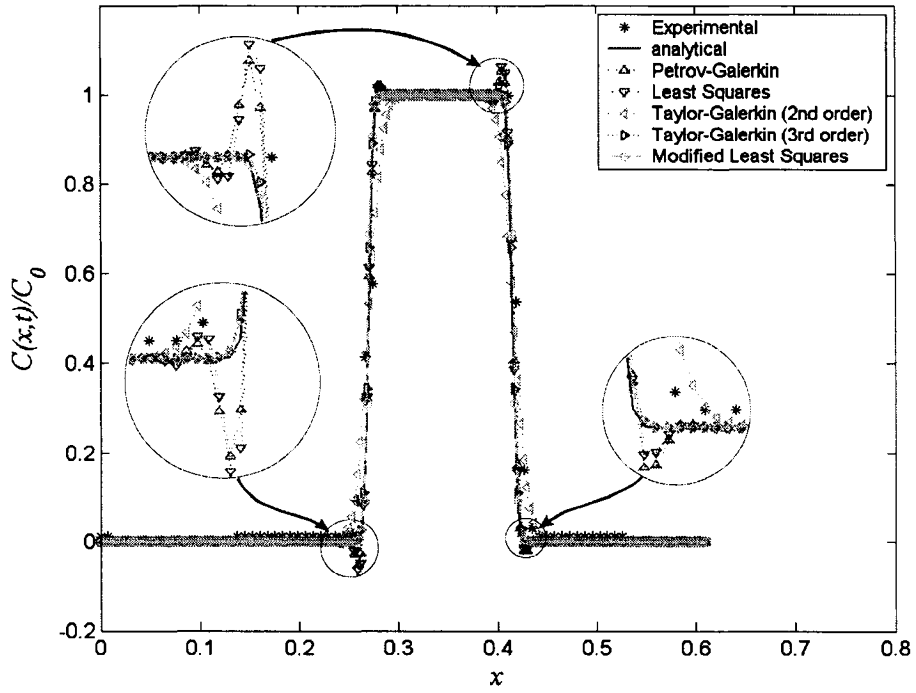

Figure 5.14 A comparison of experimental, analytical and numerical results at t=210s for the transport of the dye plug in the glass bead column with the decaying flow velocity

5.8 Discussion

In this chapter, an effective and economical colour visualization-based image processing model is developed to accurately estimate the distribution of the concentration of a chemical dye solution in the visible pore space as it migrates through an idealized porous column consisting of glass beads. A limitation of the application of the imaging technique to the transport process in the porous medium is that the visualization is restricted to the two-dimensional surface of a region of interest. Consequently, the transport phenomena of a dye solution obtained from image processing techniques are restricted to the transport characteristics of the dye solution occurring between the wall of the glass tube and the cylindrical surface of the column of glass beads. The image processing model presented in this chapter can be used to determine the flow transport process of the contaminant on the two-dimensional surface in a quantitative and non-invasive way. However, the basic concepts underlying the image enhancement and the image calibration can be extended to *Computerized Tomography* (CT) techniques to determine the transport process of contaminants in the three-dimensional porous space of the porous medium.

The inverse analysis for the parameter identification is the complementary aspect of the mathematical modelling of the transport problem in the porous medium. In the second part of this chapter, an inverse problem is created to identify the hydrodynamic dispersivity applicable to the advection-dominated transport of the dye solution in (or on the cylindrical surface of) the column of glass beads, by using the experimental results obtained from the image processing technique. The Fréchet derivative is used to determine the descent direction of the objective function employed in the optimization problem. The accuracy of the identified dispersivity coefficient, determined through the combined application of an image analysis and an inverse analysis, has been verified through numerical and experimental modelling of the movement of a plug of the dye solution in the porous column where the flow velocity is time-dependent. The close correlation between the experimental results and the numerical solutions also indicates the effectiveness of the image processing model for determining the concentration distribution of the chemical dye solution via colour visualization, and the accuracy of the time-adaptive operator splitting scheme for the advection-dominated transport problem.

CHAPTER 6

THREE-DIMENSIONAL AXISYMMETRIC ADVECTIVE TRANSPORTS

The Fourier analysis conducted in Chapter 3 indicates that the Courant number has a significant influence on the numerical behaviour of the stabilized semi-discrete Eulerian Finite Element Methods (FEMs) for the advection equation, and certain stabilized schemes can give accurate solutions for the advection equation with the Courant number criterion of $Cr = 1$. Based on this analysis, a time-adaptive operator splitting scheme was developed in Chapter 4 and successfully applied to the spherically symmetric advection-dominated transport problems for an infinite domain. In Chapter 5, the time-adaptive scheme was validated with experimental modelling of the advection-dominated transport of a chemical dye solution in a porous column. However, it should be noted that the time-adaptive scheme may not be efficient for the multi-dimensional transport problem due to the non-uniform distribution of the advective flow velocity along the steep front of the solution. On the other hand, it is implied from the definition of the Courant number (i.e. $Cr = v\Delta t/h$) that, not only the time step Δt, but also the mesh size h can be adaptively modified based on the magnitude of the flow velocity and the Courant number criterion of $Cr = 1$. The coordinate transformation and corresponding computational results for the spherically symmetric advective transport problem in Chapter 4, indicated that the mesh in the regions remote from the cavity should also be refined due to the low magnitude of the flow velocity. In this Chapter, therefore, a mesh refining adaptive scheme will be developed for the multi-dimensional transport problem, and it will be used for modelling both linear and nonlinear transport problems related to a spherical or disc-shaped cavity in a three-dimensional axisymmetric fluid saturated porous region. Only the advective transport process will be considered in this chapter for the sake of simplicity.

6.1 The Mesh Refining Adaptive Scheme

Before developing the mesh adaptive scheme, we will first review the upwind function α and the time weighting θ in the MLS scheme, which are determined by (3.37) (i.e. $\alpha = 3/2$ and $\theta = 1/3$). It has been shown that with these values of α and θ, the MLS scheme can generate an accurate solution for the purely advection equation with the additional Courant number constraint $Cr = 1$. When these constraints are satisfied it is found that no errors occur in the algorithmic amplitude and the phase velocity of the MLS scheme for the advection equation. It should be noted that this numerical advantage of the MLS scheme for the advection equation is sensitive to the Courant number. For one-dimensional problems, the conditions in (3.38) can be easily satisfied by selecting the time step via a time-adaptive procedure based on the Courant number criterion. With the multi-dimensional transport problems, however, especially with finite element discretizations that use arbitrary-shaped elements, it is difficult or even impossible to select a single time step to satisfy the Courant number criterion $Cr = 1$ at all locations of a three-dimensional contaminant migration front that has either high gradients or discontinuities. For example, if the Courant number exceeds unity in certain elements in the location of the steep front of the solution, the MLS scheme with $\alpha = 3/2$ and $\theta = 1/3$ becomes unstable in these subdomains because $\zeta^h > 1$. Therefore, conservative values of α, θ and Cr should be used to ensure that $\zeta^h \leq 1$, which would render the computations stable. This implies that the condition of $\zeta^h = 1$ may not be satisfied. The determination of conservative values of α, θ and Cr should be based on a consideration of the following aspects: (i) if $\zeta^h = 1$ is not satisfied, then the condition $v^*/v = 1$ should be satisfied; (ii) since there is only one equation available, one of two parameters α and θ can be determined beforehand, and usually the time weighting θ is taken as $\theta = 1/2$ such that the scheme has higher accuracy in time (i.e. Crank-Nicolson integral scheme). Substituting $\theta = 1/2$ into (3.36) gives the following results for the phase velocity of the MLS scheme for the advection equation

$$\left.\frac{v^*}{v}\right|_{\alpha=\frac{4}{3},\theta=\frac{1}{2},Cr=1} = 1 \tag{6.1a}$$

$$\left.\frac{v^*}{v}\right|_{\alpha=\frac{4}{3},\theta=\frac{1}{2},Cr=\frac{1}{2}}=1 \qquad (6.1\text{b})$$

Equations (6.1) imply that there is no error in the phase velocity of the Crank-Nicolson MLS (CN-MLS) scheme for $Cr = 1/2$ or $Cr = 1$ if $\alpha = 4/3$. Figure 6.1 shows the distribution of the algorithmic amplitude ζ^h and the relative phase velocity v^*/v of the CN-MLS scheme over the plane of the Courant number $Cr \in [0,3]$ vs. dimensionless wave number $\omega h \in [0,\pi]$. It should be noted from Figure 6.1 that, although (6.1) is satisfied, ζ^h will decay much faster for $Cr = 1/2$ than for $Cr = 1$. It implies that the CN-MLS scheme is more diffusive for $Cr = 1/2$ than for $Cr = 1$.

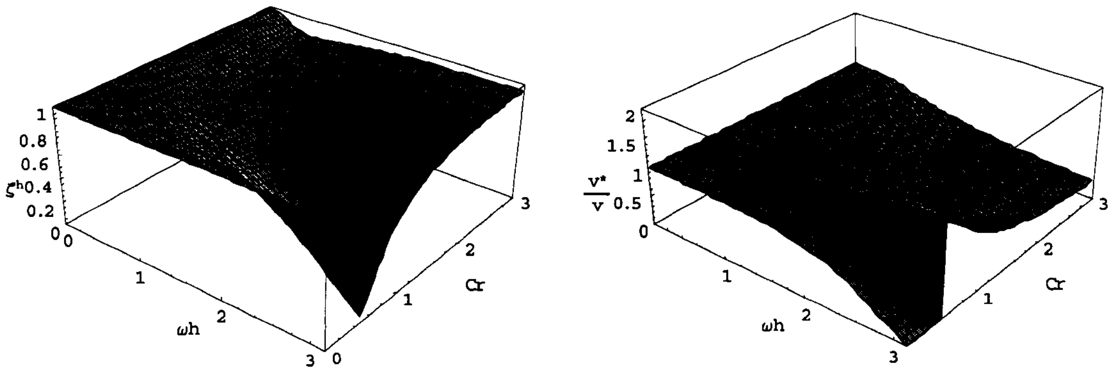

(a) (b)

Figure 6.1 Distributions of (a) the algorithmic amplitude and (b) the relative phase velocity of the MLS scheme with $\alpha = 4/3$ and $\theta = 1/2$ for the advection equation over the plane of ωh vs. Cr

Based on the above observations, the time-adaptive procedure should be coupled with the CN-MLS scheme to obtain a better numerical performance for the advection equation by using the following Courant number criterion:

$$(Cr)_{ie} = \frac{\|\mathbf{v}\|_{ie}\,\Delta t}{h_{ie}} = 1 \qquad (6.2)$$

where ie indicates the element where the steep front of the solution is located, h_{ie} and

$\|\mathbf{v}\|_{ie}$ are, respectively, the characteristic length and the magnitude of the flow velocity within the element ie. The location of the steep front of the solution in the multi-dimensional domain is determined through an error indicator $E(e)$, based on the first derivative of the solution for each element (Eriksson and Johnson, 1991)

$$E(e) = \left(\frac{1}{2} \cdot \sum_{j \in \partial e} h_j^2 [\mathbf{n}_j \cdot \nabla C]^2 \right)^2 \tag{6.3}$$

where $\mathbf{n}_j$ is the unit normal to the edge j of the element with the characteristic length h_j and ∂e is the boundary of the element. The term in square brackets in (6.3) represents the jump in the flux across the element edge. The locations (or elements) of the discontinuity or high gradient of the solution are determined by satisfying $E(e) > \beta$, and β is an error limiter which can be defined by $\beta = 0.5 \cdot \max(E(e))$.

For the transport problem of a steep front with a symmetric flow field in the computational domain discretized by the almost uniform triangle elements, the Courant number criterion can be approximately satisfied during the computation in the vicinity of the high gradient of the solution by choosing one time step Δt as follows:

$$\Delta t = \frac{1}{N_{ie}} \sum_{ie} \left(\frac{h_{ie}}{\|\mathbf{v}\|_{ie}} \right) \tag{6.4}$$

where N_{ie} is the total number of elements ie selected by (6.3). However, for the general transport problem with the arbitrary flow field, the *h*-refinement of a mesh-adaptive algorithm (Carey, 1979; George, 1991) should be used to modify the mesh size to satisfy the Courant number criterion (6.2). In such a mesh-refining adaptive scheme, the Courant number criterion (6.2) is used to refine the mesh in a quantitative way. Since the size of the element will be decreased in the mesh refinement, the elemental Courant number will increase. Therefore, in order to avoid high elemental Courant numbers, the criterion $(Cr)_{ie} \leq 0.5$ should be used in the mesh-adaptive algorithm, such that the Courant number in the refined elements is not greater than unity. In this approach, only the elements where the high gradient of the solution is present need be refined. The mesh refining algorithm within each time step can be summarized as follows:

1. Select the initial set of elements for refinement based on

$$E(e) > \beta \text{ and } (Cr)_{ie} = \frac{\|\mathbf{v}\|_{ie}\Delta t}{h_{ie}} \leq 0.5\,; \tag{6.5}$$

2. Reduce the dimensions of all the edges or the longest edge of the selected triangles into half their original length;
3. Introduce new nodes at all divided edges and construct the new elements;
4. Interpolate the variables of the unrefined mesh onto the refined mesh;
5. Return to Step 1 and repeat the procedure until no further edge division is required.

In the ensuing section, this mesh-adaptive scheme will be used to model the advective transport process of contaminants from a spherical cavity in a three-dimensional axisymmetric region.

6.2 The Advective Transport from a Spherical Cavity

In section 4.4, a time-adaptive MLS model was applied to the one-dimensional advective-dispersive transport problem in a spherically symmetric region. Here, the spherically symmetric transport problem from the cavity is recomputed using a three-dimensional axisymmetric computational model. Again, only the advective transport process will be considered in the computations. A quarter region of the three-dimensional axisymmetric computational domain of finite extent with an irregular mesh discretization is shown in Figure 6.2. Appropriate Neumann boundary conditions are prescribed on the plane surfaces to achieve the required symmetry. The parameters associated with the computations are specified as follows: the radius of the cavity $a = 3\,m$, the external radius of the domain $b = 30m$, the potential head applied on the cavity boundary $\phi_0 = 100m$ and the Dupuit-Forchheimer measure of the hydraulic conductivity $k = 0.03m/day$. If the fluid is assumed to be incompressible with respect to the porous medium, the Darcy flow velocity determined by the potential at the cavity boundary and the far-field, theoretically prescribed at $R \rightarrow \infty$, is steady and can be expressed in the spherical polar coordinate system (R,Θ,Φ) as

$$v_R(R)=\frac{\phi_0 ka}{R^2} \tag{6.6}$$

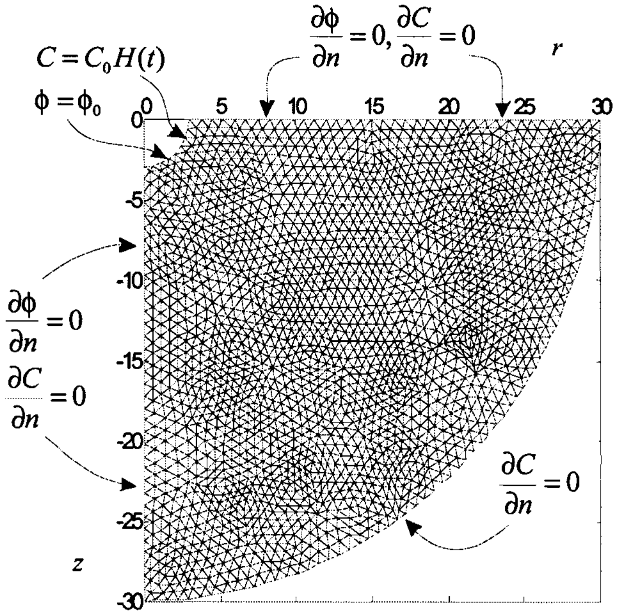

Figure 6.2 The finite element discretization (consisting of 4192 elements) of the computational domain and the associated boundary conditions for the three-dimensional axisymmetric advective transport problem from the spherical cavity

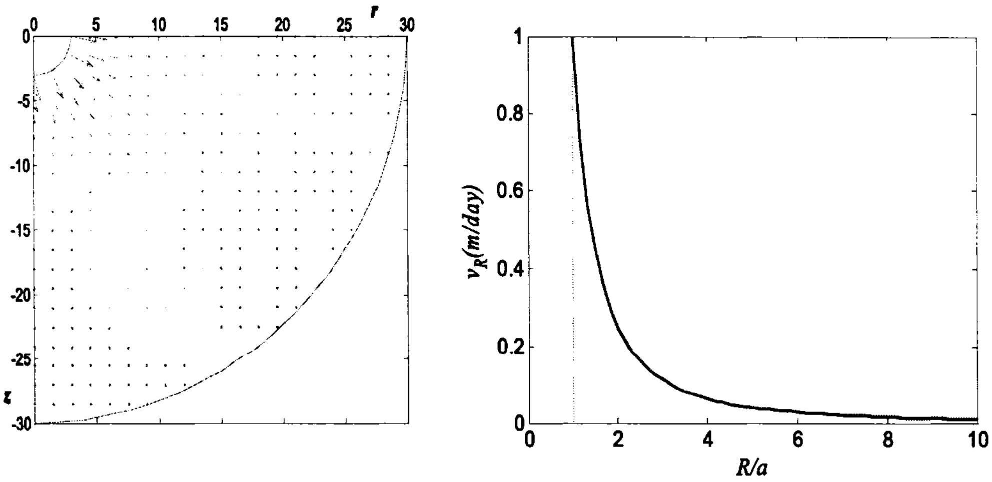

(a) (b)

Figure 6.3 Distributions of (a) the steady flow velocity pattern in the computational domain and (b) its magnitude along the radial direction

Figure 6.3 shows the pattern of velocity vectors during steady flow over the domain and its distribution along the radial direction. The radial flow velocity distribution in the computational domain (Figure 6.3(b)) indicates that the flow velocity is 1.0 *m/day* at the inner boundary $R = a$ and less than 0.01 *m/day* at the outer boundary $R = b$. The analytical solution for the advective transport of a steep front from the cavity, with the steady radial velocity (6.6), was given in Chapter 4. Figures 6.4(a) and 6.4(b) show the analytical solutions, given by (4.41) and (4.42), for the locations of the chemical concentration profile in the porous medium at t=20 *days* and t=500 *days*, respectively.

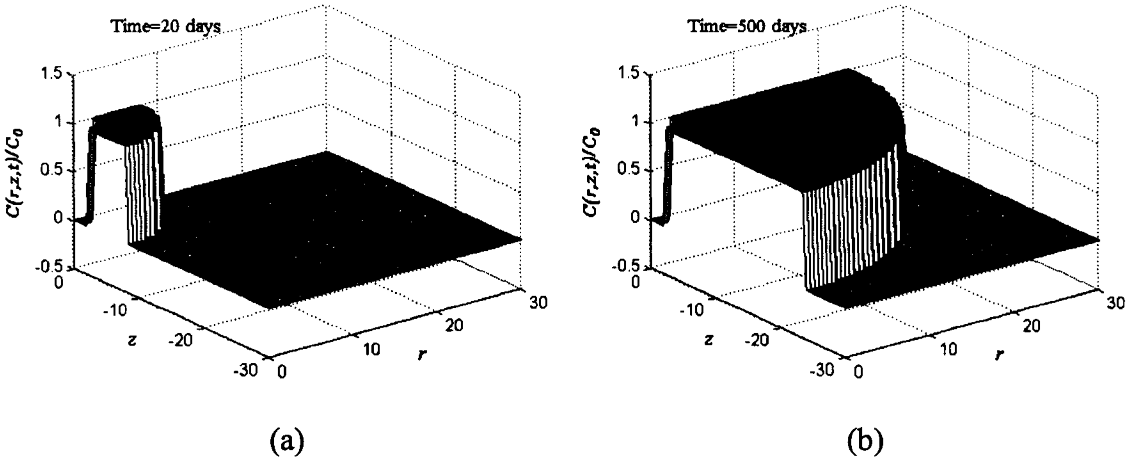

Figure 6.4 Analytical solutions of the advective transport from a spherical cavity at (a) t=20 *days* and (b) t=500 *days* (Selvadurai, 2002a)

6.2.1 Computations without Adaptive Schemes

Before the application of the adaptive computational schemes, the numerical results for the above advective transport problem from the cavity, obtained using the MLS and SUPG methods with the Crank-Nicolson time-integration scheme, are presented. Figure 6.5 shows the numerical solutions, at time t=20 *days* and t=500 *days* respectively, obtained using from CN-MLS scheme with a time step of $\Delta t = 2\,days$. It is noted that when the steep front of the solution is located in the vicinity of the cavity, numerical oscillations are introduced into the solution due to the high magnitude of the flow velocity, giving rise to a high Courant number. When the steep front of the solution migrates to a location remote from the cavity, oscillations are introduced again into the solution due to the small magnitude of the flow velocity, resulting from the low elemental Courant number in the location of the steep front. It has already been shown from Figure 6.1 that the algorithmic amplitude ζ^h will approach unity at low values (approaching zero) and high values (greater than unity) of the Courant number, but the deviations of the phase velocities of the high frequency wave components included in the solution at

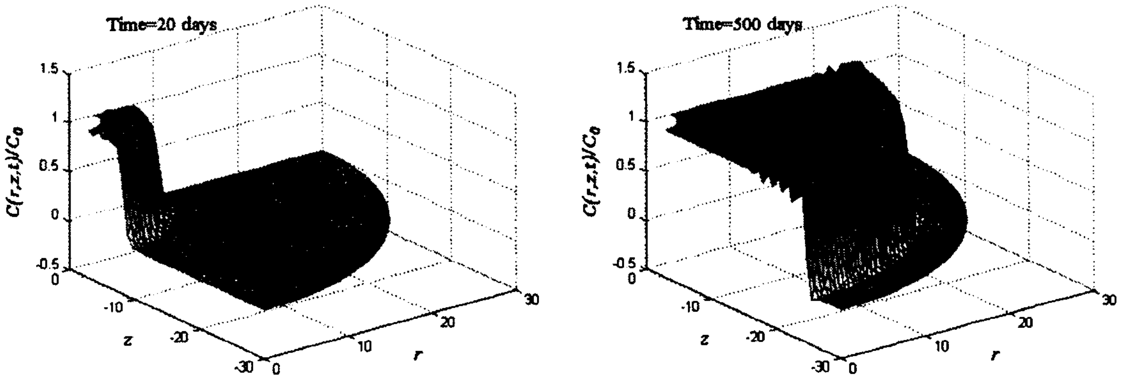

(a) (b)

Figure 6.5 Numerical results of the advective transport from a spherical cavity obtained using the CN-MLS scheme with $\Delta t = 2.0\,days$ at (a) t=20 *days* and (b) t=500 *days*

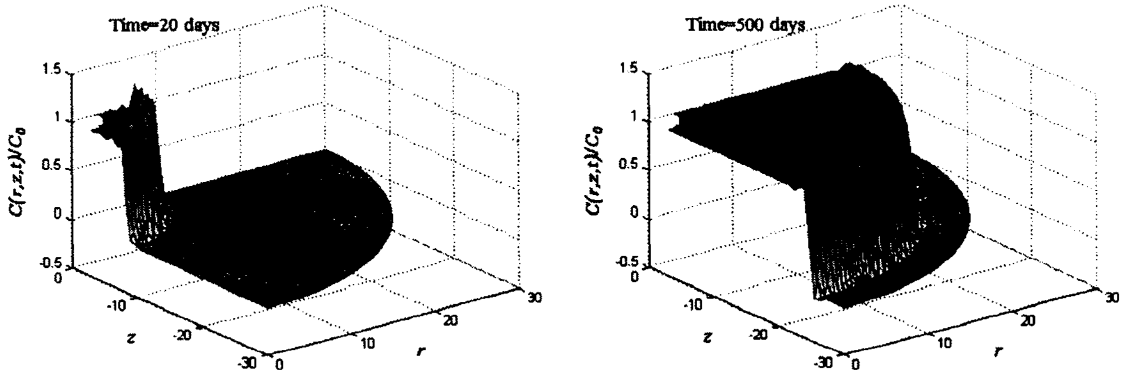

(a) (b)

Figure 6.6 Nnumerical results of the advective transport from a spherical cavity obtained using the SUPG scheme with $\Delta t = 2.0$ *days* at (a) t=20 *days* and (b) t=500 *days* low or high values of Courant number will lead to the oscillations (also referred to in the literature as 'wiggles') that either lead or trail the steep front. Similar numerical phenomena can be observed in the computational results obtained from the SUPG method for the advective transport from the cavity, which are shown in Figure 6.6. Here, the time step is also taken as $\Delta t = 2\,days$. Again, oscillations appear in the numerical solution at the start of the transport process; reasons for such oscillations were indicated previously in connection with the MLS scheme.

6.2.2 Computations with the Mesh-Adaptive Scheme

In order to remove the oscillations introduced by the numerical schemes, time- and/or mesh-adaptive procedures should be used during the computation based on the Courant number criterion of (6.2). This conclusion can be proved from the numerical computations obtained using the time-adaptive scheme, based on the observation that the advective flow field from the cavity is spherically symmetric and the elemental sizes are approximately uniform (see Figure 6.2). Figure 6.7 shows the numerical results obtained using the time-adaptive CN-MLS scheme in which the time step is determined by (6.4). Here the severe oscillations introduced by the CN-MLS (without the time-adaptive procedure) are removed. The initial time step of $\Delta t = 1\,day$ increases to $\Delta t = 22\,days$ at the end of the computation.

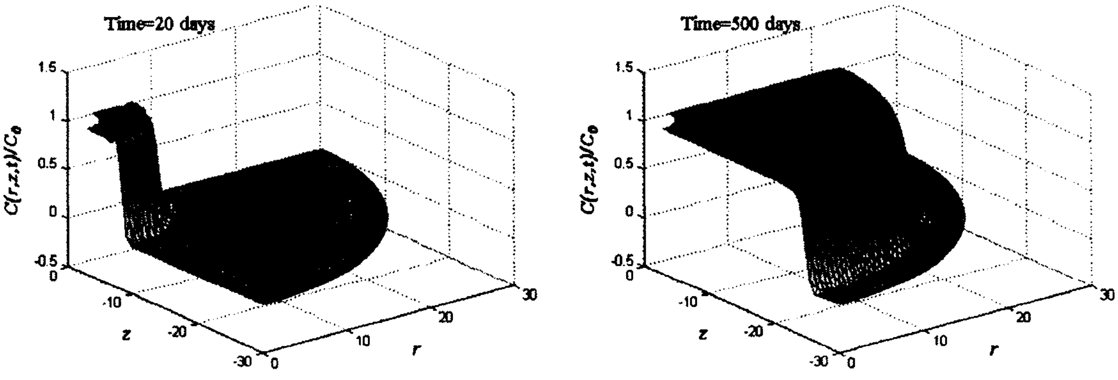

(a) (b)

Figure 6.7 Numerical results of the advective transport from a spherical cavity obtained using the time-adaptive CN-MLS scheme with $Cr = 1.0$ at (a) t=20 *days* and (b) t=500 *days*

Since arbitrary trianglar elements are used in the finite element computation and the time step determined by (6.4) is an averaged value, the Courant number in certain elements where the steep front of the solution is located may not be exactly equal to unity. This discrepancy will lead to minor oscillations which can be observed in Figure 6.7(a). In addition, since the algorithmic amplitude of the CN-MLS scheme corresponding to $Cr = 1$ decays as the dimensionless wave number increases (see Figure 4.11), the solution is also smoothed near the steep front due to numerically-induced dispersion. One way to overcome this over-diffusion of the numerical results, as the magnitude of the flow velocity decreases, is to reduce the element size based on (6.3), rather than increasing the time step. The reduction of the elemental size has an effect equivalent to that of lowering the dimensionless wave number ωh, thereby compensating for the decay in the algorithmic amplitude for the high ωh.

In order to illustrate the efficiency of the mesh-refining adaptive scheme, the computational domain is discretized with a coarse mesh consisting of 1048 elements, as shown in Figure 6.8. The corresponding computational results of advective transport from the spherical cavity at times *t*=20 *days* and *t*=200 *days*, obtained using the mesh-refining adaptive CN-MLS scheme, are shown in Figure 6.9. At these specific times, the

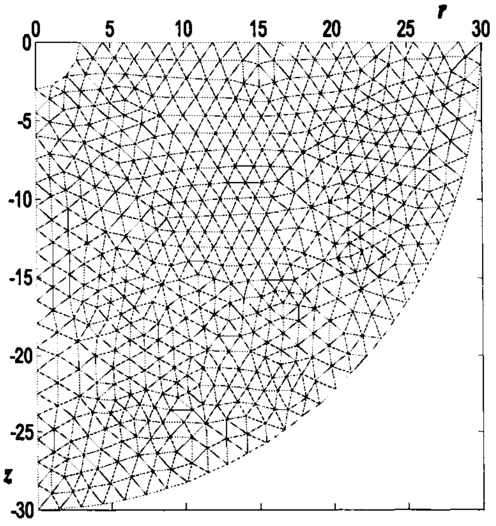

Figure 6.8 The discretization of the computational domain with a coarse mesh consisting of 1048 elements

corresponding mesh refinements yield 2035 elements and 28904 elements, respectively. Figure 6.10 shows the computational results at t=20 *days* and t=200 *days*, obtained using the mesh-adaptive SUPG scheme, where the refined meshes contain 1888 elements and 10768 elements, respectively. Judging from the flow pattern in the region shown in Figure 6.2(a) and the criterion (6.2), it should be noted that the elements located remote from the cavity region should be subject to greater refinement than those located in the vicinity of the cavity. This mesh-refining character is reflected in Figures 6.9 and 6.10. It can also be illustrated from results shown in Figure 6.10 that the time-adaptive SUPG method exhibits oscillations in the vicinity of the steep front of the solution. These

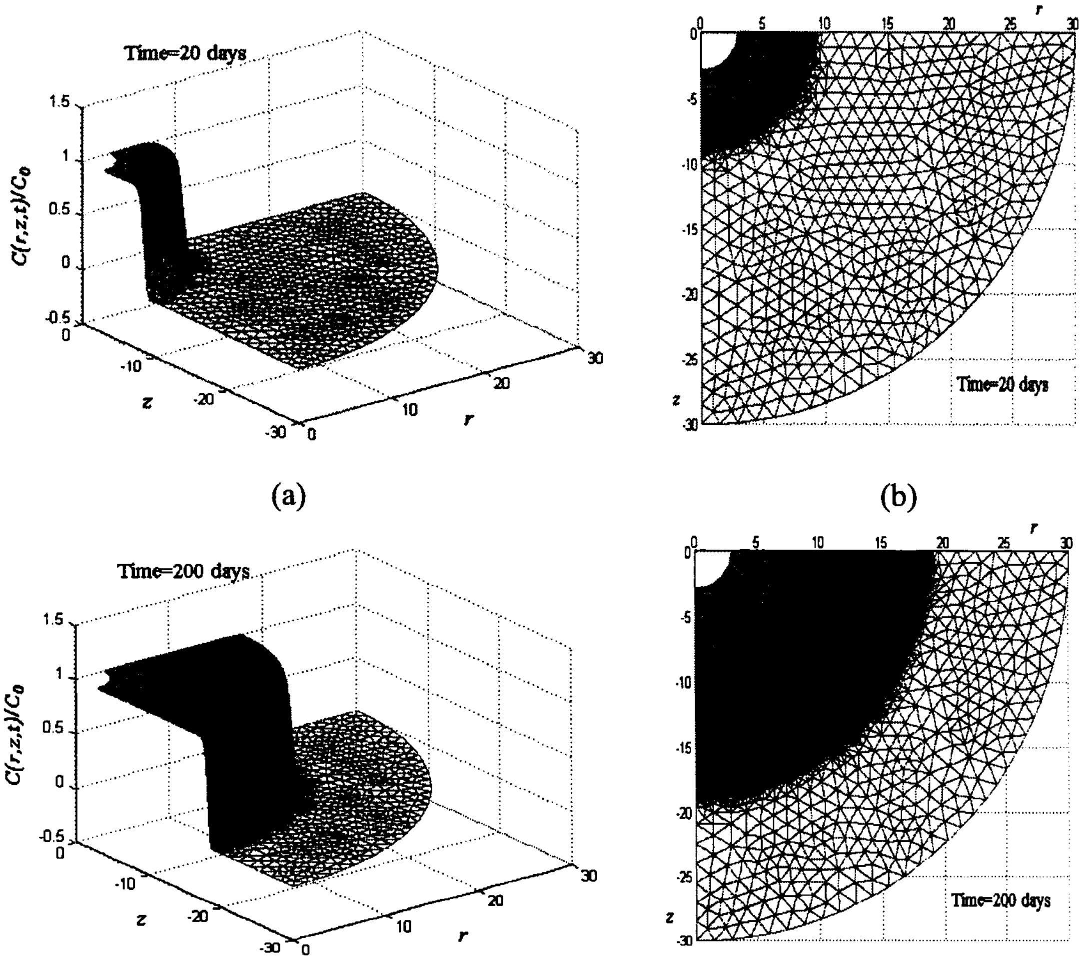

(a) (b)

(c) (d)

Figure 6.9 Numerical results and refined meshes obtained using the mesh-adaptive CN-MLS scheme, (a) 3D plot and (b) refined mesh at t=20 *days*, (c) 3D plot and (d) refined mesh at t=200 *days* oscillations are greater than those introduced by the CN-MLS scheme due to errors in both the algorithmic amplitude and phase velocity of the SUPG method as discussed in Chapter 3. The computational results illustrated in Figure 6.9 show that the mesh-refining adaptive CN-MLS scheme can generate satisfactory numerical estimates for the linear advective transport in a multi-dimensional domain.

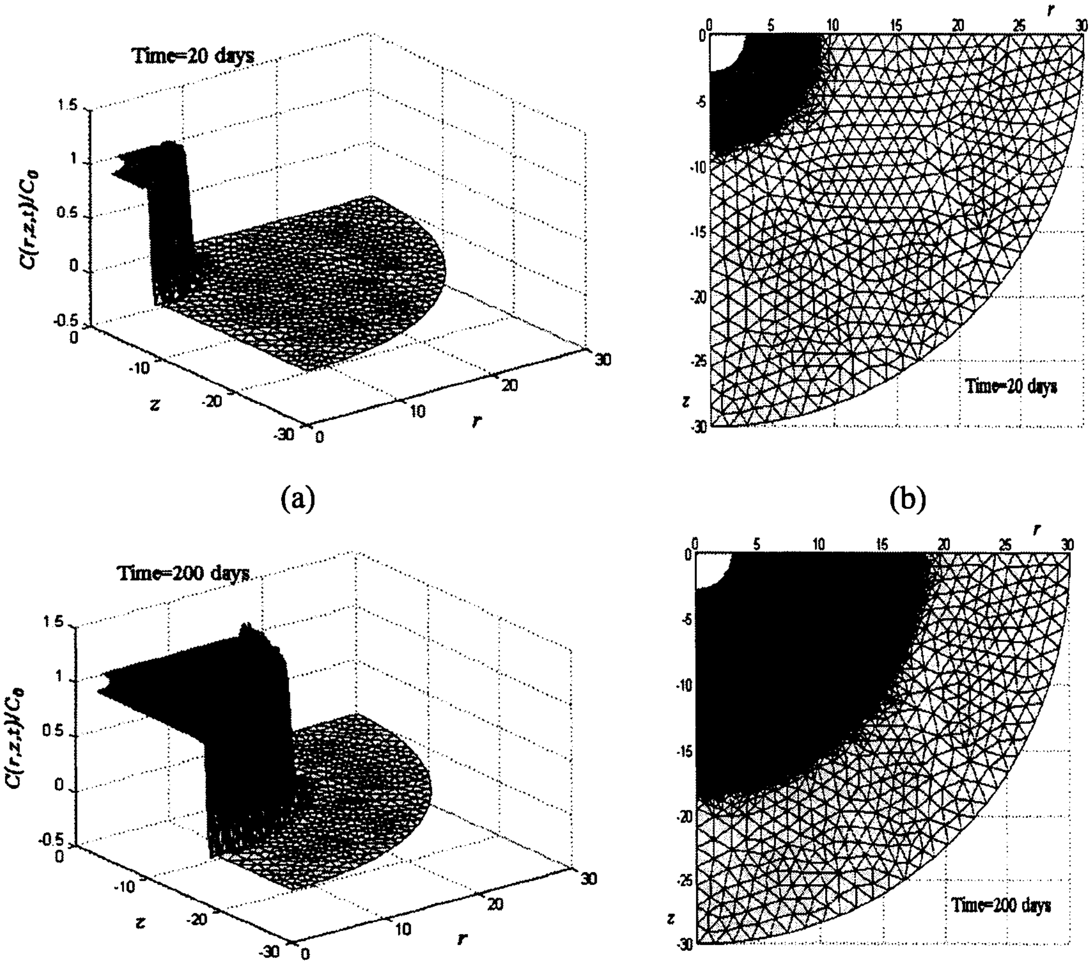

(a) (b)

(c) (d)

Figure 6.10 Numerical results and refined meshes obtained using the mesh-adaptive SUPG scheme, (a) 3D plot and (b) refined mesh at t=20 *days*, (c) 3D plot and (d) refined mesh at t=200 *days*

Incorporating the mesh-refining adaptive procedure, the MLS scheme with $\alpha = 3/2$ and $\theta = 1/3$ is now used for the solution of the advective transport problem from the spherical cavity, and the corresponding numerical results are shown in Figure 6.11. It can be noted from this figure that severe oscillations are introduced into the solution by this scheme even with the application of the mesh-adaptive scheme. This is because the MLS scheme with such defined alpha and theta is sensitive to the Courant number. During the mesh-refining adaptive procedure, the courant numbers in certain refined elements may be greater than unity, resulting to large algorithmic amplitudes greater than one and making the scheme unstable in these elements.

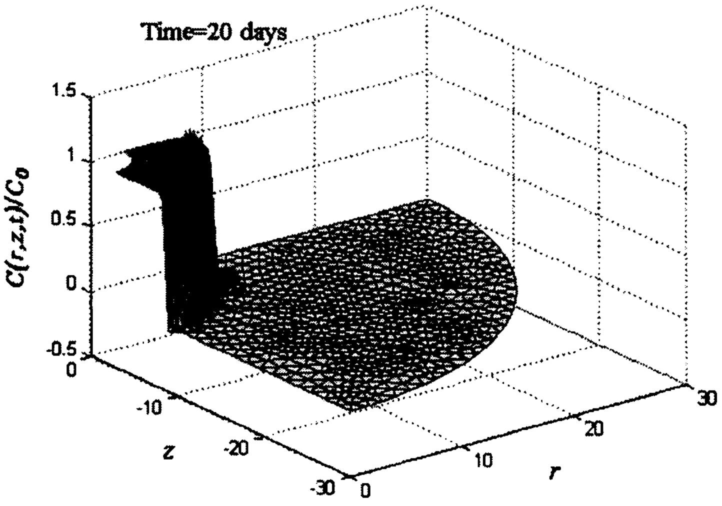

Figure 6.11 Numerical results obtained using the mesh-adaptive MLS scheme with $\alpha = 3/2$ and $\theta = 1/3$ at t=20*days* for the advective transport from a spherical cavity

6.2.3 The Advective Transport with Pressure Transients

In the modelling of the advective transport problems presented in Section 6.2.2, the pore fluid was assumed to be incompressible and the soil was considered to be rigid. Also the contaminants are released from the cavity after attainment of steady flow. In certain situations, the pore fluids and the soil skeleton are compressible, and contaminants are usually released with the establishment of the flow due to the pressurization of the contaminated pore fluids. The one-dimensional case corresponding to this situation has been already considered in Chapter 4. In this section, the three-dimensional axisymmetric advective transport from the spherical cavity, in which the flow velocities are governed by the piezo-conduction equation, is examined using the mesh-refining adaptive scheme. The numerical values of the compressibilites of the pore fluid and the soil skeleton, the porosity of the porous medium and the specific storage are taken as follows: $\kappa_s = 1.0 \times 10^{-8}\, m^2/N$, $\kappa_f = 4.4 \times 10^{-10}\, m^2/N$ and $n^* = 0.3$. The flow field in the computational domain is derived from the potential boundary conditions shown in Figure 6.2. The mesh-refining adaptive CN-MLS scheme is used to simulate such advective transport with pressure transients. The corresponding numerical results obtained using the mesh-adaptive CN-MLS scheme with a time step $\Delta t = 1\, days$ are shown in Figure 6.12.

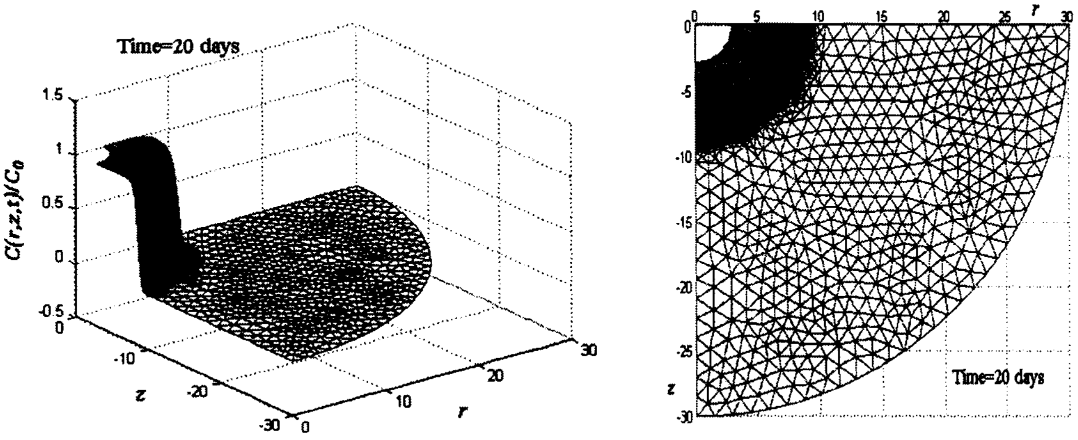

(a) (b)

Figure 6.12 The numerical result and refined mesh at t=20*days* obtained using the adaptive CN-MLS scheme for the advective transport with the pore transient, (a) 3D plot and (b) refined mesh with 2824 elements

As already mentioned, the time-dependence of the advective flow field can be caused not only by the compressibilites of the fluid-saturated porous system but also by boundary flow potentials that can vary with time. The following boundary flow potential with a pulse is considered in the computation of this cavity transport problem

$$\phi(a,t) = \begin{cases} 100 & 0 < t \le 20 days \\ 200, & 20 days < t < \infty \end{cases} \tag{6.7}$$

The computational result and the consequent refined mesh obtained using the mesh-refining adaptive CN-MLS scheme with the time step $\Delta t = 1\text{day}$ are shown in Figure

6.13. An adaptive mesh zoning can be clearly seen in the refined mesh, which corresponds to the time-dependent discontinuity in the flow velocity due to the discontinuous potential pulse applied on the cavity boundary. This increment of the flow velocity will accelerate the transport process from the spherical cavity (comparing the results shown in Figure 6.12 and Figure 6.13). Since the time- and/or the mesh-refining adaptive MLS scheme generates the symmetric matrix form and the satisfactory solutions for the advection equation, this numerical method can be confidently used with the iterative algorithm for the nonlinear transport problem in porous media.

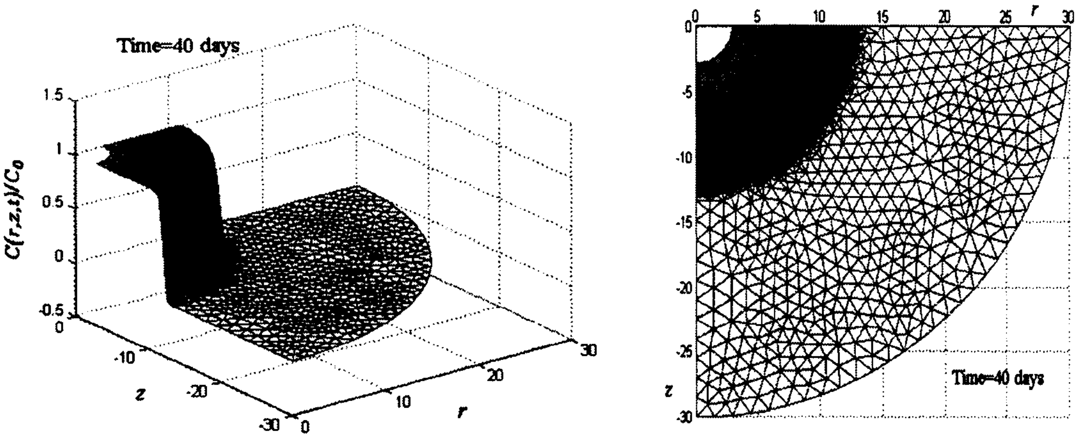

(a) (b)

Figure 6.13 The numerical result and the refined mesh at t=40*days* obtained from the adaptive CN-MLS scheme for the advective transport with the pore transient and pulsed potential boundary, (a) 3D plot and (b) refined mesh with 5672 elements

6.3 Chemically Induced Alterations of Physical Properties of Porous Media

The transport of contaminants in porous media involves complex geochemical processes that are usually influenced by nonlinear mass transfer processes between the liquid and solid phases. These geochemical reactions include sorption, complexation, ion exchange, biodegradation, etc (Von Kooten, 1996; Serrano, 2001). Compared with the magnitude of the flow velocity, such mass transfer processes can be classified into two fractions, ones that achieve equilibrium quickly and others that achieve equilibrium slowly (Kanney et al, 2003). Both fast and slow mass transfer processes can be described by a general kinetic model expressed by (2.10) that can be coupled into the transport equation as a source/sink term, but for the fast mass transfer process, the differential equation governing the kinetic model can be reduced to the algebraic equation. The geochemical reactions not only change the composition of the contaminant being transported with the groundwater but also alter the mechanical and hydrological properties of the soil skeleton, such as the deformability, compressibility, fluid transport characteristics, etc., which also have a significant influence on contaminant transport in porous media. In this section, the chemically-induced alterations of the mechanical properties of the porous medium will be briefly discussed, and these factors will be considered in the ensuing computations of the nonlinear advective transport from a disc-shaped cavity in a three-dimensional axisymmetric porous region.

6.3.1 The Alteration of the Hydraulic Conductivity

The permeability or the hydraulic conductivity of porous media is a key parameter in the modelling of fluid flow and the transport of contaminants through porous media. The assumed uniform and time-independent permeability of porous media (soil or rock) is clearly a simplification of most geological situations. The permeability is influenced by the interconnected pore structure of the soil or rock (Bear, 1972; Katz and Thompson, 1986; Doyen, 1988) and therefore any process that affects the pore structure influences the permeability. The reaction between the transporting chemical and the solid skeleton of the porous medium may alter the pore structure, and consequently lead to a variation of the permeability, which is important for quantifying the chemical mass transport in natural systems (Saripalli et al., 2001). The accurate understanding of the temporal evolution of the porosity and the permeability due to the dissolution and precipitation of the porous material can be obtained by mapping the micron scale characterization. Such mapping of pore morphologies can be revealed by techniques such as *Laser Scanning Confocal Microscopy* and *X-ray tomography* in the laboratory (Fredrich et al., 1993; 1995; Fredrich, 1999), which can be used for the direct estimation of permeability due to the alteration of the porosity of the porous medium. The photomicrographs of two representative full cross sections of Fontainebleau sandstone core samples, before and after dissolution experiments with the NaOH solution, are illustrated in Figure 6.14 (Jové

Colón et al., 2004), from which an alteration of the porosity of the sandstone sample can be clearly observed after the dissolution process. Many formulae for estimating the *phenomenological* permeability evolution of porous materials were developed based on

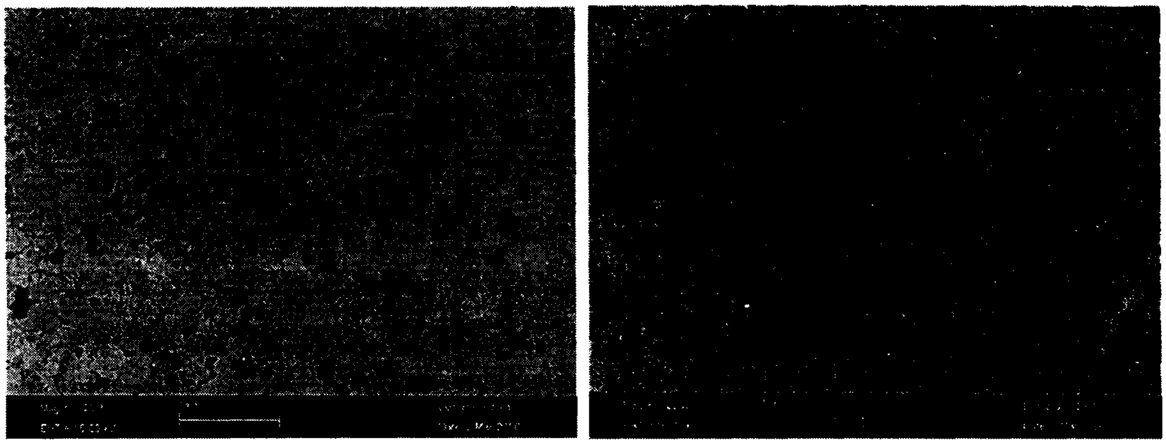

(a) (b)

Figure 6.14 Photomicrographs of core samples of sandstone (a) before and (b) after its dissolution of NaOH (Following Jové Colón et al., 2004)

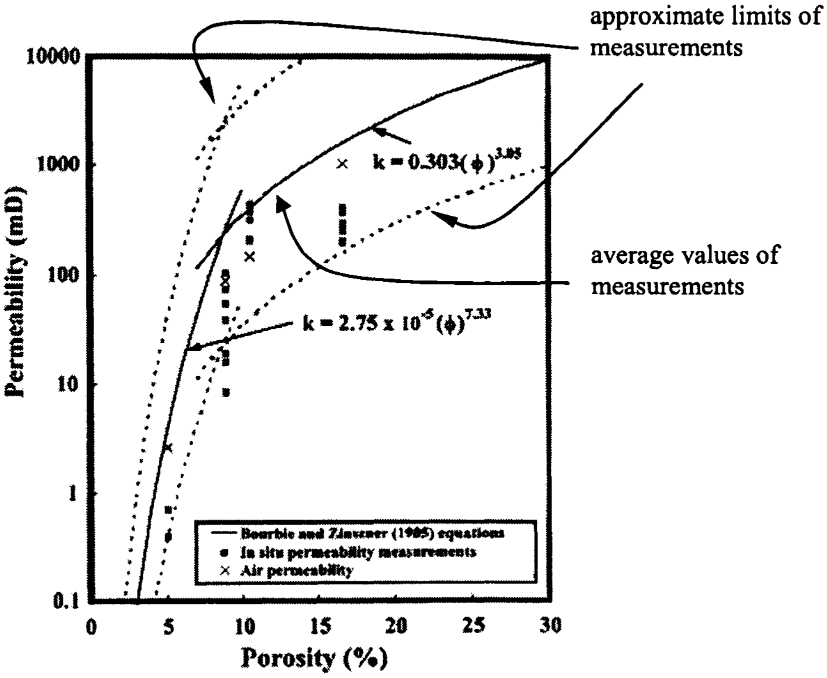

Figure 6.15 In situ permeability and air permeability, as a function of porosity, of the Fontainebleau sandstone reported by Bourbie and Zinszner (1985) (Following Kieffer et al., 1999)

the macroscopic permeability-porosity correlation and experimental observation. One simple and commonly used formula has the power law of the form (David et al., 1994)

$$k = k_0 \left(\frac{n^*}{n_0^*} \right)^j \tag{6.8}$$

where k_0 is the permeability of the untreated porous media corresponding to the initial porosity n_0^*, and j is the constant and is usually greater than 2. The commonly used cubic law is consistent with j=3 (Bear, 1972). Doyen (1988) suggested that the best fit of data is obtained using j=3.8. Recently, Kieffer et al. (1999) performed short-term dissolution experiments on Fontainebleau sandstone to obtain a relationship between the k and n^*, which is consistent with the values reported by the Bourbie and Zinzsner (1985) (see Figure 6.15).

6.3.2 The Degradation of the Elastic Stiffness

Since the precipitation and dissolution processes of the geomaterial constituents due to the chemical reaction alter the porosity of porous media, the elastic stiffness and the strength of the geomaterial can also be influenced by the alteration in the porosity. The influence of the chemical reactions, precipitation and dissolution of material constituents can be introduced in the constitutive relation in the degradation mechanisms by adding a new *ageing state variable* (Gerard et al., 1995) based on the continuum damage mechanics concept (Kachanov, 1958). The continuum damage mechanics assumes that the mechanically and chemically altered material still behaves as a continuum before the formation of macro-cracks that can lead to fractures. In general, the evolution of micro-defects of porous media due to mechanical loading and chemical flows are direction dependent, and therefore the internal variable that describes both mechanically- and chemically-induced damage should be expressed in a tensorial form. If the degradation of material properties due to chemical reactions is isotropic, i.e. no dominant directional dependency (Le Bellego et al., 2003), a more simple scalar damage variable D can be introduced into the linear stress-strain relation of the porous skeleton,

$$\sigma_{ij} = (1 - d_c) \Lambda_{ijkl} \varepsilon_{ij} \tag{6.9}$$

where Λ_{ijkl} is a 4th order elasticity tensor, $d_c(C)$ is the scalar chemical damage variable and takes a value between zero (for unreacted or chemically unaltered material) and unity (for totally dissolved material). The scalar damage variable can be defined either according to the effective load bearing area or the effective volume of a porous medium and should be determined experimentally. Figure 6.16 shows the chemical damage variable of leached cement paste samples with the calcium concentration obtained from micro-hardness experiments (Gerard et al., 1998). The solid line in the figure is a analytical relationship proposed by Fagerlund (1973).

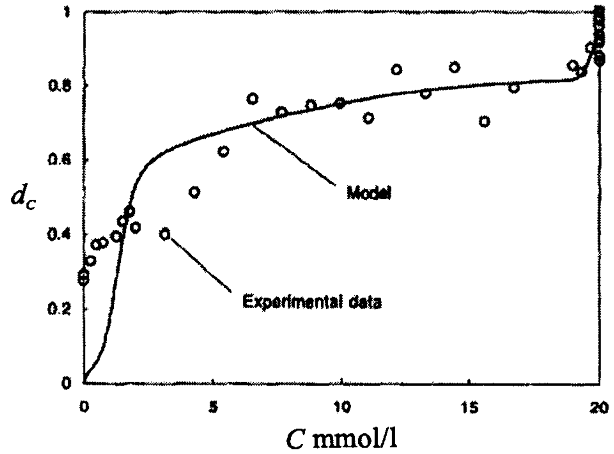

Figure 6.16 The ageing variable evolution $d_c(C)$ in concrete as a function of the calcium concentration C (Following Gerard et al, 1998)

Li et al. (2003) performed chemical acidic corrosion tests on sandstone samples to investigate the chemically-induced damage mechanism and the determination of the proper chemical–mechanical model on the rock's strength and stiffness. By dividing the rock sample into the three parts: *soluble phase*, *insoluble phase* and *porosity*, Li et al. (2003) expressed the chemical damage mechanism of the rock eroded by chemical solutes in a following quantitative way

$$E = E_d(1-d_c) + E_s \tag{6.10}$$

where E_d is the deformation modulus of the soluble cementing material, and E_s is the deformation modulus of the sample with the equivalent area when the soluble cementing material dissolves completely. They also proposed a chemical damage model to describe the process of the corrosion of sandstone and the degradation of the deformation and strength of the rock that varied with the corrosion time and the corrosion intensity. In the following section, the chemically induced alterations in the deformability and fluid-transport characteristic of the porous medium that occurs according to the prescribed relationships (6.8) and (6.10) respectively, will be considered in the numerical computation of the advective transport problem from a disc-shaped crack. Since these alterations are dependent on the chemical concentration, the resulting computational problem is non-linear, requiring an incremental iterative approach to account for the non-linearity and an adaptive approach to account for the advective transport process.

6.4 The Nonlinear Advective Transport from a Disc-Shaped Cavity

6.4.1 The Computational Modelling

A disc-shaped crack with a radius of $a = 8m$ and thickness of $2b = 2m$ is located in a fluid saturated three-dimensional axisymmetric porous medium (Figure 6.17). The contaminated fluid in the crack is pressurized and migrates into the porous medium with a Dupuit-Forchheimer hydraulic conductivity of $k = 0.03\,m/day$ and a porosity of

Figure 6.17 A schematic drawing of the advective transport from a disc-shaped crack

$n^* = 0.33$. The bulk density of the solid particle is assumed to be $\rho_b = 2.6 kg/L$. The elastic modulus and the Poisson's ratio of the porous medium are taken as $E_0 = 1.0 \times 10^8$ N/m^2 and $\nu = 0.38$, respectively, and therefore the compressibility of the porous skeleton is determined as $\kappa_s = 1/K = 3(1-2\nu)/E = 1.0 \times 10^{-8}$ m^2/N (where K is the bulk modulus). The compressibility of the fluid is assumed to be equal to $\kappa_f = 4.4 \times 10^{-10}$ m^2/N.

The finite dimensional computational domain is located within a spherical region with a radius of $R = 30\,m$. Figure 6.18 illustrates the initial finite element discretization with 301 elements of the computational domain for a quarter section of the axisymmetric region. The contaminant is released from the cavity region and is transported with the fluid movement driven by a hydraulic potential $\phi_0 = 100\,m$ applied at the cavity boundary and with zero potential at the outer boundary of the computational domain (Figure 6.18). This problem is used to examine the feasibility of the time- and mesh-adaptive scheme for modelling the nonlinear transport problem with sharp gradients and referred to a multi-dimensional region.

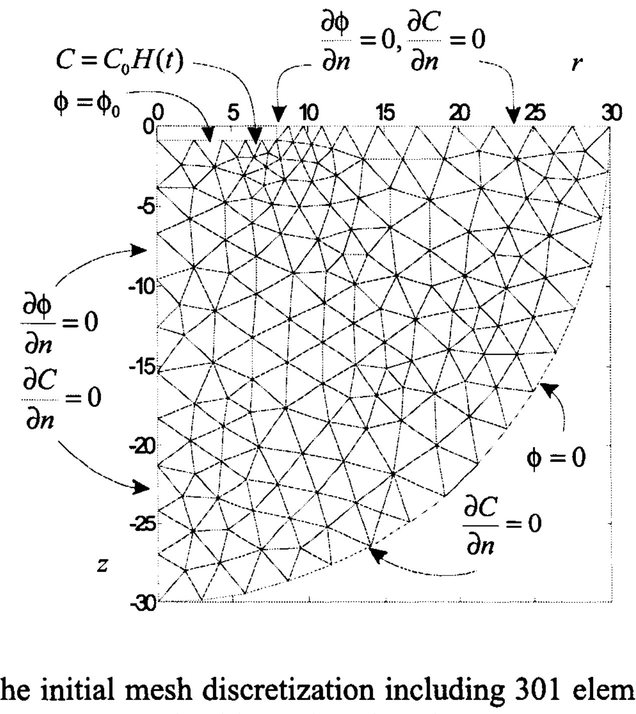

Figure 6.18 The initial mesh discretization including 301 elements and boundary conditions applicable to the advective transport problem from a disc-shaped cavity

The PDE governing the nonlinear advective transport of the contaminant in the cavity region, coupled with the mass transfer between the liquid phase and the solid phase of the contaminant, can be written in the following form

$$\frac{\partial C}{\partial t}+\mathbf{v}\cdot\nabla C+(\nabla\cdot\mathbf{v})C+\lambda\frac{\partial C_s}{\partial t}=0 \tag{6.11}$$

where C is the concentration of dissolved contaminant per unit volume of the fluid; C^s is the sorbed mass of contaminant per dry unit weight of the solid; $\lambda=\rho_b/n^*$ and $\mathbf{v}$ is the flow velocity vector. The flow velocity is assumed to be relevant to the contaminant concentration, i.e. $\mathbf{v}=\mathbf{v}(C)$, during the transport process due to the chemically-induced alterations of the hydraulic conductivity and compressibility of the porous medium. The third term on the LHS of (6.11) is non-zero if the fluid is considered to be compressible and the 4th term on the LHS of (6.11) can be used to express the Langmuir isotherm sorption that will be considered in the following computations (see the discussion in Chapter 2). The advective flow velocity is determined by the gradient of the pore pressure based on Darcy's law. The influence of the compressibility of the porous system on the pore fluid movement is considered using the *piezo-conduction* equation based on the assumption of small deformations of the soil skeleton. During the transport process, the hydraulic conductivity and elastic modulus of the porous skeleton can be altered due to the chemical reactions.

The CN-MLS scheme, introduced for the multi-dimensional transport problem in the previous section, is used to discretize the nonlinear advective transport equation (6.11), and its final stabilized weighted residual integral form can be written as follows

$$\begin{aligned}&\int_V\left[w+\frac{1}{2}\Delta t\mathbf{v}\cdot\nabla w+f(w)\right]\left[\frac{2(C^a-C^n)}{\Delta t}+(\nabla\cdot\mathbf{v})C^a+\lambda\frac{\partial C_s^a}{\partial t}\right]\mathrm{d}V\\&\quad+\int_V\left[w+\frac{2}{3}\Delta t\mathbf{v}\cdot\nabla w+f(w)\right]\left[\mathbf{v}\cdot\nabla C^a\right]\mathrm{d}V=0\end{aligned} \tag{6.12}$$

where $C^a=(C^n+C^{n+1})/2$, $f(w)$ is the perturbation term introduced in the weighting function due to the consideration of the nonlinear geochemical reaction and can be neglected in the formulation. The coefficient $2/3$ in the second integral in (6.12) results from the consideration of values of the upwind parameter α and the time weighting θ in the CN-MLS scheme (i.e. $\alpha = 4/3$ and $\theta = 1/2$). Considering linear elements, the weighted residual integral form (6.12) can be reduced to the following non-linear matrix form

$$[\mathbf{S}]\{C^a\} = \{\mathbf{F}\} \tag{6.13}$$

where

$$\mathbf{S} = (1 + \lambda \frac{\partial C_s}{\partial C})\mathbf{M} + \frac{1}{2}\Delta t \mathbf{A} \tag{6.14a}$$

$$\begin{aligned} \mathbf{A} = {} & \mathbf{v}_i \cdot \int_V w_i \nabla w_j \mathrm{d}V + \mathbf{v}_j \cdot \int_V w_j \nabla w_i \mathrm{d}V \\ & + \frac{2}{3}\Delta t \|\mathbf{v}_i\|^2 \int_V \nabla w_i \cdot \nabla w_j \mathrm{d}V + (\nabla \cdot \mathbf{v}_i) \int_V w_i \, w_j \mathrm{d}V \end{aligned} \tag{6.14b}$$

$$\mathbf{F} = \left[(1 + \lambda \frac{\partial C_s}{\partial C})\mathbf{M} - \frac{1}{2}\Delta t \mathbf{A} \right] \{C\}_j^n \tag{6.14c}$$

The matrix equation (6.13) is nonlinear about C^a since the coefficient matrix of (6.13) is assumed to be a function of C^a, and the iterative algorithm should be used for the solution of such nonlinear equations.

6.4.2 A Time- and Mesh-Adaptive Quasi-Newton Iterative Algorithm

The Newton-Raphson (N-R) iterative algorithm is regarded as an efficient iterative approach for the solution of the nonlinear algebraic equations (6.13), since it has a fast convergence rate for strongly nonlinear processes. However, the N-R method usually produces non-symmetric tangent stiffness (or Jacobian) matrices, and the updating or factorizing of such tangent matrices at each iteration results in additional computational effort, which is an impediment to the use of this procedure for the solution of large scale practical problems. The approximation of either the Jacobian matrix of the system or its inverse form leads to the *quasi-Newton* method (Engelman et al., 1981; Soria and Pegon, 1990). Such a procedure belongs to a class of methods known as *least-change secant updates*. There are several kinds of approximation formulae involved in quasi-Newton methods, and the scheme used here is the BFGS (Broyden-Fletcher-Goldfarb-Shanno) algorithm (Dennis and More, 1977), where the approximation involves the inverse of the Jacobian matrix. The N-R and/or quasi-Newton method possesses high (second-order) but local convergence, and therefore a line-search procedure is necessary to obtain the global convergence. In addition, the time- and mesh-refining adaptive procedure should be coupled with the iterative algorithm for examining the nonlinear advective transport problem. Figure 6.19 shows the flowchart of time- and/or mesh-adaptive quasi-Newton iterative algorithm for the weakly coupled piezo-conduction equation (2.8) and the nonlinear advective equation (6.11).

6.4.3 Computations for the Linear Transport

The proposed time- and mesh- adaptive quasi-Newton iterative algorithm is first applied to the linear advective transport from the disc-shaped cavity, with the consideration of a first-order reaction term, purely for the development of a reference solution. For this case, the mass transfer term in (6.11) has the form $\lambda\frac{\partial C_s}{\partial t} = rC$, where r is the coefficient for either chemical generation (+) or chemical decay (-). In the following computations, r is taken as $r = -0.01$. A computational flow velocity field corresponding to t=30*days* is shown in Figure 6.20, which indicates that the flow pattern is inhomogeneous with high velocities occurring at the boundary of the disc-shaped cavity.

Figure 6.21 shows the analytical solution, given by Selvadurai (2003, 2004a), for the advective transport from an oblate spheroidal cavity with a long axis of $a = 8m$ and short axis of $b = 1m$, in the region shown in the Figure 6.17. This analytical solution can be considered as an approximation for the linear advective transport problem from the disc-shaped crack considered in this section. Figure 6.22 shows the computational results, obtained using the mesh-refining adaptive quasi-Newton iterative scheme, for the advective transport driven by the flow pattern shown in Figure 6.20. The time step is taken as $\Delta t = 0.5$ *days*, and the initial mesh of 301 elements is refined into 5543 elements.

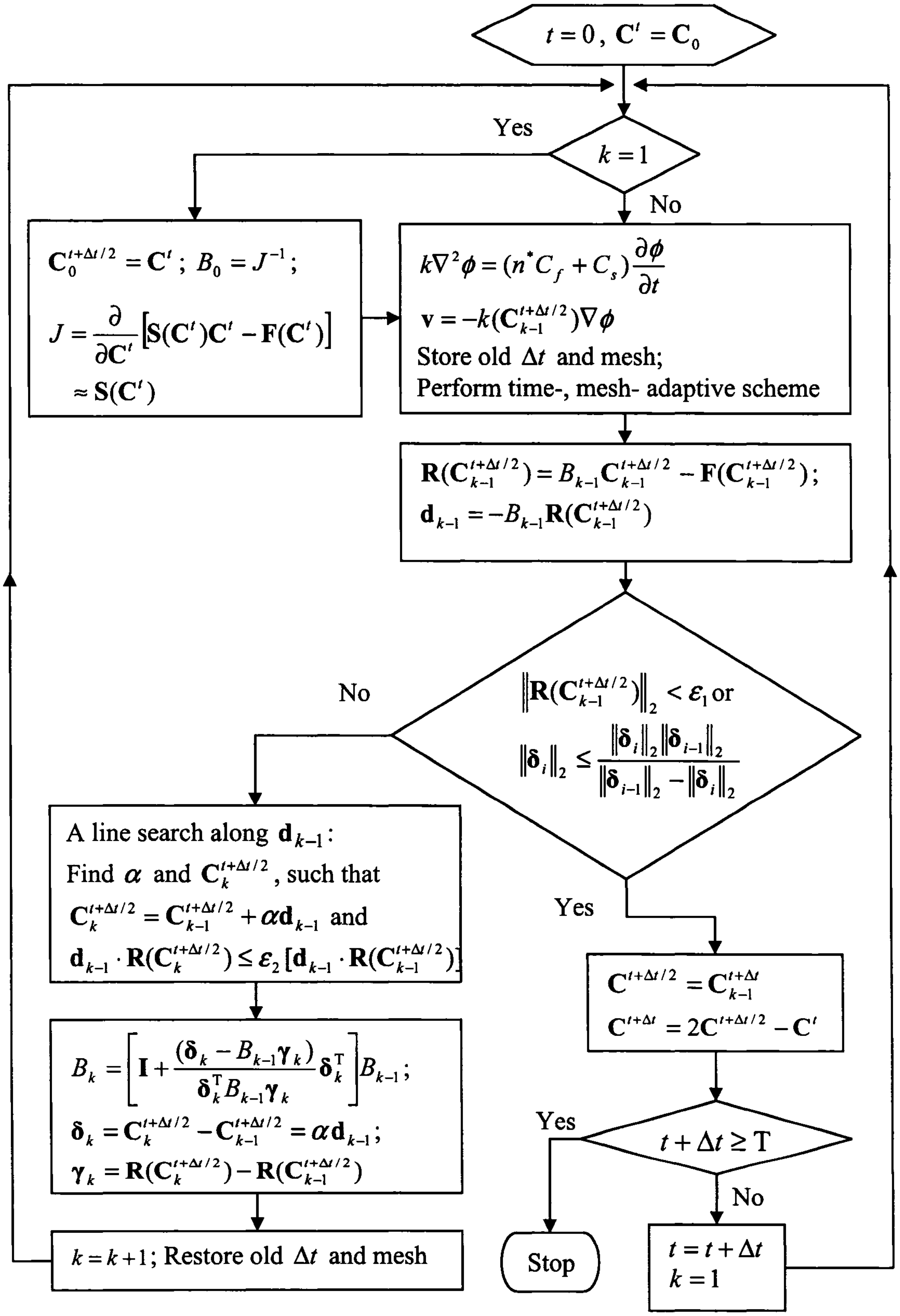

Figure 6.19 The flowchart of the time- and mesh- adaptive quasi-Newton iterative algorithm, where ε_1 and ε_2 are tolerance criteria

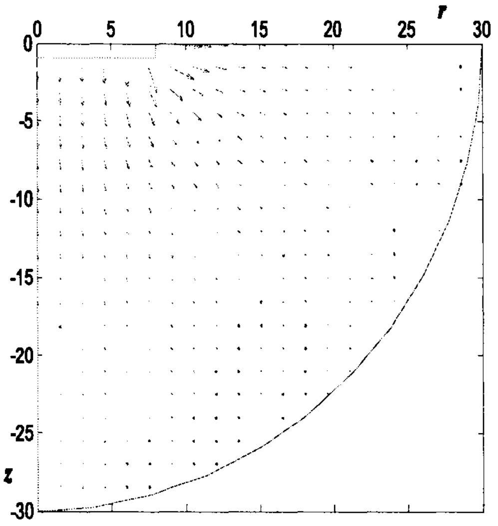

Figure 6.20 The steady flow velocity pattern in the computational domain for the axisymmetric advective transport from a disc-shaped cavity

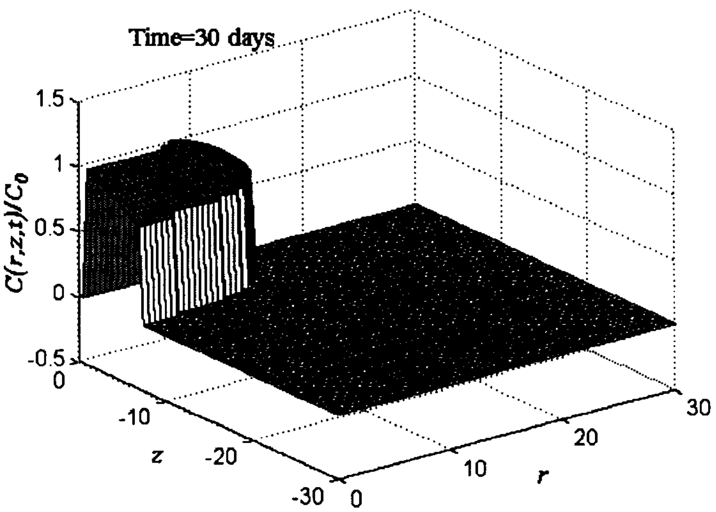

Figure 6.21 The analytical solution of the linear advective transport with decay from an oblate spheroidal cavity (a/b=8) (Selvadurai, 2004a)

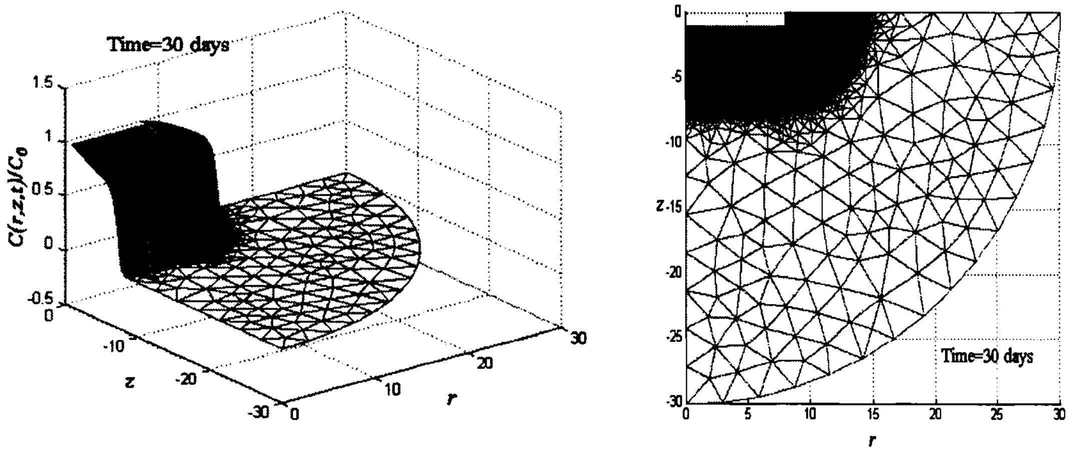

(a) (b)

Figure 6.22 The numerical result and the refined mesh at t=30*days* obtained using the mesh-adaptive iterative algorithm for the linear advective transport with decay, (a) 3D plot and (b) refined mesh with 5543 elements

Although the time-adaptive procedure can not be used on its own for such an advective transport problem for a multi-dimensional domain, it can be coupled with the mesh-refining adaptive scheme to improve the efficiency of the latter. In such a time- and mesh-refining adaptive scheme, the time step is selected first by the following equation

$$\Delta t = \min_{\text{ie}}\left(\frac{h_{ie}}{\|\mathbf{v}\|_{ie}}\right) \qquad (6.15)$$

and then the mesh-adaptive scheme is applied with the new time step. The minimum in (6.15) ensures that the elemental Courant number is not greater than unity. Figure 6.23 shows the computational results obtained using the time- and mesh-refining adaptive quasi-Newton iterative scheme. The time step is chosen as $\Delta t = 0.25\,days$ initially and increases to $\Delta t = 5.28\,days$ at the end of the computation ($t = 30\,days$); the initial mesh of 301 elements is refined into 733 elements. The results shown in Figures 6.22 and 6.23 indicate that the time- and mesh-adaptive method can give economical numerical results, but the mesh-adaptive method can generate a more accurate numerical solution for the advective transport because of the use of a finer mesh in the vicinity of the high gradient of the solution due to the application of the smaller time step.

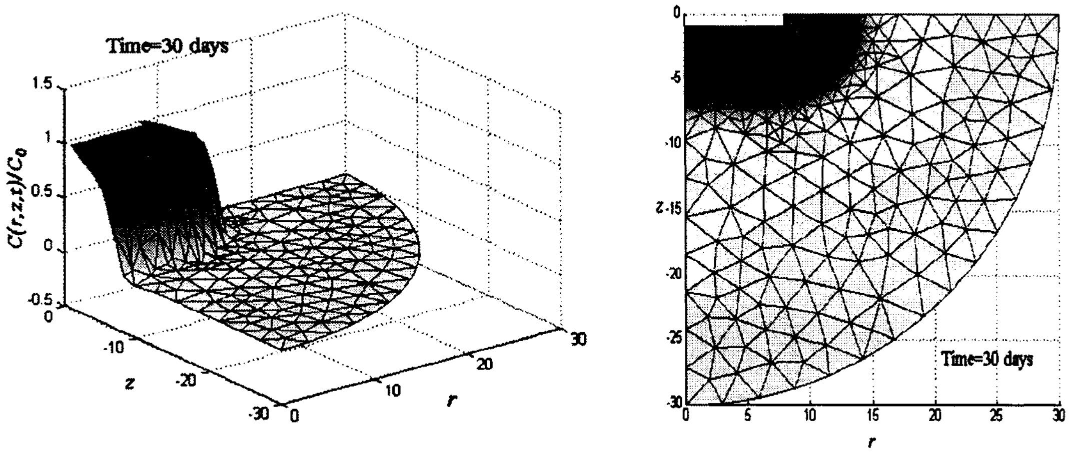

(a) (b)

Figure 6.23 The numerical result and the refined mesh at *t*=30*days* obtained using the time- and mesh-adaptive iterative algorithm for the linear advective transport with decay, (a) 3D plot and (b) refined mesh with 733 elements

6.4.4 Computations for the Nonlinear Transport

In this section, the time- and mesh-adaptive quasi-Newton iterative algorithm is used to model a nonlinear advective transport process from the disc-shaped cavity, in which Langmuir isotherm sorption is used to represent the relevant term in (6.11). For this case, the mass concentration of the solid phase of the contaminant in (6.11) is determined by (2.11a). The elastic modulus, porosity and hydraulic conductivity of the porous medium are assumed to be functions of the contaminant concentration, in order to consider the influence of the geochemical reaction. It is assumed in this computation that the chemical degradation of the porous skeleton during the computation is always isotopic. The definition of the constitutive relations and parameters involved in the nonlinear computation are listed as follows

$$k = k_0\left(\frac{n^*}{n_0^*}\right)^3, \quad n^* = n_0^* + 0.15C \tag{6.16a}$$

$$\frac{E}{E_0} = \begin{cases} 1-6.0C, & C \le 0.1 \\ 0.42-0.2C, & 0.1 < C \le 1 \end{cases} \tag{6.16b}$$

$$\kappa_s = \frac{1}{K} = \frac{3(1-2\nu)}{E} \tag{6.16c}$$

$$C_s = \frac{\alpha'\beta' C}{1+\alpha' C}, \ \alpha' = 0.01, \beta' = 1 \tag{6.16d}$$

These estimates are considered for purposes of illustration only and duplicate trends observed in the limited experimental data. First, the nonlinear advective transport of the contaminant from the disc-shaped cavity, without considering the Langmuir sorption isotherm, is examined numerically using the time- and mesh-adaptive quasi-Newton iterative scheme. In this computation, only nonlinear variations of the porosity, hydraulic conductivity and elastic modulus of the porous medium (i.e. (6.16a)-(6.16c)) are included. The numerical results and the corresponding refined mesh obtained at $t = 30\,days$ are shown in the Figure 6.24. The initial time step of $\Delta t = 0.25\,days$ increases to $\Delta t = 7.23\,days$ and the initial mesh of 301 elements is refined into 648 elements at the end of the computation. It is noted that the advective transport from the disc-shaped cavity is accelerated due to the nonlinearities involved, especially the nonlinear alteration in the hydraulic conductivity of the porous medium. Figure 6.25 shows the numerical results and the corresponding refined mesh obtained using the time- and mesh-adaptive quasi-Newton iterative scheme at $t = 30\,days$ for the nonlinear advective transport from a disc-shaped cavity with consideration of the Langmuir sorption isotherm. The initial time step of $\Delta t = 0.25\,days$ increases to $\Delta t = 3.57\,days$ finally and the initial mesh of 301 elements is refined to 692 elements at the end of the computation. The effect of retardation of the transport process due to the Langmuir sorption process can be observed in the numerical results shown in Figures 6.24 and 6.25. Finally, the numerical results, obtained using the mesh-adaptive quasi-Newton iterative scheme at $t = 30\,days$ for the nonlinear advective transport from the disc-shaped cavity, are presented in the Figure 6.26. During the computation, the time step is chosen as $\Delta t = 0.25\,days$ and the final refined mesh includes 4705 elements.

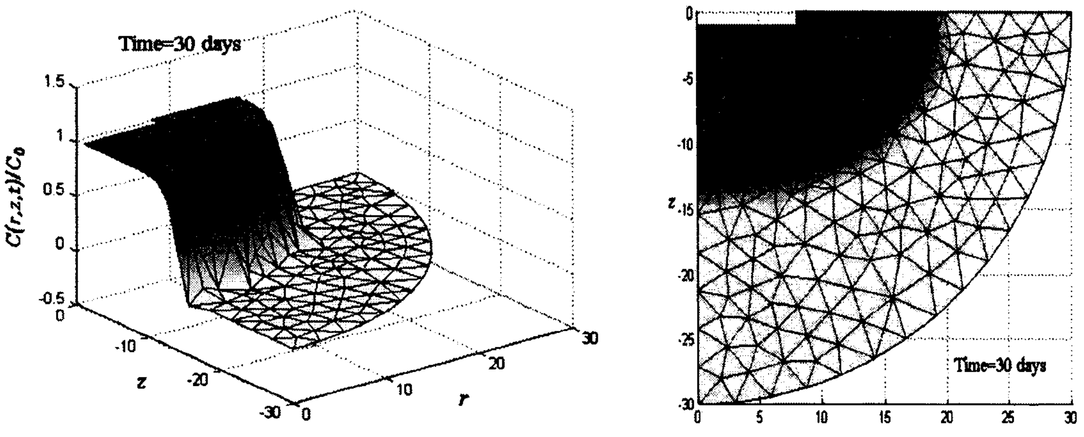

(a) (b)

Figure 6.24 The numerical result and the refined mesh at t=30*days* obtained using the time- and mesh-adaptive quasi-Newton iterative algorithm for the nonlinear advective transport without the Langmuir isotherm, (a) 3D plot and (b) refined mesh with 648 elements

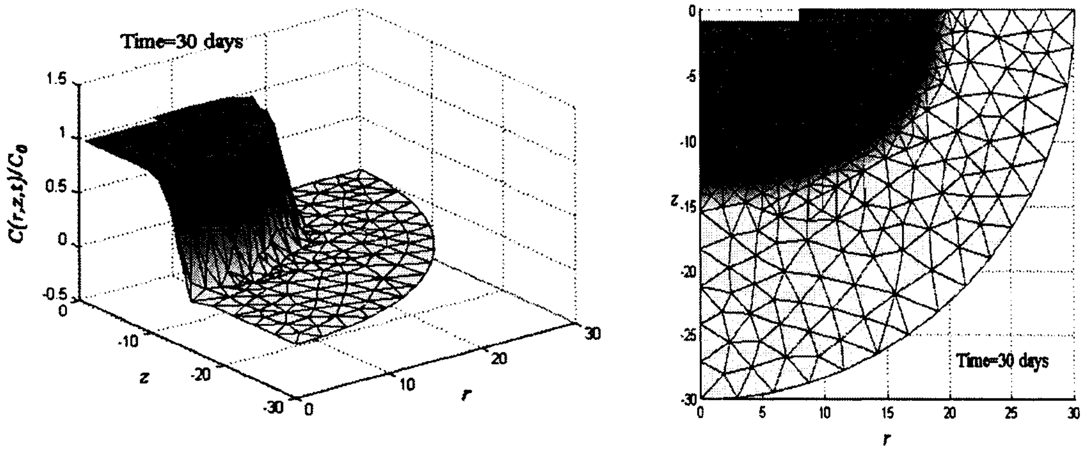

(a) (b)

Figure 6.25 The numerical result and the refined mesh at t=30*days* obtained using the time- and mesh-adaptive quasi-Newton iterative algorithm for the nonlinear advective transport with the Langmuir isotherm, (a) 3D plot and (b) refined mesh with 692 elements

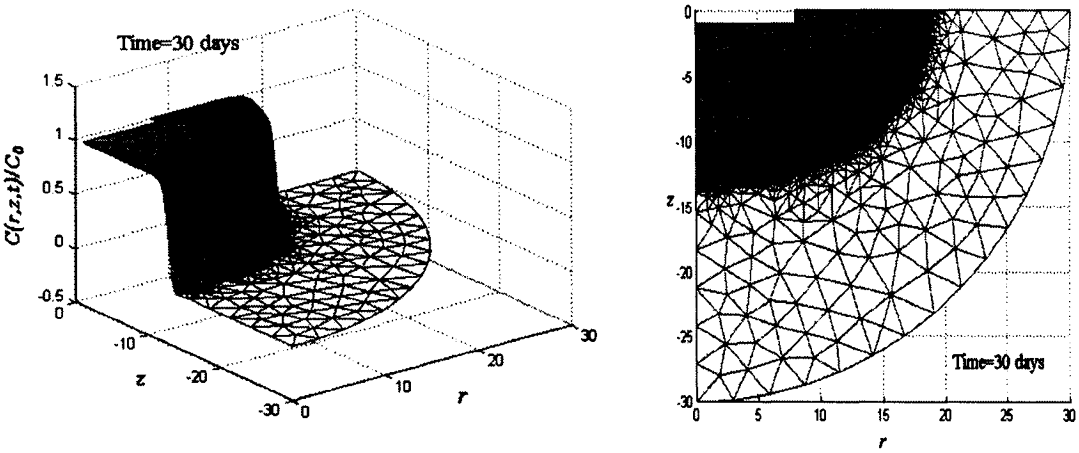

(a) (b)

Figure 6.26 The numerical result and the refined mesh at t=30*days* obtained from the mesh-adaptive quasi-Newton iterative algorithm for the nonlinear advective transport for the disc-shaped cavity, (a) 3D plot and (b) refined mesh

6.5 Discussion

Using the Fourier analysis outlined in Chapter 3, it is shown that the numerical performance of the stabilized semi-discrete methods for the advection equation is influenced by the Courant number. For one-dimensional modelling, the elemental Courant number criterion in the location of the high gradient of the solution can be easily satisfied by selecting a time step. However, for a multi-dimensional finite element computation, such an elemental Courant number criteria is hardly satisfied by simply selecting a single time step, since the flow velocities and the characteristic lengths of the elements in the locations of the high gradient of the solution may differ to a large extent. For this case, a mesh-adaptive procedure should be considered to satisfy the Courant number criteria in the vicinity of the steep front of the solution. Based on these considerations, an *h*-refinement mesh-refining adaptive scheme is developed and is successfully applied to study the linear and nonlinear three-dimensional axisymmetric advective transport problems from spherical and disc-shaped cavities in a porous region of finite extent. In comparison to the conventional mesh-adaptive schemes, which are controlled through an energy functional or a residual error of the finite element scheme and can only qualitatively identify the region to be refined, the proposed mesh-refinement strategy is quantitative.

The mesh-refining adaptive scheme proposed in this chapter can become more efficient if the mesh coarsening technique is applied, with which the mesh in the locations of the smooth part of the solution can be coarsened (or the original mesh restored). This aspect can be one focus for future work. An attempt has been made to improve the efficiency of the mesh-refining adaptive scheme by coupling it with the time-adaptive procedure. As illustrated from the computational results of the nonlinear advective transport of a steep front from the disc-shaped cavity, the time- and mesh-refining adaptive scheme can generate an oscillation-free solution for the advection equation, but the solution is relatively diffusive due to the fact that a large time step, and consequently large mesh size, was used.

CHAPTER 7

THE CONTAMINANT TRANSPORT IN A POROUS MEDIUM WITH HYDRO-MECHANICAL-CHEMICAL BEHAVIOUR

The presentations in Chapters 4 and 6 account for the influence of the deformations of the porous skeleton and the compressibility of the pore fluid on the contaminant transport process in a restricted fashion, which enables the application of the piezo-conduction equation (Barenblatt et al., 1990; Selvadurai, 2002). In certain situations, the porous geologic medium can exhibit characteristics that make the applicability of the piezo-conduction equation less accurate, and thus the complete coupling of the deformations of the porous skeleton and the pore fluid should be involved. In this case, the movement of the pore fluid that transports the contaminant needs to be described by a more accurate theory similar to that proposed by Biot (1941) (see also Lewis and Schrefler, 1998). The advection-dominated transport of the contaminant through a porous medium can be seen in geo-environmental situations, including acid drainage in mining activities, movement of chemicals retained by tailing dams, salt migration in estuaries, etc. In these situations, the movement of a chemical through the porous medium can in turn influence its deformability and fluid transport characteristics. The resulting equations governing the coupling of mechanical, hydraulic and chemical processes in the porous medium can therefore exhibit significant non-linear effects. The objective of this chapter is to present a brief introduction to the modelling of the coupled processes of the Hydro(H)-Mechanical(M)-Chemical(C) effects that can materialize as a chemical moves through a porous medium. The chapter will present a one-dimensional model of the advection-dominated transport of a reactive chemical through a deformable porous medium of the Biot-type. Although the presentation in this chapter is restricted to one-dimensional considerations, the general approach can be adopted in a three-dimensional treatment of the analogous problem.

7.1 Governing Equations

In this section, the partial differential equations governing the coupled processes of fluid movement, mechanical deformation and chemical transport are derived for completeness. The formulation is restricted to one-dimensional considerations and these governing equations are implemented in the computational approach. Attention is restricted to the quasi-static deformations of the porous medium and all inertia effects and body forces are neglected.

7.1.1 Consolidation

The development of the general equations governing both hydro-mechanical (Biot, 1941; 1955; 1956) and thermo-hydro-mechanical (Selvadurai and Nguyen, 1995; Thomas et al., 1998; Nguyen and Selvadurai, 1998; Lewis and Schrefler, 1998; Rutqvist et al., 2001; Nguyen et al., 2005) behaviour of a fluid-saturated porous medium has been extensively discussed in the literature. The mass balance equations for the fluid and solid phases of the porous medium can be written as

$$\frac{\partial(n^* \rho_f)}{\partial t} + \frac{\partial(n^* v_f \rho_f)}{\partial x} = 0 \tag{7.1}$$

$$\frac{\partial((1-n^*)\rho_s)}{\partial t} + \frac{\partial((1-n^*)v_s \rho_s)}{\partial x} = 0 \tag{7.2}$$

where x is the spatial coordinate; t is time; ρ_f and ρ_s are the densities of the pore fluid and the solid material composing the porous medium; n^* is the porosity of the porous medium; v_f is the average true fluid velocity in the porous medium relative to the spatial coordinate system; v_s is the velocity of the solid particle. Considering the definition of the material derivative (Spencer, 2004)

$$\frac{\mathrm{D}}{\mathrm{D}t} = \frac{\partial}{\partial t} + v_s \frac{\partial}{\partial x} \tag{7.3}$$

the equations (7.1) and (7.2) can now be written as

$$\frac{\mathrm{D}n^*}{\mathrm{D}t}+\frac{n^*}{\rho_f}\frac{\mathrm{D}\rho_f}{\mathrm{D}t}+\frac{1}{\rho_f}\frac{\partial}{\partial x}[n^*\rho_f(v_f-v_s)]+n^*\frac{\partial v_s}{\partial x}=0 \tag{7.4}$$

$$\frac{\mathrm{D}(1-n^*)}{\mathrm{D}t}+\frac{(1-n^*)}{\rho_s}\frac{\mathrm{D}\rho_s}{\mathrm{D}t}+(1-n^*)\frac{\partial v_s}{\partial x}=0 \tag{7.5}$$

In (7.4), $n^*(v_f-v_s)$ represents the seepage velocity of the quasi-static fluid flow through the deformable porous medium. Assuming the applicability of Darcy's law gives

$$n^*(v_f-v_s)=-\frac{k}{\gamma_w}\frac{\partial p}{\partial x} \tag{7.6}$$

where k is the hydraulic conductivity of the porous medium; $\gamma_w=\rho_f g$ is the unit weight of the pore fluid; p is the pore fluid pressure. Assuming that the densities of the fluid and the solid material in (7.6) are the functions of the pressure (Bear, 1972; Philips, 1991; Selvadurai, 2000a), i.e. $\rho_f=\rho_f(p)$ and $\rho_s=\rho_s(p)$, the following relationship for the compressibilities of the pore fluid and the solid material can be shown

$$\frac{1}{\rho_s}\frac{\partial\rho_s}{\partial p}=\frac{1}{K_s},\qquad \frac{1}{\rho_f}\frac{\partial\rho_f}{\partial p}=\frac{1}{K_f} \tag{7.7}$$

where K_f and K_s (e.g. units of stress) are, respectively, the bulk modulus of the pore fluid and the solid grain. Combining (7.4) and (7.5) and considering (7.6) and (7.7) results in the following equation

$$(\frac{n^*}{K_f}+\frac{1-n^*}{K_s})\frac{\mathrm{D}p}{\mathrm{D}t}-\frac{1}{\rho_f}\frac{\partial}{\partial x}(\rho_f\frac{k}{\gamma_w}\frac{\partial p}{\partial x})+\frac{\partial v_s}{\partial x}=0 \tag{7.8}$$

The last term in the LHS of (7.8) is the total volumetric strain of the soil skeleton in the material derivative sense, i.e.

$$\frac{\partial v_s}{\partial x}=\frac{\mathrm{D}\varepsilon}{\mathrm{D}t} \tag{7.9}$$

where ε is the one-dimensional skeletal strain. The skeletal strain is determined by the effective stress σ' applied to an element of the porous skeleton

$$\frac{\mathrm{D}\varepsilon}{\mathrm{D}t} = -\frac{1}{E_{oed}}\frac{\mathrm{D}\sigma'}{\mathrm{D}t} \tag{7.10}$$

where $E_{oed} = \dfrac{E(1-\nu)}{(1+\nu)(1-2\nu)}$ is the oedometric modulus; E is elastic modulus; ν is Poisson's ratio of the skeletal fabric. The negative sign is indicative of the sign convention where compressive stresses are negative. For the porous medium saturated with an incompressible pore fluid (i.e. $K_f \to \infty$), the effective stress is defined as the difference between the total vertical stress σ and the pore pressure p (Terzaghi, 1923), i.e.

$$\sigma' = \sigma - p \tag{7.11}$$

where σ is total vertical stress. Substituting (7.10) and (7.11) into (7.9) gives

$$\frac{\partial v_s}{\partial x} = \frac{\mathrm{D}\varepsilon}{\mathrm{D}t} = \frac{1}{E_{ode}}(\frac{\mathrm{D}p}{\mathrm{D}t} - \frac{\mathrm{D}\sigma}{\mathrm{D}t}) \tag{7.12}$$

Identifying the displacement of the one-dimensional region, $u(x,t)$, as the displacement of the porous skeleton, (7.12) gives

$$\frac{\partial u}{\partial x} = -\frac{1}{E_{oed}}(\sigma - p) \tag{7.13}$$

Substituting (7.12) into (7.8) and considering $K_f \to \infty$ in (7.8) give

$$\frac{1-n^*}{K_s}\frac{\mathrm{D}p}{\mathrm{D}t} - \frac{1}{\rho_f}\frac{\partial}{\partial x}(\rho_f \frac{k}{\gamma_w}\frac{\partial p}{\partial x}) + \frac{1}{E_{ode}}(\frac{\mathrm{D}p}{\mathrm{D}t} - \frac{\mathrm{D}\sigma}{\mathrm{D}t}) = 0 \tag{7.14}$$

In instances where the total vertical load σ is constant, $\mathrm{D}\sigma/\mathrm{D}t = 0$. For small deformation of the soil skeleton, it is also assumed that the convective rate of change in pore pressure with the solid particle in (7.14) is negligible, i.e. $\mathrm{D}/\mathrm{D}t \approx \partial/\partial t$. This reduces (7.14) to

$$(\frac{1-n^*}{K_s} + \frac{1}{E_{ode}})\frac{\partial p}{\partial t} - \frac{1}{\rho_f}\frac{\partial}{\partial x}(\rho_f \frac{k}{\gamma_w}\frac{\partial p}{\partial x}) = 0 \tag{7.15}$$

When the solid material of the porous skeleton is non-deformable, $K_s \to \infty$, and (7.15) reduces to the classical diffusion equation of the distribution of the pore pressure p in the porous medium fully saturated with the incompressible pore fluid

$$\frac{\partial p}{\partial t} = c_v \frac{\partial^2 p}{\partial x^2} \tag{7.16}$$

where c_v is the coefficient of consolidation applicable to the one-dimensional consolidation of a poroelastic solid

$$c_v = \frac{kE(1-\nu)}{\gamma_w(1+\nu)(1-2\nu)} \tag{7.17}$$

Implicit in the development presented here is the assumption of the absence of the chemical influences on both the deformability and flow properties of the porous medium. This is recognized as a limitation of the development. An indirect form of coupling can, however, be introduced by assuming that E, ν and k are dependent on the chemical concentration.

7.1.2 The Contaminant Transport

The conservation of the contaminant mass in a fixed Representative Element Volume (REV) or control volume for its liquid phase leads to (Bear and Verruijt, 1990; Lewis and Schrefler, 1998; Smith, 2000; Peters and Smith, 2002)

$$\frac{\partial (n^* C)}{\partial t} + \frac{\partial}{\partial x}(n^* v_f C) - \frac{\partial}{\partial x}(n^* D \frac{\partial C}{\partial x}) + s = 0 \tag{7.18}$$

where $C(x,t)$ is the concentration of the contaminant in the pore fluid (*mg/L*), D is the diffusion or dispersion coefficient and s is the attenuation rate of the contaminant mass per unit volume. The conservation of the contaminant mass for its solid phase without the consideration of the diffusion within solid particles leads to

$$\frac{\partial ((1-n^*)\rho_s C_s)}{\partial t} + \frac{\partial}{\partial x}((1-n^*)v_s \rho_s C_s) - s = 0 \tag{7.19}$$

where $C_s(x,t)$ is the mass of the contaminant sorbed per dry unit weight of the solid particle (*mg/kg*), and s is the rate of absorption/adsorption of the contaminant mass. The rate of contaminant loss from the liquid phase onto the solid phase is assumed to be equal to the rate of contaminant gain by the solid phase from the liquid phase. Mass conservation within a fixed control volume requires that the source and sink terms in (7.18) and (7.19) are the same. Therefore, the transport equation for a contaminant in a deforming porous medium is given by combining (7.18) and (7.19), i.e.

$$\frac{\partial(n^*C+(1-n^*)\rho_sC_s)}{\partial t}+\frac{\partial}{\partial x}(n^*v_fC+(1-n^*)v_s\rho_sC_s)-\frac{\partial}{\partial x}(n^*D\frac{\partial C}{\partial x})=0 \qquad (7.20)$$

Considering the mass balance equations (7.1) and (7.2) for the pore fluid and the solid material of the porous skeleton, the equation (7.20) can be written as

$$\begin{aligned}&n^*\frac{\partial C}{\partial t}+n^*v_f\frac{\partial C}{\partial x}-[\frac{n^*}{\rho_f}\frac{\partial \rho_f}{\partial t}+\frac{n^*v_f}{\rho_f}\frac{\partial \rho_f}{\partial x}]C-\frac{\partial}{\partial x}(n^*D\frac{\partial C}{\partial x})\\&+(1-n^*)\frac{\partial \rho_sC_s}{\partial t}+(1-n^*)v_s\frac{\partial \rho_sC_s}{\partial x}\\&-[\frac{(1-n^*)}{\rho_s}\frac{\partial \rho_s}{\partial t}+\frac{(1-n^*)v_s}{\rho_s}\frac{\partial \rho_s}{\partial x}]\rho_bC_s=0\end{aligned} \qquad (7.21)$$

Substituting (7.7) into (7.21) gives

$$\begin{aligned}&n^*\frac{\partial C}{\partial t}+(1-n^*)\frac{\partial \rho_sC_s}{\partial t}+n^*v_f\frac{\partial C}{\partial x}+(1-n^*)v_s\frac{\partial C_s}{\partial x}-\frac{\partial}{\partial x}(n^*D\frac{\partial C}{\partial x})\\&-[(\frac{n^*}{K_f}C+\frac{1-n^*}{K_s}\rho_sC_s)\frac{\partial p}{\partial t}+(\frac{n^*}{K_f}v_fC+\frac{1-n^*}{K_s}v_s\rho_sC_s)\frac{\partial p}{\partial x}]=0\end{aligned} \qquad (7.22)$$

If the pore fluid is incompressible, then $K_f \rightarrow \infty$ in (7.22). If the soil skeleton is also in small deformation, i.e. $v_s \approx 0$, the effects of convection resulting from the movement of the solid particles can be neglected, then (7.22) can be written as

$$n^*\frac{\partial C}{\partial t}+(1-n^*)\frac{\partial \rho_sC_s}{\partial t}+n^*v_f\frac{\partial C}{\partial x}-\frac{\partial}{\partial x}(n^*D\frac{\partial C}{\partial x})-\frac{1-n^*}{K_s}C_s\frac{\partial p}{\partial t}=0 \qquad (7.23)$$

If the solid phases of the porous medium are further assumed to be incompressible, i.e. $\rho_s = const$, the contaminant transport equation (7.23) can be simplified to the standard advection-dispersion equation for a rigid porous medium (Bear, 1972; Loroy et al., 1996)

$$n^* \frac{\partial C}{\partial t} + \rho_b \frac{\partial C_s}{\partial t} + v \frac{\partial C}{\partial x} - \frac{\partial}{\partial x}(n^* D \frac{\partial C}{\partial x}) = 0 \tag{7.24}$$

where $v = n^* v_f$ is the seepage velocity and $\rho_b = (1 - n^*)\rho_s$ is the bulk density of the solid skeleton of the porous medium (*kg/L*).

The second term on the LHS of (7.23) or (7.24) represents the mass transfer between the liquid phase of the contaminant dissolved in the groundwater and the solid phase sorbed by the solid particles. For the single-component system, this mass transfer can be described by the kinetic model expressed as (Kanney et al., 2003)

$$\frac{\partial C_s}{\partial t} = \lambda_1 (\lambda_2 C - \lambda_3 C_s) \tag{7.25}$$

where λ_i ($i = 1,2,3$) are constants, and further details about determination of λ_i can be found in Chapter 2.

7.2 The Computational Modelling

The partial differential equations governing the HMC processes in a porous medium through which a contaminant migrates include (7.13), (7.15) (7.23) and (7.25). The dependency of the physical, mechanical and transport parameters on the chemical concentration makes the problem non-linear and amenable only to computational treatment. In this section, the computational modelling of the coupled transport problem governed by (7.13), (7.15) (7.23) and (7.25) is developed via an iterative non-linear finite element approach. In this computational modelling, the physical and transport parameters of the porous medium that are susceptible to chemical influences can be altered using the experimental investigations available in the literature. The conventional Galerkin finite element technique is used to computationally solve the partial differential equations governing the hydro-mechanical coupling of the porous medium and the stabilized semi-discrete MLS scheme is used to solve the partial differential equation governing the contaminant transport process. The corresponding discretization equations of the HMC transport model can be expressed as follows:

$$\begin{bmatrix} \mathbf{S}_{uu} & \mathbf{S}_{up} & 0 & 0 \\ 0 & \mathbf{S}_{pM} + \Delta t\theta' \mathbf{S}_{pK} & 0 & 0 \\ 0 & \mathbf{S}_{Cp} & \mathbf{S}_{CM} + \Delta t\theta \mathbf{S}_{pK} & \mathbf{S}_{Cs} \\ 0 & 0 & -\Delta t\theta'\lambda_2 \mathbf{S}_{sC} & [1/\lambda_1 + \Delta t\theta'\lambda_3]\mathbf{S}_{ss} \end{bmatrix} \begin{Bmatrix} \mathbf{u} \\ \mathbf{p} \\ \mathbf{C} \\ \mathbf{C}_s \end{Bmatrix}^{n+1} = \begin{Bmatrix} \mathbf{f}_u \\ 0 \\ 0 \\ 0 \end{Bmatrix} + \begin{bmatrix} 0 & 0 & 0 & 0 \\ 0 & \mathbf{S}_{pM} - \Delta t(1-\theta')\mathbf{S}_{pK} & 0 & 0 \\ 0 & \mathbf{S}_{Cp} & \mathbf{S}_{CM} - \Delta t(1-\theta)\mathbf{S}_{pK} & \mathbf{S}_{Cs} \\ 0 & 0 & \Delta t(1-\theta')\lambda_2 \mathbf{S}_{sC} & [1/\lambda_1 - \Delta t(1-\theta')\lambda_3]\mathbf{S}_{ss} \end{bmatrix} \begin{Bmatrix} \mathbf{u} \\ \mathbf{p} \\ \mathbf{C} \\ \mathbf{C}_s \end{Bmatrix}^{n} \tag{7.26}$$

where

$$\mathbf{S}_{uu} = \int_0^l w_i^u \frac{\mathrm{d}w_j^u}{\mathrm{d}x}\mathrm{d}x \tag{7.27a}$$

$$\mathbf{S}_{up} = \frac{1}{E_{oed}} \int_0^l w_i^u w_j^p \mathrm{d}x \tag{7.27b}$$

$$\mathbf{f}_u = \int_0^l w_i^u w_j^\sigma \mathrm{d}x \{p - \sigma_0\}_j^n \tag{7.27c}$$

$$\mathbf{S}_{pM} = (\frac{1-n^*}{K_s} + \frac{1}{E_{oed}}) \int_0^l w_i^p w_j^p \mathrm{d}x \tag{7.27d}$$

$$\mathbf{S}_{pK} = \frac{k}{\gamma_w} \int_0^l \frac{\mathrm{d}w_i^p}{\mathrm{d}x} \frac{\mathrm{d}w_j^p}{\mathrm{d}x} \mathrm{d}x \tag{7.27e}$$

$$\mathbf{S}_{Cp} = -\frac{1-n^*}{n^*} \frac{1}{K_s} C_{s\,i}^{\,n} \int_0^l w_i^C w_j^p \mathrm{d}x \tag{7.27f}$$

$$\mathbf{S}_{CM} = \int_0^l w_i^C w_j^C \mathrm{d}x \tag{7.27g}$$

$$\mathbf{S}_{CK} = \int_0^l v_{f\,i} w_i^C \frac{\mathrm{d}w_j^C}{\mathrm{d}x}\mathrm{d}x + \int_0^l \frac{\mathrm{d}w_i^C}{\mathrm{d}x} v_{f\,j} w_j^C \mathrm{d}x + [D + \alpha\theta\Delta t v_{f\,i}^{\;2}] \int_0^l \frac{\mathrm{d}w_i^C}{\mathrm{d}x} \frac{\mathrm{d}w_j^C}{\mathrm{d}x} \mathrm{d}x \tag{7.27h}$$

$$\mathbf{S}_{Cs} = \frac{1-n^*}{n^*} \rho_b \int_0^l w_i^C w_j^s \mathrm{d}x \tag{7.27i}$$

$$\mathbf{S}_{sC} = \int_0^l w_i^s w_j^C \mathrm{d}x \tag{7.27j}$$

$$\mathbf{S}_{ss} = \int_0^l w_i^s w_j^s \mathrm{d}x \tag{7.27k}$$

In (7.27), l is the length of the one-dimensional computational domain, w^m ($m = u, p, C, s$) are the weighting functions and they are all taken as the linear interpolation function in the modelling, $\theta' \in [0,1]$ and $\theta \in [0,1]$ are two time weightings, α is the upwind parameter introduced by the MLS scheme. The time weighting θ' for the equations governing the dissipation of the pore fluid pressure and the kinetics of the chemical reaction is taken as unity for better numerical stability; however, the time weighting θ for the contaminant transport equation should be determined in order for the MLS scheme to have the optimal performance. The fact that the operator splitting technique is not used for solving the advection-dispersion-reaction transport equation (7.23) implies that the optimal value of θ and α determined by (3.37) (i.e. $\theta = 1/3$ and $\alpha = 3/2$), cannot be used in the MLS formulation. For this case, the conservative values of θ and α have to be adopted in the modelling (see the relevant discussions in Section 4.3). A conservative optimal value of the time weighting and the upwind parameter can be $\theta = 1/2$ and $\alpha = 4/3$ (see the relevant discussion in Section 6.1). This corresponds to the use of the Crank-Nicolson time integration strategy for the temporal term of the transport equation (7.23). In Chapter 6, it was shown from a Fourier analysis that for a better numerical performance of the MLS scheme with $\theta = 1/2$ and $\alpha = 4/3$ for the transport equation, the Courant number should be kept equal to unity. Therefore, the time-adaptive procedure should be used during the HMC modelling of the advection-dominated contaminant transport process. Figure 7.1 shows a flowchart of the time-adaptive quasi-Newton iterative algorithm for modelling the HMC coupling transport processes defined by (7.26) and (7.27). In Figure 7.1, $\mathbf{S}$ represents the stiffness matrix of the system shown in (7.26), $\mathbf{X}$ represents the unknown nodal variables of u, p, C and C_s at the time level t^{n+1}, and $\mathbf{F}$ represents the RHS vector of (7.26).

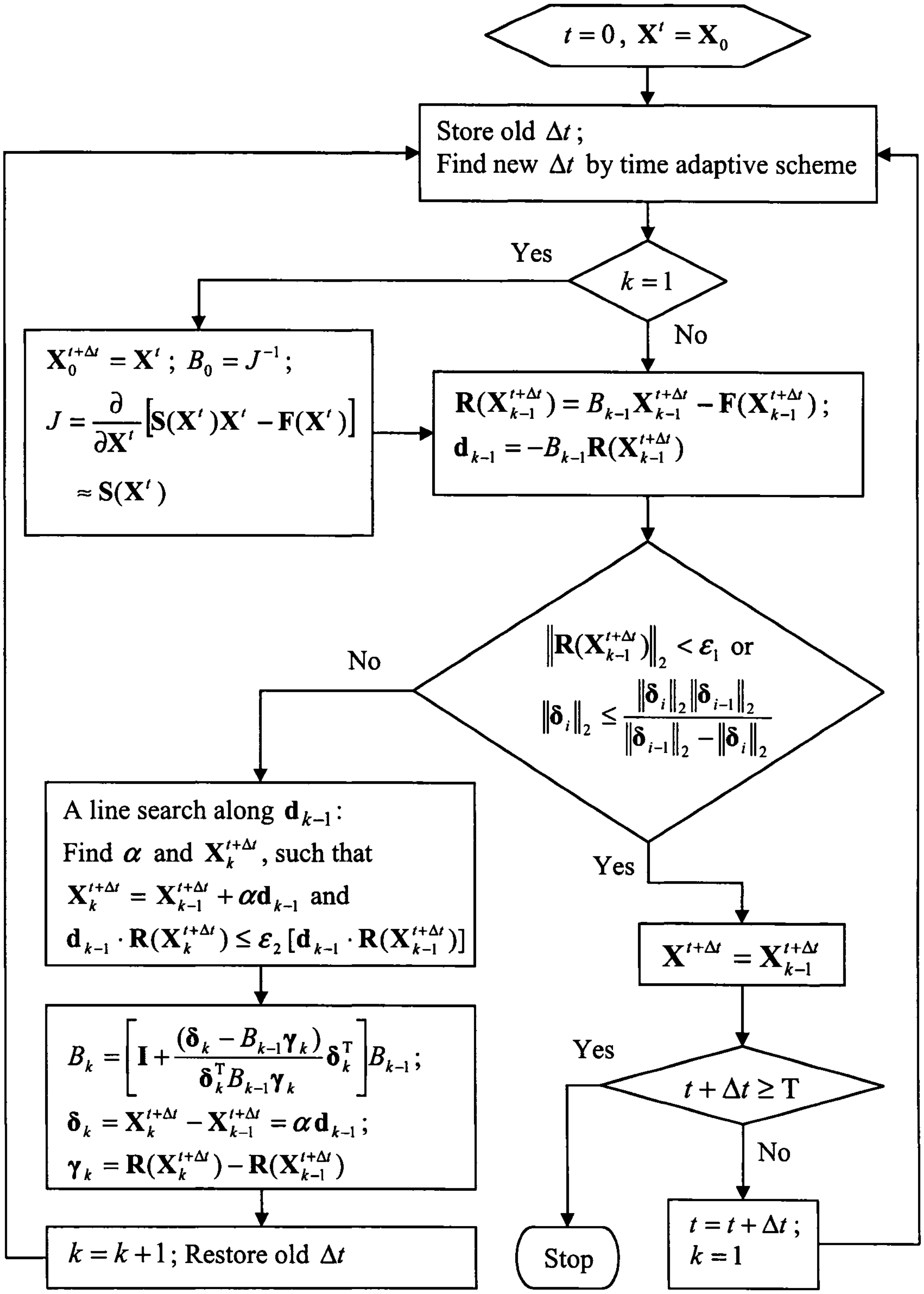

Figure 7.1 The flowchart of the time-adaptive quasi-Newton iterative algorithm, where ε_1 and ε_2 are tolerance criteria

7.3 Numerical Examples

As a numerical example, we examine the nonlinear advective-dispersive-reactive contaminant transport problem in a one-dimensional column of the porous medium of length H that is saturated with an incompressible pore fluid (i.e. $K_f \to \infty$). The skeleton of the porous medium is assumed to be linearly elastic, and the solid material of the porous skeleton is assumed to be compressible. The soil column rests on a permeable rigid base, and is subjected to a surface injection of the chemical solution with a concentration of C_0. After such chemical solution penetrates into the upper 5 meters of the soil column, the soil column is subjected to an external total vertical stress σ_0 at the surface. The strict one-dimensional conditions imply that the deformation in the z-direction is suppressed by specifying a plane strain condition. The geometry of the region and associated boundary conditions for the skeletal displacement u, the pore fluid pressure p and the contaminant concentration C are shown in Figure 7.2. The physical and mechanical parameters of the pore fluid and the poroelastic medium are given as

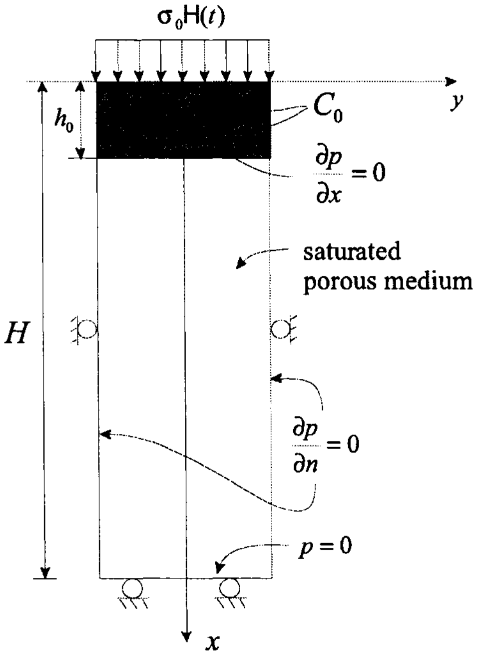

Figure 7.2 One-dimensional computational domain of the transport and consolidation problem

$$H = 30m;\ \sigma_0 = 100kPa;\ C_0 = 1;\ h_0 = 5m; \tag{7.28a}$$

$$\rho_b = 2.6kg/L;\ \rho_w = 1.0kg/L;\ K_s = 0.14\times10^{10}Pa \tag{7.28b}$$

$$E = 8000kPa;\ \nu = 0.4;\ n^* = 0.36 \tag{7.28c}$$

$$k = 6\times10^{-4}m/day;\ D = 10^{-4}m^2/day \tag{7.28d}$$

7.3.1 Elastic Consolidation

The first example deals with a comparison of the analytical and computational results for the one-dimensional consolidation of the porous elastic soil column subjected to a constant total stress σ_0. The chemical load, intrusion and transport are not considered during this computation. Initially, the total stress σ_0 is completely carried by the pore fluid, and the excess pore pressure will dissipate in accordance with the Dirichlet boundary condition applied at the base and the Neumann boundary condition applied at the surface of one-dimensional domain. The analytical solution for the time-dependent variation in the pore fluid pressure for a porous medium consisting of an incompressible pore fluid and non-deformable grains (i.e. $K_s = K_f = \infty$) was given by Terzaghi (1943), and takes the following form

$$p = \sigma_0 \frac{4}{\pi}\sum_{m=0}^{m=\infty}\frac{1}{2m+1}\sin\left(\frac{(2m+1)\pi(H-x)}{2H}\right)\exp\left(-\frac{(2m+1)^2\pi^2T_v}{4}\right) \tag{7.29}$$

where $T_v = c_v t/H^2$ is a dimensionless time factor. Figure 7.3 gives the variation in the excess pore pressure p (*kPa*) in the soil column ([0,30*m*]) given by (7.29) over a 150-day period.

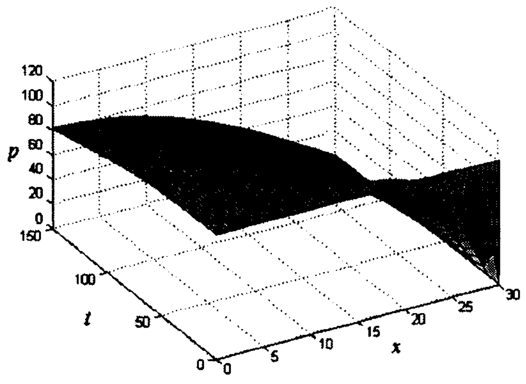

Figure 7.3 The analytical solution for the dissipation of the excess pore fluid pressure in the soil column during a 150-day period

In the numerical computations, the computational domain is discretized into 60 elements with an elemental length of $h = 0.5m$, and the time step Δt is taken as 10 *days*. The corresponding computational results for the dissipation of the excess pore fluid pressure p (*kPa*) and time-dependent deformation u (*m*) of the soil column during a 150-day period are shown in Figure 7.4. It should be noted that the numerical results for the dissipation of the excess pore fluid pressure shown in Figure 7.4(a) are close to its analytical solution shown in Figure 7.3.

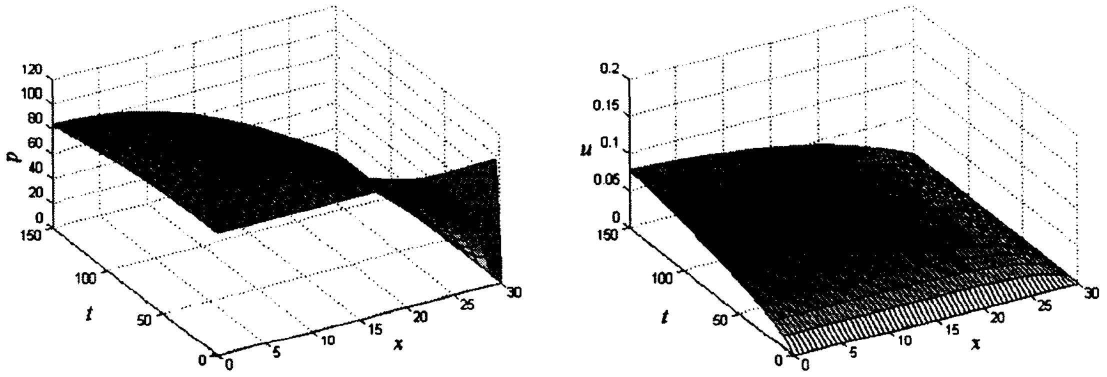

(a) (b)

Figure 7.4 Computational results during a 150-day period of (a) the dissipation of the excess pore fluid pressure and (b) the consolidation of the soil column

7.3.2 The Chemical Transport Driven by Consolidation

The second example deals with the problem of the contaminant transport in the soil column induced by the poroelastic response of the porous medium. The problem formulation with respect to the hydro-mechanical aspects, is identical to that described in section 7.3.1. In this case, however, the surface of the soil column is subjected to a chemical solution of concentration C_0, and such chemical solution already penetrates into the upper 5 meters of the soil column before the application of the surcharge σ_0. The diffusion or dispersion of the contaminant is considered during the contaminant transport process with the dispersion coefficient defined in (7.28d). The transport process is assumed to be influenced by the nonlinear Langmuir isotherm sorption, which can be described by the kinetic model described by the equation (7.25) with the following model parameters and sorption coefficients

$$\lambda_1 = 10^8; \quad \lambda_2 = \alpha'\beta'; \quad \lambda_3 = 1 + \alpha' C; \quad \alpha' = 0.01; \quad \beta' = 1 \qquad (7.30)$$

Figure 7.5 shows the computational results of the advective-dispersive-reactive contaminant transport processes during a 150-day period obtained from the HMC model, with and without the time-adaptive scheme. During computations, the initial time step is taken as $\Delta t = 10\,days$. It can be seen from Figure 7.5 that the dissipation of the excess pore fluid pressure drives the migration of the contaminated solution trapped in upper part soil column, and such a contaminant transport process is accelerated after 60 days, when the flow velocity increases at the interface between the contaminated and uncontaminated region. Due to this dissipation of the pore water pressure, the advective flow velocity presents a transient character, and therefore it is necessary to use the time-adaptive procedure in the computation to obtain the optimal solution of the transport process. Without the time-adaptive scheme, oscillations are introduced into the solution in the vicinity of its steep front (Figure 7.5(a)); these oscillations are avoided by using the time-adaptive procedure. It should be noted that in order to avoid the too large time increment, a constraint of $\Delta t \leq 20\,days$ is applied to the time step during the time-adaptive procedure, which results in small oscillations in the solution at the beginning of the transport process (Figure 7.5(b)).The variation of the time step during the computation determined by the time adaptive procedure is clearly illustrated by the grid line distribution of the time shown in the Figure 7.5(b).

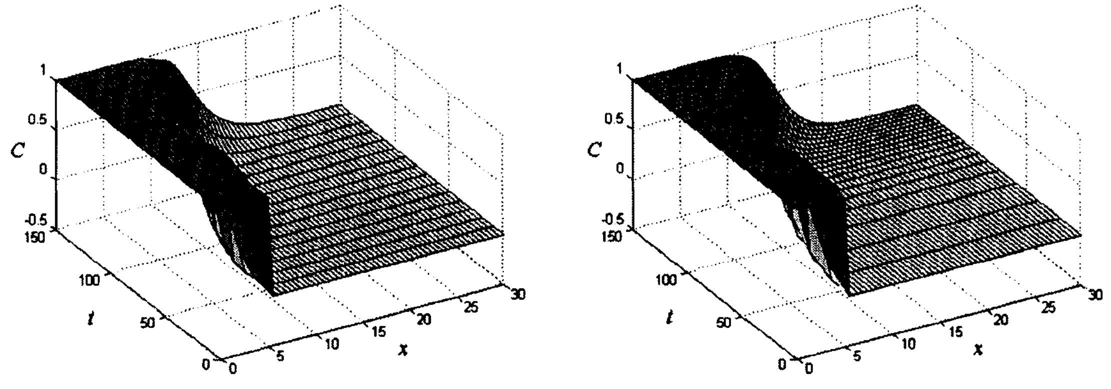

(a) (b)

Figure 7.5 Computational results during a 150-day period of the contaminant transport processes in the soil column, (a) without and (b) with the time-adaptive procedure

7.3.3 The Chemical Transport with Material Property Alterations

In this section, attention is focused on the influences of chemically-induced alterations in the deformability and fluid transport characteristics of the poroelastic medium. In general, the geochemical reaction between the contaminant solution and the porous solid is a complex, time and space dependent process (Saripalli et al., 2001). But it is assumed in this section that a space-independent leaching of the porous material is caused by the reactive interaction between the contaminant and the porous solid, resulting in the alteration of the porosity of the poroelastic medium. This is regarded as an approximation of a much more complex process where dominant flow paths, particularly in three-dimensional problems, can results in the development of chemically-induced anisotropy in the poroelastic medium. This approximation is retained in view of the fact that only the one-dimensional problem is examined. The parameters that can be influenced by the porosity, which in turn can be influenced by the chemical concentration, include the hydraulic conductivity k and elasticity parameters E and ν. The results presented by Bourbie and Zinszner (1985) (see Figure 6.15) for Fontainebleau sandstone indicate that the hydraulic conductivity of porous media subjected to chemical reaction changes according to the relationship

$$k = k_0 \left(\frac{n^*}{n_0^*} \right)^3 \tag{7.31}$$

where $k_0 = 6 \times 10^{-4} m/day$ and $n_0^* = 0.36$ are, respectively, the initial porosity and hydraulic conductivity; n^* is the chemically altered porosity, which is assumed to relate to the chemical concentration according to

$$n^* = n_0^* + 0.15C \tag{7.32}$$

Similarly, from experimental results given by Gerard et al. (1998) on leached cement paste, the elastic modulus of the porous medium is assumed to vary with the chemical concentration according to

$$\frac{E}{E_0} = \begin{cases} 1 - 6.0C, & C \leq 0.1 \\ 0.42 - 0.2C, & 0.1 < C \leq 1 \end{cases}, \tag{7.33}$$

where $E_0 = 8000 kPa$ is the elastic modulus of the porous medium in the chemically unreacted state. The Poisson's ratio ν of the porous medium is assumed to be invariant during the contaminant transport process.

Figure 7.6 shows computational results for the reactive transport process of the contaminant and the consolidating process of the soil column with the chemical-induced alteration of the hydraulic conductivity k of the porous medium defined by (7.31) and (7.32). In this and following computations, the other system parameters are those defined in (7.28) and (7.30). The initial time step is taken as $\Delta t = 20\, days$ and a time adaptive procedure with the constraint of $\Delta t \leq 20\, days$ is used. Comparing the results shown in Figure 7.6(a) with those shown in Figure 7.5(b), it is evident that the increase in the hydraulic conductivity of the soil material, caused by the chemical reaction, accelerates the contaminant transport processes.

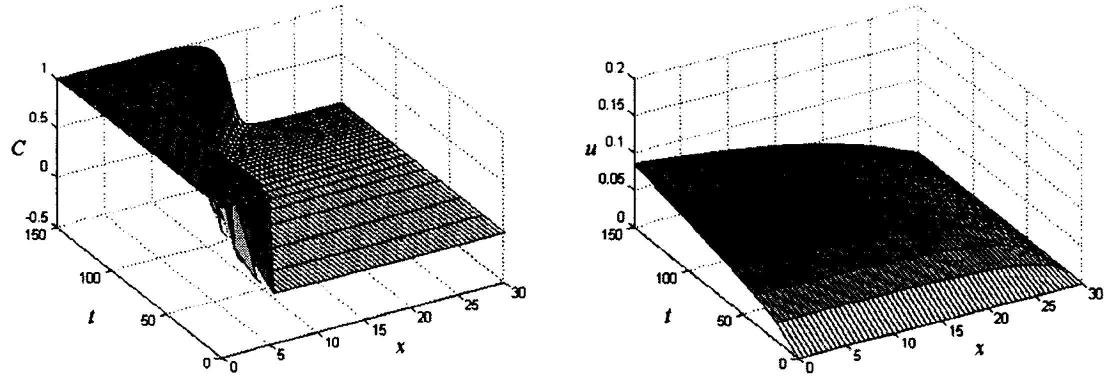

(a) (b)

Figure 7.6 Computational results during a 150-day period of (a) the contaminant transport process and (b) the consolidation of the soil column, corresponding to the altered hydraulic conductivity

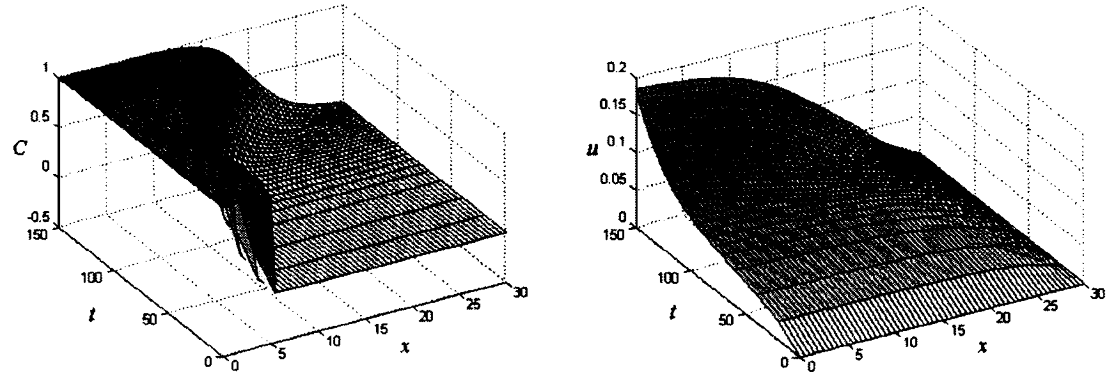

(a) (b)

Figure 7.7 Computational results during a 150-day period of (a) the contaminant transport process and (b) the consolidation of the soil column, corresponding to the altered elastic modulus

Figure 7.7 shows the computational results of the contaminant transport process and the consolidating process of the soil column with an alteration of the elastic modulus defined by (7.33). It should be noted from this figure that the chemically-induced reduction of the elastic modulus of the porous material contributes more to the consolidation of the soil skeleton and therefore accelerates the dissipation of the excess pore fluid pressure in the soil column. Such an enhancement in the dissipation of the pore fluid pressure will accelerate the contaminant transport processes, which will in turn influence the consolidation of the porous skeleton and the dissipation of the pore fluid pressure.

Finally, the chemically-induced alterations of both the hydraulic conductivity and the elastic modulus are considered in the contaminant transport driven by the consolidation of the soil column. The corresponding computational results obtained from the HMC transport model are shown in Figure 7.8. The influence of the chemically-induced alterations of the transport and mechanical properties of the soil column on the contaminant transport process can be clearly observed in Figure 7.8(a). The accelerated contaminant transport process enhances the consolidating process of the soil column due to the reduction of the elastic modulus (see Figure 7.8(b)).

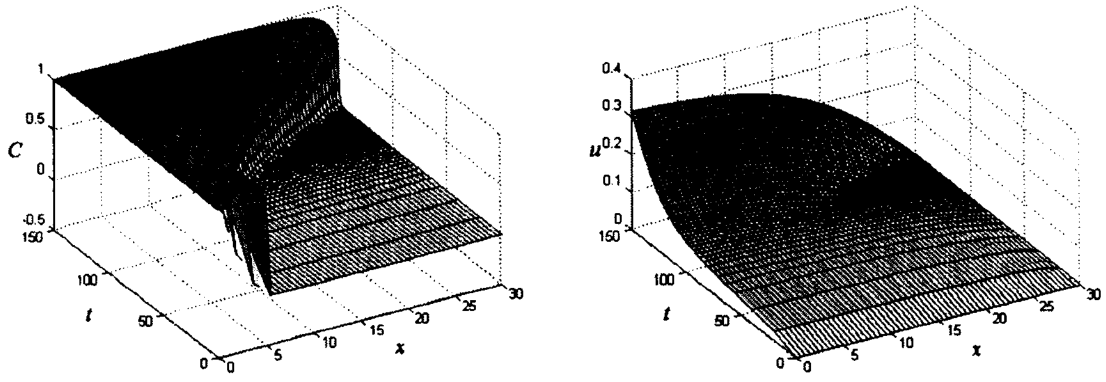

(a) (b)

Figure 7.8 Computational results during a 150-day period of (a) the contaminant transport process and (b) the consolidation of the soil column, corresponding to the altered hydraulic conductivity and the elastic modulus

7.4 Discussion

This chapter considered a HMC transport model that can be used to simulate the advection-dominated transport process of a contaminant in a deforming porous medium. The influences of the chemically-induced alterations of the mechanical and transport properties of the porous medium on the contaminant transport process were considered in the HMC transport model, using experimental results found in the published literature. The time-adaptive scheme is coupled in the HMC model to obtain the optimal solution of the advective-dispersive-reactive transport process. However, since conservative values of the time-weighting and the upwind function were adopted in the MLS formulation of the transport equation, an artificial diffusion is embedded in the model solution for the transport process. Such artificial diffusion can be observed in the numerical results of the contaminant transport processes shown in Figures 7.5-7.8, and it is enhanced by the dissipation of the excess pore fluid pressure. Further effort should be made to improve the accuracy of the HMC transport model by using an operator-splitting technique with an iterative algorithm for the accurate solution of the advection-dominated transport problem.

CHAPTER 8
CONCLUSIONS AND RECOMMENDATIONS

8.1 Summary and Conclusions

Contaminant transport in porous media is one of the most important geo-environmental problems related to the human life and activities, since the transported chemicals or hazardous materials may contaminate the groundwater and aquifers making them unusable for a long time. The prediction of the time- and space-dependent movement of contaminants in porous media is important for contaminant management and environmental decision-making processes in such endeavours as groundwater remediation and soil cleanup. In general, the factors contributing the migrations of contaminants in porous media are complex and include the processes of advective-dispersive transport, dissipation of the pore fluid pressure, deformation of the porous medium, geochemical reactions and heat transfer. These coupled nonlinear processes, when applied to practical problems, can only be investigated through a numerical modelling.

However, numerical models currently in use encounter difficulties in obtaining the accurate solution for the advection-dominated transport equation with a solution containing high gradients or discontinuities: they introduce either mathematical oscillations or artificial diffusion into the solution in the vicinity of the high gradients in the contaminant concentration. Developing high-order accurate stabilized numerical methods for solving the advection-dominated transport equation has become an important topic in the field of science and engineering, since the classical advection-dispersion equation can be used to describe a variety of physical processes associated with a wide range of problems, such as waves in shallow water, heat transfer in fluids, salt movement in the oceans, the flow of vehicular traffic, movement of charged particles like electrons, gas dynamics, biological processes and sediment contamination of aquifers, etc. To date, many attempts have been made to develop stabilized numerical methods for the solution the advection-dominated equation. A review and classification of the research on the development of stabilized Finite Element Methods (FEMs) for the advection equation were given in Chapter 1 and a summary table is given in the Appendix.

Stabilized FEMs for the advection equation have undergone development for four decades since the upwind scheme was first introduced into the Galerkin method in the late of 1970s, by using the asymmetric weighting function. However, the theoretical fundamentals of the stabilized FEMs were not realized until almost 20 years later when the concepts of the Multiscale and the Bubble function were proposed. The origins of stabilized FEMs for the advection equation with a solution containing a discontinuity were reviewed in Chapter 1 by means of the Péclet number and the Fourier mode. When the Péclet number is greater than unity, the variation of the unknown variable over the element can be considered to be discontinuous in the discretization sense. Fourier expansion shows that a step wave (which contains a discontinuity) consists of the wave components of high frequency that are referred to as the fine scales of the solution. The conventional finite element space with the lower-order polynomial is not appropriate for these fine scales, and need to be augmented with certain high-order polynomials (or bubble functions). However, effects of the fine scales can also be considered in the normal finite polynomial space, and this is equivalent to adding a stabilizing term to the weak form of the conventional Galerkin method for the advection equation. This leads to a general weighted residual integral form of stabilized FEMs for the advection equation, details of which were given in Chapter 2.

The assessment of numerical methods for the advection-dispersion equation has kept pace with their development, using mathematical tools such as maximum principles, hyperbolic conservation law, error analysis, Fourier analysis, etc. In particular, the Fourier analysis can illustrate the mathematical properties of numerical methods in the frequency domain by means of the alterations, caused by the numerical scheme, of the algorithmic amplitudes and the phase velocities of different wave components involved in the solution. From this view of point, Fourier analysis can be used to investigate the mathematical nature underlying the difficulties embedded in the numerical schemes for the hyperbolic equation, such as oscillations and artificial diffusion. Such an investigation can be used to derive the conditions for the optimal numerical performance of stabilized schemes for the hyperbolic equation, which contains a discontinuous solution. Due to these considerations, the Fourier analysis has become a powerful tool for the stability analysis of numerical schemes and the determination of stabilized parameters.

It is evident that besides the spatial discretization, the time integration strategy also has an influence on the performance of the numerical scheme for the advection-dispersion equation, and this influence should be included in the assessment. Based on this consideration, this thesis performs a Fourier analysis on stabilized semi-discrete FEMs using different time integration schemes to investigate their overall numerical behaviour for the advection equation. The Fourier analysis is performed on several representations of stabilized semi-discrete Eulerian FEMs, such as Petrov-Galerkin, Taylor-Galerkin, Least Squares and Modified Least Squares (MLS) methods, since they can be easily implemented for the solution of practical problems. The formulations of these stabilized methods for the advection equation are briefly described in Chapter 2.

The analytical expressions of the algorithmic amplitudes and phase velocities of these semi-discrete Eulerian stabilized FEMs for the advection equation with forward-Euler, backward-Euler and Crank-Nicolson time integration schemes are given in Chapter 3. Using these analytical expressions, the numerical performance of the semi-discrete stabilized FEMs for the advection equation can be easily and accurately investigated by illustrating the variations of their algorithmic amplitudes and phase velocities with the Courant number and the dimensionless wave number. These variations show that the time integration scheme and the Courant number have a significant influence on the behaviour of these stabilized FEMs for the advection equation, and their optimal performances can be obtained by properly choosing the time-weighting or the stabilized parameter under certain Courant number criteria. In particular, it was found that the MLS scheme with a specified upwind parameter $\alpha = 3/2$ and the time-weighting $\theta = 1/3$ could generate an oscillation-free and non-diffusive numerical solution to the advection equation under a Courant number condition of $Cr = 1$. This conclusion is confirmed by the numerical computation of a one-dimensional advective transport problem given at the end of Chapter 3.

The numerical advantage of the MLS scheme allows the development of an accurate numerical modelling of the practical advective transport process in a porous medium. In Chapter 4, a one-dimensional advective transport problem of a contaminant in the poroelastic geological material is examined numerically. A simplified treatment of the fully coupled behaviour of the volumetric deformation of the porous medium (i.e. the compressibilities of both the pore fluid and the porous skeleton) and the dissipation of the pore fluid pressure is utilized in the numerical examination of this advective transport problem. In this case, a piezo-conduction equation was used to describe the transient nature of the pore fluid pressure, which is responsible for Darcy flow in the porous medium. Based on the Courant number criterion developed by Fourier analysis discussed in Chapter 3, a time-adaptive procedure is proposed, coupled with the MLS scheme, to generate an accurate solution of above one-dimensional advective transport process induced by a time- and space-dependent flow associated with a pore fluid pressure transient. In such a time-adaptive scheme, the time step is determined, based on the Courant number criterion $Cr = 1$, by the magnitude of the flow velocity and the elemental length at the locations where the discontinuity of the solution presents.

In Chapter 4, the time-adaptive scheme was also used to examine an advection-dominated transport process of a contaminant from a spherical cavity in a fluid-saturated isotropic porous region. Such a transport problem can be encountered in the geo-environmental problem associated with the deep disposal of hazardous waste material. A Fourier analysis was carried out to show the need to use an operator splitting approach with the MLS scheme for solving the advection-dispersion equation. Therefore, a time-adaptive operator splitting numerical model was developed for the spherically symmetric advection-dominated transport problem. In this numerical modelling, a coordinate transformation was applied, transforming the spherically radial advection equation to the classical advection equation in order to utilize the numerical advantages of the MLS scheme. In addition to the compressibility of the porous system, the infinite extent of the porous region, usually encountered in the contaminant transport processes in the geo-environmental field, was considered in this model: an infinite element was used to solve the piezo-conduction equation to obtain an accurate approximation of the flow field. The computational results showed that small physical dispersions can be captured by the time-adaptive operator splitting scheme without introducing numerical oscillations and artificial diffusion.

Experimental research work is important when modelling transport problems in environmental geosciences, both for the verification of the theoretical or numerical model and for the identification of the parameters governing the physical phenomenon. In Chapter 5, the advection-dominated transport process is experimentally simulated by considering the migration of a chemical dye solution in the idealized porous medium consisting of glass beads. A colour visualization-based image processing method was developed for quantitatively determining the transport process of the dye solution on the cylindrical surface of the porous column without any physical disturbance. Using the experimental results determined from this image processing method, an inverse analysis of the transport problem was carried out, by means of the *Output Least Squares Criterion*, to identify the dispersivity of the transport process in the porous column. The identified transport parameter was used for the validation of the numerical modelling. The close correlation between the experimental results, the analytical solution and the numerical estimation of the advection-dominated transport process of a dye plug indicates the effectiveness and the accuracy of the colour visualization-based image processing method and the time-adaptive operator splitting scheme for the one-dimensional advection-dominated transport problem with a time-dependent flow velocity.

The numerical computations and the experimental validation presented respectively in Chapters 4 and 5 indicate that the time-adaptive scheme is sufficient to give an accurate solution for the one-dimensional advection-dominated transport problem. However, for the multi-dimensional advection-dominated transport problem, the flow velocity in the vicinity of high gradients or discontinuities of the solution is usually not uniformly distributed; in such cases, it is not possible to select a single time step to satisfy the Courant number criterion at the locations of the high gradients of the solution, which is discretized with a set of arbitrary-shaped elements. Due to this observation, a mesh-refining adaptive scheme is developed in Chapter 6 for modelling a three-dimensional axisymmetric advective transport problem from a spherical cavity in a fluid saturated porous region. This advective transport problem was computed with a one-dimensional time-adaptive model in Chapter 4, but it was recomputed in Chapter 6 using a mesh-refining adaptive three-dimensional axisymmetric model. Compared with conventional mesh-adaptive methods, the mesh-refining adaptive scheme developed in Chapter 6 is quantitative in the sense that the size of the refined element can be determined by the Courant number criterion. The time-adaptive procedure can be coupled with mesh-refining adaptive scheme to improve the efficiency of the later, and this time- and mesh-refining adaptive scheme was successfully used with a quasi-Newton iterative algorithm to model a nonlinear three-dimensional axisymmetric advective transport problem from a disc-shaped cavity. In this computation, the influence of nonlinear sorption and chemically-induced alterations of the stiffness and transport properties of the porous medium are considered, by weakly coupling the advection-dispersion equation and the piezo-conduction equation. Computational results show the feasibility of applying the time- and mesh-adaptive iterative schemes to model practical nonlinear contaminant transport problems in porous media.

Finally, a numerical HMC model was developed in Chapter 7 to couple processes of the advection-dominated transport of a contaminant, the mechanical deformation of the porous skeleton, the dissipation of the pore fluid pressure, and the geochemical reactions, applicable to the one-dimensional behaviour of a fully-saturated soil column. In this numerical modelling, the mechanical and transport properties of the porous medium are assumed to be altered by a simplified space-independent leaching of the porous material due to the reaction between the contaminant and the solid particles of the porous medium.

8.2 Recommendations for Future Work

In this thesis, Fourier analysis was used to investigate the numerical performance of several stabilized semi-discrete Eulerian FEMs for the advection equation. Based on this investigation, the time- and/or mesh-adaptive numerical schemes were developed for modelling the one- and multi-dimensional advection-dominated contaminant transport problems with the time- and space-dependent flow field. An image processing method was developed in the experimental modelling to determine the transport process of a chemical solution on the cylindrical surface of the porous column. With respect to these aspects, future research work can be extended in the follow ways:

- Application of the Fourier analysis to a wider range of the stabilized finite element methods to investigate a general stabilized weighted residual integral form for the accurate solution of the advection equation.
- Coupling of the mesh coarsening technique with the mesh-refining adaptive scheme to develop a more efficient truly mesh-adaptive scheme, in which the mesh near the locations of high gradients of the solution can be refined based on the Courant number criterion; while the mesh in the locations of smooth parts of the solution can be coarsened (or the original mesh restored). Using such a technique, the refined region in the computational domain would alter with the migration of the steep front of the solution.
- Application of a colour visualization-based image processing method to determine the transport process of the chemical solution in practical geomaterials, such as sand, clay and aggregate, etc., by using a coloured chemical solution which contrasts the colour composition of the geomaterial.
- Application of the imaging processing method developed in this thesis to the laboratory study of the flow transport pattern of a chemical solution on a two-dimensional homogeneous or inhomogeneous porous region in a quantitative, economical and non-invasive way.
- Extending the one-dimensional HMC transport model developed in this thesis to model multi-dimensional advection-dominated contaminant transport processes coupled with Hydro-Mechanical-Chemical behaviour of the porous medium. This is important topic in the field of geo-environmental engineering for accurate assessment of subsurface flow transport, contaminant migration and deformation of the porous medium.

APPENDIX.

A SUMMARY OF STABILIZED SCHEMES FOR THE ADVECTION EQUATION

Authors	Year	Characteristics
		Upwind
Courant	1952	Sided spatial difference in characteristic direction for the upwind direction (the first one in Upwind techneque)
Spalding	1972	Discussion of UDS and CDS FDM
Bori & Book	1973	Flux Corrected Transport (FCT) FDM with SHASTA algorithm
Raymond & Garder	1976	Asymmetric test functions and optimal value for upwind function for PG scheme
Christie et al.	1976	1D Asymmetric linear and quadratic basis functions
Heinrich et al.	1977	2D Upwind finite element scheme
Hughes	1978	Unsymmetrical weighting function for the advective term
Griffiths & Mithchell	1979	Biased weighting functions
Heinrich & Zienkiewicz	1979	Biased weighting functions
Belytschko & Eldib	1979	Analysis of upwind method based on amplifying transport term
Carey	1979	Analysis of stability and oscillations using the Gershgorin circle theory and oscillation matrices
Gresho and Lee	1979	Analysis of oscillations
Heinrich	1980	PG with 1D quadratic and 2D biquadratic element
Morton & Parrott	1980	Modified weighting functions satisfying unit CFL property for an upwind effect
Kelly et al.	1980	Anisotropic balancing dissipation
Huyakorn et al.	1983	Upwind application to practical problems
Yu & Heinrich	1986	PG method for 1D time dependent AD equation
Yu & Heinrich	1987	PG method for multi dimensional time dependent AD equation
Galeao & Dutra do Carmo	1988	A consistent approximation Upwind PG method
Steffler	1989	QUICK: Quadratic Upwind Interpolation for Convective Kinematics
Leismann & Frind	1989	Optimal upwind through an error analysis with implicit dispersion and explicit advection
Idelsohn	1989	Upwind technique via variational principles
Dutra do Carmo	1991	CAU: Consistent Approximate Upwind Method

Codina et al.	1992	Optimal intrinsic time for 1D and Characteristic length for 2D
Khelifa et al.	1993	Douglas-Wang (DW) approach for AD equation.
Codina	1993a	Discontinuity-capturing crosswind-dissipation
Harari & Hughe	1994	Stabilized FEM for steady ADE
Carrano & Yeh	1994	Optimization of spectrally weighted average phase error method based on a Fourier analysis
Paillere et al.	1996	Upwind Resedual distribution schemes
Oñate	1998	Artificial or balancing diffusion in the stabilized equation
Bradford et al.	2000	Discussion of monotonicity of PG method
Hendriana	2000	Various upwind techniques for imcompressible high Reynolds flow
		Petrov-Galerkin
Hughes & Brooks	1979	Streamline diffusion method, Upwind only in flow direction
Hughes & Brooks	1982	SUPG: Streamline Upwind Petrov-Galerkin.
Brooks & Hughes	1982	SUPG for incompressible Navier-Stokes equation
Johnson et al.	1984	Mathematical analysis of SUPG
Mizukami & Hughes	1985	A new PG method satisfying the maximum principle
Hughes & Mallet	1986a	Errors estimates for SUPG with linear element
Hughes et al.	1986	SUPG with discontinuity capturing
Hughes & Mallet	1986b	Discontinuity Capturing (DC) operator
Tezduyar & Ganjoo	1986	Algorithmic Courant number
Tezduyar & Park	1986	DC for convection and reaction dominated problem
Hughes et al.	1987	Convergence analysis of the generalized SUPG
Hughes	1987	Convergence (stability and consistency) of SUPG for ADE
Tezduyar et al.	1987	SUPG for the convection and reaction dominated problem
Franca et al.	1992	Analysis of Stabilized FEM, i.e., SUPG, GLS, DW
Codina	1993b	Stability analysis of scheme with Forward Euler in time and SUPG in space
Cardle	1995	Modified PG method for the transient problem
Ganesan & Salamon	1996	Multilevel PG method: the virtual mesh refinement technique.
Idelsohn et al.	1996	(SU-C)PG: Streamline Upwind-Centred Petrov-Galerkin
Oñate et al.	1997	Derivation of the stabilization parameter, i.e., intrinsic time, characteristic length
Codina	1998	Comparisons of SUPG, ST-GLS, SGS, CG, TG in terms of
Sheu & Fortin	2001	SUPG for 1 and 2D problem with quadratic element
		Taylor-Galerkin
Lax-Wendroff	1960	Taylor series expansion in temporal derivative term (FDM)

Donea et al.	1984	Taylor Galerkin (TG) method for advection diffusion equation
Donea	1984	Euler-Taylor/Galerkin method: Taylor series expansions in time and Bubnov-Galerkin FEM in space, first one in FEM
Löhner et al.	1984	Nonlinear hyperbolic equation
Selmin et al.	1985	TG method for nonlinear advection diffusion equation
Donea et al.	1987	Lax-Wendroff TG and Crank-Nicolson TG
Choe & Holsapple	1992	TG-DFEM: Taylor-Galerkin Discontinuous FEM
Noorishad et al.	1992	Review of CNG, SUPG and CNTG throughout Pe-Cr space
Comini	1995	Analysis of diffusion, dispersion errors and stability of TG and BG schemes
		Least-Squares FEM
Carey & Jiang	1987a	Least-Squares FEM and Parallel Conjugate Gradient Solution
Carey & Jiang	1987b	LS FEM and Preconditioned CG (PCG) for nonlinear problems
Carey & Jiang	1988	Comparison of Least-Squares FEM with PG and TG method
Bensabat	1990	Optimal control problem for PDE, created by Least square procedure and solved by conjugate gradient method
Park & Liggett	1990	TLS, Taylor-Least-Square FEM for 1D
Park & Liggett	1991	Application of TLS to 3D problem with operator splitting
Franca & Hughes	1993	Convergence analyses of GLS
Idelsohn	1996	Generalization of GLS method for the 2D transient problem
Carey et al.	1998	Least-Squares Mixed FEM
Carey et al.	1998	Parallel Conjugate Gradient for Least-Squares Mixed FEM
		Characteristic Galerkin method (Euler-lagrange)
Garder et al.	1964	Particle tracking method for Method of characteristics (MOC)
Neuman	1981	A review of Eulerian-Lagrangian method
Douglas & Russell	1982	Characteristics method with FEM or FDM
Varoglu & Liam Finn	1982	Eulerian-Lagrangian method in 2D problem
Zienkiewicz et al.	1984	Lagrange and Euler method
Neuman	1984	Basic discussions of the Eulerian-Lagrangian approach and applications of article tracking
Löhner et al.	1984	ECG: Euler Characteristic Galerkin
Morton	1985	Nonlinear problem
Demkowitz & Oden	1986	Adaptive PG method for multidimensional problem
Celia et al	1990	ELLAM: Eulerian-Lagrangian Localized Adjoint Methods
Szymkirewicz	1993	Spline functions for determination of the characteristics
Ijiri & Karasaki	1994	Time-dependent adaptive mesh generation for dispersion using the finite element method

Celia	1994	Solute mass conservation for finite volumes using ELLAM
Binning & Celia	1994	Finite volume ELLAM for contaminant transport in saturated and unsaturated zone
Ewing et al.	1994	Coupled simulation of fluid, heat and radioactive transport using ELLAM
Hinkelmann & Zielke	1995	Flow and salt transport on shadow systems
Dahle et al.	1995	EL localized adjoint method.
Oliveira & Baptista	1995	comparison of integration and interpolation EL methods
Allievi et al.	1997	Generalized particle search-locate algorithm
Le Roux et al.	1997	Semi-lagrangian method
Le Roux & Lin	1999	Semi-implicit semi-lagrangian finite-element
Allievi & Bermejo	2000	FEMMC: Finite Element Modified Method of Characteristics
Zoppou et al.	2000	Exponebtial spline interpolation in characteristic based scheme
Sheng & Smith	2000	TEPG: Transport-Equilibrium Petrov-Galerkin methods with nonlinear adsorption isotherm
Li et al.	2000	CG with implicit scheme for non-equilibrium sorption
Li et al.	2000	Implicit characteristic Galerkin method, with 2^N exponential algorithm for convective term
		Space-time Galerkin
Varoglu & Liam Finn	1980	1D Space-Time Galerkin method
Nguyen & Reynen	1984	Space-time least-squares FEM
Yu & Heinrich	1986	PG method for transient problem in space-time FE mesh
Hughes et al.	1989	GLS/ST: The Galerkin/Least-Squares Space-Time
Sharkib & Hughes	1991	Space-Time Galerkin/Least-Squares Algorithms
Hansbo	1992	CSD: Characteristic Streamline Diffusion method in space-time space
Pironneau et al.	1992	Analysis of CG and GLS/ST
Oñate & Manzan	1999	Stabilized space-time FEM
N'dri et al.	2001	Space-time Galerkin for 2D and 3D incompressible viscous flow
		Operator split
Douglas & Rachford	1956	Heat transport using the Alternating Direction Implicit (ADI) scheme
Marchuk	1975	Mathematical description of the operator split technique
LeVeque & Oliger	1983	Additive Operator Splitting for hyperbolic equation
Morshed & Kaluarachchi	1995	Operator splitting procedure applied to the advection-dispersion-reaction equation

Marchuk	1995	Overview of different splitting-up techniques
Zienkiewicz &Codina	1995	CBS: The Character Based Split scheme
Siegel et al.	1997	Discontinuous FEM on advection and mixed hybrid FEM on diffusion
Khan & Liu	1998a	Numerical analysis of operator Splitting for 2D equation
Khan & Liu	1998b	Operator Splitting for 3D equation
Karlsen et al.	1998	COS:Corrected Operator Splitting methods
Zienkiewicz et al.	1999	Semi-implicit and implicit scheme for CBS
Wendland & Schmid	2000	S3: Symmetrical Streamline Stabilization OS scheme
		Residual-Free Bubbles
Brezzi et al.	1992	Relationship between stabilized FEM and Galerkin method using bubble
Baiocchi et al.	1993	Virtual bubbles and GLS method
Brezzi & Russo	1994	bubbles for advection-diffusion problems
Hughes	1995	DtN (Dirichlet-to Neumann) formulation, Subgrid scale models, Bubbles, and Intrinsic time
Franca & Farhat	1995	Stabilized FEM with bubble functions
Franca & Russo	1997	RFB and mass lumping
Brezzi et al.	1997	Equivalence of variational multiscale and residual-free bubbles approach
Brezzi et al.	1998	RFB for 2D ADE
Franca & Macedo	1998	RFB for ADE and approximation of TLFEM
Brezzi et al.	1998	Intrinsic time in SUPG and pseudo REB functions
Franca et al.	1998	RFB and TLFEM for Helmholtz equation
Franca & Valentin	2000	USFEM (Unusual Stabilized FEM) with large zero-order term
Franca & Hwang	2002	TLFEM (Two-Level FEM) for ADE with bubbles function
		Recently work on Finite Difference Methods
Bruneau et al.	1997	Back characteristics and Flux limiter scheme
Keppens et al.	1999	Implicit and semi-implicit TVD and CG-type iterative schemes
Balzano	1999	2D QUICKEST scheme
Pereira & Pereira	2001	Fourier analysis of several FD schemes for 1D problem
Wang & Hutter	2001	Comparisons of 1D FDM numerical methods
Kalita et al.	2002	HOC: higher Order Compact schemes

REFERENCES

Aboustit B.L., Advani S.H. and Lee J.K., 1985, Variational principles and finite element simulations for thermo-elastic consolidation, *Int. J. Num. Ana. Meth. Geomech.*, **9**, 49-69.

Allersma H.G.B., 1990, On line measurement of soil deformation in centrifuge tests by image processing, *9th Int. Conf. on Experimental Mechanics*, Copenhagen, 1739-1748.

Allievi A. and Bermejo, R., 1997, A Generalized Particle Search –Locate Algorithm for Arbitrary Grids, *J. Comput. Phys.*, **132**, 157-166.

Allievi A. and Bermejo R., 2000, Finite element modified method of characteristics for the Navier-Stokes equations, *Int. J. Numer. Meth. Fluids.*, **32**, 439-463.

Alonso E.E, Gens A. and Josa A., 1990, A constitutive model for partially saturated siols, *Geotechnique*, **40**, 405-430.

Asundi A.K., 2002, *MATLAB for Photomechanics: A Primer*, Elsevier, Amsterdam; Boston; London.

Atluri S.N., 2004, *The Meshless Local-Petrov-Galerkin Method for Domain & BIE Discretizations*, Tech Science Press, Encino, CA.

Atluri S.N. and Zhu T. 1998, A new meshless local Petrov-Galerkin (MLPG) approach in computational mechanics, *Comput. Mech.*, **22**, 117-127.

Atluri S.N., Kim H.G. and Cho J.Y., 1999, A critical assessment of the truly meshless local Petrov-Galerkin (MLPG), and local boundary integral equation (LBIE) methods, *Comput. Mech.*, **24**, 348-372.

Atluri S.N., Han Z.D. and Rajendran A.M., 2004, A new implementation of the meshless finite volume method, through the MLPG "Mixed" approach, *CMES:Computer Modeling in Engineering & Sciences*, **6**, 491-513.

Baiocchi C., Brezzi F. and Franca L.P., 1993, Virtual bubbles and the Galerkin-least-square method, *Comput. Methods Appl. Mech. Engrg.*, **105**, 125-142.

Balzano A., 1999, MOSQUITO: An efficient finite difference scheme for numerical simulation of 2D advection, *Int. J. Numer. Meth. Fluids.* **31**, 481-496.

Banks R.B., 1994, *Growth and Diffusion Phenomena: Mathematical Frameworks and Applications*, Springer-Verlag, Berlin.

Barenblatt G.I., Entov V.M. and Ryzhik V.M., 1990, *Theory of Fluid Flows Through*

Natural Rocks, Kluwer Academic Publishers, Dordrecht, The Netherlands.

Bathe K.J., 1996, *Finite Element Procedures*, Englewood Cliffs, N.J.: Prentice Hall.

Batu V. 1993, A generalized two-dimensional analytical solute transport model in bounded media for flux-type finite multiple sources, *Water Resour. Res.*, **29**, 2881-2892.

Bear J., 1961, Some experiments in dispersion, *J. Geophys. Res.*, **66**, 2455–2267.

Bear J., 1972, *Dynamics of Fluids in Porous Media*, Dover Publications, New York.

Bear J. and Bachmat Y., 1992, *Introduction to the modelling of transport phenomena in porous media*, D. Reidel Publ. Co, Dordrecht, the Netherlands.

Bear J. and Verruijt A., 1990, *Modeling groundwater flow and pollution*, D. Reidel Publ. Co, Dordrecht, the Netherlands.

Bedient P. B., Rifai H.S., Newell C.J., 1999, *Ground water contamination: transport and remediation*, Prentice Hall PTR, Upper Saddle River, NJ.

Belytschko T. and Eldib I., 1979, Analysis of a finite element upjwind scheme, in *Finite Element Methods for Convection Dominated Flows,* Hughes T.J.R. ed., AMD, **34**, 195-200, ASME, New York.

Belytschko T., Gu L. and Lu Y.Y., 1994, Element-free Galerkin methods, *Int. J. Numer. Methods eng.,* **37**, 229-256.

Bensabat J. and Zeitoun D. G., 1990, A least-squares procedure for the solution of transport problems, *Int. J. Numer. Meth. Fluids.*, **10**, 623-636.

Binning P. and Celia M. A., 1994, Two-dimensional Eulerian Lagrangian localized adjoint method for the solution of the contaminant transport equation in the saturated and unsaturated zones, *Proc. Computational Methods in Water Resources X*, Vol. **1**, 165-172, Heidelberg.

Biot M.A., 1941, General theory of three-dimensional consolidation, *J. Appl. Phys.*, **12**, 155-164.

Biot M.A., 1955, Theory of elasticity and consolidation for a porous anisotropic solid, *J. Appl. Phys.*, **26**, 182-185.

Biot M.A., 1956, General solution of the equation of elasticity and consolidation for a porous material, *J. Appl. Mech.*, **23**, 91-95.

Biot M.A. and Willis D.G., 1957, The elastic coefficient of the theory of consolidation, *J. Appl. Mech.*, **24**, 594-601.

Bishop A.W., 1973, The influence of an undrained change in stress on the pore pressure in porous media of low compressibility, *Geothechnique*, **23**, 435-442.

Bishop A.W. and Blight G.E., 1963, Some aspects of effective stresses in saturated and partly saturated soils, *Geotechnique*, **13**, 177-197.

Bokota A. and Iskierka S., 1995, An analysis of the diffusion-convection problem by the boundary element method, *Engng. Anal. Boundary Elem.*, **15**, 267-275.

Book D.L., Boris J.P. and Hain, K., 1975, Flux-corrected transport. II. Generalization of the method, *J. Comput. Phys.*, **18**, 248-283.

Book D.L., Boris J.P. and Zalesak, S.T., 1981, Flux corrected transport, In *Finite Difference Techniques for Vectorized Fluid Dynamics Circulations*, Book D.L. ed., Springer-Verlag: Berlin, 29-55.

Boris J.P. and Book D.L., 1973, Flux-corrected transport. I. SHASTA, a fluid transport algorithm that works, *J. Comput. Phys.*, **11**, 38-69.

Bourbie T. and Zinszner B., 1985, Hydraulic and acoustic properties as a function of porosity in Fontainebleau sandstone, *J. Geophys. Res.*, **90**, 11524–11532.

Bradford S.F. and Katopodes N.D., 2000, The anti-dissipative, non-monotone behavior of Petrov-Galerkin upwinding, *Int. J. Numer. Meth. Fluids.*, **33**, 583-608.

Brebbia C.A. and Dominguesz J., 1992, *Boundary Elements: An Introductory Course, 2^{nd} ed.,* Computional Mechanics publications.

Brebbia CA, Telles JFC, Wrobel LC., 1984, *Boundary Element Techniques: Theory and Applications in Engineering*, Springer: Berlin and New York.

Brezzi F., Bristeau M.O., Franca L., Mallet M., Roge G., 1992, A relationship between stabilized finite element methods and Galerkin method with bubbles functions, *Comput. Methods Appl. Mech. Engrg.* **96**, 117-129.

Brezzi F., Franca L.P., Hughes T.J.R. and Russo A., 1997, b $=\int$ g, *Comput Methods Appl Mech Engrg.*, **145**, 329-339.

Brezzi F., Franca L.P. and Russo A., 1998a, Further considerations on residual-free bubbles for advective–diffusive equations, *Comput. Methods Appl. Meth. Engrg.* **166**, 25-33.

Brezzi F., Marini, D. and Russo A., 1998b, Applications of the pseudo residual-free bubbles to the stabilization of convection-diffusion problems, *Comput. Methods Appl. Meth. Engrg.*, **166**, 51–63.

Brezzi F. and Russo A., 1994, Choosing bubbles for advection-diffusion problems, *Math. Models Methods Appl. Sci.*, **4**, 571-587.

Brooks A.N. and Hughes T.J.R., 1982, Streamline Upwind/Petrov-Galerkin formulations for convective dominated flows with particular emphasis on the incompressible Navier-Stokes equations, *Comput. Methods Appl. Mech. Engng.*, **32**, 199-259.

Bruneau C.H., Fabrie H., and Rasetarinera P., 1997, An accurate finite scheme for solving convection-dominated diffusion equations, *Int. J. Numer. Meth. Fluids.*, **24**, 169-183.

Burns S. E. and Zhang M., 1999, Digital image analysis to assess microbubble behavior in porous media, *J. Comp. in Civ. Engrg.*, **13**, 43-48.

Cardle J.A., 1995, A modification of the Petrov-Galerkin method for the transient convection-diffusion equation, *Int. J. Numer. Meth. Engng.* **38**, 171-181.

Carey C., 1979, An analysis of stability and oscillations in convection-diffusion computations, in *Finite Element Methods for Convection Dominated Flows*, Hughes T.J.R. ed., AMD, **34**, 63-71, ASME, New York.

Carey G.F and Jiang B.N., 1987a, Least square finite element method and preconditioned conjugate gradient solution, *Int. J. Numer. Meth. Engng.*, **24**, 1283-1296.

Carey G.F and Jiang B.N., 1987b, Nonlinear preconditioned conjugate gradient and least squares finite elements, *Comput. Methods Appl. Mech. Engrg.*, **62**, 145-154.

Carey G.F and Jiang B.N., 1988, Least square finite elements for first order hyperbolic systems, *Int. J. Numer. Meth. Engng.*, **26**, 81-93.

Carey G.F., Pehlivanov A.I., Shen Y., Bose A. and Wang K. C., 1998, Least-squares finite elements for fluid flow and transport, *Int. J. Numer. Meth. Fluids.*, **27**, 97-107.

Carey G.F., Shen Y. and Mclay R.T., 1998, Parallel conjugate gradient performance for least-squares finite elements and transport problems, *Int. J. Numer. Meth. Fluids.*, **28**(10), 1421-1440.

Carrano C.S. and Yeh G.T., 1994, A Fourier analysis and dynamic optimization of the Petrov-Galerkin finite element method, *Proc. Computational Methods in Water Resources X*, **1**, 191-198, Heidelberg.

Caruana A. and Dawe R.A., 1996, Experimental studies of the effects of heterogeneities on miscible and immiscible flow processes in porous media, *Transport in Chemical Engineering*, **3**, 185-203.

Cederberg G.A., Street R. and Leckie J.O., 1985, TRANQL: A groundwater mass transport and equilibrium chemistry model for multi-component systems, *Water Resour. Res.*, **21**, 1095-1104.

Celia M.A., 1994, Eulerian Lagrangian localized adjoint method for contaminant transport simulations, *Proc. Computational Methods in Water Resources X*, Vol. **1**, 207-216, Heidelberg.

Celia M.A. Russell T.F., Herrera I. and Ewing R.W., 1990, An Eulerian-Lagrangian localized adjoint method for the advection-diffusion equation, *Adv. Water Res.*, **13**, 187-205.

Chandan C., Sivakumar K., Masad E. and Fletcher T., 2004, Application of Imaging Techniques to Geometry Analysis of Aggregate Particles, *J. Comp. in Civ. Engrg.*, **18**, 75-82

Charbeneau R.J., 2000, *Groundwater Hydraulics and Pollutant Transport*, Prentice-Hall PTR, Upper Saddle River, NJ.

Choe K.Y. and Holsapple K.A., 1992, The discontinuous finite element method with the Tylor-Galerkin approach for nonlinear hyperbolic conservation laws, *Comput. Methods Appl. Mech. Engrg.*, **95**, 141-167.

Christie I., Griffiths D., Mitchell A., and Zienkiewicz O.C., 1976, Finite element methods for second-order differential equations with significant first derivatives, *Int. J. Numer. Meth. Engng.*, **10**, 1389-1396.

Cleall P.J., Thomas H.R., Seetharam S.C. and Melhuish T.A., 2004, Thermal-hydraulic-chemical-mechanical (THCM) behaviour of unsaturated siols-application in the nuclear waste disposal context, *Proceedings of the 9th Symposium on Numerical Models in Geomechanics-NUMOG IX*, Ottawa, Canada, 311-317.

Codina R., 1993a, Stability analysis of the forward Euler scheme for the convection-diffusion equation using the SUPG formulation in space, *Int. J. Numer. Meth. Engng.*, **36**, 1445-1464.

Codina R., 1993b, A discontinuity-capturing crosswind-dissipation for the finite element solution of the convection-diffusion equation, *Comput. Methods Appl. Mech. Engrg.*, **110**, 325-342.

Codina R., 1998, Comparison of some finite element methods for solving the diffusion-convection-reaction equation, *Comput. Methods Appl. Mech. Engrg.*, **156**, 185-210.

Codina R., Oñate E. and Cervera M., 1992, The intrinsic time for the SUPG formulation using quadratic element, *Comput. Methods Appl. Mech. Engrg.*, **94**, 239-262.

Coles M.E., 1999, X-ray imageing, *Experimental Methods in the Physical Sciences, Vol. 35, Method in the Physics of Porous Media*, Academic Press, San Diego, CA, Chapter 8, 301-336.

Comini G., Manzan M. and Nonino C., 1995, Analysis of finite element schemes for convection-type problems, *Int. J. Numer. Meth. Fluids.*, **20**, 443-458.

Corapcioglu M.Y. and Fedirchuk P., 1999, Glass bead micromodel study of solute transport, *J. Contam. Hydrol.*, **36**, 209-230.

Courant R., Isaacson, E. and Rees H., 1952, On the solution of nonlinear hyperbolic differential equation, *Comm. Prue Appl. Math.*, **5**, 243-55.

Dahle H.K., Ewing R.E. and Russell T.F., 1995, Eulerian-Lagrangian localized adjoint methods for a nonlinear advection-diffusion equation, *Comput. Methods Appl. Mech. Engrg.*, **122**, 223-250.

David C., Wong T.-F., Zhu W., and Zhang J., 1994, Laboratory measurement of compaction-induced permeability change in porous rock: Implications for the generation and maintenance of pore pressure excess in the crust, *Pure Appl. Geophys.*, **143**, 425– 456.

Dawe R.A., Wheat M.R. and Biener M.S., 1992, Experimental investigation of capillary pressure effects on immiscible displacement in lensed and layered porous media, *Transport in Porous Media*, **7**, 83-101.

Demkowitz L. and Oden J.T., 1986, An adaptive characteristic Petrov-Galerkin finite element methods for convection-dominated linear and nonlinear parabolic problems in two space variables, *Comput. Methods Appl. Mech. Engrg.*, **55**, 63-87.

Dennis J.E. and More J.J., 1977, Quasi-Newton methods, motivation and theory, *SIAM Rev.*, **19**, 46-89.

Domenico P.A., 1987, An analytical solution model for multidimensional transport of a decaying contaminant species, *J. Hydrol.*, **91**, 49-58.

Donea J., 1984, A Taylor-Galerkin method for convection transport problems, *Int. J. Numer. Meth. Engng.*, **20**, 101-119.

Donea J., Giulian S., Laval H. and Quartapelle L., 1984, Time-accurate solution of advection-diffusion problem by finite elements, *Comput. Methods Appl. Mech. Engrg.*, **45**, 123-145.

Donea J., Quartapelle L. and Selmin V., 1987, An analysis of time discretization in the finite element solution of hyperbolic problems, *J. Comput. Phys.*, **70**, 463-499.

Douglas J. Jr. and Rachford H.H.J., 1956, On the numerical solution of heat conduction problems in two and three space variables, *Trans. Amer. Math. Soc.*, **82**, 421-439.

Douglas J. Jr. and Russell T.F., 1982, Numerical methods for convection-dominated diffusion problems based on combining the method of characteristics with finite element of finite difference procedures, *SIAM J. Num. Anal.*, **19**, 871-885.

Doyen P.M., 1988, Permeability, conductivity, and pore geometry of sandstone, *J. Geophys. Res.*, **93**, 7729–7740.

Driessen B.J. and Dohner J.L., 2001, A finite element-boundary element method for advection-diffusion problems with variable advective fields and infinite domains, *Int. J. Heat Mass Transfer*, **44**, 2183-2191.

Dutra do Carmo E.G. and Galeao A.C., 1991, Feedback Petrov-Galerkin methods for convection-dominated problems, *Comput. Methods Appl. Mech. Engrg.*, **88**, 1-16.

Engelman M.S., Strang G. and Bathe K.J., 1981, The application of quasi-Newton methods in fluid mechanics, *Int. J. Numer. Meth. Engng.*, **17**, 707-18.

Eriksson K. and Johnson C., 1991, Adaptive Finite Element Methods for Parabolic Problems I: A Linear Model Problem, *SIAM J. Numer. Anal.*, **28**, 43–77.

Ewing R.E., Wang H. and Sharpley R.C., 1994, Eulerian Lagrangian localized adjoint method for transport of nuclear-waste contaminant in porous media, *Proc. Computational Methods in Water Resources X*, Vol. **1**, 241-248, Heidelberg.

Fagerlund G., 1973, The elastic moduli of concrete, *Proceedings ofthe International RILEM Symposium on Pore Structures and Properties of Materials*, *Prague*, Rilem ed., D129-Dl41. Paris, France.

Franca L.P. and Farhat C., 1995, Bubbles functions prompt unusual stabilized finite element methods, *Comput. Methods Appl. Mech. Engrg.*, **123**, 299-308.

Franca L.P., Frey S.L. and Hughes T.J.R., 1992, Stablized finite element methods: I. Application to the advective-diffusive model, *Comput. Methods Appl. Mech. Engrg.*, **95**, 253-276.

Franca L.P. and Hughes T,J.R., 1993, Convergence analyses of Galerkin least-squares methods for symmetric advective-diffusive forms of Stokes and incompressible Navier-Stokes equations, *Comput. Methods Appl. Mech. Engrg.*, **105**, 285-298.

Franca L.P. and Hwang F., 2002, Refining the submesh strategy in the two-level finite element method: application to the advection-diffusion equation, *Int. J. Numer. Meth. Fluids.*, **39**, 161-187.

Franca L.P., Macedo A.P., 1998, A two-level finite element method and its application to Helmholtz equation, *Int. J. Numer. Meth. Engng.*, **43**, 23-32.

Franca L.P., Nesliturk A. and Stynes M., 1998, On the stability of residual-free bubbles for convection–diffusion problems and their approximation by a two-level finite element method, *Comput. Methods Appl. Meth. Engrg.*,**166**, 35-49.

Franca L.P. and Russo A., 1997, Mass lumping emanating from residual-free bubbles, *Comput. Methods Appl. Mech. Engrg.*, **142**, 353-360.

Franca L.P., Valentin F., 2000, On an improved unusual stabilized finite element method for the advective-reactive-diffusive equation, *Comput. Methods Appl. Meth. Engrg.*, **190**, 1785–1800.

Fredlund D. G., 1979, Appropriate concepts and technology for unsaturated soils, *Canad. Geotech. J.*, **16**, 121–139.

Fredrich J.T., 1999, 3D imaging of porous media using laser scanning confocal microscopy with application to microscale transport processes, *Phys. Chem. Earth A*, **24**, 551–561.

Fredrich J.T., Greaves K.H., and Martin J.W., 1993, Pore geometry and transport properties of Fontainebleau sandstone, *Int. J. Rock Mech. Min. Sci.*, **30**, 691–697.

Fredrich J.T., Menendez B., and Wong T. F., 1995, Imaging the pore structure of geomaterials, *Science*, **268**, 276–279.

Freeze R.A. and Cherry J. A., 1979, *Groundwater*, Prentice-Hall, Englewood Cliffs, N.J.

Fromm J.E., 1968, A method for reducing dispersion in convective difference schemes, *Applled. Mathematics Modelling*, **19**, 640-653.

Galeao A.C. and Dutra do Carmo E.G., 1988, A consistent approximate upwind Petrov-Galerkin method for convection dominated problems, *Comput. Methods Appl. Mech. Engrg.*, **68**, 83-95.

Gander W. and Gautschi W., 2000, Adaptive Quadrature - Revisited, *BIT*, **40**, 84-101.

Ganesan R. and Salamon N.J., 1996, Solution of the one-dimensional convection-diffusion equation by a multilevel Petrov-Galerkin method, *Int. J. Numer. Meth. Engng.*, **39**, 2095-2109.

Ganzha V.G. and Vorozhtsov E.V., 1998, *Computer-Aided Analysis of Difference Schemes for Partial Differential Equation*, CRC Press, Boca Raton.

Garbocai E.J., Bentz D.P., and Martys N.S., 1999, Digital images and computer modeling, In *Experimental Methods in the Physical Sciences*, Vol. **35**, *Method in the Physics of Porous Media*, Academic Press, San Diego, CA, Chapter 1, 1-41.

Garder A. O., Peaceman D.W. and Pozzi A.L., Jr., 1964, Numerical calculations of multidimensional miscible displacement by the method of characteristics, *Soc. Petrol. Engng. J.*, **4**, 26-36.

George P.L., 1991, *Automatic Mesh Generation—Application to Finite Element Methods*, Wiley, Chichester.

Gerard B., Didry O., Marchand J., Breysse D. and Hornain H., 1995, Modelling the long term durability of concrete barriers for radioactive waste disposals. In *Mechanisms of Chemical Degradation of Cement Based Systems*, Scrivener K. L. and Young F. J. eds. E&FN Span.

Gerard B., Pijaudier-Cabot G. and Laborderie C., 1998, Coupled diffusion-damage modelling and the implications on failure due to strain localization, *Int. J. Solids Struct.*, **35**, 4107-4120.

Gonzalesz R.C. and Woods R.E., 2002, *Digital image processing, 2nd ed.*, Upper Saddle River, N.J.: Prentice Hall.

Gottlieb J. and DuChateau P. eds, 1996, *Parameter Identification and Inverse Problems in Hydrology, Geology, and Ecology*, Kluwer Academic Publishers, Dordrecht; Boston.

Grathwohl P., 1998, *Diffusion in natural porous media: contaminant transport, sorption/ desorption and dissolution kinetics*. Kluwer Academic Publishers, Boston.

Grenier A., Schreiber W., Brix G and Kinzelbach W., 1997, Magnetic resonance imaging of paramagnetic tracers in porous media: quantification of flow and transport parameters, *Water Resour. Res.*, **33**,1461–1473.

Gresho P.M. and Lee R.L., 1979, Don't suppress the wiggles-they're telling you something, in *Finite Element Methods for Convection Dominated Flows*, Hughes T.J.R. ed., AMD, **34**, 37-61, ASME, New York.

Griffiths D.F. and Mithchell A.R., 1979, On generating upwind finite element methods, in *Finite Element Methods for Convection Dominated Flows*, Hughes T.J.R. eds., AMD, **34**, 91-104, ASME, New York.

Grove D.B, and Wood W.W., 1979, Prediction and field verification of subsurface-water quality changes during artificial recharge, Lubbock, Texas. *Groundwater*, **17**, 250-257.

Hansbo P., 1992, The characteristic streamline diffusion method for convection-diffusion problems, *Comput. Methods Appl. Mech. Engrg.*, **96**, 239-253.

Harari I. and Hughes T.J.R., 1994, Stabilized finite element methods for steady advection-diffusion with production, *Comput. Methods Appl. Mech. Engrg.*, **115**, 165-191.

Harten A., 1983, High resolution schemes for hyperbolic conservation laws, *J. Comput. Phys.*, **49**, 357-393.

Heinrich J.C., 1980, On quadratic elements in finite element solutions of steady state convection-diffusion equations, *Int. J. Numer. Meth. Engng.*, **15**, 1041-1052.

Heinrich J.C., Huyakorn P., Zienkiewicz O.C. and Mitchell A.M., 1977, An upwind finite element scheme for two dimensional convective transport equation, *Int. J. Numer. Meth. Engng.*, **11**, 131-143.

Heinrich J.C. and Zienkiewicz O.C., 1979, The finite element method and 'upwind' techniques in the numerical solution of convection dominated flow problems, in *Finite Element Methods for Convection Dominated Flows*, Hughes T.J.R. eds., AMD, **34**, 105-136, ASME, New York.

Hendriana D. and Bathe K. J., 2000, On upwind methods for parabolic finite elements in incompressible flows, *Int. J. Numer. Meth. Engng.*, **47**, 317-340.

Hinkelmann R. and Zielke W., 1995, A parallel 2D Lagrangian-Eulerian model for the shallow water equations, *Proc. Computational Methods in Water Resources*, Vol. **1**, 537-543. Berlin.

Huang W.E., Smith C.C., Lerner D.N., Thornton S.F. and Oram A., 2002, Physical modelling of solute transport in porous media: Evaluation of an imaging technique using UV excited fluorescent dye, *Water Research.*, **36**, 1843-1853.

Hudson J.A., Stephansson O., Andersson J., Tsang C.F., Jing L., 2001, Coupled T-H-M issues relating to radioactive waste repository design and performance, *Int. J. Rock Mech. Min.*, **38**, 143-161.

Hughes T.J.R., 1978, A simple scheme for developing upwind finite elements, *Int. J. Numer. Meth. Engng.*, **12**, 1359-1368.

Hughes T.J.R., 1987, Recent progress in the development and understanding of SUPG methods with special reference to the compressible Euler and Navier-Stokes equations, In: *Finite Elements in Fluids,* Gallagher R.H. et al. eds., **7**, 273-287, Wily, Chichester.

Hughes T.J.R., 1995, Multiscale phenomena: Green functions, the Dirichlet-to-Neumann formulation, subgrid scale models, bubbles, and the origins of stabilized methods, *Comput. Methods Appl. Mech. Engrg.*, **127**, 387-401.

Hughes T.J.R. and Brooks A., 1979, A multidimensional upwind scheme with no cross-wind diffusion, In *Finite Element Methods for Convection Dominated Flows*, Hughes T.J.R. ed., AMD, **34**, 19-36, ASME, New York.

Hughes T.J.R. and Brooks A., 1982, A theoretical framework for Petrov-Galerkin methods with discontinuous weighting functions: Application to the Streamline-Upwind Procedure, In *Finite Elements in Fluids*, Gallagher R.H. et al. eds., **4**, 47-65, Wiley, Chichester.

Hughes T.J.R., Franca L.P. and Mallet G., 1987, A new finite element formulation for computational fluid dynamics: VI. Convergence analysis of the generalized SUPG formulation for linear time-dependent multidimensional advective-diffusive system, *Comput. Methods Appl. Mech. Engrg.*, **63**, 97-112.

Hughes T.J.R., Franca L.P. and Hulbert G.M., 1989, A new finite element formulation for computational fluid dynamics: VIII. The Galerkin/least-squares method for advective-diffusive equation, *Comput. Methods Appl. Mech. Engrg.*, **73**, 173-189.

Hughes T.J.R. and Mallet, M., 1986a, A new finite element formulation for computational fluid dynamics III. The general Streamline operator for multidimensional advective-diffusive systems, *Comput. Methods Appl. Mech. Engrg.*, **58**, 305-328.

Hughes T.J.R. and Mallet M., 1986b, A new finite element formulation for computational fluid dynamics IV. A discontinuity-capturing operator for multidimensional advective-diffusive systems, *Comput. Methods Appl. Mech. Engrg.* **58**, 329-336.

Hughes T. J. R., Mallet, M. and Mizukami A., 1986, A new finite element formulation for computational fluid dynamics II. Beyond SUPG, *Comput. Methods Appl. Mech. Engrg.*, **54**, 341-355.

Huyakorn P.S., Lester B.H. and Mercer J.W., 1983, An efficient finite element technique for modeling transport infractured porous media: 1. single species transport, *Water Resour. Res.*, **19**, 841-854.

Idelsohn S.R., 1989, Upwind techniques via variational principles, *Int. J. Numer. Meth. Engng.*, **28**, 769-784.

Idelsohn S.R., Heinrich J.C. and Oñate E., 1996, Pertrov-Galerkin methods for the transient advective-diffusive equation with sharp gradients, *Int. J. Numer. Meth.*

Engng., **39**, 1455-1473.

Idelsohn S.R, Nigro N., Storti M. and Buscaglia G., 1996, A Petrov-Galerkin formulation for advection-reaction-diffusion, *Comput. Methods Appl. Mech. Engrg.*, **136**, 27-46.

Ijiri Y. and Karasaki K., 1994, A Lagrangian-Eulerian finite element method with adaptive gridding for advection-dispersion equation, *Proc. Computational Methods in Water Resources X*, Vol. **1**, 291-298, Heidelberg.

Isakov V., 1998, *Inverse Problems for Partial Differential Equations*, Springer, New York.

Jennings A.A., Kirkner D.K. and Theis T.L., 1982, Multicomponent equilibrium chemistry in groundwater quality models, *Water Resour. Res.,* **18**, 1089-1096.

Jia C., Shing K. and Yortsos Y.C., 1999, Visualization and simulation of non-aqueous phase liquids solubilization in pore networks, *J. Contam. Hydrol.*, **35**: 363–387.

Jiang B.N., 1998, *The Least-Squares Finite Element Method: Theory and Application in Computational Fluid Dynamics and Electromagnetics*, Springer-Verlag, Berlin Heidelberg.

Johnson C., Navert U. and Pitkarantas J., 1984, Finite element methods for linear hyperbolic systems, *Comp. Methods Appl. Mech. Eng.*, **45**, 285–312.

Jové Colón C.F., Oelkers E. and Schott J., 2004, Experimental investigation of the effect of dissolution on sandstone permeability, porosity, and reactive surface area, *Geochimica et Cosmochimica Acta*, **68**, 805–817.

Kanney J.F., Miller C.T., Barry D.A., 2003, Comparison of fully coupled approaches for approximating nonlinear transport and reaction problems, *Adv. Water Res.*, **26**, 353-372.

Kachanov L.M., 1958, Time of rupture process under creep conditions, *Isv. Akad. Nauk SSR Otd. Teck.*, **8**, 26-31.

Kalita J.C., Dalal D.C. and Dass A.K., 2002, A class of higher order compact schemes for the unsteady two-dimensional convection-diffusion equation with variable convection coefficients, *Int. J. Numer. Meth. Fluids.*, **38**, 1111-1131.

Karlsen K.H., Brusdal K., Dahle, H.K., Evje, S. and Lie, K.-A., 1998, The corrected operator splitting approach applied to a nonlinear advection-diffusion problem, *Comput. Methods Appl. Meth. Engrg.*, **167**, 239-260.

Katz A.J. and Thompson A.H., 1986, Quantitative prediction of permeability in porous rocks, *Physical Reviews B*, **34**, 8179-8181.

Kelly D.W., Nakazawa S., Zienkiewicz O.C. and Heinrich J.C., 1980, A note on upwinding and anisotropic balancing dissipation in finite element approximations to convective diffusion problems, *Int. J. Numer. Meth. Engng.*, **15**, 1705-1711.

Keppens R., Toth G.T., Botchev M.A. and Van Der Ploeg A., 1999, Implicit and semi-implicit schemes: Algorithms, *Int. J. Numer. Meth. Fluids.*, **30**, 335-352.

Khalili A, Basu A.J. and Pietrzyk U., 1998, Flow visualization in porous media via Positron Emission Tomography, *Phys Fluid*, **10**,1031–1033.

Khan L.A. and Liu P.L.-F., 1998a, Numerical analyses of operator-splitting algorithms for the two-dimensional advection-diffusion equation, *Comput. Methods Appl. Meth. Engrg.*, **152**, 337-359.

Khan L.A. and Liu P.L.-F., 1998b, An operator splitting algorithm for the three-dimensional advection-diffusion equation, *Int. J. Numer. Meth. Fluids.* **28**, 461-76.

Khelifa A., Robert J.L. and Ouellet Y., 1993, A Douglas-Wang finite element approach for transient advection-diffusion problems, *Comput. Methods Appl. Mech. Engrg.*, **110**, 113-129.

Kieffer B., Jové C.F., Oelkers E.H. and Schott J., 1999, An experimental study of the reactive surface area of the Fontainebleau sandstone as a function of porosity, permeability, and fluid flow rate, *Geochimica et Cosmochimica Acta*, **63**, 3525–3534.

Kirkner D.J., Theis T.L. and Jennings A.A., 1984. Multicomponent solute transport with sorption and soluble complexation, *Adv. Water Resour.*, **7**, 120-125.

Kocabas I. and Islam M.R., 2000, Concentration and temperature transients in heterogeneous porous media Part II: Radial transport, *J. Petrol. Sci. Eng.*, **26**, 221-233.

Lax P.D. and Wendroff B., 1960, Systems of conservation laws, *Comm. Prue Appl. Math.*, **13**, 217-237.

Le Bellégo C., Pijaudier-Cabot G., Gérard B., Dubé J-F and Molez L., 2003, Coupled mechanical and chemical damage in calcium leached cenentitious structures, *J. Eng. Mech.*, **129**, 333-341.

Le Roux D.Y., Lin C.A. and Staniforth A., 1997, An accurate interpolation scheme for semi-Lagrangian advection on an unstructured mesh for ocean modelling, *Tellus*, **49A**, 119-138.

Le Roux D.Y. and Lin C.A., 1999, A semi-implicit semi-Lagrangian finite-element shallow-water ocean model, *Monthly Weather Rev.*, **128**, 1384-1401.

Leij F.J. and Dane J.H., 1990, Analytical solution of the one-dimensional advection equation and two- or three-dimensional dispersion equation, *Water Resources Res.*, **26**, 1475-1482.

Leij F.J., Toride N. and van Genuchten M.Th., 1993, Analytical solutions for non-equilibrium solute transport in three-dimensional porous media, *J. Hydrol.*, **151**,193-228.

Leismann H. M. and Frind E. O., 1989, A symmetric-matrix time integration scheme for the efficient solution of advection-dispersion problems, *Water Resources Res.*, **25**, 1133-1139.

Leonard B.P., 1979, A stable and accurate convective modeling procedure based on quadratic upstream interpolation, *Comput. Meth. Appl. Mech. Engrg.*, **19**, 59-98.

LeVeque R.J., 1992, *Numerical Method for Conservation Laws*. Birkhäuser Verlag Basel-Boston Berlin.

LeVeque R.J. 2002, *Finite volume methods for hyperbolic problems*. Cambridge; New York: Cambridge University Press.

Lewis F.M., Voss C.I. and Rubin J., 1987, Solute transport with equilibrium aqueous complexation and either sorption or ion exchange: Simulation methodology and applications, *J. Hydrol.*, **90**, 81-115.

Lewis R.W. and Schrefler B.A., 1998, *The finite element method in the static and dynamic deformation and consolidation of porous media*, John Wiley, Chichester, England; New York.

Li N., Zhu Y., Su B. and Gunter B., 2003, A chemical damage model of sandstone in acid solution, *Int. J. Rock Mech. Min. Sci.*, **40**, 243-249.

Li S.F. and Liu W.K., 2004, Meshfree and particle methods and their applications, *Appl. Mech. Rev.*, **55**(1), 1-34.

Li X., Wu W. and Cescotto S., 2000, Contaminant transport with non-equilibrium processes in unsaturated soils and implicit characteristic Galerkin scheme, *Int. J. Numer. Anal. Meth. Geomech.* **24**, 219-243.

Li X., Wu W. and Zienkiewicz O. C., 2000, Implicit characteristic Galerkin method for convection-diffusion equations, *Int. J. Numer. Meth. Engng.*, **47**, 1689-1708.

Lichtner P.C., Steefel C.I. and Oelkers E.H., eds., 1996, *Reactive Transport in Porous Media, Reviews in Mineralogy*, Min. Soc. Amer., Washington, DC.

Lin H., and Atluri S.N., 2000, Meshless Local Petrov-Galerkin (MLPG) method for convection-diffusion problems, *CMES:Computer Modeling in Engineering & Sciences*, **1**, 45-60.

Liu G.R. and Yan L., 1999, A study on numerical integrations in element free methods, in *Proc. APCOM 99*, Singapore, 979-984.

Liu W.K., Jun S. and Zhang Y., 1995, Reproducing kernel particle methods, *Int. J. Numer. Methods Fluids*, **20**, 1081-1106, 1995.

Liu G.R., 2003, *Mesh free methods: moving beyond the finite element method*, Boca Raton, Fla.: CRC Press.

Löhner R., Morgan K. and Zienkiewicz O.C., 1984, The solution of non-linear hyperbolic equation systems by the finite element method, *Int. J. Numer. Meth. Fluids.*, **4**, 1043-1063.

Loroy J.J.C., Soga K., Savvidou C. and Britto A.M., 1996, Finite element analysis of consolidation and contaminant transport in porous media, In *Environmental Geotechnics*, Kamon M. ed., 263–268, Balkema: Rotterdam.

Macari E.J., Parker J.K. and Costes N.C., 1997, Measurement of volume changes in triaxial tests using digital imaging techniques, *Geot. Testing Journal*, **20**, 103-109.

Majors P.D., Smith D.M. and Davis P.J., 1991, Effective diffusivity measurement in porous-media via NMR radial imaging, *Chem. Eng. Sci.* . **46**: 3037–3043.

Marchuk G. I., 1975, *Methods of Numerical Mathematics*, Springer, New York.

Marchuk G.I., 1995, *Adjoint Equation and Analysis of Complex Systems*, Kluwer, Academic Publisher, Dordrecht.

Meyerhoff K. and Hesse D., 1997, Determination of effective macropore diffusion coefficients by digital image processing, *Chem. Eng. Technol.*, **20**, 230-239.

Mizukami A. and Hughes T.J.R., 1985, A Petrov-Galerkin finite element method for convection-dominated flows: An accurate upwind technique for satisfying the maximum principle. *Comput. Methods Appl. Mech. Engrg.*, **50**, 181-193.

Montemagno C.D. and Gray W.G., 1995, Photoluminescent volumetric imaging-a technique for the exploration of multiphase flow and transport in porous-media, *Geophys Res. Lett.*, **22**, 425–428.

Morshed J. and Kaluarachchi J.J., 1995, Critical assessment of the operator-splitting technique in solving the advection-dispersion-reaction equation: 2. Monod kinetics and coupled transport, *Adv. Water Res.*, **18**, 89-100.

Morton K.W., 1980, Stability of finite difference approximations to a diffusion-convection equation, *Int. J. Numer. Meth. Engng.*, **15**, 677-683.

Morton K.W., 1985, Generalised Galerkin methods for hyperbolic problems, *Comput. Methods Appl. Mech. Engrg.*, **52**, 847-871.

Morton K.W. and Parrott A.K., 1980, Generalised Galerkin methods for first order hyperbolic equations, *J. Comput. Phys.*, **36**, 249-270.

Morton K.W., 1996, *Numerical Solution of the Convection-Diffusion Problem*, Chapman & Hall, London.

Murray W. ed., 1972, Numerical methods for unconstrained optimization. Academic Press, London.

N'dri D., Garon A. and Fortin A., 2001, A new stable space-time formulation for two-dimensional and three-dimensional incompressible viscous flow, *Int. J. Numer. Meth. Fluids.*, **37**, 865-884.

Neuman S.P., 1981, A Eulerian-Lagrangian numerical scheme for the dispersion-convection equation using conjugate space grids, *J. Comput. Phys.*, **41**, 270-294.

Neuman S.P., 1984, Adaptive Eulerian-Lagrangian finite element method for advective-dispersion, *Int. J. Numer. Meth. Engng.*, **20**, 321-37.

Nguyen H. and Reynen J., 1984, A space-time least-squares finite element finite element scheme for advection-diffusion equations, *Comput. Methods Appl. Mech. Engrg.*, **42**, 331-342.

Nguyen T.S., Selvadurai A.P.S. and Armand G., 2005, Modelling of the FEBEX THM experiment using a state surface approach, *Int. J. Rock Mech. Min. Sci.*, **42**, 639-651.

Nguyen T.S. and Selvadurai A.P.S., 1998, A model for the coupled mechanical and hydraulical behaviour of a rock joint, *Int. J. Numer. Anal. Meth. Geomech.*, **22**, 29-48.

Nordstrom D.K., Plummer L.N., Wigley T.M.L., Wolery T.J., Ball J.W., Jenne E.A., Bassett R.L., Crerar D.A., Florence T.M., Fritz B., Hoffman M., Holdren G.R., Lafon G.M. Jr., Mattigod S.V., McDuff R.E., Morel F., Reddy M.M., Sposito G. and Thraikill J., 1976, A comparison of computerized chemical models for equilibrium calculations in aqueous systems, in *Chemical Modeling in Aqueous Systems*, Jenne E.A., eds., American Chemical Society, Wasington, D.C.

Noorishad J., Tsang C.F., Perrochet P. and Musy A., 1992, A perspective on the numerical solution of convection dominated transport problems: a price to pay for the easy way out, *Water Resources Res.*, **28**, 551–561.

Ogata A. and Banks R.B., 1961, A solution of the differential equation of longitudinal dispersion in porous media, *Geological Survey Professional Paper 411-A*, U.S. Govt. Printing Office, Washington, DC, A1-A7.

Okamoto N., 1988, Analysis of convective diffusion problem with first-order chemical reaction by boundary element method, *Int. J. Numer. Meth. Fluid*, **8**, 55-64.

Okamoto N. and Kawahara M., 1991, Numerical analysis of convection-diffusion with chemical reaction by combined finite and boundary element methods, *Int. J. Numer. Meth. Fluid*, **13**, 465-479.

Oliveira A. and Baptista A.M., 1995, A comparison of integration and interpolation Eulerian–Lagrangian methods, *Int. J. Numer Methods Fluids*, **21**, 183–204.

Oñate E., 1998, Derivation of stabilized equations for numerical solution of advective-diffusive transport and fluid flow problems, *Comput. Methods Appl. Mech. Engrg.*, **151**, 233-265.

Oñate E., García J. and Idelsohn S., 1997, Computation of the stabilization parameter for the finite element solution of advective-diffusive problems, *Int. J. Numer. Meth. Fluids*, **25**, 1385-1407.

Oñate E. and Manzán M., 1999, A general procedure for deriving stabilized space-time finite element methods for advective-diffusive problems, *Int. J. Numer. Meth. Fluids.*, **31**, 203-221.

Paillere J., Boxho H., Degrez G. and Deconinck H., 1996, Multidimensional upwind residual distribution schemes for convection-diffusion equation, *Int. J. Numer. Meth. Fluids.*, **23**, 923-936.

Papanicolaou A.N., Diplas P., Balakrishnan M. and Dancey C.L., 1999, Computer vision technique for tracking bed load movement, *Comp. in Civ. Engrg.*, **13**, 71-79.

Park D.J. and McNeil P.A., 1996, Positron emission tomography for process applications, *Meas. Sci. Technol.*, **7**, 287-296.

Park E. and Zhan H., 2001, Analytical solutions of contaminant transport from finite one-, two-, and three-dimensional sources in a finite-thickness aquifer, *J. Contam. Hydrol.*, **53**, 41-61.

Park N.-S. and Liggett J.A., 1990, Taylor-least-squares finite element for two-dimensional advection-dominated unsteady advection-diffusion problems, *Int. J. Numer. Meth. Fluids.*, **11**, 21-38.

Park N.-S. and Liggett J.A., 1991, Application of Taylor-least-squares finite element to three-dimensional advection-diffusion equation, *Int. J. Numer. Meth. Fluids.*, **13**, 759-773.

Partridge P.W., Brebbia C.A., Wrobel L.C., 1992, *The Dual Reciprocity Boundary Element Method.* Computational Mechanics Publications: Southampton and Boston.

Pereira J.M.C. and Pereira J.C.F., 2001, Fourier analysis of several finite difference schemes for the one-dimensional unsteady convection-diffusion equation, *Int. J. Numer. Meth. Fluids*, **36**, 417-439.

Peters G.P. and Smith D.W., 2002, Solute transport through a deforming porous medium, *Int. J. Numer. Anal. Meth. Geomech.*, **26**, 683-717.

Philips O.M., 1991, *Flow and reactions in permeable rocks*, Cambridge University Press.

Pironneau O., Liou J. and Tezduyar T., 1992, Characteristic-Galerkin and Galerkin/least-squares space-time formulations for the advection-diffusion equation with time-dependent domains, *Comput. Methods Appl. Mech. Engrg.*, **100**, 117-141.

Quarteroni A. and Valli A., 1997, *Numerical Approximation of Partial Differential Equations, 2nd ed.*, Springer Series in Computational Mathematics, Springer-Verlag.

Raymond W.H. and Garder A., 1976, Selective damping in a Galerkin method for solving wave problems with variable grids, *Monthly Weather Rev.*, **104**, 1583-1590.

Richtmeyer R.D. and Morton K.W., 1967, *Difference Methods for Initial Value Problem*, Wiley, New York.

Robbins G.A., 1989, Methods for determining transverse dispersion coefficients of porous-media in laboratory column experiments, *Water Resour. Res.*, **25**,1249–1258.

Rubin J., 1983, Transport of reacting solutes in porous media: relation between mathematical nature of problem formulation and chemical nature of reactions, *Water Resour. Res.*, **19**, 1231-1252.

Russ J.C., 1994, *The Image Processing Handbook.* CRC Press, Cleveland, OH.

Rutqvist L., Borgesson L, Chijimatsu M., Kobayashi A., Jing L., Nguyen T.S., Noorishad J. and Tsang C-F, 2001, Thermohydromechanics of partially saturated geological media: governing equations and formulation of four finite element models, *Int. J. Rock Mech. Min. Sci.*, **38**, 105-128.

Saripalli K.P., Meyer P.D., Bacon D.H. and Freedman V.L., 2001, Changes in hydrologic Properties of aquifer media due to chemical reactions: a review, *Critical Reviews in Environmental Science and Technology*, **31**, 311-349.

Sauty J.P., 1980, An analysis of hydrodispersive transfer in aquifers. *Water Resour. Res.*, **16**, 145-158.

Selmin V. Donea, J. and Quartapelle L., 1985, Finite element methods for nonlinear advection, *Comput. Methods Appl. Mech. Engrg.*, **52**, 817-845.

Selvadurai A.P.S. ed., 1996, *Mechanics of Poroelastic Media*, Kluwer Academic Publ., Dordrecht, The Netherlands.

Selvadurai A.P.S., 2000, *Partial Differential Equation Mechanics: Vol. 1: Fundamentals, Laplace's Equation, diffusion equation, wave equation,* Springer-Verlag, Berlin.

Selvadurai A.P.S., 2000, *Partial Differential Equation Mechanics: Vol. 2: The Biharmonic Equation, Poisson's Equation*, Springer-Verlag, Berlin.

Selvadurai A.P.S., 2002a, The advective transport of a chemical from a cavity in a porous medium, *Computers and Geotechnics*, **29**, 525-546.

Selvadurai A.P.S., 2002b, Some remarks on the elastic drive equation, In *Environmental Geomechanics*, L. Vulliet, L. Laloui and B. Schrefler, eds., 253-258, EPFL press, Switzerland.

Selvadurai A.P.S., 2003, Contaminant migration from an axisymmetric source in a porous medium, *Water Resources Res.*, **39**, 1203 doi:10.1029/2002WR001442.

Selvadurai A.P.S. 2004a, Advective transport from a penny-shaped crack in a porous medium and an associated uniqueness theorem, *Int. J. Num. Analytical Meth. Geomech.*, **28**,191-208.

Selvadurai A.P.S., 2004b, On the advective-diffusive transport in porous media in the presence of time-dependent velocities, *Geophysical Research Letters*, **31**(13), L13505.

Selvadurai A.P.S. and Nguyen T.S., 1995, Computational modelling of isothermal consolidation of fractured porous media, *Computers and Geotechnics*, **17**, 39-73

Serrano S.E., 2001, Solute transport under non-linear sorption and decay, *Water Res.*, **35**, 1525–1533.

Sharkib F. and Hughes T.J.R., 1991, A new finite element formulation for computational fluid dynamics: IX. Fourier Analysis of space-time Galerkin/least-squares algorithms, *Comput. Methods Appl. Mech. Engrg.*, **87**, 35-58.

Shattuck M.D., Behringer R.P., Johnson G.A. and Georgiadis J.G., 1997, Convection and flow in porous media. Part 1. Visualization by magnetic resonance imaging, *J. Fluid Mech.*, **332**, 215-245.

Sheng D. and Smith D.W., 2000, Numerical modelling of competitive components transport with non-linear adsorption, *Int. J. Numer. Anal. Meth. Geomech.* **24**, 47-71.

Sheu T.W.H. and Shiah H.Y., 2001, The two-dimensional streamline upwind scheme for the convection-reaction equation, *Int. J. Numer. Meth. Fluids.*, **35**, 575-591.

Shin S. and Hryciw R.D., 2004, Wavelet analysis of soil mass images for particle size determination, *J. Comp. in Civ. Engrg.*, **18**, 19-27.

Siegel P., Mose R., Ackerer and Ph., Jaffre, J., 1997, Solution of the advection-diffusion equation using a combination of discontinuous and mixed finite elements, *Int. J. Numer. Meth. Fluids.*, **24**, 595-613.

Simmons C.T., Fenstemaker T.R. and Sharp J.M.Jr., 2001, Variable-density groundwater flow and solute transport in heterogeneous porous media: approaches, resolutions and future challenges, *J. Contam. Hydrol.*, **52**, 245-275.

Smith D.W., 2000, One-dimensional contaminant transport through a deforming porous medium: theory and a solution for a quasi-steady-state problem, *Int. J. Numer. Anal. Meth. Geomech.*, **24**, 693-722.

Soria A. and Pegon P., 1990, Quasi-Newton iterative strategies applied to the heat diffusion equation, *Int. J. Numer. Meth. Engng.* **30**, 661-677.

Spalding D.B., 1972, A novel finite difference formulation for differential expressions involving both first and second derivatives, *Int. J. Numer. Meth. Engng.*, **4**, 551-59.

Spencer A.J.M., 2004, *Continuum Mechanics, 3rd ed.*, Dover Publ., London.

Steffler P. M., 1989, Upwind basis finite elements for convection-dominated problems, *Int. J. Numer. Meth. Fluids.*, **9**, 385-403.

Sun N-Z, 1994, *Inverse Problems in Groundwater Modeling*, Kluwer Academic, Dordrecht; Boston.

Szymkiewicz R., 1993, Solution of the advection-diffusion equation using the spline function and finite element, *Commun. Numer. Meth. Engng.*, **9**, 197-206.

Taylor G.I., 1953, Dispersion of soluble matter in solvent flowing slowly through a tube, *Proc. Roy. Soc. Ser. A*, **210**, 186-203.

Terzaghi K., 1923, Die berechnung der druchlasigkeitszifer des tones aus dem verlauf der hydrodynamischen spannungserscheinumgen, *Ak. Der Wissenschaften, Sitzungsberichte Mathematisch-Naturwissenschaftliche Klasse*, Part II **132**,125-138.

Terzaghi K., 1943, *Theoretical Soil Mechanics*, John Wiley and Sons, New York.

Tezduyar T.E. and Park Y.J., 1986, Discontinuity capturing finite element formulations for nonlinear convection-diffusion-reaction, *Comput. Methods Appl. Mech. Engrg.*, **59**, 307-323.

Tezduyar T.E. and Ganjoo D.K., 1986, Petrov-Galerkin formulation with weighting functions dependent upon spatial and temporal discretization: applications to transient convection-diffusion problems, *Comput. Methods Appl. Mech. Engrg.*, **59**, 49-71.

Tezduyar T.E., Park Y.J. and Deans H.A., 1987, Finite element procedures for time-depeendent convection-diffusion-reaction systems, *Int. J. Numer. Meth. Fluids.*, **7**, 1013-1033.

Thomas H.R. and Cleall P.J., 1999, Inclusion of expansive clay behaviour in coupled thermo hydraulic mechanical models, *Engineering Geology*, **54**, 93-108.

Thomas H.R. and He Y., 1995, Analysis of coupled heat, moisture and air transfer in a deformable unsaturated soil, *Geotechnique*, **46**, 677-689

Thomas H.R. and He Y., 1997, A coupled heat-moisture transfer theory for deformable unsaturated soil and its algorithmic implementation, *Int. J. Numer. Methods Engng* **40**, 3421-3441.

Thomas H.R., He Y. and Onofrei C., 1998, An examination of the validation of the model of the hydro/thermo/mechanical behaviour of engineered clay barriers, *Int. J. Num. Ana. Mech. Geomech*, **22**, 49-71.

Van Genuchten M.Th., 1981, Analytical solutions for chemical transport with simultaneous adsorption, zero-order production and first-order decay, *J. Hydrol.*, **49**, 213-233.

Varoglu E. and Liam Finn W.D., 1980, Space–time finite elements incorporating characteristics for one-dimensional diffusion-convection equation, *J. Comput. Phys.*, **34**, 371–389.

Varoglu E. and Liam Finn W.D., 1982, Utilisation of the method of characteristics to solve accurately two-dimensional transport problems by finite elements, *Int. J. Numer. Meth. Fluids.*, **2**, 173–184.

Vichnevetsky R. and Bowls J.B., 1982, *Fourier Analysis of Numerical Approximations of Hyperbolic Equations*, SIAM Philadelphia, PA.

Von Kooten J.J.A., 1996, A method to solve the advection-dispersion equation with a kinetic adsorption isotherm, *Adv. Water Res.*, **19**, 193-206.

Von Neumann J., 1944, Proposal and analysis of a numerical method for the treatment of hydrodynamical shock problems, *National Defense and Research Committee Report* AM-551.

Vulliet L., Laloui L. and Harding R., 2002, Environmental geomechanics: An introduction, In *Environmental Geomechanics*, L. Vulliet, L. Laloui and B. Schrefler, eds., 3-12, EPFL press, Switzerland.

Wang Y. and Hutter K., 2001, Comparisons of numerical methods with respect to convectively dominated problems, *Int. J. Numer. Meth. Fluids,* **37**, 721-745.

Warner G.S., Nieber J.L., Moore I.D. and Gesie R.A., 1989, Characterizing macropores in soil by computed tomography, *Soil Sci. Soc. Am. J.*, **53**, 653-660.

Wendland E. and Schmid G., 2000, A Symmetrical Streamline Stabilization scheme for high advective transport, *Int. J. Numer. Anal. Meth. Geomech.* **24**, 29-45.

Wexler, E.J., 1992, Analytical solution for one-, two-, and three-dimensional solute transport in ground-water systems with uniform flow, *Techniques of Water-Resources Investigations of the U.S. Geological Survey*, Book 3, Ch. B7.

Whitaker S., 1977, Simultaneous heat mass and momentum transfer in porous media: a theory of drying, In: Advances in Heat Transfer, Hartnett J.P. and Irvine T. F. eds., Vol. **13**, 119-203, Academic Press, New York.

Xu T. and Pruess K., 2001, Modelling multiphase nonisothermal fluid flow and reactive geochemical transport in variably saturated fractured rocks: methodology, *Am. J. Sci.*, **301**, 16-33.

Yanenko N.N., 1971, *The Method of Fractional Steps*, Springer-Verlag, Berlin.

Young D.L., Wang Y.F. and Eldho T.I., 2000, Solution of the advection-diffusion equation using the Eulerian-Lagrangian boundary element method, *Engng. Anal. Boundary Elem*, **24**, 449-457.

Yu C.C. and Heinrich J.C., 1986, Petrov-Galerkin methods for the time-dependent convective transport equation, *Int. J. Numer. Meth. Engng.*, **23**, 883-901.

Yu C.C. and Heinrich J.C., 1987, Petrov-Galerkin method for multidimensional, time dependent convection diffusion equation, *Int. J. Numer. Meth. Engng.*, **24**, 2201-2215.

Zhao C.B. and Valliappan S., 1994, Transient infinite elements for contaminant transport problems, *Int. J. Numer. Meth. Engng.*, **37**, 1143-1158.

Zienkiewicz O.C., and Codina R., 1995, A general algorithm for compressible and incompressible flow- Part I. The split, character based scheme, *Int. J. Numer. Meth.*

Fluids., **20**, 869-885.

Zienkiewicz O.C. Kelly D.W. and Bettess P., 1977, The coupling of the finite element method and boundary solution procedures, *Int. J. Numer. Meth. Engng.*, **11**, 355-375.

Zienkiewicz O.C., Löhner R., Morgan K. and Nakazawa S., 1984, The finite elements in fluid mechanics-a decade of progress, in *Finite Elements in Fluids*, Gallagher R.H. et al. eds., **5**, 1-26, Wily, Chichester.

Zienkiewicz O.C., Löhner R., Morgan K. and Pereira, J., 1985, High-speed compressible flow and other adavection-dominated problems of fluid dynamics, in *Finite Elements in Fluids*, Gallagher R.H. et al. eds., **6**, 41-88, Wily, Chichester.

Zienkiewicz O.C., Nithiarasu P., Codina R. and Vázquez M., 1999, The characteristic based split procedure: An efficient and accurate algorithm for fluid problem, *Int. J. Numer. Meth. Fluids.*, **31**, 359-392.

Zienkiewicz O.C. and Taylor R.L., 2000, *The Finite Element Method, 5th ed., Vol.1: The Basis; Vol.2: Solid Mechanics; Vol.3: Fluid Dynamics*, Butterworth-Heinemann, Oxford ; Boston.

Zoppou C., Roberts S. and Renka R.J., 2000, Exponential spline interpolation in characteristic based scheme for solving the advective-diffusion equation', *Int. J. Numer. Meth. Fluids.*, **33**, 429-452.